Constraints on the carbon dioxide (CO2) deglacial rise based on its stable carbon isotopic ratio (δ13CO2)

Anna Lourantou

LABORATOIRE DE GLACIOLOGIE
ET GEOPHYSIQUE DE L'ENVIRONNEMENT
UMR5183
Centre National de la Recherche Scientifique
Université Joseph Fourier
54, rue Molière – Domaine Universitaire
BP 96 – 38402 – Saint Martin d'Hères Cedex (France)

Constraints on the carbon dioxide (CO_2) deglacial rise based on its stable carbon isotopic ratio ($\delta^{13}CO_2$)

Anna LOURANTOU

Thèse de doctorat de l'Université Joseph Fourier (Grenoble 1)
(Arrêtés ministériels du 5 juillet 1984 et 30 mars 1992)

Spécialité : Sciences de la Terre et de l'Univers

Date de Soutenance :
22 Décembre 2008

Composition du jury :

Mme Catherine Chauvel	*Présidente*
M. Philippe Ciais	*Rapporteur*
M. Eric Wolff	*Rapporteur*
M. Andrew Friend	*Examinateur*
M. Laurent Labeyrie	*Examinateur*
Mme Valérie Masson-Delmotte	*Examinateur*
M. Jérôme Chappellaz	*Directeur de thèse*

CENTRE NATIONAL DE LA RECHERCHE SCIENTIFIQUE

Observatoire OSUG des Sciences de l'Univers de Grenoble

UNIVERSITE JOSEPH FOURIER SCIENCES.TECHNOLOGIE.SANTÉ

Σα βγεις στον πηγαιμό για την Ιθάκη,	*Quand tu te mettras en route pour Ithaque*
να εύχεσαι νάναι μακρύς ο δρόμος,	*Souhaite que long soit le chemin*
γεμάτος περιπέτειες, γεμάτος γνώσεις.	*Plein d'aventures, plein de connaissances*
Τους Λαιστρυγόνας και τους Κύκλωπας,	*Ne crains pas les Lestrygons et les Cyclopes*
τον θυμωμένο Ποσειδώνα μη φοβάσαι,	*Ni le redoutable Poseidon*
τέτοια στον δρόμο σου ποτέ σου δεν θα βρεις,	*Tu ne trouveras jamais de telles choses sur ton chemin*
αν μέν' η σκέψις σου υψηλή, αν εκλεκτή	*Si ta pensée reste élevée, si une émotion noble*
συγκίνησις το πνεύμα και το σώμα σου αγγίζει.	*Habite ton esprit et ton corps .*
Τους Λαιστρυγόνας και τους Κύκλωπας,	*Tu ne rencontreras ni les Lesrtrygons ni les Cyclopes, ni le*
τον άγριο Ποσειδώνα δεν θα συναντήσεις,	*farouche Poseidon,*
αν δεν τους κουβανείς μες στην ψυχή σου,	*Si tu ne les portes pas dans ton âme*
αν η ψυχή σου δεν τους στήνει εμπρός σου.	*Si ton âme ne les dresse pas devant toi.*
Να εύχεσαι νάναι μακρύς ο δρόμος.	*Souhaite que long soit le chemin*
Πολλά τα καλοκαιρινά πρωιά να είναι	*Que nombreuses soient les matinées d'été*
που με τι ευχαρίστησι, με τι χαρά	*Lorsque avec un tel plaisir et une telle joie*
θα μπαίνεις σε λιμένας πρωτοειδωμένους ·	*Tu entreras dans des ports vus pour la première fois, que tu*
να σταματήσεις σ' εμπορεία Φοινικικά,	*fasses escale dans des ports phéniciens et que tu acquières*
και τες καλές πραγμάτειες ν' αποκτήσεις,	*les bonnes marchandises, des nacres et des coraux, des*
σεντέφια και κοράλλια, κεχριμπάρια κ' έβενους,	*ambres et des ébènes*
και ηδονικά μυρωδικά κάθε λογής,	*De voluptueuses essences de toutes sortes*
όσο μπορείς πιο άφθονα ηδονικά μυρωδικά ·	*Le plus d'essences voluptueuses possible*
σε πόλεις Αιγυπτιακές πολλές να πας,	*Que tu ailles dans de nombreuses villes égyptiennes*
να μάθεις και να μάθεις απ' τους σπουδασμένους.	*Que tu apprennes et apprennes encore auprès des savants.*
Πάντα στον νου σου νάχεις την Ιθάκη.	*Garde toujours Ithaque présente à l'esprit*
Το φθάσιμον εκεί είν' ο προορισμός σου.	*Y arriver c'est ta destinée*
Αλλά μη βιάζεις το ταξείδι διόλου.	*Mais ne hâte point ton voyage*
Καλλίτερα χρόνια πολλά να διαρκέσει ·	*Il vaut mieux qu'il dure beaucoup d'années*
και γέρος πια ν' αράξεις στο νησί,	*Et que devenu vieux, dans l'île tu jettes l'ancre, riche de ce*
πλούσιος με όσα κέρδισες στον δρόμο,	*que tu as gagné en chemin*
μη προσδοκώντας πλούτη να σε δώσει η Ιθάκη.	*Sans attendre qu'Ithaque te comble de richesses.*
Η Ιθάκη σ' έδωσε τ' ωραίο ταξίδι.	*Ithaque t'a donné le beau voyage*
Χωρίς αυτήν δεν θάβγαινες στον δρόμο.	*Sans elle tu ne serais jamais parti*
Άλλα δεν έχει να σε δώσει πια.	*Maintenant elle n'a plus rien à te donner*
Κι αν πτωχική την βρεις, η Ιθάκη δεν σε γέλασε.	*Et si elle te paraît pauvre, Ithaque ne t'a pas trompé*
Έτσι σοφός που έγινες, με τόση πείρα,	*Sage comme tu l'es devenu, avec tant d'expérience*
ήδη θα το κατάλαβες η Ιθάκες τι σημαίνουν.	*Tu auras déjà compris ce que signifient les Ithaques*
Ιθάκη - Κ.Π. Καβάφης	***Ithaque – K.P. Kavafis***

Remerciements

Merci …

- aux *membres du jury* d'avoir accepté lire et examiner ce manuscrit ainsi qu' assister à ma soutenance de thèse, 3 seuls jours avant Noël !! Merci de leur patience (les « Parisiens » ont eu de problème de train ce jour-là), leurs commentaires fructueux qui m'ont poussé à bien argumenter ainsi qu'à voir le problématique d'un point de vue plus « sphérique ».

- à *Jérôme*, pour m'avoir accepté dans l'équipe « gaz » lors d'un entretien téléphonique (!), de sa confiance, ses encouragements aux moments où il fallait et son recul lors de mes réactions au niveau diplomatique…cette thèse a été une grande école pour moi !

- plus particulièrement à *Jost*, pour son encadrement initial, sa patience *ou pas*, les moments agréables à travailler ensemble et bien sûr à argumenter !! Sincèrement, si *Jost* avait pas été là, le déroulement de ma thèse aurait été complètement différent.. Je le suis donc reconnaissante.. Merci aussi à *JC*, de m'avoir montré comment on broie la glace, ainsi que pour les pauses-clope de 1ère année de thèse.

- à l'équipe gaz, *Dominique*, *Jean-Marc* et *Greg*, ces stagiaires, doctorants et post-docs pour les réguliers « cafés gaziers » de mardi ou mercredi ou même vendredi. Les gâteaux succulents, les tasses de thé qui permettaient nettoyer ma tasse –constamment sale– à café, les discussions scientifiques (*ou pas..*), les invités-surprise.. Merci à *Joël* pour ses remarques et ses conseils sur le spectro ! Un merci aussi à *Hinrich* lors de son passage rapide par le labo, ainsi que les « évènements Heinrich » qu'il a provoqués !

- aux scientifiques du LSCE lors de mon détachement en hiver 2006-2007 : merci *Didier P.*, qui, avec l'aide de *Julien B.* l'informaticien j'ai eu BOXKIT à ma disposition et avec lequel j'ai pu m'amuser pendant ma thèse ! Merci *Elisabeth M.* et *Claire W.* pour nos conversations électroniques surtout, merci *Laurent B.* pour le parrainage pendant ces 3 mois. Merci à l'ensemble des doctorants (*ou autres*) du LSCE pour les discussions lors des pauses cafés ainsi que les pauses – déjeuners agréables à la cantine du CEA, la plupart desquels je fréquente actuellement étant en post-doc au LSCE, ce qui fait plus que plaisir !!

- à *Peter K.*, acharné modélisateur du cycle du carbone du passé, pour sa collaboration précieuse, les discussions scientifiques lors de ma visite à AWI, les conférences mais surtout par voie électronique.

- aux scientifiques engagés aux projets dans lesquels j'ai eu l'occasion de participer : EPICA-MIS et INSU/QUEST DESIRE, avec qui j'ai pu discuter un peu plus science. En particulier pour le cas d'EPICA, merci à la stratégie des scientifiques de l'*UBern*, responsables pour mon moral *« en berne »* pendant la totalité de cette thèse…

- à *Samuel*, compagnon fidèle du bureau Δ (pour lui), δ (pour moi), de m'avoir donné l'opportunité jouer le rôle de 'rapporteuse' pour un stage M1 et ses moqueries tout au long de ces 2+ ans, *« enfin, toujours la même courbe ? » ou « tu écris un review avec tous ces publis ou*

quoi ? ». Merci également aux passagers de notre bureau international, car à deux c'est bien mais à trois encore mieux : le super salsa danseur basque *Ben*, le bosseur et organisé Allemand *Markus*, la joyeuse et bavarde Vénézuélienne *Giuliat,* entre autres...

- à mes *collocs*, de m'avoir motivé de leur manière finir ma thèse plus tôt que prévu !! *Nico*, j'oublierai quand même pas ton limoncello ni les soirées bien arrosées où on se retrouvait dans n'importe quelle pièce dans la maison. Merci *Sylvain* pour tes cadeaux d'ex-colloc ! GR*Isa* et (surtout) *Alvaro*, bon courage pour la suite. *Adrien* et *Masha*, restez tant amoureux ! Merci en particulier à *Temilotzin*, avec qui j'ai partagé de bons et de mauvais moments en été 2008, restant toujours solidaires.. muchas gracias !

- aux *doctorants* du réseau international GREENCYCLES, pour les journées scientifiques et les soirées arrosées lors des réunions du réseau à Lisbonne, à Barcelone, à Cannes et à Vienne, ainsi que pour la communication hors-réunions.. Le fou *Trevor* d'Irlande, la sage *Raquel* l'Espagnole, le doux *Marcin* le Polonais& papa_1, le rigolo *Maciej* le Polonais & papa_2, la timide *Marlies* d'Autriche, la sensible (après le 5ème verre) *Roxana* de Roumanie, la joyeuse *Valentina* l'Italienne, la cool *Sarah* d'Irlande, la familière Meike la Suisse, l'attachant *Yannick* de France…Bienvenus aussi aux « nouveaux » du réseau, *Federica* et *Helena*. Bon vent à vous tous, j'espère que l'on se retrouvera bientôt ! Merci aux post-docs de GREENCYCLES, en particulier mon sémi-mentor, *Sönke*, pour ses conseils et son encouragement tout au long de cette thèse.

- toujours dans le réseau GREENCYCLES, un grand merci à *Marion*, notre 'project manager' pour ses nombreux conseils, son aide considérable, ses encouragements, son support pour les aspects du projet, ainsi que les « hors-projet » sujets (*ex.* impôts, thèse en générale)..Merci *Marion*, pour ta disponibilité et ton aide si précieuse là où j'en avais vraiment besoin..

- merci à l'ensemble des permanents, personnel administratif et informatique, la secrétariat ainsi que les doctorants/stagiaires du LGGE, pour leurs sourires du matin, du soir (des fois de la nuit, même), les discussions autour d'un café, d'une bière ou d'une courbe $\delta^{13}CO_2$ (!) *Michel F.* merci de ton temps et désolée des retards des rendez-vous.. *Maud, Elisabeth, Amélie, Leila, Michèle, Marie, Eric, Gaetan, Sandrine* merci pour tout! *Fred, Paul, Manu, Delphine, Olivier, Eric, Yves, Bruno,* restez le plus fous possibles ! *Jacques, Philippo, Olivier, Patricia* merci la compagnie lors des pauses-clopes ! *Vinc, Béné, Laetitia, Hélène, Alexandrine, Maxime, « le branlo » (Pierre), Gaël*, j'ai été plus qu'enchantée vous rencontrer ! *Irina, Florence, JC, Christine, Daphné, Marie, Marie, Cath, Martina, Amandine, Olivier, Xavier, Ludo* bon vent pour vos projets futurs !

- un merci particulier à *Jean-Philippe* pour ta collaboration et ton enthousiasme à la cité des Sciences, ainsi que ton aide lors des périodes des chutes à vélo.. *Merci Martine des Anges* pour les discussions autour d'une bière (*Béné* incluse), merci *Jean-Robert* pour ta simple existence au labo.. on a des points faibles dans cette vie..

- à mes amis de Grèce, qui, via le réseau Internet ou par voie téléphonique on a pu garder même renforcer notre amitié. Parmi eux je mentionne *Dioni*, *Kostas* (ou *Ksanthia*), *Nefeli*, *Maria*, *Efi*, *Lily* (la super cousine), *Efi*, *Zacharias*, *Kostakis* (ou *génie*) basés partout en Grèce, de Xanthi à Crète, en Angleterre même en Afrique centrale !! Merci aux amis qui ont

trouvé le temps de me rendre visite et passer de vraiment super moments sur Grenoble ; j'oublierai pas *Manolis* (Crète), *Lefteris* (Athènes et cosmopolite !), *Vincent* & *Vincent* (Belgique), *Dioni* et *Takis* (France à l'époque), *Margot-Morgane* (France) et *Vilo* (Slovakie) et bien sûr ma famille, notamment *Deppy*, ma sœur. Pour ceux que j'ai oubliés (il y en a surtout beaucoup) mes excuses mais vous savez que je tiens à vous ! Merci aussi à *Costas le géologue* de Crète, avec qui on a fait des séances de musique pendant la période dure de la rédaction.. tes mojitos me manquent déjà !

- je pourrais pas ne PAS mentionner *Raph*, bien sûr ! D'où commencer ? Merci de ton amitié, les discussions, les soirées, les conseils, les encouragements, les emmerdements (!), tes amis qui sont devenus mes amis, ta maison et ton offre de colloc les périodes difficiles…t'as été la meilleure, d'ailleurs ! Merci pour tout et je te souhaite un avenir brillant comme ta personnalité exige..

- à mes *parents*, ma *sœur* et mes *petits frères* pour leurs présence forte même par distance, leurs encouragements constants, leur envies de savoir sur mon évolution professionnel ainsi que personnel, leur suprême aide à ma soutenance, qui m'a tant soulagée et rendue fière de ma famille, merci, efharisto, pour tout !!

- last but not least, un grand grand merci à *JD* ou *Zidé* ou *Rhou* de ces 3 ans de support, de patience, d'amour, de voyages, de conseils, de discussions sans but et sans fin, de moments de silence, de surprises, de sourires, de désespoir (y en avait par moments !), d'encouragement, de nihilisme, de rêve, de rencontres, de joie totale, de confusion aussi totale, de billets de train SNCF, beaucoup de billets SNCF… Merci pour ces 3 ans et surtout pour la dernière semaine de la thèse, là, où tout était si sombre et t'es venu avec une bonne bouteille de vin et plein de bon fromage…

Si j'ai oublié des gens soit c'est fait inconsciemment, soit ça veut dire qu'ils appartiennent à la catégorie plus générale, à laquelle ce manuscrit est dédié, d'ailleurs… *(tourner la page)*

…to the ones I have injured with my bike…

Abstract

We currently live in a world undergoing constant climate perturbations, due to human contribution. At this emergent moment, scientists and policy makers tend to anticipate against further climatic reconstructions, by quantifying the effects of actual CO_2 emissions in the future. Huge mathematical equations have been therefore set to predict our future climate.

Still, open questions exist on the climate – carbon cycle interactions, that have to be answered in order to obtain a more complete picture of what occurred in the past (where no human action existed) and to better constrain the models. Ice cores provide the only direct archive from which valuable information can be retrieved on the atmospheric components of the last ~800000 years. On such means this study leans in order to contribute to some past major climate questions.

One of these major questions deals with the causes of the rapid rise of carbon dioxide (CO_2), that occurred in a periodic way, between glacial and interglacial periods. This CO_2 increase was in pace with atmospheric temperature oscillations. A question of cause and effect is risen between climate (represented by temperature) and carbon cycle (depicted by CO_2) throughout the Earth history.

A way to comprehend the origin of CO_2 gas lies in the analytical measurement of its stable carbon isotopic ratio, $\delta^{13}CO_2$. $\delta^{13}CO_2$ helps in defining the prevailing sources for the CO_2. The principle lies on the different isotopic signal the Earth's reservoirs carry (being notably the ocean and the terrestrial biosphere on a glacial-interglacial scale).

This study provides new CO_2 and $\delta^{13}CO_2$ data from Antarctic ice over the past 160000 years, covering the past two deglaciations. The delicate analytical protocol applied for the first time in LGGE is presented, by which we obtained the stable carbon isotopes out of CO_2 in the air occluded in the ice. We achieved in proposing a consistent causal scenario, out of the results obtained for both deglaciations. This scenario involves an interplay between solar (external) forcing, climate and carbon cycle interactions. S. Ocean appears to be first affected by orbital forcing changes and in turn, be the main protagonist over the deglacial CO_2 rise.

The obtained coupled results of CO_2 and $\delta^{13}CO_2$ throughout the last two deglaciations, permitting to suggest a consistent causal deglaciation scenario, as well as aspects dealing with the behaviour of ice of different physical nature against the analytical efficiency and the obtained atmospheric signal, constitute the major highlights of this study.

Abbreviations

(already seen in the main text with bold types)

Chapter I

AABW	Antarctic Bottom Waters
AIM	Antarctic Isotope Maxima
Alk	Alkalinity
BP	before present (present being 1950)
C	carbon
CAM	Crassulacean Acid Metabolism
CFCs	chlorofluorocarbons
CH_4	methane
CO_2	Carbon dioxide
δD	deuterium/hydrogen isotopic record
DIC	Dissolved Inorganic Carbon
D/O	Dansgaard-Oeschger
DOC	dissolved organic carbon
EDC	EPICA Dome C
EDML	EPICA Dronning Maud Land
EPICA	European Project on Ice Cores in Antarctica
G	glacial
GHG	greenhouse gas
GPP	Gross Primary Production
HNLC	High Nutrient Low Chlorophyll
H_2O	water vapour
IG	interglacial
IR	Infra-Red
Ma (y) or ka (y)	for millions (10^6) or thousands (10^3) of years / annum
MIS	Marine Isotope Stages
NADW	North Atlantic Deep Waters
NH	North Hemisphere
N_2O	nitrous oxide
NPP	Net Primary Production
PI	pre-industrial

POC	particulate organic carbon
Rh	heterotrophic respiration
SH	South Hemisphere
SST	sea surface temperature
T	Termination
TD	Taylor Dome
THC	thermohaline circulation
V-PDB	Vienna- Pee Dee Belemnite

Chapter II

COD	Close-Off Depth
ECM	electrical conductivity
LID	Lock-In Depth
VOC	volatile organic compounds

Chapter III

BFI	Bubble Free Ice
GC	Gas Chromatograph
GC/C	Gas Chromatograph/ Combustion interface
GC-IRMS	Gas Chromatograph- Isotope Ratio Mass Spectrometer
CF	Continuous Flow
CSIRO	Commonwealth Scientific and Industrial Research Organization
FID	Flame Ionization Detector
IRLS	Isotope Ratio Laser Spectroscopy
LN2	liquid nitrogen
MEMCO	Multi Element Multi Collector
PLOT	Porous Layer Open Tubular
SIO	Scripps Institute of Oceanography
TCD	Thermal Conductivity Detector
WMO	World Meteorological Organization

Chapter IV

AAIW	Antarctic Intermediate Waters
ACR	Antarctic Cold Reversal
APF	Antarctic Polar Front
B/A	Bølling/Allerød event
CCD	carbonate compensation depth
CLIMAP	Climate: Long-range Investigation, Mapping and Prediction
EH	Early Holocene
GCM	General Circulation Models
GNAIW	Glacial North Atlantic Intermediate Waters
H	Heinrich events (***H1:*** *Heinrich 1)*
IRD	Ice Rafted Debris
LGM	Last Glacial Maximum
MWP-1A	Meltwater pulse 1A
RR	rain ratio
SP	sub-periods
TI	Termination I
YD	Younger Dryas

Chapter V

CDW	Circumpolar Deep Water
ITCZ	Intertropical Convergence Zone
MOC	Meridional Oceanic Circulation

Table of contents

Chapter I. Introduction

I.1. General context

The industrialised world has unintentionally initiated a long-term experiment with Earth's climate, with great uncertainties and debates about its long-term consequences. On a short-term scale, emissions from fossil fuel burning, land change as induced by deforestation, cement production, biomass burning, crop production, and grassland-to-cropland changes, have been increasing since, thus leading to elevated carbon (**C**) sources into the atmosphere (IPCC, 2007). The actual energy problem, closely related to the economic crisis, further combined with the demographic evolution, have been leading our Earth towards a non-reversible ecological destruction. Carbon dioxide, $\mathbf{CO_2}$, being the major human-induced greenhouse gas (**GHG**), has been emitted since with a constantly increasing rate. The ensemble of GHG such as methane, $\mathbf{CH_4}$, or nitrous oxide, $\mathbf{N_2O}$, also increase as a consequence of anthropogenic activities, contributing to the so-called "global warming". An exception to this general increasing pattern concerns chlorofluorocarbons (**CFCs**), with the signature of the Montreal protocol in the 1990's[1]. Human kind actually lives under a long-lasting interglacial state, which is linked with cultural evolution and well-being when compared to glacial states, but an evident problem keeps arising since the long-term feedback of this rapid GHG increase on climate, cannot be fully anticipated.

I.2. The global carbon cycle

I.2.1. Coupling C-cycle with climate: greenhouse effect

Definitions

Carbon (C) cycle *is the steps by which carbon is exchanged among the Earth's biosphere, pedosphere, geosphere, hydrosphere and atmosphere. These exchanges occur in biogeochemical terms, thus involving processes dealing with geological, physical biological or chemical interactions, depending on the examined time or spatial scale*	**Climate** *contains all meteorological factors, constituting the actual weather, integrated over a generation time scale (~35 y). Temperature, humidity, rainfall are the major climate notions. Among these factors, temperature will be extensively used throughout this study as climate representative.*

There is a tight correlation between climate and C cycle, the CO_2 gas being the most evident witness. The atmospheric CO_2 content reflects the dynamic exchanges of C with the rest of Earth's major C reservoirs, such as the oceans and the continents. It is thus primordial to

[1] Since, NF_3 has been widely used for electronic applications, which will be potentially effecting Earth's climate, see Weiss R. F., Mühle J., Salameh P. K. and Harth C. M. (in press) Nitrogen trifluoride in the global atmosphere. *Geophysical Research Letters.*

comprehend all potential interactions occurring between the different reservoirs in order to interpret CO_2 variations as registered in the ice cores.

The general property of GHGs can be summarized as follows: molecules such as **H_2O** (water vapour), CO_2, or CH_4 and N_2O absorb the emitted Earth energy (as a response to the reception of sun energy) in the long wavelength domain (Infra-Red, **IR**), and re-emit this energy at the temperature of the atmosphere, with a part being returned back to the Earth.

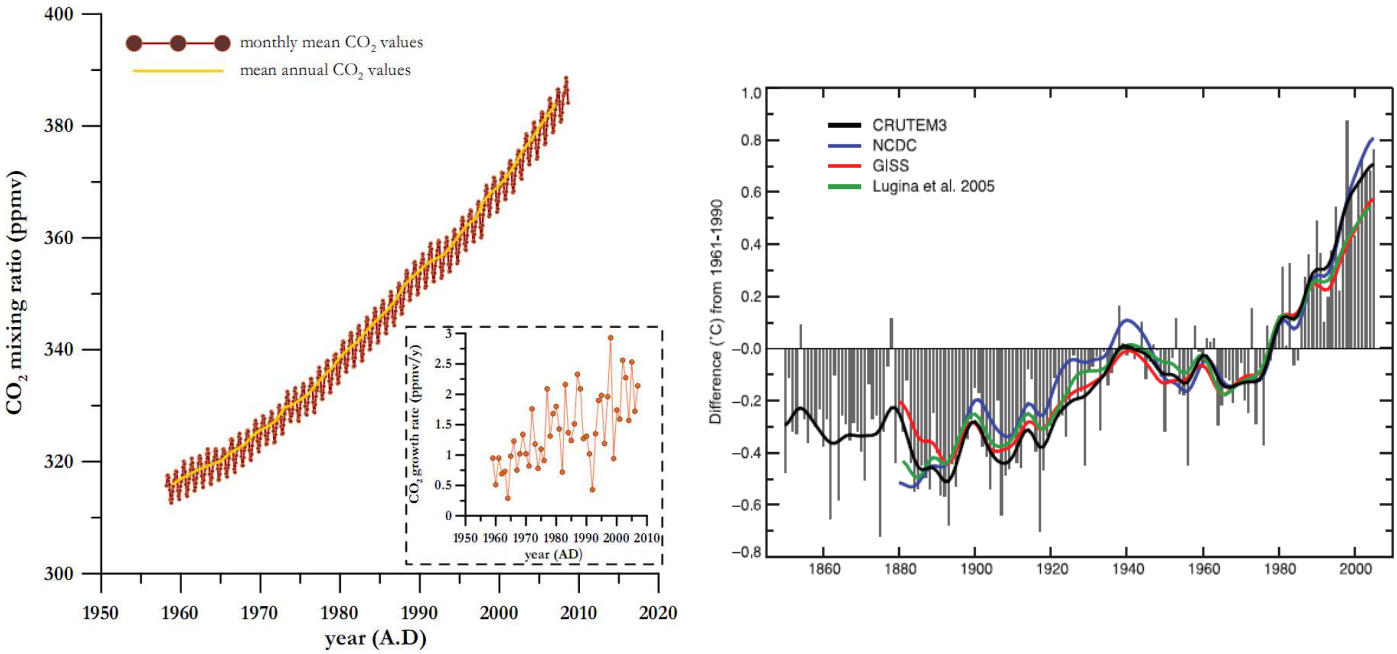

Fig. 1-1: *left panel: "Keeling curve", representing CO_2 evolution from 1958-2008 at Mauna Loa (19°54'N; 155°58'W; 3397m a.s.l.) including seasonal variations; dotted framed graph: mean annual growth rate (NOAA ESRL data of 03/09/2008); right panel: annual anomalies of global land- surface air temperature (°C), relative to 1961-1990 mean reference (IPCC, 2007)*

The Greenhouse Effect, mainly ensured by the naturally-induced H_2O, is vital for life existence on Earth. Without it, the mean Earth surface temperature would be down to –18°C, *i.e.* below the freezing point of water. GHGs naturally rise temperatures up to +15°C.

Nowadays, man intervenes to this phenomenon, by emitting more and more CO_2 into the atmosphere. Humans became aware of this with the onset of direct atmospheric CO_2 measurements by *Charles Keeling* in 1958. Fig. 1-1 (left panel) shows this historical curve, as captured from Mauna Loa station in Hawaii, as well as the annual growth trends. The measurements precision allowed scientists to accurately distinguish between pure multi-annual anthropogenic influence and the natural annual cycle of C exchange between the atmosphere and the biosphere. In parallel, air temperature rises, as seen in fig. 1-1 (right panel), notably since the late 70s.

I.2.1.1. notion of feedbacks

Within the climatic system, one encounters several feedbacks susceptible either to amplify (positive feedback) or attenuate/dampen (negative feedback) an initial radiative perturbation, and can even generate new forcings. For the actual human prevailing state, a negative feedback example can be cited for the N. Hemisphere (**NH**)[2], where the human-induced sulphate aerosols tend to cool the Earth, thus "masking" a portion of warming induced by the greenhouse effect. A positive feedback involves (i) the impact of increased temperatures to reduced C storage of tropical ecosystems, via increased evapo-transpiration, or (ii) less C export from surface to deep ocean, via deep ocean circulation slowdown (Friedlingstein, 2008).

The ocean plays a considerable role in the atmospheric CO_2 increase, since it contains 50 times more C than the atmosphere. In a natural world, rising sea surface temperature (**SST**) can have two different effects on atmospheric CO_2 : either more CO_2 is absorbed by the oceans, due to the enhanced marine productivity (SST constituting a limiting factor for photosynthesis), or less CO_2 is absorbed by the ocean, resulting from the reduced capacity of the ocean in dissolving gases (Henry's law). SSTs augmentation can generate many other feedbacks such as melting of ice sheets and elevation of sea level, thus complicating things more.

Regarding natural feedbacks between climate and continental ecosystems, an increase in temperature and precipitations can favour photosynthesis and consequently plants growth. This process results in a rise of continental C storage, leading to a decline in CO_2 (negative feedback). On the contrary, soil C storage tends to decrease when temperature rises, as a result of enhanced decomposition of organic matter; in this case, CO_2 rises (positive feedback).

I.2.2. Description of global C-cycle

I.2.2.1. comparison of different time scales

On geological time scales, global atmospheric CO_2 is regulated by the slow (millions of years) C-exchange between the atmosphere, ocean, buried organic matter and lithosphere (Berner, 1994; Berner and Kothavala, 2001). The main driving factors are volcanism (bringing C to the atmosphere) and continental weathering associated with plate tectonics (removing C from the atmosphere). On shorter time scales, the C-cycle is dominated by faster processes of atmosphere-ocean gas exchange, as well as by the growth and decay of the terrestrial biosphere, through photosynthesis and respiration. Fig. 1-2 illustrates this difference.

[2] Equally for the S. Hemisphere, which will be abbreviated as **SH**

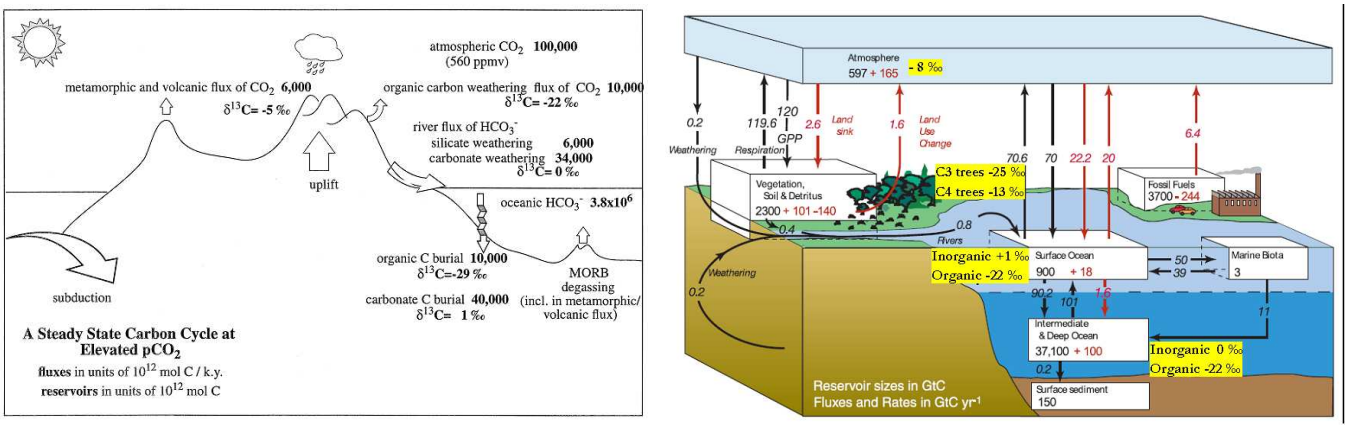

Fig. 1-2: *long- (left panel) and short- (right panel) term C-cycle: arrows showing fluxes direction between reservoirs. For the modern C cycle case, red numbers and arrows represent the anthropogenic perturbations to the system, while values in yellow frames are the stable carbon isotope values for the separate reservoirs (IPCC, 2007)*

I.2.2.2. The natural carbon cycle relevant to Quaternary time scales

In the framework of this study, C cycle will be examined from a CO_2-centric point of view, since, foremost, the CO_2 evolution is of main interest for this study and secondly, because CO_2 acts as a "conveyor" of C-exchange between two major reservoirs, the terrestrial biosphere (including the soils) and the ocean (including sediments). The amount of CO_2 in the atmosphere is small, when compared with the gross exchange fluxes between the three main reservoirs. The ocean and terrestrial biosphere amounts to 38000 and 2000 GtC[3], respectively while the atmosphere represents only ~730 GtC. Atmospheric CO_2 is therefore expected to react sensitively to changes in the global C cycle.

Before the industrial revolution of the mid 1800's, CO_2 was stable and the C-reservoir exchanges were under a dynamic equilibrium. We actually recognize the perturbation of this dynamic balance by the human intervention (*cf.* I.1), further seen in the right panel of fig. 1-2 *(as red arrows and numbers)*

- Terrestrial Biosphere

CO_2 exchange between the atmosphere and the biosphere results from three different processes: photosynthesis, respiration and biodegradation. These processes are directed by the biochemical reaction, described by the two-way equation (1-1):

$$CO_2 + H_2O \leftrightarrow CH_2O + O_2 \qquad (1\text{-}1)$$

Plant photosynthesis corresponds to the conversion of water and CO_2, under the influence of light and specific enzymes, to glucose molecules and oxygen (right direction of eq. 1-1). Respiration is the opposite reaction, where the plants consume oxygen, rejecting CO_2 in the

[3] GtC corresponds to Giga (=10^9 Tonnes of C)

atmosphere. When respiration occurs in the soil, it is called biodegradation, and atmospheric CO_2 is produced by the oxidized ("decomposed") organic matter.

Some numbers

Total CO_2 quantity dissolved in the leaves *stomata* amounts to ~270GtC/y, *i.e.* 1/3 of total atmospheric CO_2 (Farquhar et al., 1993; Ciais et al., 1997). The "fixed" quantity, consists of CO_2 converted to carbohydrate during photosynthesis and corresponds to the Gross Primary Production (**GPP**). Ciais et al., 1997 measured it through the stable oxygen isotopes of atm. CO_2 and found it to be of ~120 GtC/y. It is equally supposed that half is incorporated in new tissues (leaves, roots, wood) and the other half is converted to CO_2 with autotrophic respiration (Lloyd and Farquhar, 1996). Net Primary Production (**NPP**) corresponds to the difference between photosynthesis and respiration; it is estimated to be of ~60GtC/y (IPCC, 2001). NPP returns to atm. CO_2 pool via two processes: heterotrophic respiration, **Rh** and combustion. Fig. 1-2 gives provides more numbers.

- Ocean

The ocean covers 3/4 of the Earth' surface, thus constituting a major area for C exchange with the atmosphere. It acts either as a source or a sink for CO_2 through various physical, chemical (both related to temperature, salinity, pH..), dynamical (*e.g.* circulation) or biological processes.

Physical-chemical processes

In the ocean, CO_2 exists in three different inorganic forms: as free CO_2 (~1%), $CO_{2,aq}$, as bicarbonate ion, HCO_3^- (~91%) and as carbonate ion, CO_3^{2-} (~8%), all three constituting the Dissolved Inorganic Carbon, **DIC**. A fourth form is the true carbonic acid, H_2CO_3, whose concentration is much smaller than that of $CO_{2,aq}$ ($\leq$ 0.3%) (Zeebe and Wolf-Gladrow, 2003).
Surface water temperature changes influence the atmospheric CO_2 value, resulting from Henry's law of temperature-dependent gas dissolution effect on liquids (cooler water → enhanced CO_2 dissolution → lower atm. CO_2). CO_2 dissolution in water also depends on salinity and alkalinity (pH indirectly). The equilibrium between gas and dissolved phase is represented in eq. 1-2:

$$CO_{2,gas} \xleftrightarrow{K_0} CO_{2,aq.} \qquad (1\text{-}2)$$

Where K_0 the solubility coefficient of CO_2 in seawater.

Then, dissolved CO_2 reacts with water, to form carbonic acid, H_2CO_3, a weak acid leading to a double dissociation:

$$H_2O + CO_2 \leftrightarrow H_2CO_3 \xleftrightarrow{K_1} HCO_3^- + H^+ \quad (1\text{-}3)$$

$$HCO_3^- \xleftrightarrow{K_2} CO_3^{2-} + H^+ \quad (1\text{-}4)$$

K_1 and K_2 are the equilibrium constants and depend on the temperature and salinity, the latter having the opposite effect on solubility than temperature.

The partitioning between the three inorganic forms of CO_2 also depends on the pH, or the alkalinity of waters (Sanyal et al., 1995). Alkalinity (**Alk**) corresponds to the water capacity in capturing a sufficient number of H^+ protons, which permits the complete dissolution of carbonic acid (eq. 1-3 and 1-4). The transformation from gaseous to dissolved CO_2 is favoured by rising the pH (reducing the water acidity), since the pH is related to carbonates ($CaCO_3$) chemistry. Therefore, a pH rise transfers atmospheric CO_2 into the surface ocean.

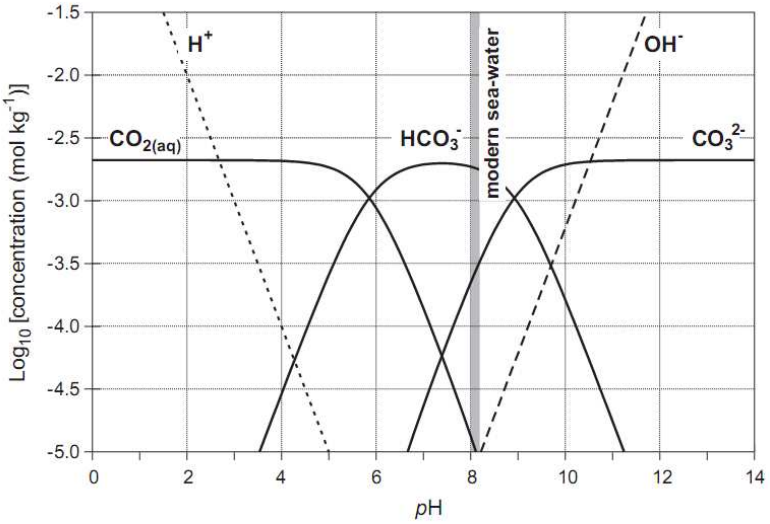

***Fig. 1-3**: Bjerrum plot showing changes of CO_2, HCO_3^- and CO_3^{-2} against pH variations (Ridgwell and Zeebe, 2005)*

Fig. 1-3 illustrates this phenomenon with the so-called Bjerrum plot[4]. The plot highlights the dominance of bicarbonate ions through natural pH range, the mean pH in the ocean ranging between 7.9-8.3 units (IPCC, 2007).

Thermohaline circulation and CO_2 cycle

Temperature or salinity changes in the surface water at the air/ocean interface provoke changes in density. Such modifications can generate an instability of the water column, accompanied by a new regime of water flow, following the new density configuration. Ocean circulation driven by the interplay of temperature and salinity gradients, is defined as thermohaline circulation (**THC**). Deep cold and salty waters are formed at high latitudes of both hemispheres: in the N. Atlantic, more specifically the Labrador, Norwegian and Greenland seas for the NH, and the S. Ocean and

[4] after the researcher who initiated the graphical representation of equilibrium relationships in 1914

the Weddell Sea for the SH. They are represented as **NADW**[5] and **AABW**[6] in fig. 1-4. The former move southwards, where they join the latter and together they raise (upwell) to the surface in the Pacific/Indian regions. This circuit is closed back to the Atlantic ocean, by a surface counter-current, principally driven by Coriolis force and winds. This oceanic journey largely contributes to climate patterns throughout the globe (Rahmstorf, 2002).

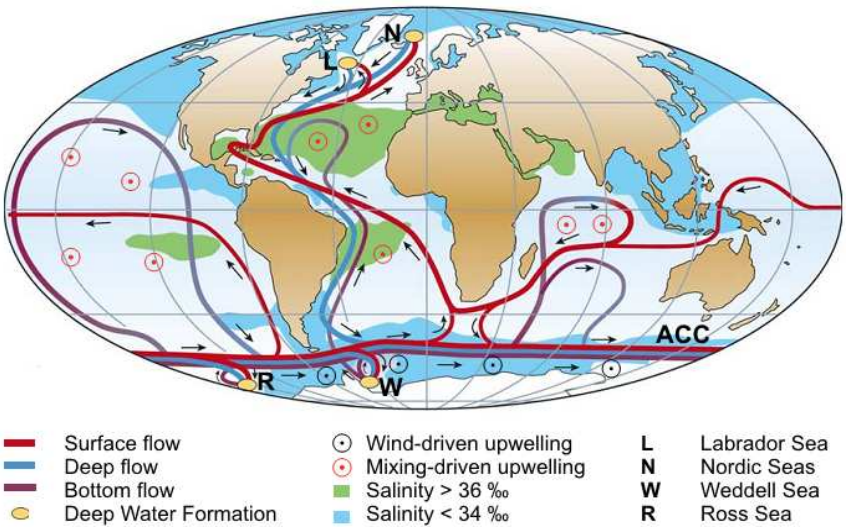

Fig. 1-4: *THC scheme as taken from Rahmstorf, 2002 and modified from Kuhlbrodt et al., 2007*

In principle, enhanced deep water formation implies reduced atm. CO_2 values due to stronger ocean pumping. Still, reality is more complex since deep water formation enhancement in one ocean area may provoke increased upwelling elsewhere, thus equilibrating the CO_2 oceanic sources and sinks.

Biological processes

The marine "biological pump" first consists of photosynthesis, *i.e.* CO_2 assimilation from microscopic algae (phytoplankton) under light presence, producing living organic matter (either dissolved or particulate, **DOC** or **POC**[7], respectively). Apart from soft tissues, marine biological processes also produce shells, containing carbonate ($CaCO_3$) particles in surface waters; this is called "(counter) carbonate pump". IPCC, 2001 reported 90 GtC/y of exchanged CO_2 through this step, from which 88Gt are returned to the atmosphere.

The phytoplankton is consumed in a second step by the zooplankton (planktonic animals), which is further eaten by bigger predators, (*e.g.* fish). Therefore, the initially photosynthesized carbon is either transformed in short-living detritus stock, such as skeletons or faecal particles or is already being demineralised by the respiratory pathway. If the latter occurs in surface waters, CO_2 is

[5] North Atlantic Deep Waters
[6] Antarctic Bottom Waters
[7] DOC for Dissolved Organic Carbon and POC for Particulate Organic Carbon

directly exchanged with the atmosphere; the percentage of this reaches ~90%, according to IPCC, 1995. A non-negligible quantity is furthermore exported in a third step towards the deep ocean, either through organisms effectuating vertical transects or under detritus form being denser than water (e.g. dead phytoplankton cells, animal skeletons in form of calcareous shells). 45 GtC/y is the calculated flux for these transports. A very small fraction of this (of the order of 0.01 GtC/y) will be definitely stored in marine sediments during millions of years and will later constitute the sedimentary rocks, which on geological time-scales will return as CO_2 in the atmosphere through volcanism (*cf.* left panel of fig. 1-2).

Biological processes require light, CO_2, nutrients (nitrogen, phosphorous) and oligo-elements (Fe). Nutrients in particular are known to be the main limiting factor for most of oceanic regions. An exception, more discussed in *Ch. IV*, concerns the **HNLC**[8] regions: such regions (*e.g.* S. Ocean, N. and Equat. Pacific) experience low productivity, as deduced from the low chlorophyll content, while their nutrients are abundant. They are therefore supposed to be biologically limited by iron, **Fe** (Martin et al., 1990; Kumar et al., 1995).

Fig. 1-5 presents a schematic combination of the three main oceanic pumps.

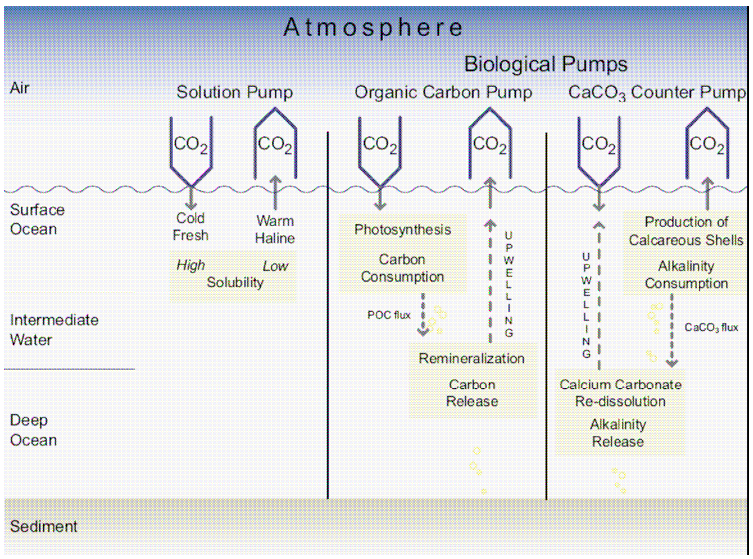

Fig. 1-5: *different oceanic pumps representation synthesis, taken from IPCC, 2007*

I.3. CO_2 evolution in different past time scales

I.3.1. Beyond ice cores

A visualization of the actual atmospheric CO_2 behaviour is already presented in the left panel of fig. 1-1, from the beginning of continuous direct atm. CO_2 measurements in 1958, until now

[8] High Nutrient Low Chlorophyll

(mid-2008). In the right panel, the temperature anomaly is illustrated. For both cases, similarities are distinguished.

The notion of global warming is linked to the Earth's climate. If one compares this situation with previous decades, or even hundreds of thousands of years, neither temperature (via proxies), nor CO_2 show such big values. Still, on time scales of millions of years (**Ma or My**), the atmospheric CO_2 mixing ratio was far more elevated than nowadays, reaching 20-fold higher CO_2 values than present, during the early Phanerozoic (until ~550 Ma). Fig. 1-6 illustrates this difference in atm. CO_2, in a cover up of the whole Phanerozoic, compared to model predictions for the future. Atmospheric CO_2 in such early periods has been estimated from equation-based CO_2 variations governing the outgassing and weathering reactions, formulated in the GEOCARB model of Berner, 1994; Berner and Kothavala, 2001.

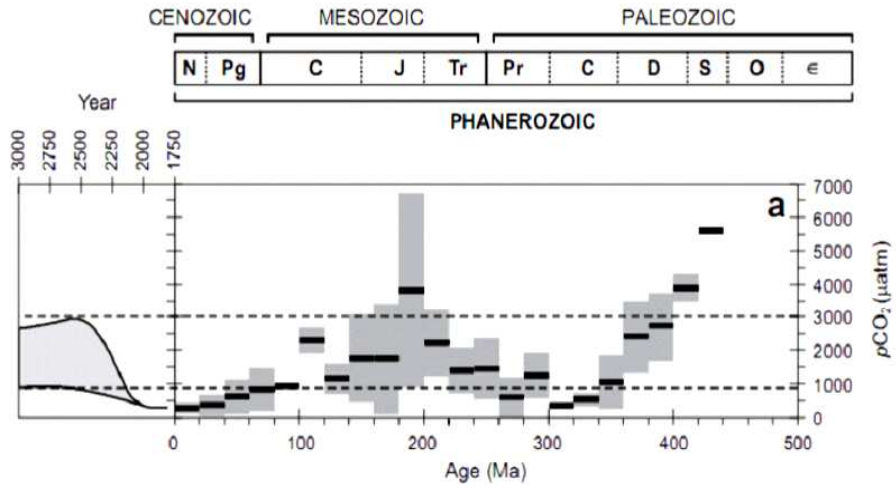

Fig. 1-6: *atmospheric CO_2 in the geological past against future predictions (Ridgwell and Zeebe, 2005)*

Fig. 1-7 leans on the Cenozoic era (until 60 My) and the relation of CO_2 with ice volume (expressed through $\delta^{18}O$ of benthic foraminifera). The so-called "hyperthermals", occurring during the Eocene and Paleocene, are warm events accompanied by elevated CO_2 concentrations (*e.g.* Mid-Eocene Climatic Optimum, Early Eocene Climatic Optimum). Based on these observations, a number of studies suggest CO_2 to be the driver for these warm phenomena (Zachos et al., 2008; Bains et al., 2000; Berner and Kothavala, 2001; Bowen et al., 2004; Lowenstein and Demicco, 2006), following the baseline theory first proposed by Arrhenius, 1896 and which possibly has extensions to nowadays. The opposite effect is observed for later (closer to today) time scales, such as the Mid-Miocene Climatic Optimum, an important transition in the Earth's history, marking the passage from Greenhouse to Icehouse climate status. During this optimum, temperature is elevated but CO_2 values remain low (Pagani et al., 1999; Holbourn et al.,

2005). For this second case, theories lean on the leading role of tectonics or orbital forcing on the temperature configuration.

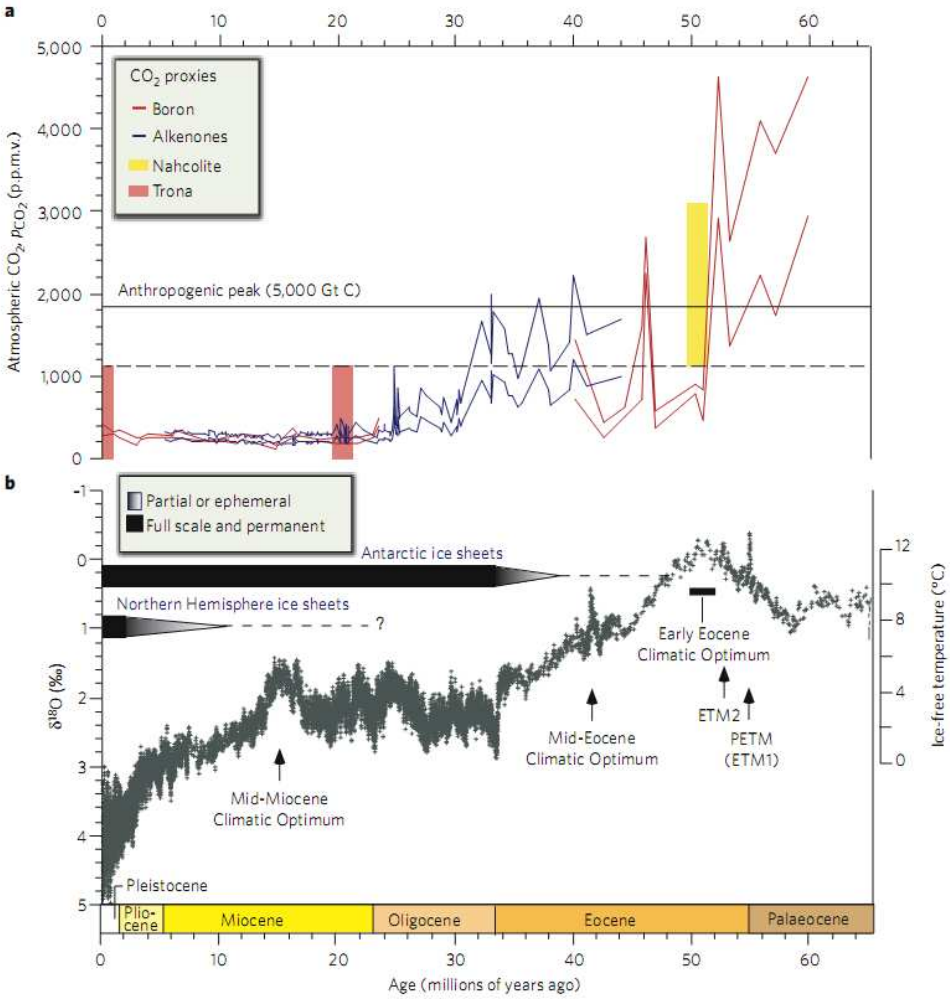

Fig. 1-7: *CO_2 (upper curve) and benthic $\delta^{18}O$ (lower curve), as a representation of climate – C cycle relationship for the Cenozoic (Zachos et al., 2001); scheme information used in IPCC, 2007*

For such early time scales, CO_2 is reconstructed from:

- boron measurements in the ocean
- $\delta^{13}C$ from alkenones
- paleosols (carbonate nodules in ancient soils)
- stomata density of fossilized leaves

These methods are applicable to all geologic periods, the Cenozoic being a period of major interest. Nevertheless, they suffer from high uncertainties. Ice cores provide the oldest direct means in reconstructing the atm. CO_2 with lower uncertainties than the methods exposed before.

I.3.2. Ice core studies

I.3.2.1. The oldest up-to-date direct record of atm. CO_2

Overall, it seems difficult to deduce an unifying historical relationship between CO_2 and climate by extracting a simple correlation between the two variables throughout the Earth's history, as other important factors (notably plate tectonics affecting atmospheric and oceanic circulations and thus climatic patterns) intervene. It thus appears appropriate to focus on more recent time periods, when plate tectonics did not change significantly the configuration of Earth surface.

High-resolved ice core records cover the recent Quaternary period. They permit to examine the relative phasing between CO_2 and temperature, thus extracting useful information on leads and lags for the last 800 ky BP[9]. Fig. 1-8 presents the correlation between CO_2 and temperature, the latter being reconstructed from the deuterium/hydrogen measurements. The tight relationship between these two variables is obvious, since warm events are accompanied by elevated CO_2 concentrations and vice versa.

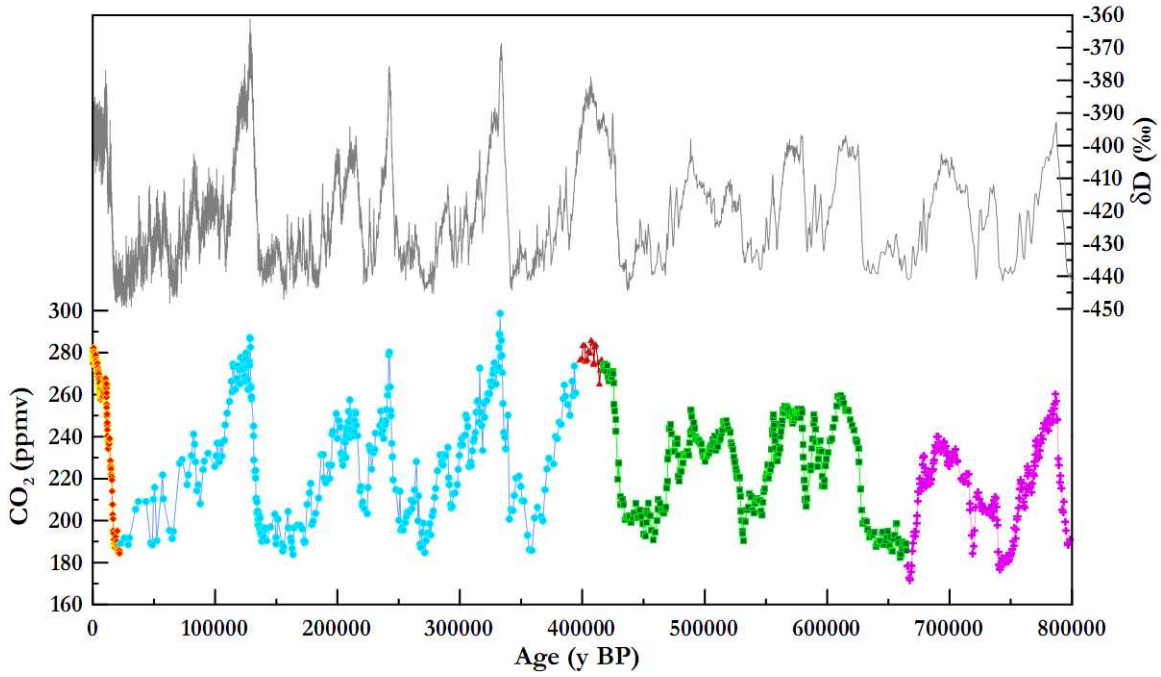

Fig. 1-8: *ice core CO_2 (lower curve) and temperature (upper curve) reconstructions from the major part of the Quaternary, now covering the last 800ka data from Lüthi et al., 2008 and Jouzel et al., 2007; different colours in the CO_2 curve correspond to sources or UBern / LGGE measurements on Vostok and EDC data*

I.3.2.2. Glacial- interglacial cycles

The recent 800-ky CO_2 record, corresponds to 8 climatic cycles. These cycles are represented by saw-tooth shaped curves involving a rapid temperature rise followed by a slow decline (see framed box). Similar behaviour is observed for a number of climatic variables, originating from

[9] ky for kilo (10^3) years, while BP corresponds to Before Present, the present being 1950

various means (marine sediments, continental flora, fauna and loess) other than ice cores. These records reveal a main 100-ky glacial (**G**) /interglacial (**IG**) periodicity, accompanied by secondary frequencies of 41, 23 and 19 ky, the *so-called* orbital parameters (eccentricity, obliquity and precession of the Earth's orbit). The leading role of these "Milankovitch cycles" on the G-IG transition has been widely recognized.

Definitions

The transition from glacial to interglacial state ("deglaciation") is widely expressed by the "Termination, ***T***" notion (Broecker and van_Donk, 1970), followed by a Latin number (***I, II, III*** etc.). Further back one goes in time, higher the number is. In ice core data, Ts are best represented by: (i) the deuterium/hydrogen isotopic record, **δD**, an atmospheric temperature indicator showing higher values for IG state and (ii) the atmospheric oxygen isotopic record, $\delta^{18}O_2$, a "proxy" of mainly global ice volume and, consequently, sea level changes, which gets depleted during IG state (Broecker and Henderson, 1998).

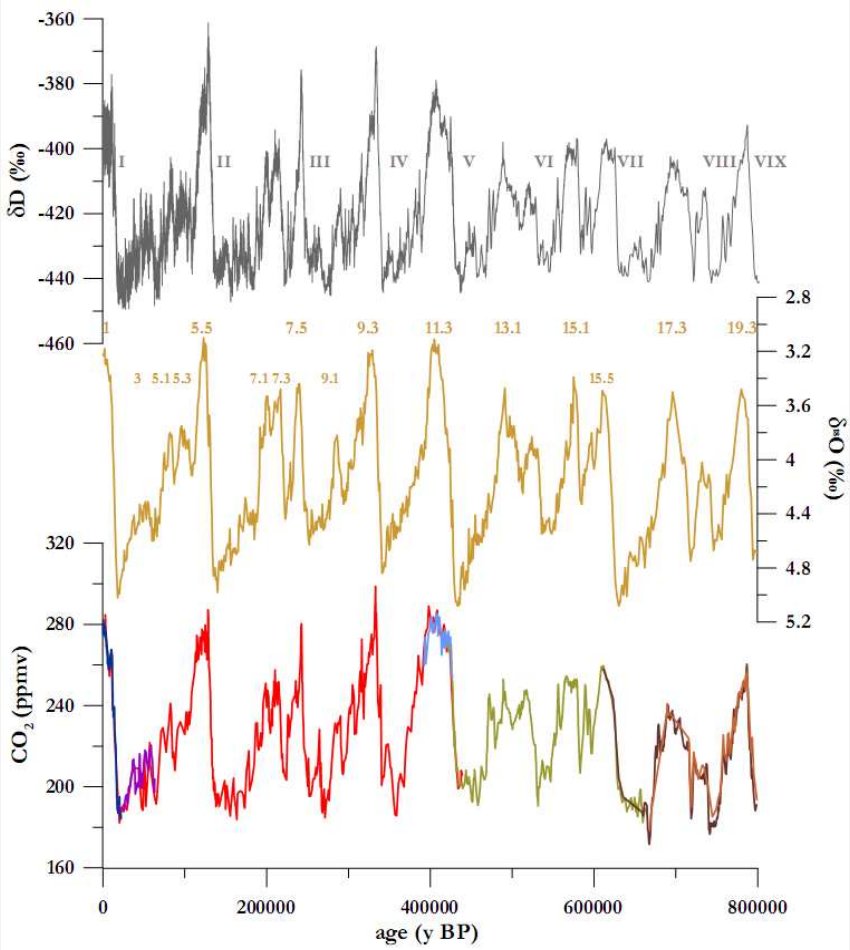

Fig. 1-9*: benthic $\delta^{18}O$ –CO_2 –δD correlation for the last 800 ka; data from (Jouzel et al., 2007;Lisiecki and Raymo., 2005; Lüthi et al., 2008)*

In the marine world, the G-IG transition is best reconstructed via the benthic oxygen isotope record, $\delta^{18}O$. $\delta^{18}O$ is influenced by global ice volume, temperature and salinity (Shackleton and Opdyke, 1973). It declines when reaching an IG state. Shackleton, 1967 first provided evidence that the benthic $\delta^{18}O$ record is dominated by the effect of $\delta^{18}O$ changes in the global ocean; the shifts between elevated and low benthic $\delta^{18}O$ define isotope stages (called Marine Isotope Stages, ***MIS***) which are numbered and used as a means of global sediment stratigraphic framework. Analogously to T numbering, higher MIS numbers go further back in time, with certain differences: i. MIS is represented by Arabic numbers (***1, 2, 3*** etc.) and ii. MIS numbering is more detailed (as it "counts" the $\delta^{18}O$ "peaks" throughout an IG, for *e.g.*); these sub-divisions are shown with a Latin letter (***a, b, c*** etc.). In MIS "numbering", always an IG is represented by an odd number (***1, 3*** etc.), while a G by an even number (***2, 4*** etc.).
The above nomenclature, used by the ice core community, was first conceived from the marine world. Both marine sediments and ice cores describe past oceanic and atmospheric trends. Paleo-scientists tend to superimpose these datasets onto a common time scale, in order to examine phenomena concomitance and leads and lags. Fig. 1-9 shows a combination of these indicators.

Deglaciation causes

According to the Milankovitch theory, high NH (65°N) summer insolation plays a leading role in forcing the ice age climate cycles, mainly paced by either obliquity or precession. Insolation extremes occur when eccentricity is high, an element justifying the dominant 100-ky periodicity in G-IG cycles (Cheng et al., 2006). This would imply that times of ice sheet collapse should correspond to peaks in NH June insolation.

Since this study will be focused on the past two deglaciations, some discrepancies of orbital nature are introduced below, which will be further discussed in *Ch. V*.

Although Milankovitch forcing of Pleistocene ice ages is universally accepted, it has been revealed problematic on the timing of TII, since paleo-records change towards the IG values before the June insolation at 127 ky (Henderson and Slowey, 2000; Gallup et al., 2002; Spötl et al., 2002). Karner and Muller, 2001 provide a historical overview and a thorough explanation of this "causality problem". In a recent dating correlation study between ice cores and marine sediments, Waelbroeck et al., 2008 deduce that the NH deglacial initiation theory cannot stand on its own. Furthermore, Parrenin and Paillard, 2003 in a modeling study, propose a combined additional role of insolation and ice volume to explain the deglaciations onset, which can solve this TII particularity. A more complete theory, also including the earlier glacial transitions, constitutes the 'insolation canon hypothesis'. This theory supports the deglaciation trigger to have been caused by a prolonged synchronous increase of insolation at both hemispheres, with a temporal lead of the SH The overlaps timing are mainly modulated by an obliquity and

precession-driven insolation, while eccentricity paces the overlaps duration (Schulz and Zeebe, 2006).

Alone orbital parameters cannot account for the observed sawtooth amplitudes in CO_2, though. Amplifying mechanisms residing mainly in the Earth's ocean or atmosphere are additionally required. The final interplay between the orbital forcing and the Earth's amplifiers (such as GHGs ot THC changes) will lead to the atmospheric signal we capture in ice cores.
A number of studies on the relative phasing of CO_2, Antarctic temperature (δD) and ice volume ($\delta^{18}O$) show the temperature leading over CO_2 and CO_2 over ice volume for the ensemble of deglaciations (Fischer et al., 1999; Broecker and Henderson, 1998; Sowers et al., 1991). Temperature increase could for *e.g.* lead to ocean stratification breakdown via an ensemble of mechanisms (*cf.* Ch. IV; V), thus more CO_2 flushed to the atmosphere by the deep ocean; this CO_2 rise, in turn, leads to more IR capture and thus higher temperatures. Without this feedback of the carbon cycle, the initial insolation forcing warming up in particular the S. Ocean and Antarctica would not be able to carry the Earth system into a new stable mode corresponding to interglacial conditions (IPCC, 2007).

I.4. Stable carbon isotopes – a climatic tool

I.4.1. Introduction on the notion of isotopes

The concept of isotopes was introduced in the beginning of the 2nd century. The word "isotope", originating from the Greek *ίσος* (*isos*, equal) and *τόπος* (*topos*, place), means that two elements belong to the same position in Mendeleïev's periodic table (Mendeleev, 1889). An element X can be illustrated as ${}^{A}_{Z}X$. Two isotopes of the same element have the same number of protons (atomic number, Z) inside their nucleus, but they differ in their neutrons number, N. They consequently differ in their mass number, A, being the sum of Z+N.
In nature, most of the elements possess isotopes. A common situation corresponds to the preponderance of one isotope (being associated to at least another one), being generally heavier than the dominant one. Isotopes have the same chemical properties, they just differ in some mass-dependent physical properties, such as kinetic energy. Carbon has two stable isotopes: ^{12}C, which is the most abundant with 98.9% and ^{13}C with an abundance of only of 1.1%. These configurations are presented in fig. 1-10. In this figure, the unstable radioactive of cosmogenic origin isotope ^{14}C (10^{-10}%), is equally presented.

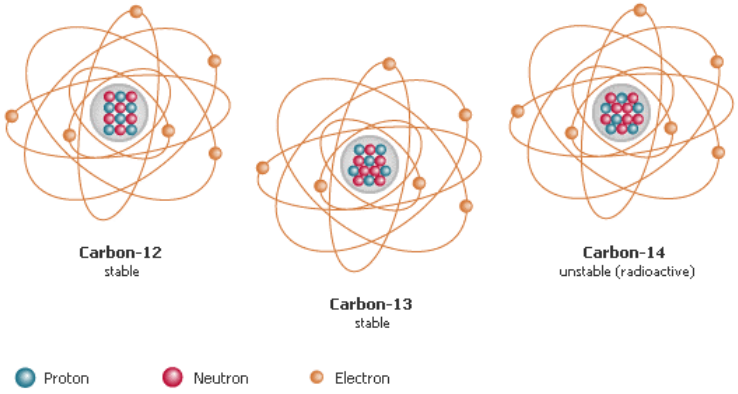

Fig. 1-10: *visualisation of C isotopes nuclear structure,* ${}^{6+N}_{6}C$ *for N=6, 7 or 8*

Different CO_2 isotopes can be also called **isotopologues**: Isotopologue is a molecular entity that differs only in at least one isotopic composition, *i.e.* in the number of isotopic substitutions (*e.g.* $^{12}C^{16}O^{16}O$, $^{12}C^{16}O^{18}O$, $^{12}C^{18}O^{18}O$).

I.4.2. δ notion – application on C - $\delta^{13}C$ definition

The change in proportion between two isotopologues of the same element in nature is usually very small. Therefore, differences in the isotopic ratios ought to be exposed in a relative way and in the case of carbon isotopes, should be multiplied by a factor of 1000, in order to provide readable numbers (Coplen et al., 2006). Eq. 1-5 introduces the corresponding notion of **δ** (delta) notation. It is reported in per mil (‰), comparative to a standard:

$$\delta^{13}C = \left[\frac{R_{sample} - R_{standard}}{R_{standard}} \right] [‰] \qquad (1\text{-}5)$$

with $R = \frac{^{13}C}{^{12}C}$,

R_{sample} = isotopic ratio of the sample and

$R_{standard}$ = isotopic ratio of the standard

The "reference" or natural standard is considered as having a δ=0‰. The current reference standard for stable carbon analysis is a Belemnite calcite fossil collected from the banks of the Pee Dee River in South California and therefore called "Pee Dee Belemnite, PDB". Its absolute carbon isotopic ratio R equals 0.0112372. For carbon isotope measurements this ratio is defined as the International Standard (Craig, 1957). The original Carbon Standard being exhausted, a new standard of similar isotopic ratio has been established and is referred as the Vienna-PDB standard (**V-PDB**) (Hut, 1987).

I.4.3. Isotopic fractionation

I.4.3.1. Theoretical aspects

As shown in fig. 1-2, different reservoirs do not only exchange carbon in large quantities, but each reservoir has a distinct carbon isotopic composition. This is due to the fact that exchange processes between two reservoirs lead to carbon isotope fractionation. The concept of isotopic fractionation was first introduced by Urey, 1947, who, by using the principles of quantum physics and mechanics, achieved in predicting (in a theoretical way) fractionation factors and their dependence on temperature. Fractionation among isotopes are either produced kinetically or during equilibration processes (Young et al., 2002). Kinetic fractionations are generally related to physical transport effects and are often observed during diffusion processes, where the lighter molecules diffuse faster than the heavier ones. Equilibrium fractionations are witnessed among chemical species, *e.g.* between CO_3^{2-}, HCO_3^- and dissolved CO_2, as well as during phase changes, *e.g.* gas-liquid equilibrium. The fractionation factor α is defined as:

$$\alpha_{A\rightarrow B} = \frac{R_A}{R_B} \tag{1-6}$$

The absolute value of α is near 1, as the fractionations of natural origin are generally small; in order to use readable numbers, the term ε is used:

$$\varepsilon = (\alpha - 1) \times 1000 [‰] \tag{1-7}$$

ε is called fractionation constant.

In both cases, the degree by which two or more isotopes are fractionated is usually mass-dependent. Thiemens and Heidenreich, 1983 introduced the notion of mass-independent isotopic fractionation taking place through some chemical reactions. In this study all processes studied deal with mass-dependent fractionation.

I.4.3.2. Applications

Applications in C isotopic fractionations are encountered in several scientific domains, such as archaeology, medicine, biochemistry, microbiology, food science. The determination of isotopic composition has largely expanded its field of application over the last 20 years, due to the rapid development of molecular-selective isotope techniques. An overview of $\delta^{13}C$ applications can be found in Lichtfouse, 2000, while more details on technical aspects are given in *Ch. III*.

Carbon isotopic fractionation in the terrestrial biosphere

When primary production occurs, the additive effects of many consecutive steps during the photosynthesis result in a depletion of plants in the heavier isotope, ^{13}C, against ^{12}C. The reason lies on (1) the enzymatic preference for ^{12}C during carboxylation reaction and (2) the slower ^{13}C

diffusion into the stomatal cavity (Ciais et al., 1995a). This depletion is primarily species-dependent, as three kinds of plants exist, according to their photosynthetic pathway (**C3**, **C4** and **CAM**[10], (O'Leary, 1981)). The whole photosynthetic process discriminates against ^{13}C with a fractionation factor of ~19-20‰ according to (Peterson and Fry, 1987; Yakir and Sternberg, 2000; Ciais et al., 1995; Francey et al., 1999 ; Brovkin et al., 2002), while the equivalent fractionation for C4 plants is of the order of ~7‰. Given an atmospheric value of -8‰, the biomass of C3 plants has a typical $\delta^{13}C$ value of ~-28‰ and for C4 plants of ~-15‰. As the removed carbon has a light signature, in turn, the remaining CO_2 in the atmosphere gets isotopically enriched in ^{13}C. The following isotopic mass balance (eq. 1-8) formulates in the simplest form two reservoirs inter-connections:

$$C_{mixture} \times \delta^{13}C_{mixture} = C_{reservoir-A} \times \delta^{13}C_{reservoir-A} + C_{reservoir-B} \times \delta^{13}C_{reservoir-B} \quad (1\text{-}8)$$

With ***Ci*** the amount of carbon for the reservoirs A and B and the mixture, while ***δ^{13}Ci*** represents the isotopic composition of the reservoirs or mixture.

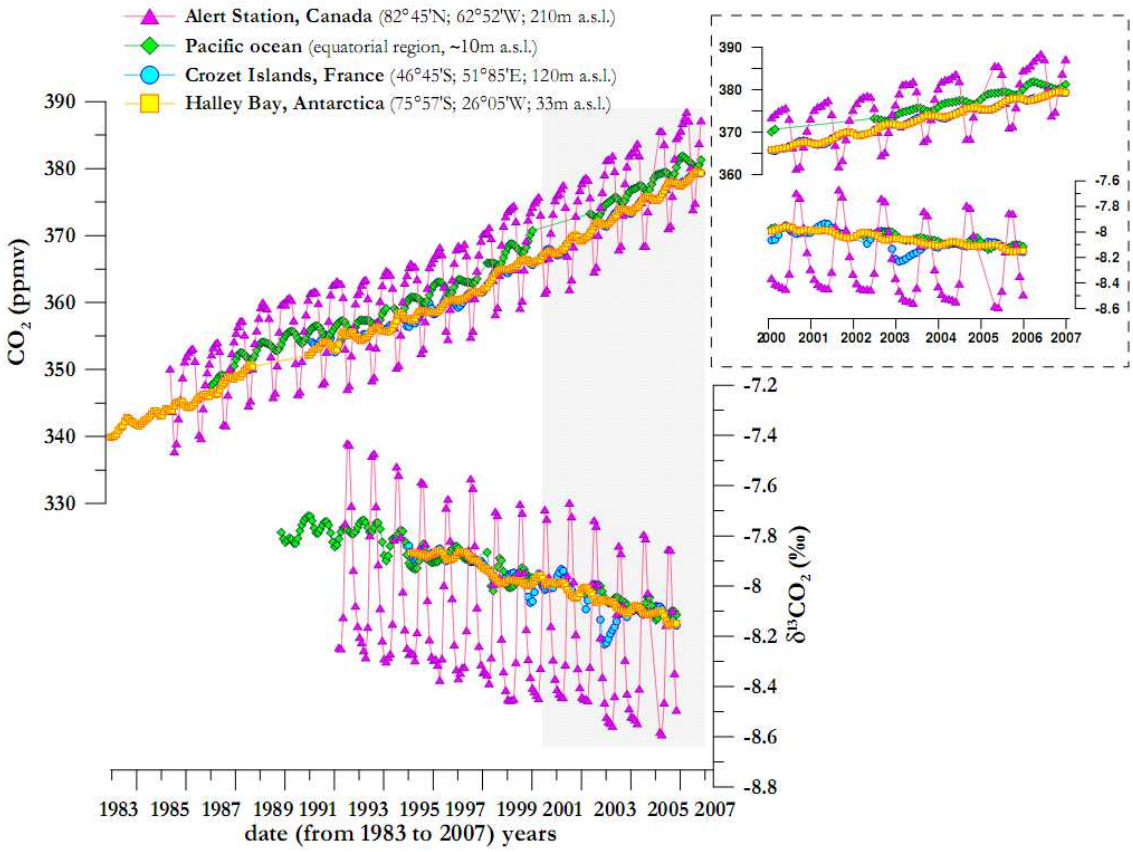

Fig. 1-11: *reconstruction of CO_2 and $\delta^{13}C$ atm. data in flasks from 4 different stations; shadowed part is given more in detail in the dotted smaller graph part on the right. Source from sources: Dr. Pieter Tans, NOAA/ESRL - http://www.esrl.noaa.gov/gmd/ccgg/trends/; WMO WDCCGG - http://gaw.kishou.go.jp/wdcgg/*

[10] C3 and C4 denote the number of carbon atoms of the first photosynthetic product, while CAM stands for Crassulacean Acid Metabolism

Fig. 1-11 illustrates the atmospheric effect of isotopic fractionation during plant photosynthesis on a global scale. Four sites have been selected from different latitudes. One easily observes the waxing and waning of the terrestrial biosphere, depicted differently in these four stations: the record of Alert Station (82°N) demonstrates a more pronounced carbon cycle when compared to equatorial Pacific ocean stations or Crozet Islands (46°S) and Halley Bay (75°S). During late summer time, where light availability is at its peak and ambient temperature at its highest, photosynthesis gets enhanced and C gets assimilated more easily in form of CO_2. This is shown as a CO_2-dip in the upper CO_2-curve of fig. 1-11 (more detailed in the small frame, depicting seasonal variations). This phenomenon is accompanied by a ^{13}C-enrichment (lower panel), as predicted by the mass balance equation. The opposite trends occur during the late winter, when light availability and temperature are low. Within the same figure, one observes atmospheric variations of the order of ~15 ppmv and ~0.8‰ for CO_2 and $\delta^{13}C$, respectively. Even on a daily basis, these fluctuations can be ever higher (Fisher et al., 2005; Ribas-Carbo et al., 2002).

Carbon isotopic fractionation in the ocean

Contrary to the terrestrial biosphere, the ocean – atmosphere relative $\delta^{13}C$ values are of opposite signs, the ocean being more enriched in ^{13}C than the atmosphere. A temperature-dependent fractionation of carbon isotopes exists and is dominated by the ocean carbonate chemistry and the diffusive $air \longleftrightarrow sea$ carbon transfer (Mook, 1986). In contrast to the high exchange fluxes registered between atmosphere and terrestrial biosphere, these changes are less pronounced for the ocean. However, on decadal or millennial time scales, it is the ocean which dictates the atmospheric CO_2 level, as well as the $\delta^{13}C$ value, due to its large reservoir size and the quasi-permanent diffusive equilibrium taking place between the surface ocean and the atmosphere. The main forcing factor on the carbon isotopic fractionation between the atmosphere and the ocean is the temperature influence during the air/sea exchange, while the biology pump generates vertical $\delta^{13}C$ oceanic gradients. As for the continental biosphere, the photosynthetic process in the surface ocean removes preferentially the lighter ^{12}C, thus enriching surface waters in ^{13}C. The opposite effect of organic matter remineralization, occurring in intermediate waters, below euphotic zone, leads to a ^{13}C depletion of surrounding deep waters.

On long time scales, water masses mixing also constitute a leading factor on oceanic $\delta^{13}C$ values (and eventually on atmospheric $\delta^{13}C$ ones). In NH areas of deep water formation (fig. 1-4), superficial, ^{13}C-enriched waters are transported towards the deep ocean; therefore the sinking fresh waters have higher ^{13}C values. These deep waters circulate in the bottom ocean, being isolated from the surface, while they constantly receive an organic carbon rain enriched in ^{12}C due

to the biological pump. The longer these waters remain isolated in the deep ocean, the more they lose their elevated ^{13}C-signature, due to the increased amount received of remineralized organic carbon. Fig. 1-12 (left panel) shows the $\delta^{13}C$ partitioning throughout the Atlantic transect. The equatorial and Northern Atlantic reveal a large difference between ^{13}C-depleted bottom waters and ^{13}C-enriched surface waters, due to the above-mentioned processes. This is not the case for the S. Ocean, where bottom and intermediate waters are more ^{13}C-depleted than the rest of the Atlantic sector. The major differences concern the NADW and AABW formation regions, leaving a signal distinction that may help distinguishing the water masses origin in the mid-to-high- latitude deep Atlantic (*cf. Ch. IV*).

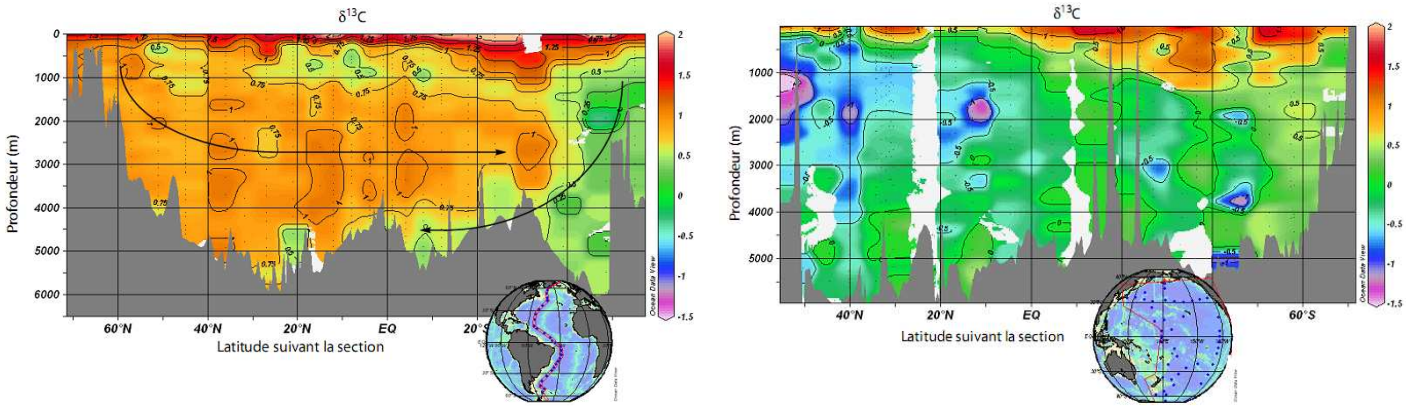

Fig. 1-12: *distribution of $\delta^{13}C$ and surface – bottom waters differences at the Atlantic section (left panel) and Indo-Pacific section (right panel). Courtesy of Roche, 2006*

The reason for this high-latitude difference can be found among the following points: a. the air-sea CO_2 exchanges are limited in the SH, especially on winter, due to sea-ice formation; b. the AABW are simultaneously formed and recycled in the Antarctic edge, implying a re-usage of already ^{13}C-depleted waters; c. S. Ocean constitutes a HNLC region, primarily limited by Fe. Overall, AABW waters are less enriched in ^{13}C and they mix in a smaller-sized reservoir than NADW.

As far as the Pacific/Indian sector is concerned (shown in right panel of fig. 1-12), it appears to be the most ^{13}C-depleted area, as they correspond to mixing points of waters originating from the N. Atlantic and the S. Ocean. The more ^{13}C-depleted values are encountered in the N. Pacific region, which is principally due to the age of the waters, and indirectly to the absence of deep water formation.

From this simplified global carbon cycle view, it appears critical to evaluate temporal changes of each reservoir size as well as isotopic composition, in order to explain past changes in atmospheric CO_2 mixing and isotopic ratios.

I.4.4. Previous studies using carbon isotopes to constrain the global C cycle

I.4.4.1. Ocean

In this section some milestones on the application of stable carbon isotopes in illuminating the C-cycle will be exposed. One of the most 'historical' application (dating back to the ensemble of Phanerozoic, 550Ma ago) lies in the reconstruction of past atmospheric CO_2 values based on oceanic $\delta^{13}C$ data, as exposed in I.3.1 section. Two methods have been used : (1) $\delta^{13}C$ of alkenones (biomarkers of marine sedimentary org. C) *e.g.* Pagani et al., 1999; (2) $\delta^{13}C$ analysis of pedogenic carbonates in paleosols *e.g.* Cerling, 1991. More details on these two approaches are synthesized in Ghosh and Brand, 2003. Ever since, the study of marine $\delta^{13}C$ has been tightly related with the evolution of atmospheric CO_2. Periods of large temperature anomalies and rather rapid on geological time-scales, have been the focus of major research.

Veizer et al., 1999 first compiled oceanic $\delta^{13}C$ data during the whole Phanerozoic (Cambrian to Tertiary) and concluded on the primal biology-driven character of the data (fig. 1-13).

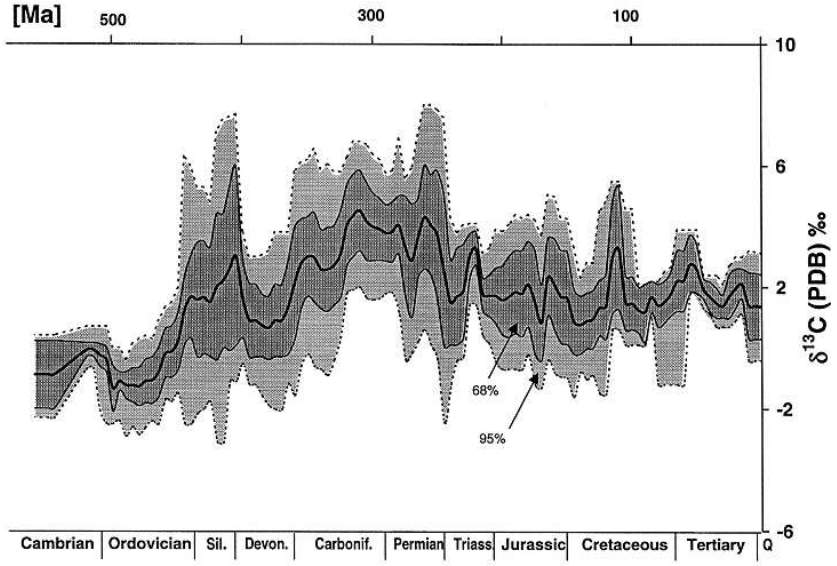

Fig. 1-13: *oceanic $\delta^{13}C$ compilation throughout Phanerozoic from Veizer et al., 1999*

In the far past, anticorrelations of atm. CO_2 and marine $\delta^{13}C$ have been found and can be visualized here when comparing fig. 1-6 with fig. 1-13; e.g. the "Oceanic Anoxic Event" at ~120 My (Kuypers et al., 1999; Van Breugel et al., 2007), or the Paleocene/Eocene Thermal transition, ~55My (Bowen et al., 2004; Norris and Röhl, 1999), or later on, at 51-53 My, the Early Eocene Climatic Optimum (Lowenstein and Demicco, 2006; Edgar et al., 2007), during which ^{13}C-depleted waters were related to elevated CO_2 values. This implied an injection of a large ^{13}C-depleted mass into the atmosphere or ocean (Zachos et al., 2008). The reasons for these events

out-pass the study area, though, since another time scale is studied, dominated by more long-term processes. The propagation of the oceanic signal towards the atmosphere, will be still discussed in the framework of this study.

For decades now, carbon isotopic composition has been available from the oceanic reservoir, derived mainly from shells found in marine sediments or from dead organic matter (Curry et al., 1988). On a G-IG scale, benthic $\delta^{13}C$ is known to have shifted towards 0.3-0.4‰ higher values (Bird et al., 1994). This isotopic shift has been interpreted as a 500 GtC transfer from the "lowered" ocean to the expanding terrestrial biosphere. This, in combination with the buffering capacity and the carbonate compensation oceanic mechanism, a part of the CO_2 deglacial atmospheric rise could be explained (see more in *Ch. IV*). The millennial-scale past evolution of benthic $\delta^{13}C$, allows to elucidate marine productivity and THC changes (Raymo et al., 1996; Oppo et al., 1997; Rickaby and Elderfield, 2005; Lototskaya and Ganssen, 1999; Skinner and Shackleton, 2006), notably based on the anticorrelated signal N-sourced waters carry against S. – sourced one in the Atlantic ocean (*cf. Ch. IV*). Planktic $\delta^{13}C$ data are generally considered as less reliable, due to the dominant influence of the local and short-term character, such as light availability leading to photosynthesis and the consequent time and space-dependent C-fixation. Still, there exist cases of exploiting planktic $\delta^{13}C$ data, when related to water masses changes (Spero and Lea, 2002). For both $\delta^{13}C$ cases, the propagation of the oceanic signal towards the atmosphere will be studied.

I.4.4.2. Atmosphere

The continuous increase in the concentration of atm. CO_2 over the beginning of the industrialized world is due to addition of ^{13}C-depleted CO_2 from organic sources (fossil fuel and biomass burning), a process that has progressively changed the isotopic composition in the atmosphere (Keeling et al., 1995) *(fig. 1-11)*. The combination of direct atmospheric measurements with other means of reconstructing atm. $\delta^{13}CO_2$, such as speleothems (Baskaran and Krishnamurthy, 1993), tree rings (Francey and Farquhar, 1982) or firn air and ice cores (Francey et al., 1999), extended the actual trend of decreasing atm. $\delta^{13}CO_2$ back to pre-industrial times. This makes the most direct and quantitative proof that the current increase in atm. CO_2 results from fossil fuel burning and anthropogenic activities.

I.5. CO_2 and $\delta^{13}CO_2$: combined reconstruction from ice cores

I.5.1. Significance in measuring $\delta^{13}CO_2$ in ice cores

- $\delta^{13}CO_2$ constitutes the sole direct indicator of CO_2 mixing ratio origin, of either oceanic or terrestrial biospheric source (since both reservoirs carry different isotopic signals)
- it is concomitantly measured with the CO_2 mixing ratio, thus avoiding external (analytical or environmental) biases
- $\delta^{13}CO_2$ can be measured with a high resolution from ice cores, allowing to examine C-cycle dynamics and feedbacks with climate. Stable carbon isotopes of CO_2 in ice can contribute in answering questions on the causes of the CO_2 / temperature correlation or on the "Ruddiman hypothesis" of early human impact on atmospheric CO_2 (Ruddiman, 2003).
- Measurements of C-isotopes in ice cores can help additionally in elucidating the origin of CO_2 during rapid natural climatic changes such as deglaciations or brief Antarctic oscillation analogues (**AIM**[11] **events)** to the NH **D/O**[12] events (EPICA, 2006).

I.5.2. State of the art

For over 30 years, analytical effort has been made not only for the case of CO_2 concentration analysis in the air trapped in ice cores, but also on its isotopic composition. The analysis of the latter been certainly more delicate, less data have been produced so far.

First $\delta^{13}CO_2$ results have been presented for the last two thousand years on S. Pole and 50ky before from the Byrd ice core (Friedli et al., 1984); 2 years later, Friedli et al., 1986 combined the S. Pole $\delta^{13}C$ data with new results from Siple core covering the last two centuries. They were the first to superpose ice core data with direct atmospheric data from Keeling et al., 1995, thus providing an integrated $\delta^{13}CO_2$ record over industrial times, in which the $\delta^{13}C$ decrease related to CO_2 rise becomes evident. The average $\delta^{13}C$ value before 1800 A.D. as found at Siple Station is –6.41‰, very close to the extrapolated PI mean value (-6.44‰) for the S. Pole, having been measured directly in air samples (Keeling et al., 1995).

This very first pre-industrial (**PI**) to industrial record was considerably improved later on by Francey et al., 1999. The examined ice core was the high-resolution Law Dome coastal site, combined with air samples from the Cape Grim archive. The record covers the last millennium. The dataset of high quality allowed the authors to establish a well defined PI atmospheric $\delta^{13}C$ level of –6.4‰. Prior to the anthropogenic CO_2 increase starting around 1750 AD, the global C-

11 Antarctic Isotope Maxima
12 Dansgaard-Oeschger

cycle was relatively stable according to the Law Dome dataset, showing only minor variability in mixing and isotopic CO_2 ratios. Fig. 1-14 shows the compilation of the majority of pre-mentioned important datasets, thus superimposing atmospheric with firn air and ice core datasets.

The first $\delta^{13}CO_2$ data dating from the last glacial period were retrieved from the Byrd core (Leuenberger et al., 1992). The measured data do not provide enough temporal resolution to allow an adequate C-cycle reconstruction of the glacial period. Nevertheless, the Byrd data showed a ^{13}C- depleted atm. glacial signal against Holocene (by an average of 0.3±0.2‰). This is in line with the rough assumption that during the cold periods, the C reservoir of the terrestrial biosphere was reduced, as large areas in the N. Hemisphere were covered with continental ice sheets, thus reducing the photosynthesis which normally enriches the atmosphere with ^{13}C.

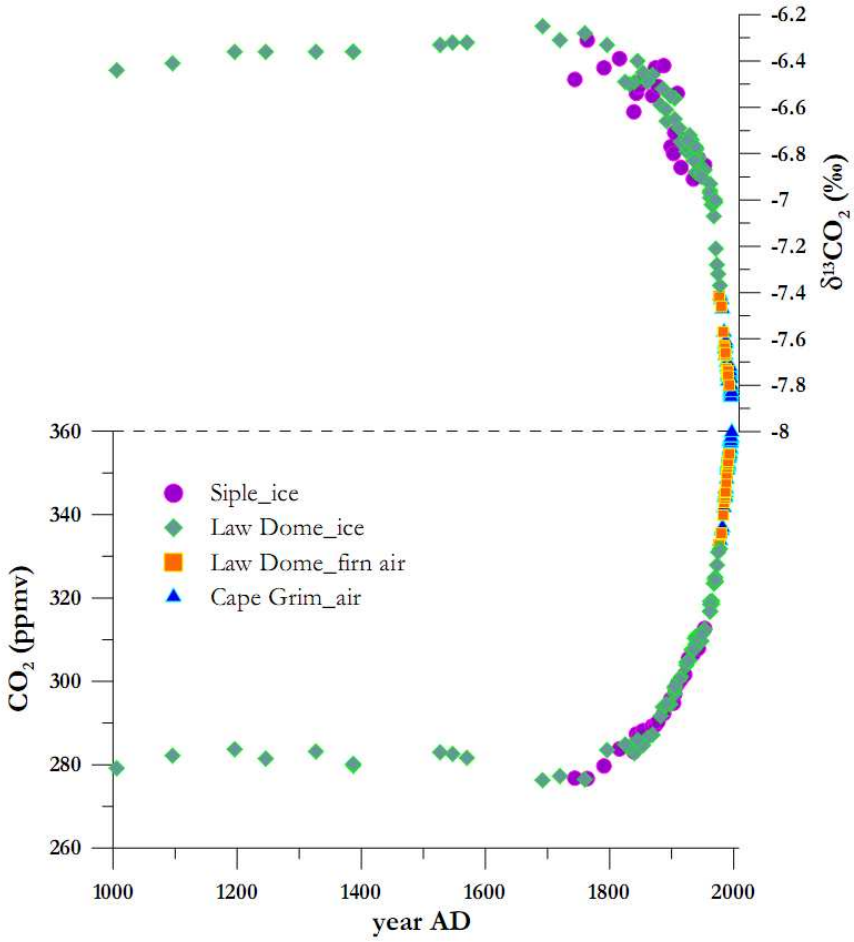

Fig. 1-14: *data compilation from selected studies on air (Francey et al., 1999), firn (Francey et al., 1999) and ice (Friedli et al., 1986; Francey et al., 1999)*

A more detailed picture came recently from the Taylor Dome (**TD**) ice core, showing millennial scale $\delta^{13}C$ variability within the Holocene (Indermühle et al., 1999). Analysis of the same core during the last deglaciation, gave another "milestone" by (Smith et al., 1999). While the

deglaciation CO_2 signal seemed to have been dominated by oceanic changes, terrestrial biosphere intervened at equal terms with the ocean during the Holocene. Still, the temporal resolution of these pioneering analyses remain very low, and the initial interpretation was based in the Keeling plot principle which was proved to be inadequate during deglaciations (Köhler et al., 2006). Therefore, many questions remain unanswered. Several carbon model studies leaned on this TI dataset from (Smith et al., 1999) in an attempt to interpret the ensemble of available signals (Brovkin et al., 2002; Köhler et al., 2005). Such studies attributed the CO_2 evolution either to marine biology or terrestrial biosphere changes through different time-frames of the last deglaciation. Original TD dataset is exposed in fig. 1-15.

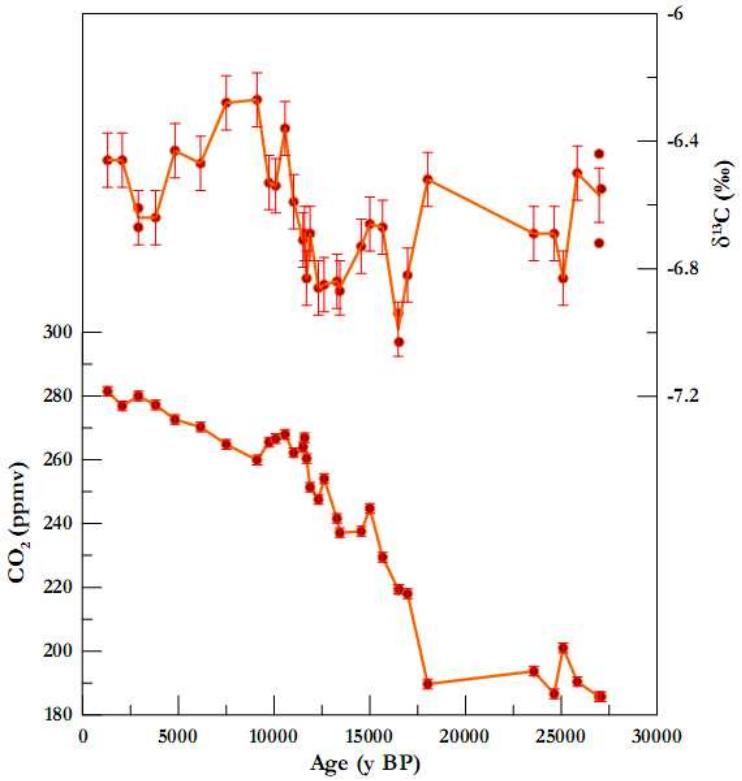

Fig. 1-15: *atmospheric CO_2 and $\delta^{13}CO_2$ data from Taylor Dome on its original age scale, as provided by (Smith et al., 1999), averaged error bars as stated by the authors included*

In order to improve the temporal resolution within the Holocene, while providing an extension of the $\delta^{13}C$ record further into the glacial period, (Eyer, 2004) produced two highly resolved $\delta^{13}C$ records from the two **EPICA**[13] ice cores (**EDML**[14] and **EDC**[15]). The EDML Holocene $\delta^{13}C$ record deviates from that from TD core (Indermühle et al., 1999). Even when large dating errors between the two ice cores were taken into account, the disagreement between the two datasets

[13] European Project on Ice Cores in Antarctica
[14] EPICA Dronning Maud Land
[15] EPICA Dome C

persisted. In particular, during the time interval older than 6 ky BP, the $\delta^{13}C$ average for EDML is ~0.3‰ lighter compared to TD. In addition to this, the analytical scatter in the (Eyer, 2004) data is quite considerable.

If the above mentioned data are superposed for the last 60 ky BP, fig. 1-16 provides the result:

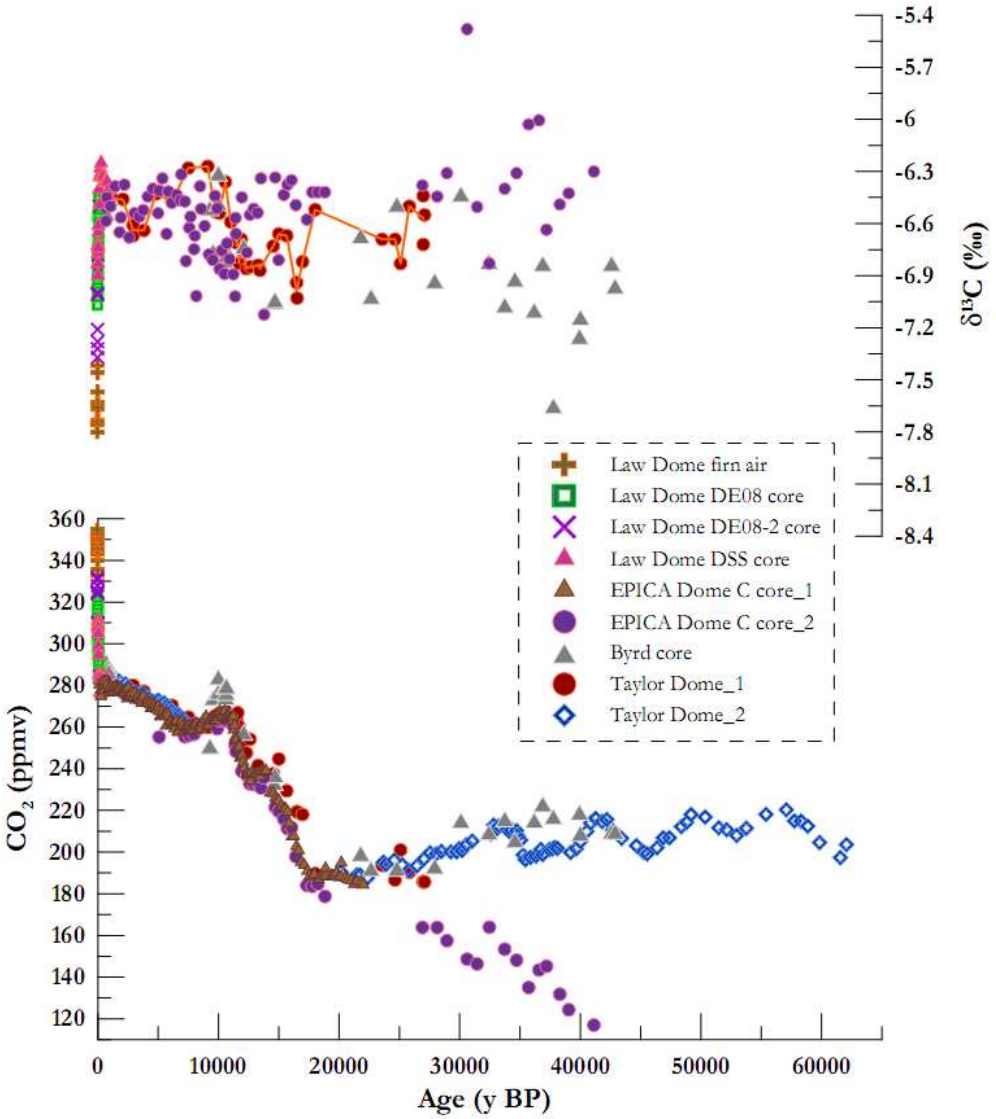

Figure 1-16 : *data compilation on atm. CO_2 and $\delta^{13}CO_2$ reaching back to the last glacial period taken from Law Dome firn and ice (Francey et al., 1999); Byrd ice (Leuenberger et al., 1992); TD ice (Smith et al., 1999; Indermühle et al., 1999 ; Indermühle et al., 2000; EDC ice (Monnin et al., 2004; Bellier, 2004; Eyer, 2004)*

Recently, Schmitt, 2006 developed a new extraction technique, based on the sublimation of ice samples. This helps in recovering ~100% of the air trapped in the ice, which gives more confidence in measuring clathrate ice, consisting ~90% of *e.g.* the entire EDC ice core record (Schmitt, 2006). Therefore, some analytical biases are avoided, such as those encountered with the mechanical ice grinding techniques *(cf. Ch. III)*. After numerous analytical improvements, Schmitt (2006) achieved in obtaining an analytical error of 0.05‰.

As far as LGGE is concerned, an attempt had been made in the early to mid 90s to measure $\delta^{13}CO_2$ on large ice core samples, using a cheese grater coupled to CO_2 freezing in glass ampoules and subsequent measurements by dual-inlet at LSCE (*E. Michel and J.M. Barnola, pers. comm.*). Unfortunately, this method never reached a routine status. More recently, some initial tests were carried on using the continuous-flow technique installed at LGGE for CH_4 isotopic measurements, adapted for CO_2 isotopes (Bellier, 2004). No results of stable C isotope ratios were finally produced. As it will be extensively discussed in *Ch. III*, the $\delta^{13}CO_2$ chapter in LGGE starts with Jost Lavric, a post-doctoral who managed to put all pieces together and permitted the first tests accomplishment in the lab. Without his contribution, this PhD thesis would be surely of a different nature.

I.6. Scope of this study

With the present study we aim to provide new carbon isotopic data constraints on the origin of CO_2 and the interactions with climate, focused on the recent two deglaciations.
The following major tasks are to be accomplished:

- analytical technique testing
- data production
- data interpretation

The **analytical -based objectives** include :

- the air extraction procedure testing, based on blank tests and standard gas tests;
- the establishment of a complete analytical protocol, which, when fully followed, leads to directly comparable results;
- intercomparison tests with the other two European laboratories which belong to the same network (UBern and AWI), as a means of evaluating each lab reproducibility and accuracy ;
- the testing of the air extraction efficiency, in relation with the ice physical properties

The **data production objective** includes the production of new datasets of CO_2 and their stable isotopes on past periods, aiming to constitute the new "data milestones" on the domain. Main sampling periods of interest throughout this study will be: Termination I (last deglaciation) with MIS 2, Termination II (penultimate deglaciation) with MIS 6, the last millennium, Antarctic Isotopic Maxima 12. EDC core will be the main study core. Fig. 1-17 exposes a data compilation

for this core back to the LGM. Fig. 1-18 further shows the CO_2 Vostok record for the past 160 ky BP.

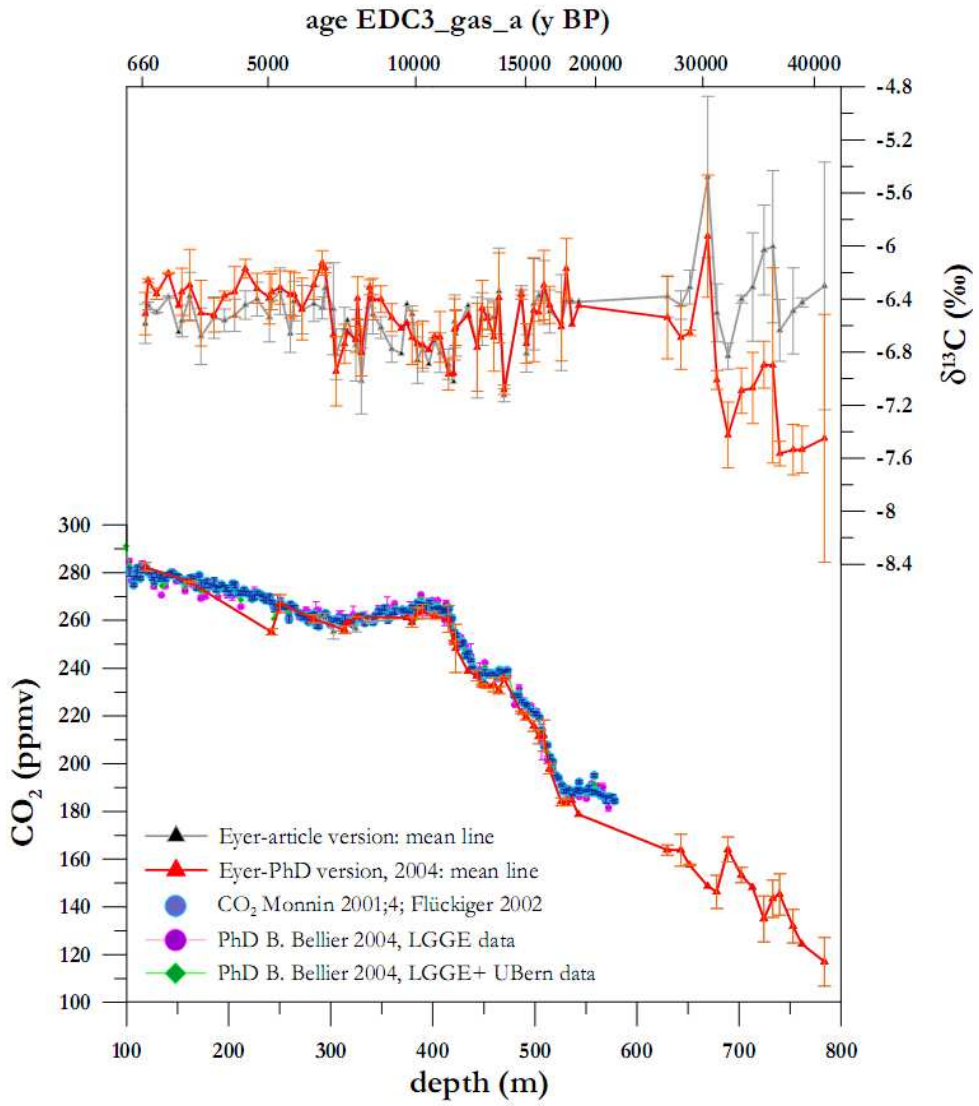

Fig. 1-17: *data compilation from EDC core on atm. CO_2 and $\delta^{13}CO_2$ up to date, found in Eyer, 2004; Bellier, 2004; Monnin et al., 2004*

Our objective will be to complete these records back to the penultimate glacial and proceed to data intercomparison and discussion. The comparison with existing ice-deduced millennium data will permit to test our calibration system. As far as TII and AIM 12 are concerned, the data produced during this thesis will be the first ever, from the EDC core.

The **data interpretation objective** includes:

- the contribution in resolving the C-cycle problem during the glacial/ interglacial transitions, which requires the use of models, permitting to test scenarios with a "sensitivity tests" approach;

- the validation or rejection of such scenarios, by further proposing a combined hypothesis;
- the comparison with data acquired from other means, such as marine sediments, invoking the challenge of records synchronization, which when over-passed, provides useful information at a global scale

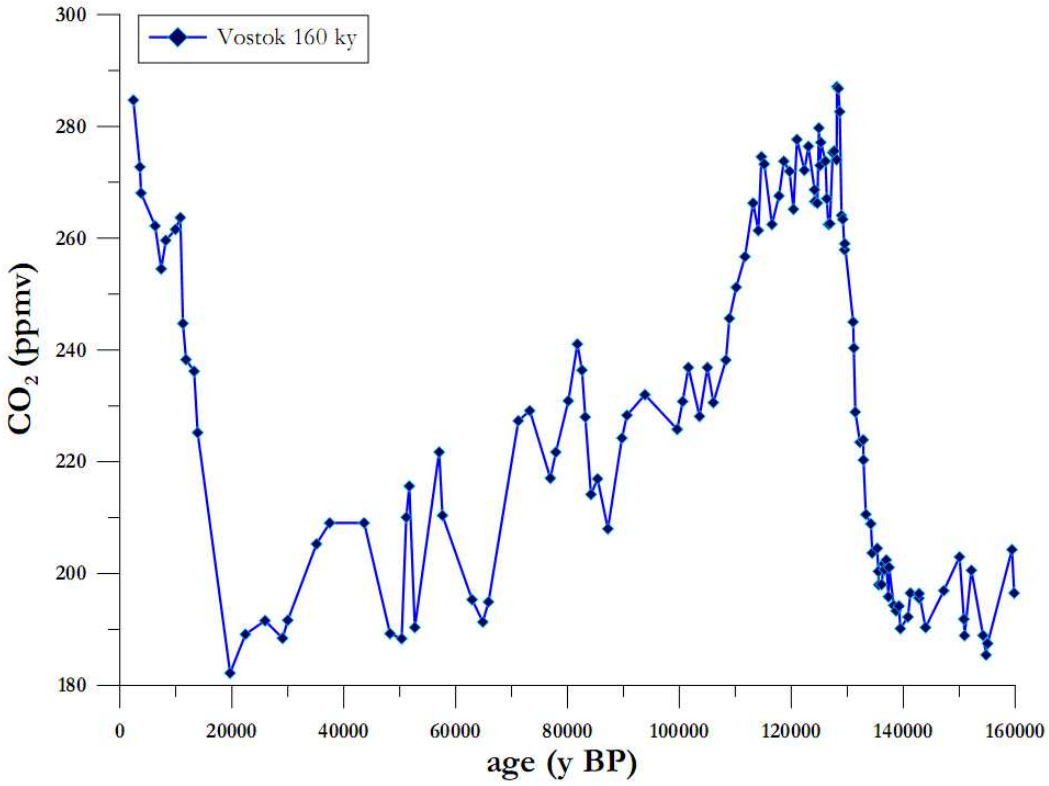

Figure 1-18 : *atm. CO_2 data from Vostok ice core for the last 160 ky (Barnola et al., 1987) synchronized against EDC3_gas_a by Lüthi et al., 2008*

INTERLUDE *…always to keep in mind throughout this study*

Man's tendency to lean on the past, in order to search questions concerning the future

Earth System Scientists illustrate the Greek historian Thucidides quotation: *"History repeats itself"*, subsequently enriched by Karl Marx by: *"first as tragedy, second as farce"*. Since planet Earth responds quite rapidly to the current human (abusing) intervention with surprisingly negative results, scientists proceed in the first place to direct inter-comparisons with similar past conditions, their goal being the projection of the actual situation to potentially equivalent past ones (that does not exist) and of course, the anticipation.
When looking into the past planet history for clues of the future, one finds general support for the notion that atmospheric CO_2 increase will cause global warming. However, this relationship (extrapolation) is neither linear nor in phase with the ensemble of past timescales.
Therefore, the sayings of George Bernard Shaw would be the most appropriate: *"If history repeats itself, and the unexpected always happens, how incapable must Man be of learning from experience."*

Chapter II. The ice core archive

II.1. Introduction

II.1.1. Interest in studying polar ice cores

Since the 1960s, polar ice core drillings give access to climatic archives accumulated for thousands of years. The isotopic composition of the ice permits a quantitative reconstruction of past temperature variations, while the air bubbles occluded in the ice preserve the past atmospheric composition signal. Dust and aerosol records witness atmospheric circulation patterns, as well as their source changes, such as volcanoes, oceans or deserts. Interior sites of polar ice sheets, being isolated from atmospheric humidity sources, present weak accumulation rates and thick ice layers, thus reconstructing up to several past climatic cycles. On the contrary, coastal sites, being of lower altitude and characterized by a higher accumulation rate, have lower ice thickness, thus offering records of smaller duration but of better resolution. These sites are important since the calculated age difference between ice and occluded gas (Δage) is smaller, which allows for a better estimate of time relationships between markers in the gas and the ice phases. Furthermore, ice core archives permit continuous tropospheric measurements, initiated in the late 50s for CO_2 and the late 70s for CH_4 (Etheridge et al., 1996; Etheridge et al., 1992).

All the above highlight the importance of studying the air contained in the ice and in the firn, as it offers the opportunity to (nearly) directly reconstruct the past atmospheric composition. Within this chapter, the main characteristics of the ice cores studied are provided. A detailed discussion on the physical and chemical properties of the ice susceptible to affect our signal (mixing or isotopic ratio) follows. Some first applications to the main sampling periods of this study are equally provided.

INTERLUDE *….what might have related Antarctica with Aegean Sea and the Louvre Museum*

It all started in 1775, with the British explorer *James Cook,* who successfully navigated around the Antarctic peninsula. The naval officer of the Russian Empire *Fabian von Bellingshausen* was the second person to see the Antarctic continent in 1820, while the French explorer *Jules Sebastien Dumont d'Urville,* in one of his several expeditions with the Astrolabe vessel in 1840, was the first to land in this unknown cold place, which he named *"terre Adélie",* inspired from his wife's name. *(I wouldn't be flattered if my husband baptised a white, cold and remote place upon my name …)* Still *Dumont d'Urville* was a highly cultivated person and to my knowledge he also did expeditions in the *Aegean Sea,* which is surely less important for this PhD framework. But permit me to inform you, that it was *Dumont d'Urville* who "transported" the famous *Greek statue Venus of Milos* to its actual place in *Louvre Museum in Paris,* 20 years before his experience with the white continent.

II.1.2. Ice cores of interest during this PhD

All ice cores analyzed during this study originate from the Antarctic continent and are shown in fig. 2-1. The reason for selecting the Antarctic continent will be exposed in the following sections.

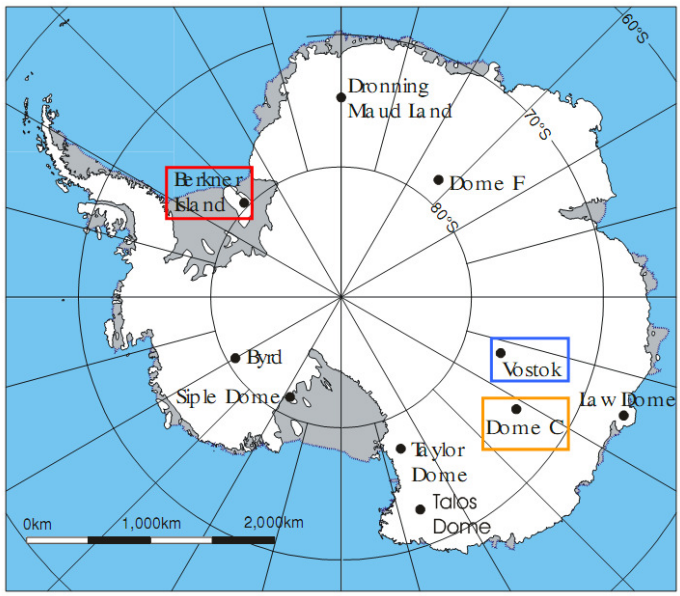

***Fig. 2-1**: map of Antarctica, highlighting the locations examined in this study*

Core	EDC	Vostok	Berkner
Geographical name	Dome C	Vostok	Berkner island South Dome, Thyssenhöhe
Station name	Concordia station	Vostok	
Coordinates	75°06'S, 123°21'E	78°28'S, 106°48'E	79°32'S, 45°31'W
Altitude	3233m	3500m	890m
Annual mean Temperature	-54.5°C	-57.3°C	-26°C
Accumulation rate	2.85cm/y*	2.2cm/y*	26cm/y*
Drilling depth	3270.2m	3667m	949m
Climatic record reached	800 ky	420 ky (for 3300m)	~120ky
Depths measured	* 102.3 – 126.5m *(last millennium)* * 178.2 – 222.2m *(E. Holocene)* * 346.5 - 578.05m *(TI)* * 800.3 – 860.8m *(AIM 12)* * 1669.3 – 1872.8m *(TII)*	* 161m *(3073.4 y BP)*	* 729.3 - 755.7m *(AIM 12)*
* expressed as the ice-equivalent thickness of annual layers			

***Table 2-1** : characteristics of sites of our interest. Sources: EPICA, 2004; Parrenin et al., 2007; Petit et al., 1999; Mulvaney et al., 2002 and J.-M. Barnola, pers. comm.*

Each site's characteristics are exposed in table 2-1.

EDC was the main ice core analyzed throughout the PhD, covering different time frames (*cf. table 2-1*). One Vostok (BH7) sample (divided into 8 pieces) was used to test the reproducibility of the experimental setup (work in collaboration with J.-V. Lavric, *cf. Ch. III*). Finally, Berkner ice was also measured during this PhD, in order to investigate the effect of hydrate formation in the ice (*cf. Ch. III*).

II.2. Gas trapping in the ice

Fig. 2-2 illustrates the physical and chemical processes susceptible to affect atmospheric air finally trapped in the ice. In the following section, the processes linked with the main location where fractionation processes occur, the firn column, will be further discussed.

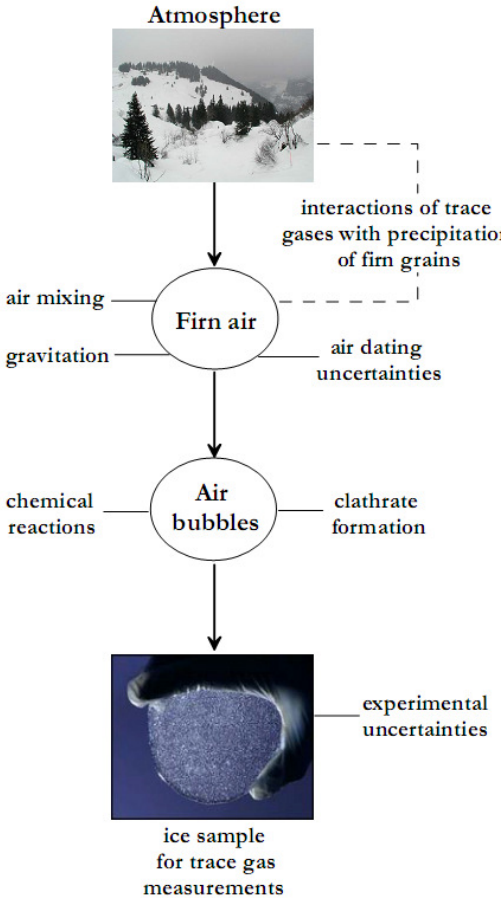

Fig. 2-2: *scheme of general physical and chemical processes potentially affecting air trapped in the ice*

II.2.1. Densification process

The densification process consists in the progressive transformation of the initially deposited snow on the polar icecaps, into firn and subsequently in ice. It can be briefly described as follows: fresh snow is of low density and is highly porous. It is quickly reformed by wind, temperature and pressure gradient. Sublimation processes driven by daily and seasonal temperature cycles tend

to reduce the surface area and the snow is transformed into firn. With progressive accumulation of snow layers on top, the snow particles get rounded, they slide between each other and develop grain joints (Alley, 1987). In-between, tiny openings (pores) are formed. By sintering and creep, this compaction increases the firn density, while the open porosity decreases. When relative density ($\mathbf{D_o}=\varrho/\varrho_{ice}$) reaches ~0.6, the grain-boundary sliding process stops. Then snow particles, under the increasing pressure of the snow column with depth, undergo a plastic deformation at their contact points (Arzt et al., 1983). At a density of ~0.84 g/cm^3, the pores between the snow grains get isolated from one another, forming individual bubbles. The transition from firn to ice has been reached, the so-called 'Close-Off Depth" (**COD**), or pore closing zone. The above processes occur gradually, and the transition depths between different densification regimes vary according to the site. The COD varies between 60 and 150 m in Antarctic sites, depending on mean surface temperature, pressure, accumulation rate and wind speed (Kaspers et al., 2004). The time required for the transformation of surface snow layers into ice layers may thus vary from ~100 to ~6000 years (Blunier et al., 2007).

These processes occur in cold sites; if surface melting happens during summer, liquid water percolation and refreezing deeper in the firn affect the firn structure and its densification. In addition, CO_2 dissolves in melt layers and chemical reactions can occur, making such sites unsuitable for accurately recording this trace-gas evolution (Stauffer et al., 2002).

II.2.2. Gas transport within the firn column

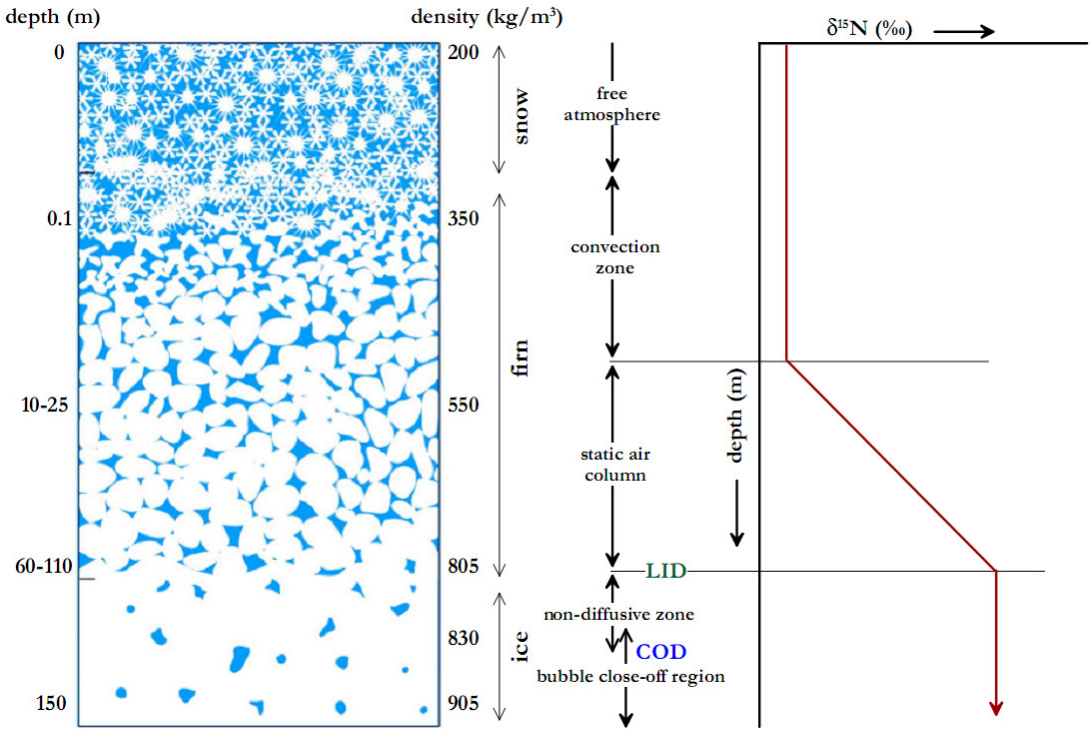

Fig. 2-3: *different air movement zones encountered within the firn layer; from left to right: (1) firn air depth evolution, with densification process; (2) density profile; (3) definition of different zones of gas transport and (4) $\delta^{15}N$ profile showing an increase with depth within the diffusive zone, due to gravitational enrichment. Original work from Sowers et al., 1992, inspiration from adapted work of J.-M. Barnola*

The firn column constitutes the upper layer of the ice sheet. It is both porous and permeable. It can be further separated into three zones (*cf.* fig. 2-3) according to the prevailing air movement and fractionation affecting the gases (Sowers et al., 1992):

- the **convective zone** constitutes the uppermost layer, extending down to ~10m of the firn column (Bender et al., 1997). From porosity observations, convective zone is considered well-mixed, because atmospheric pressure and temperature fluctuations produce a turbulent regime and air convection within the firn pores, resulting in rapid response to atmospheric composition changes (Bender et al., 1997). Within this zone, pressure variations originate principally from meteorological phenomena, such as relief effects of the specific site and wind pumping (Colbeck, 1989). The convective zone can be thicker than 10 m under special climatic conditions, *e.g.* in 'megadune' areas with large pressure waves (Kawamura et al., 2006). Surface snow density is typically of 0.3-0.35g/cm^3 (Arnaud, 1997; Bender et al., 1997), but it can vary according to the grain size, itself depending on insolation (Raynaud et al., 2007), wind and temperature (Colbeck, 1989). The corresponding porosity is of 62-67%.
Within the convective zone, thermal gradients are encountered, which can potentially affect the isotopic ratios of gases due to thermal diffusion. If convective mixing exceeds molecular diffusivity in this firn part, the latter being of ~1m^2/day (Schwander et al., 1988), isotopic fractionation due to thermal diffusion can be considered negligible (Severinghaus et al., 2003).
- the **diffusive zone,** also called "stagnant/static air column", represents the thickest firn part, reaching 50 to 100m, depending on the accumulation rate and the mean annual temperature. Within this zone, elemental and isotopic air composition depends on molecular diffusion (Bender et al., 1997). Annual temperature cycles or convective mixing do not reach the diffusive zone. On the other hand, longer-term temperature changes (such as ample decadal-scale climatic changes at the snow surface) can propagate through this zone and fractionate gases and their isotopes through thermal diffusion. Lastly in the diffusive zone, gravitational settling also occur, generating the most important correction to apply to *e.g.* the isotopic ratio of CO_2 measured in air bubbles.
- the **non-diffusive zone** or pore closing or bubble formation zone, has a thickness from 2 to 12 m, depending on the seasonal snow and firn layer anisotropy. Within this zone, open pores and

formed 'closed' bubbles coexist. Vertical gas exchange and diffusion processes cease in its upper layer, the so-called Lock-In Depth (**LID**). On the contrary, horizontal gas movement can remain active along permeable layers, due to differences in vertical firn permeability. The layers stop vertical diffusion but they allow air fractionation with expulsion through tiny capillaries linking together the porosity of the underlying, still permeable layers ("effusion" effect). The lower part of this zone, constitutes the COD, where all interstitial air gets completely trapped in bubbles and where firn air porosity becomes nil. In densification models, the bubble closing zone corresponds to the density interval between 0.815 and 0.845 g/cm^3 (Arnaud, 1997), where 10-15% of the volume is air (Bender et al., 1997). The density at the COD is more important at cold sites (Pimienta, 1987), as they receive less precipitation, thus snow settling is slower.

This third and last zone does not affect the difference of age between trapped air and the surrounding ice.

II.3. Physical processes affecting gases occluded in ice

In the following sections, processes potentially affecting the CO_2 mixing ratio and stable isotopic ratio in trapped bubbles are detailed and quantified.

Three physical processes, linked with the diffusive zone, affect the gas composition in the open porosity :

- Gravitative settling
- Thermal diffusion
- Molecular diffusion provoked by concentration gradients

They are interrelated as gravitative settling and thermal diffusion create concentration gradients whereas molecular diffusion attenuates these gradients until the establishment of a new steady state equilibrium. The following differential equation combines these three driving forces (Severinghaus et al., 2001) :

$$\frac{\partial C}{\partial t} = \frac{\partial}{\partial z}\left(D_{eff}(z,T)\left[\underbrace{\frac{\partial C}{\partial z}}_{(1)} - \underbrace{\frac{\Delta m g}{RT}}_{(2)} + \underbrace{\Omega \frac{dT}{dz}}_{(3)} \right] \right) \qquad (2\text{-}1)$$

being (1) the ordinary diffusion; (2) the gravitative settling and (3) the thermal diffusion mathematical representations

With $\boldsymbol{C}$: concentration of a gas species (*e.g.* CO_2); $\boldsymbol{t}$: time; $\boldsymbol{z}$: depth; $\boldsymbol{D_{eff}}$: effective molecular diffusivity of a gas species in the firn; $\boldsymbol{T}$: absolute temperature; $\boldsymbol{\Delta m}$: mass difference between the gas species and air; $\boldsymbol{g}$: acceleration due to gravitation; $\boldsymbol{R}$: ideal gas constant; $\boldsymbol{\Omega}$: thermal diffusion sensitivity of the gas species

II.3.1. Gravitational separation of gases and isotopes

Under turbulence-free conditions, air subject to a gravitational field tends to fractionate by a process called gravitational settling. The relative difference of molecular weight of gases or isotopes with respect to air provokes a preferential accumulation of heavier species at the bottom part of the firn column (Craig et al., 1988; Schwander et al., 1993). A steady state is reached during which gravitational settling in one direction is balanced by diffusion along a concentration gradient in the other direction. In the case of isotopic ratios, the isotopic enrichment in the LID (at the very bottom of the diffusive zone) is calculated by the following barometric equation:

$$\delta = \left[\frac{R}{R_0} - 1\right] \times 10^3 = \left(e^{\frac{\Delta m g}{RT}} - 1\right) \times 1000 \cong \frac{\Delta m g z}{RT} (‰) \qquad (2\text{-}2)$$

Where $\boldsymbol{\Delta m}$: absolute mass difference of isotopes of the same gas species (kg/mol); $\boldsymbol{g}$: gravitational acceleration (=9.82 m/s^2); $\boldsymbol{T}$: mean annual firn temperature (K); $\boldsymbol{z}$: diffusive column height or **DCH** *(=thickness of the diffusive zone);* $\boldsymbol{R}$: ideal gas constant

The equation can be validated experimentally by measuring the isotopic ratio of a molecule being constant in the atmosphere. This is done with the application of molecular nitrogen isotope, $\delta^{15}N$ (Sowers et al., 1992), being of proportional value to the thickness of the diffusive zone, in absence of thermal gradient (*cf. below*). As CO_2 is heavier than air, similarly to its isotopes, gravitative settling provokes an increase of its mixing ratio with depth.

The isotopic fractionation of a gas species due to gravitation is a function of the difference of mass between the two isotopologues. The mass difference between ^{13}C and ^{12}C (Δmass=1) being identical to ^{15}N versus ^{14}N, justifies the $\delta^{15}N$ application in correcting gravitationally our data.

II.3.1.1. Application to data from this study

The gravitational effect, originated from the favoured sedimentation of the heavy isotopes in the firn layer before the air entrapment in bubble form can be applied as a correction to our data with the following equations:

<u>CO_2-case:</u>

$$CO_{2,corr} = CO_{2,obs} - (M_{CO_2} - M_{air}) \times \delta^{15}N \times CO_{2,obs} = CO_{2,obs} \times (1 - \frac{\delta^{15}N \times 15.2}{1000}) \qquad (2\text{-}3)$$

where $\boldsymbol{M}$ the molecular mass

Isotopes-case :

$$\delta^{x}A_{corr} = \delta^{x}A_{meas} - \left[(x-\alpha)\times\delta^{15}N\right] \quad (2\text{-}4)$$

x the atom's ***A*** mass number, the ***a*** being the dominant isotopologue

for the case of C:

$$\delta^{13}C_{corr} = \delta^{13}C_{meas} - \left[(13-12)\times\delta^{15}N\right] \quad (2\text{-}5)$$

for the case of O:

$$\delta^{18}O_{corr} = \delta^{18}O_{meas} - \left[(18-16)\times\delta^{15}N\right] \quad (2\text{-}6)$$

$\delta^{15}N$ can be deduced from an empirical relationship from deuterium data measured in the same depth as our air-deduced $\delta^{15}N$ values. δD, measured in the ice matrix is projected versus ice age whereas $\delta^{15}N$, originally measured in the enclosed bubbles, are visualized vs. the gas age. We thus use the same depths for our samples and values of correction, taking into consideration the Δage for the analyzed ice core (Gabrielle Dreyfus, *pers. comm.*). The empirical equation applied for the ensemble of data correction, is the following:

$$\delta^{15}N = 0.0020032\times\delta D + 1.2969 \quad (2\text{-}7)$$

In the meantime, for the case of Terminations, which constitute the "basic" results of this PhD, Gabrielle Dreyfus provided me with data of direct $\delta^{15}N$ values measured by her. In fig. 2-4, an intercomparison between the two $\delta^{15}N$-correction methods is presented. Still, the availability of measured $\delta^{15}N$ data (interpolated at the depths of our samples) was restricted over the full depth range; this fact, combined with the possibility of introducing the analytical noise of the measured value to our correction and for uniform corrections application, we "officially" adopted the above empirical equation for our data gravitational corrections.

Fig. 2-5 to 2.7 show the gravitational effect on TI and TII sampling periods. The fig. are followed by tables, 2-2 to 2-4, exposing in numbers the deviation from the uncorrected value.

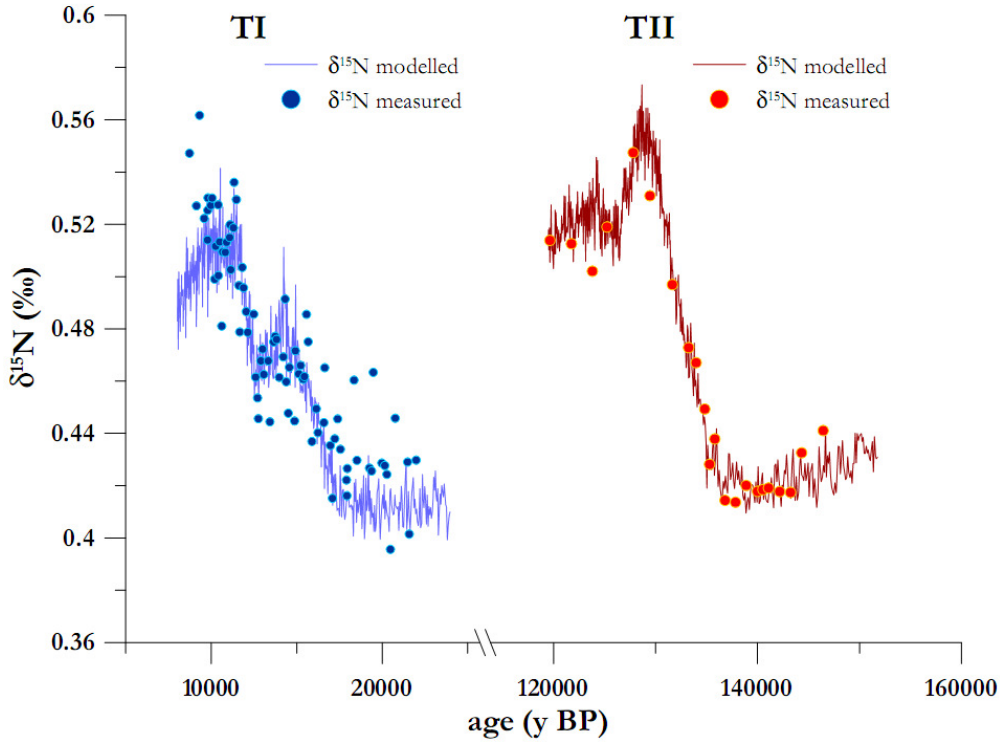

Fig. 2-4: *$\delta^{15}N$ measured (G. Dreyfus, pers. comm.) and reconstructed from the eq. 2-7 (Jouzel et al., 2007; G. Dreyfus, pers. comm.)*

Application on CO_2 from TI and TII sampling periods:

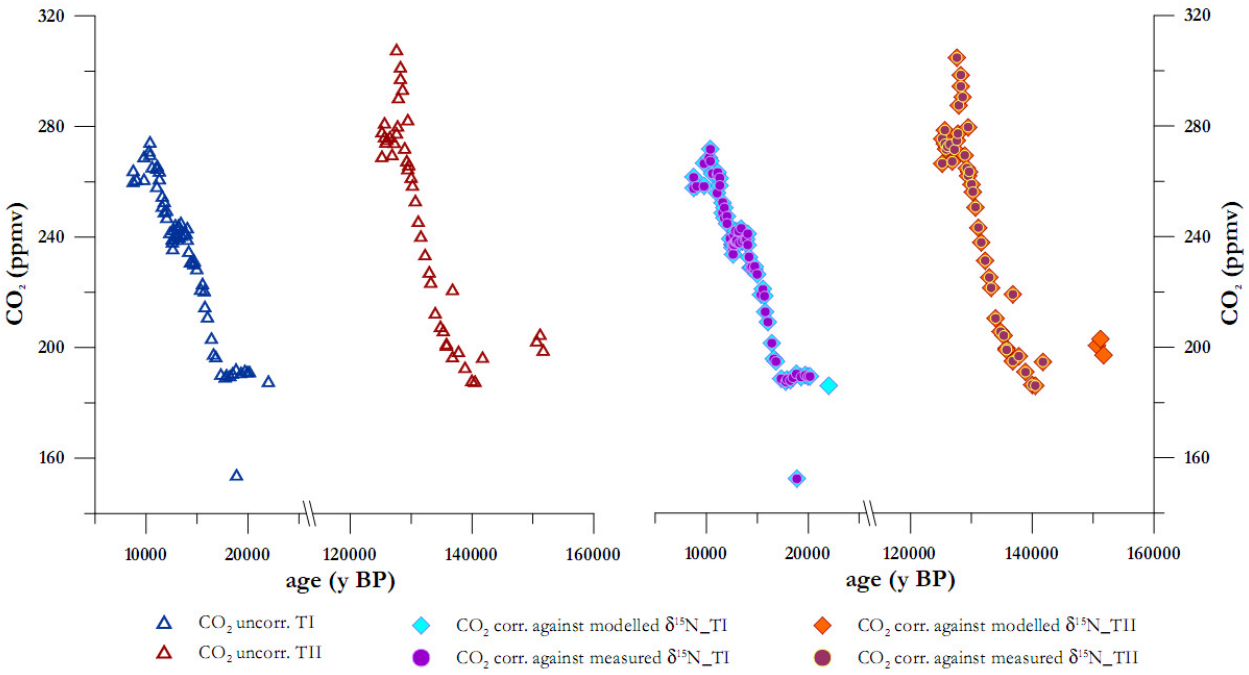

Fig. 2-5: *(left panel): uncorrected CO_2 data; (right panel): both kinds of gravitational correction on CO_2 for TI and TII. y-axis did not change for intercomparison reasons, while all measured data are plotted; scientific analysis after outliers rejection will be exposed in Ch. IV and V*

	Equation -based	Measured
ΔCO_2 (vs. uncorr)	-1.66 (-2.15; -0.97)	-1.69 (-2.23; -1)

***Table 2-2**: deviations from corrected CO_2 values against uncorrected ones, for both methods applied: mean value is exposed, whereas in parenthesis the (max; min) boundary values. Calculations applied for all expansions, outliers included (cf. also fig. 2-5)*

Application on $\delta^{13}CO_2$ from TI and TII sampling periods:

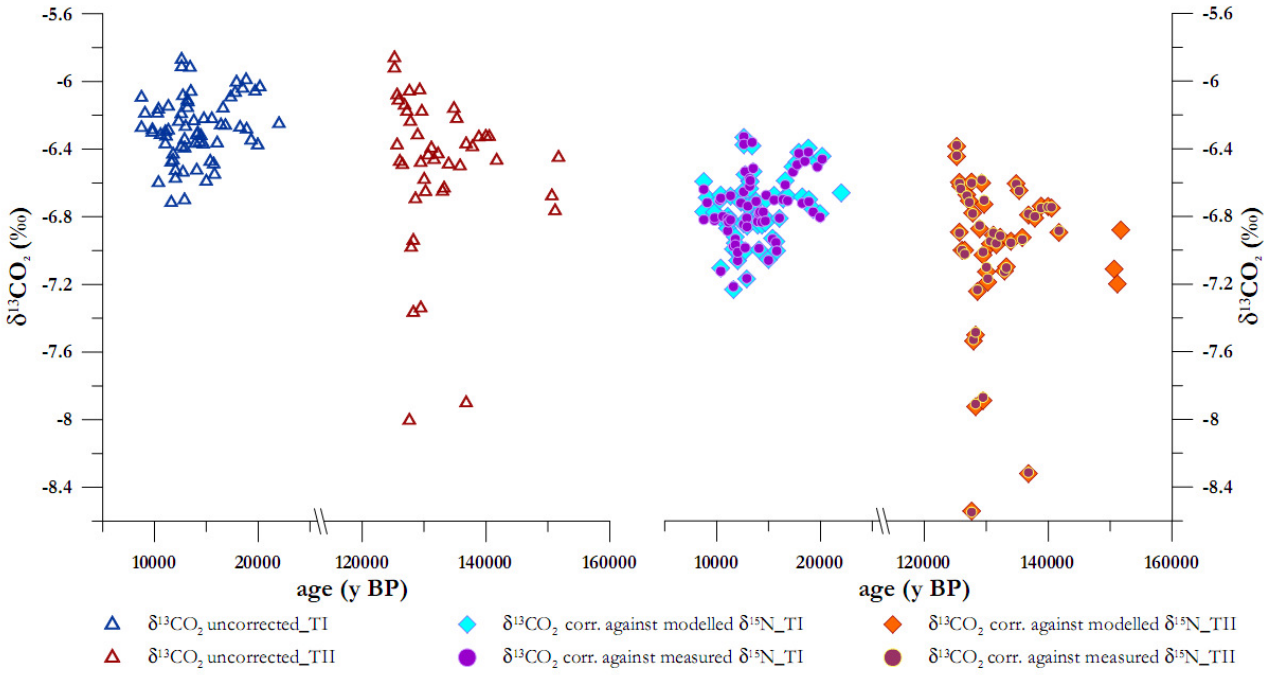

***Fig. 2-6:** (left panel): uncorrected $\delta^{13}CO_2$ data; (right panel): both kinds of gravitational correction on $\delta^{13}CO_2$ for TI and TII. y-axis did not change for intercomparison reasons, while all measured data are exposed; scientific analysis after outliers rejection will be discussed in Ch. IV and V*

	Equation -based	Measured
$\Delta\delta^{13}CO_2$ (vs. uncorr)	-0,467 (-0,533; -0.405)	-0,473 (-0,546; -0,422)

***Table 2-3**: deviations from corrected $\delta^{13}CO_2$ values against uncorrected ones, for both methods applied: mean value is exposed, whereas in parenthesis the (max; min) boundary values. Calculations applied for all expansions, outliers included (cf. also fig. 2-6)*

Application on $\delta^{18}O$-CO_2 from TI and TII sampling periods:

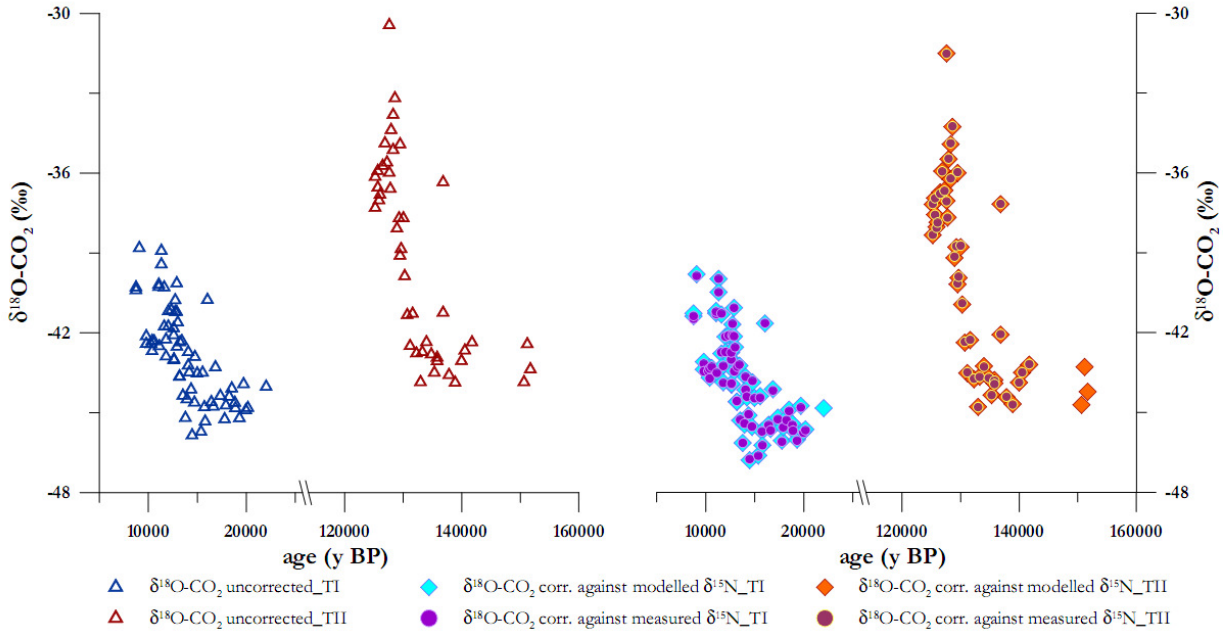

Fig. 2-7: *(left panel): uncorrected $\delta^{18}O\text{-}CO_2$ data; (right panel): both kinds of gravitational correction on $\delta^{18}O\text{-}CO_2$ for TI and TII. y-axis did not change for intercomparison reasons, while all measured data are plotted; scientific analysis after outliers rejection will be exposed in annex IV*

	Equation -based	Measured
$\Delta\delta^{18}O\text{-}CO2$ (vs. uncorr)	-0,934 (-1,066; -0.810)	-0,946 (-1,091; -0,844)

Table 2-4*: deviations from corrected $\delta^{18}O\text{-}CO_2$ values against uncorrected ones, for both methods applied: mean value is exposed, whereas in parenthesis the (max; min) boundary values. Calculations applied for all expansions, outliers included (cf. also fig. 2-7)*

Table 2-5 compares the two correction applications, (data-based) – (model-based) for both TI and TII, since $\delta^{15}N$ measurements were effectuated by the same person, while the equation related to δD remained the same (2-7):

Sampling period	$\Delta^*\delta^{15}N$	Δ^*CO_2	$\Delta^*\delta^{13}C$	$\Delta^*\delta^{18}O$
TI	0.005	-0.017	-0.005	-0.010
TII	-0.003	0.013	0.004	0.006

Table 2-5*: comparison of $\delta^{15}N$ values: (i) measured $\delta^{15}N$ interpolated for our data depths and (ii) "modelled" $\delta^{15}N$ as calculated by the equation (2-7) and projected to our depths; difference ⊿ defined as (data) – (model). Similar exercise for CO_2 and its stable isotopes corrections.*

From the above we deduce same magnitude of changes for each questioned variable and anti-correlated results for the two sampling periods. The overall difference between the two methods is negligible.

II.3.2. Thermal diffusion

A gas mixture in the diffusive zone can undergo thermal fractionation, if a large temperature change takes place at the surface, generating a temperature gradient within the diffusive zone. Then, in general heavier (lighter) isotopes preferentially accumulate at the cooler (warmer) end of the thermal gradient (Severinghaus et al., 2001; Grachev and Severinghaus, 2003). More specifically, this phenomenon is significant when:

(i) gas diffusion takes place faster than heat diffusion in the corresponding firn. Severinghaus et al., 1998 mention that gases diffuse about 10 times faster than heat in firn, so the thermally fractionated gas will penetrate to the bottom of the firn long before the temperature equilibrates, and the gas composition will approach a steady state with respect to the new firn temperature at close-off, following the equation given below (eq. 2-8)

(ii) the temperature gradient is large. Temperature differences can reach 20°C in the upper 5m, depending on the season (Severinghaus et al., 2001). ΔTemperature between surface and COD vary from 16°C for the case of Greenland (Landais et al., 2006) and 2-3°C every 1 or 2 ky in Antarctica (Caillon et al., 2001).

A rapid rise of surface temperature is accompanied by a positive anomaly of ex. ^{15}N and ^{40}Ar in the trapped air. The anomaly can be used to quantify the amplitude of temperature variations at the surface, independently of conventional measurements of water isotopes (Severinghaus and Brook, 1999; Severinghaus et al., 2001; Caillon et al., 2001; Landais, 2004), which has further applications in the in-parallel independent calculation of the close-off depth, during rapid temperature variations (Caillon et al., 2003). The thermal isotopic fractionation is represented by the following equation:

$$\delta = \left[\frac{R}{R_0} - 1\right] \times 10^3 = \left[\left(\frac{T_t}{T_b}\right)^{\alpha_T} - 1\right] \times 1000 \cong \Omega \Delta T \left(‰\right) \qquad (2\text{-}8)$$

With δ : fractional deviation; ΔT : temperature difference between the boundary layers of the diffusive zone (T_t and T_b, top and bottom, respectively); α_T : constant of thermal diffusion and Ω : thermal diffusion sensitivity (‰/°C). The latter parameters (a_T and Ω) being T-dependent are determined experimentally (Grachev and Severinghaus, 2003).

II.3.2.1. Application to $\delta^{13}C$

Leuenberger and Lang, 2002 calculated the thermal diffusion sensitivity for some isotope mixtures, using the Lennard-Jones model. Fig. 2-8 illustrates the results. Ω of C isotopes in CO_2 appears very small at polar temperatures, and largely smaller than for isotopes of N_2.

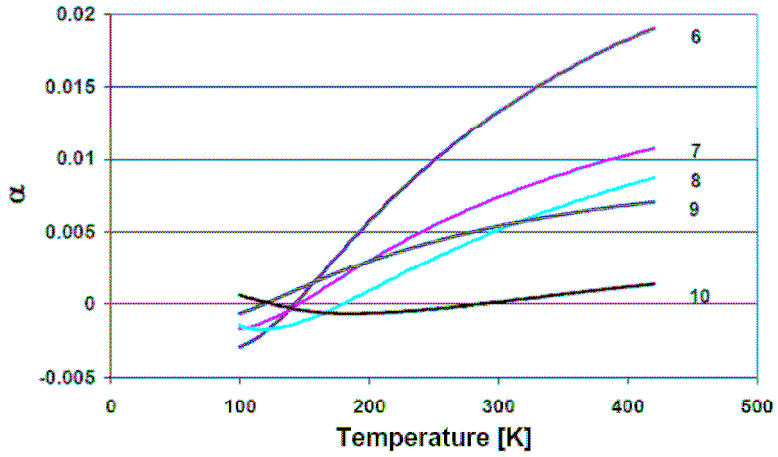

Fig. 2-8: *thermal diffusion factor against temperature for the following isotope mixtures: 6.* $^{40}Ar/^{36}Ar$*; 7.* $^{18}O/^{16}O$*; 8.* $^{13}C/^{12}C$ *of* CH_4*; 9.* $^{15}N/^{14}N$ *of* N_2*; 10.* $^{13}C/^{12}C$ *of* CO_2*; from Leuenberger and Lang, 2002*

Since thermal correction for C isotopes is based on the atmospheric $\delta^{15}N$ signal (as is the case for gravitational correction) and since no thermal anomaly was detected with $\delta^{15}N_2$ in the core sections of EDC and Berkner that we analyzed for CO_2 isotopes, we thus did not apply any thermal correction to our signal.

II.3.3. Diffusion along a concentration gradient

Atmospheric gas species or isotopes diffuse in a firn column according to their concentration gradient between the top and bottom part (Schwander, 1996). This gradient is the "motor" of molecular diffusion processes, carrying trace gases or isotopes between the atmosphere and the COD. This process is slow, which tends to smooth atmospheric variations. For instance, seasonal changes of atmospheric CO_2 are smoothed out in the upper half of the firn column (Trudinger et al., 1997). Based on Fick's law, the diffusive flux of a gas along a concentration gradient is:

$$F = -D\frac{dC}{dx} \qquad (2\text{-}9)$$

Where $\boldsymbol{F}$: net flux; $\boldsymbol{dC/dx}$: concentration gradient in the diffusion direction and $\boldsymbol{D}$: diffusion constant, being inversely proportional to the square root of the molecular mass.

Eq. 2-9 results from the fact that all molecules of a gas mixture have the same kinetic energy ($E=1/2mv^2$). As a consequence, gas species or isotopes of lower mass have the tendency to move faster and thus have higher diffusion constants, D. If the diffusion involves the movement of one gas through a second one, then molecular masses have to be replaced by their 'reduced' ones (as for the case of the collision), denoted with μ:

$$\mu = \frac{m_A \times m_B}{m_A + m_B} \qquad (2\text{-}10)$$

Applying the above equation, Bernard, 2004 shows that 50 years can intervene for concentrations or isotopic ratios transfer from the surface until the COD.

The ratio between the diffusion coefficient of the two stable carbon isotopologues of CO_2, $^{13}CO_2$ and $^{12}CO_2$ (having masses 45 (=m_A^*) and 44 (=m_A), respectively) in air (having a mean mass of 29g/mol), $^{13}\alpha$, can be written as:

$$^{13}\alpha = \frac{D_{^{13}CO_2}}{D_{^{12}CO_2}} = \sqrt{\frac{m_A^* + m_B}{m_A^* \times m_B} \times \frac{m_A \times m_B}{m_A + m_B}} = \sqrt{\frac{45+29}{45\times 29} \times \frac{44\times 29}{44+29}} = 0.9956 \qquad (2\text{-}11)$$

In δ notation, a fractionation factor of $^{13}\alpha$=0.9956 translates into a heavy isotope depletion of 4.4‰.

The two pre-mentioned physical processes affecting firn pore composition, gravitative settling and thermal diffusion, favour enrichment of the bottom firn layers with heavy isotopes. On the contrary, molecular diffusion enriches bottom firn layers with light isotopes. The steady state equilibrium resulting from the three processes is already given by eq. 2-1.

II.3.3.1. Application to our case

The difference of diffusion coefficient in air generates changes in the $\delta^{13}CO_2$ signal in both firn and trapped bubbles, whenever CO_2 varies in the atmosphere. Natural changes of CO_2 concentration are marginal when compared to the mean age of the firn air. Monnin et al., 2001 report an increase of CO_2 by 1-2 ppmv every 100 years for the last glacial maximum time span. Furthermore, rapid CO_2 fluctuations are unlikely to occur, due to the equilibration with the ocean surface, causing a "buffering" effect.

Therefore, diffusion effects originated from natural CO_2 changes on the CO_2 isotopic composition are minor compared to the gravitational effect. When dealing with current anthropogenic conditions, though (when CO_2 increases by about 2 ppmv/y), they have to be taken into account since the diffusion correction on firn air and trapped bubbles composition amounts to about 0.10‰ on a 70-m thick firn column (Trudinger et al., 1997). As the correction is at first order proportional to the CO_2 rate of change, and as the largest observed CO_2 rate of change during deglaciations is about 20 times smaller than the present-day rate of increase (Joos and Spahni, 2008), the correction would amount to less than 0.01‰ on the EDC $\delta^{13}CO_2$ profile, and is thus neglected here.

II.3.4. Bubble close-off processes

Diffusion processes also occur within the ice matrix. Recent studies on elemental air ratios extracted in polar firn layers close to the firn-ice transition, show systematic enrichment of Ne/N_2, O_2/Ar, O_2/N_2 and Ar/N_2 (Severinghaus and Battle, 2006; Huber et al., 2006), while the same ratios seem depleted near the COD. This process is called effusion (Craig et al., 1988 ; Sowers et al., 1989 ; Bender et al., 1997). For this diffusion case, the diameter of the species counts, contrary to the mass (being the case for the previous processes). In case of a diameter inferior to 3.6 Å, species migrate through the ice lattice, marking a partial, non-linear disappearance to the firn column (Severinghaus and Battle, 2006) to get finally depleted within the formed air bubble. CO_2, having a molecular "collision" diameter of 3.94 Å (as derived from viscosity experiments), lies in the safe region of the above size criterion. Its "effective" diameter, derived from experiments of permeation and diffusion through porous membranes, is found at 3.3 Å and thus it can pass through inorganic membranes (Hirayama et al., 1999; Yeom et al., 2000). Since firn air measurements near the COD do not indicate any effect on the CO_2 mixing ratio (information given in Schmitt, 2006) and the fact that this diameter does not change between the different isotopologues examined in this study, no such diffusion is considered as 'hazardous' for the data treatment.

It is not clear if effusion takes place *in situ* during bubble close-off or after ice cores are retrieved (Bender et al., 1997). A similar diffusion process occurs during the ice storage after the drilling process, which may be responsible for further gas composition offset (Bender, 2002). Cracks and imperfections in the ice of about 3 Å spacing would allow O_2 and Ar loss while selectively retaining nitrogen. Due to this diffusive loss risk, being valid also for our case when treating the ice sample, the external cm of the ice sample should be removed.

II.3.4.1. Application within this study

The firn - ice transition, where air is supposed to circulate within a depth range, has been examined during this PhD study. *Annex VI* presents the results of EDC core for depths that correspond the last millennium, aiming to compare our mixing and isotopic results with those from Francey et al., 1999 and propose further corrections to our data.

II.3.5. Clathrate formation and decomposition

Fig. 2-9 is a Temperature – Pressure phase diagram for CO_2. Such diagrams demonstrate that a gas (here CO_2) cannot co-exist on thermodynamical means with ice phase, beyond a pressure threshold.

Application of this diagram is encountered in ice core air content, being dependent on pressure changes with depth. A set of thermodynamic conditions are fulfilled in order to achieve phase stability. The bubble ice zone corresponds to only 15% of the total core length; in dating terms, this percentage is even smaller, considering the layer thinning with increasing depth.

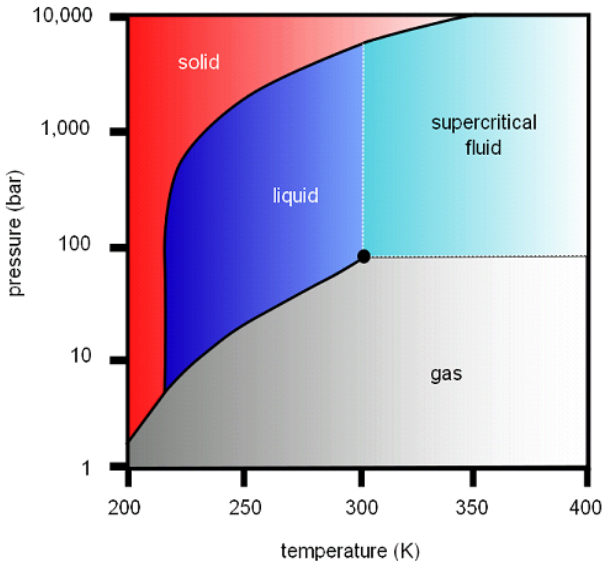

Fig. 2-9: *phase diagram for the CO_2 case*

For each gas and temperature, a special dissociation pressure has to be reached before the dominance of the clathrate form (Ikeda-Fukazawa et al., 2001). After the pore close-off, the ice matrix keeps condensing under the pressure of the superior layers of snow, firn and ice (Anklin et al., 1997). At depths varying from 500-1200m for Vostok or from 900-1600m for GRIP (Kipfstuhl et al., 2001), hydrostatic pressure exceeds dissociation pressure of the ice, P^d (defined in *eq. 2-12*), encouraging the clathrate formation. This occurs at shallower depths (at an earlier time scale) at cold locations with low accumulation rates. This phenomenon was introduced by Miller, 1969, while in 1982 the first application has been registered for Dye-3 core (Shoji and Langway, 1982).

$$P^d = \frac{P^d_{N_2} \times P^d_{O_2}}{Z_{N_2} P^d_{O_2} + Z_{O_2} P^d_{N_2}} \qquad (2\text{-}12)$$

where $P^d_{N_2}$ and $P^d_{O_2}$ are the respective dissociation pressures of pure N_2 and O_2-clathrate hydrates and Z_{N_2} and Z_{O_2} are the mole fractions of N_2 and O_2 in the gas phase, respectively (Ikeda et al., 1999)

Fig. 2-10 (left panel) gives the relationship of depth with temperature for a number of ice cores. Square points indicate the boundary limit below which air bubble formation is ceased. At this

depth, bubbles are entirely replaced by clathrates. The right panel of the same figure shows in detail the bubble properties evolution with depth, for the old Vostok and EDC cores.

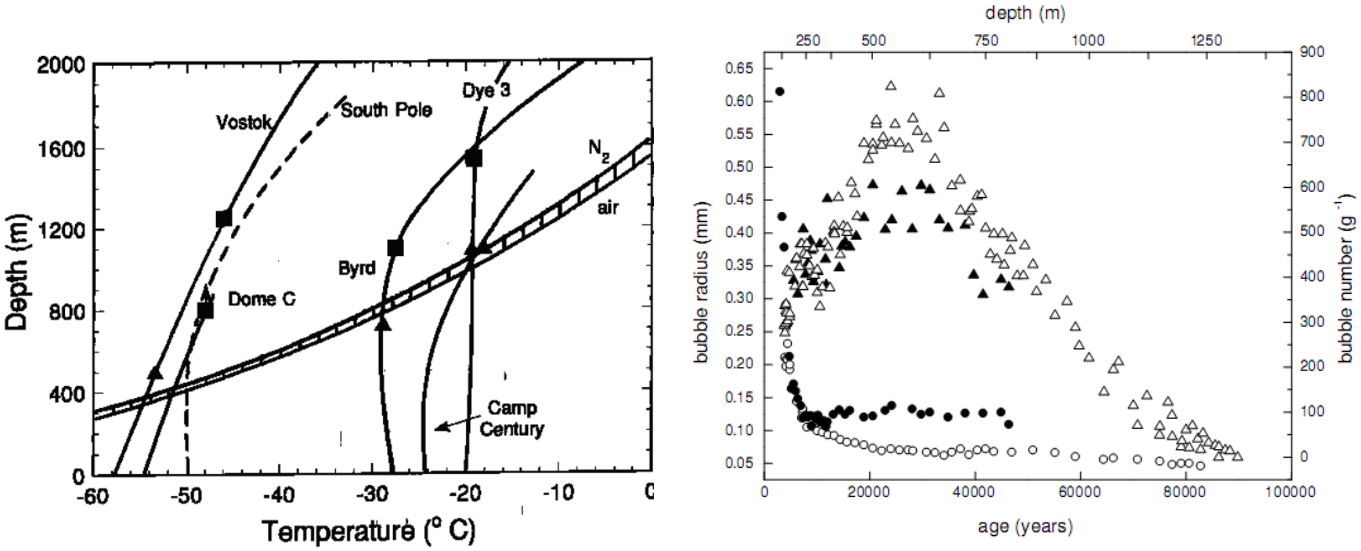

Fig. 2-10: (left panel): *temperature vs. depth in ice, compared with equilibrium pressures (converted to depths) for co-existence of bubbly ice with clathrated ice, from Price, 1995. Temperature gradually rises with depth as a consequence of the thermal heat flux from the bedrock. For the EDC core case, clathrate formation starts at 400-500m, while bubbles stop forming at 800m;* ***(right panel):*** *evolution of the average bubble radius (circles) and of the bubble density (triangles) with depth. White symbols: Vostok core; black symbols EDC core, from Durand et al., 2006*

Air hydrates have a cubic crystal symmetry and are translucent. This property differentiates clathrate ice from bubbly ice. Clathrates are formed in the first place in the borderline of ice with bubbles, to be afterwards slowly propagated within the air bubble by diffusion of water and gas molecules (Uchida et al., 1994). In some cases (*e.g.* in sites of low accumulation) the transition zone from bubbles to clathrates extends over several hundreds of meters (Salamatin et al., 2003), corresponding to several thousands of years (Ikeda et al., 1999). Therefore, a highly-unstable "transition" bubble-clathrate zone exists. Fig. 2-11 shows the instability encountered in this transition zone, as seen in two Antarctic ice cores, Vostok and Dome F. This zone, is also called "brittle zone" out of the physical ice condition (*cf. Ch. III*).

Gas molecules behave differently against this physical ice state change, according to their partial pressure and their own P-T phase diagram (*e.g.* fig. 2-9 for CO_2 case). The different dissociation pressures of the air components may provoke changes within the gas composition. For *e.g.*, the major air content, O_2, diffuses much faster than N_2, the latter becoming progressively enriched within the bubble. As a consequence, mixing ratios anomalies have been reported for the ratio O_2/N_2 especially at the transition zone (Ikeda et al., 1999), see *fig. 2-11*.

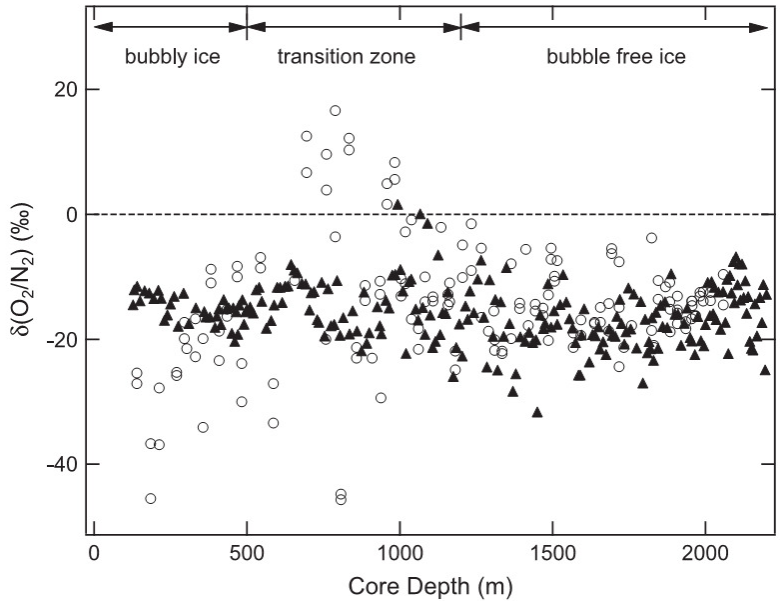

Fig. 2-11: *evolution of O_2/N_2 ratio in different ice levels: bubble, 'transit' and clathrate zone for Vostok (open circles) and Dome Fuji (black triangles); horizontal line represents the atm. value from Ikeda-Fukazawa et al., 2005*

Both the pure clathrate zone as the bubble-clathrate brittle zone constitute analytical challenges when quantitative results are needed. Clathrates are metastable. They slowly disintegrate due to pressure release after drilling to reform after years back bubbles. This reformation, involving kinetics and gas specific dissociation pressures, affects gas mixing ratios between the hydrate and non-hydrate phases (Eyer, 2004; Ikeda-Fukazawa et al., 2005). This is thought to be depicted in results from non-quantitative air extraction techniques from ice, such as milling. One recent representative study on EDC ice comes from UBern and the PhD thesis of Eyer, 2004, who, when studying the last glacial period he found CO_2 mixing ration depleted by max. 60 ppmv against the 180-ppmv threshold known (*cf. Ch. I*). Still, the studied EDC period does not belong to the purely clathrated zone, but to the highly-unstable transition "brittle" zone, of potential different characteristics. Pauer et al., 1995 and Pauer et al., 1997 after having proceeded to N_2/O_2 Raman spectroscopy measurements on GRIP core, found that all, at least most of, the atmospheric air is quantitatively trapped into the clathrate form.

In contrast to mixing ratios anomalies of gases related to clathrates processes, no equivalent carbon isotope effects have been reported yet (Eyer, 2004; Hachikubo et al., 2007), the latter for the $\delta^{13}CH_4$. This may be due to the process of the clathrate cages filling, being related to the molecule geometry, and thus to the volume and not the mass of the molecule. Though the binding energy of the ^{13}C-^{16}O bond is slightly higher than for ^{12}C-^{16}O (implying a shorter bond strength), the difference is too small to induce a steric isotopic effect.

II.3.5.1. Contribution of this study

In this PhD study, two sets of tests will be carried out on the properties of (i) brittle ice (EDC), compared to a bubble one (Berkner) and (ii) clathrate ice (EDC during TII). Results of the above exercises, focused on the isotopic behaviour, will be presented in *Ch. III and V,* respectively.

II.4. Chemical processes affecting gas composition in ice

II.4.1. Greenland observations

A number of studies focused on CO_2 mixing ratio reconstructions from Greenland ice cores (Eurocore, GISP2, GRIP and NGRIP) showed a typical 10-15 ppmv scatter between neighbouring ice layers (Anklin et al., 1995; Tschumi and Stauffer, 2000; Ahn et al., 2004). As smoothing effects of gas diffusion and trapping preclude recording of short-term atmospheric fluctuations, and as measurements precision are typically of ~3ppmv, these variations cannot be explained by physical mechanisms or analytical uncertainties.

The comparison with results from Antarctic cores for the same time periods, not showing such fluctuations, strengthens the suggestion on artefacts existence in Greenland cores (Barnola, 1999; Stauffer et al., 2002; Siegenthaler et al., 2005). Anklin et al., 1995 found considerable deviations, far larger than the expected inter-hemispheric gradient (being limited between –1 and +5 ppmv). Smith et al., 1997a ; Smith et al., 1997b reached the same conclusions by measuring CO_2 mixing ratios from GISP2 core either over D/O events during glacial times, or during the last G/IG transition, and by comparing with Antarctic cores. The Greenland records show up to 50 ppmv higher values. No dating constraints can either explain this inter-hemispheric inconsistency, since the use of atmospheric CH_4 in synchronizing records is considered accurate (Blunier et al., 1998; Blunier and Brook, 2001; EPICA, 2006; Blunier et al., 2007; Loulergue et al., 2007). Such large CO_2 difference between the two hemispheres, not only is not observed today for annual means, but is not compatible with the inter-hemispheric air mass exchange and the regional distribution of CO_2 sources and sinks (Denning et al., 1995; Dargaville et al., 2003). One could partly involve the so-called "rectifier effect" caused by the inter-seasonal co-variation of vertical and surface fluxes of CO_2. Denning et al., 1999 propose a "rectification" of 2.5 ppmv. But such possible effect appears meaningless over polar ice caps where no surface CO_2 fluxes take place.

The only explanation to these observations is to consider *in situ* CO_2 production occurring in Greenland ice cores.

II.4.1.1. Greenland contamination sources

Tschumi and Stauffer, 2000 compared their Greenland CO_2 records with chemical components also measured within the ice matrix, such as dust (calcium Ca^{+2}), hydrogen peroxide H_2O_2 and formaldehyde HCHO. Electrical conductivity of the melt-water, combined with the direct-current ice conductivity (**ECM**) were additionally measured. Protons concentration, H^+ could be then derived from ECM as an acidity tracer. After proceeding to statistical analysis, Tschumi and Stauffer, 2000 deduced that the Greenland CO_2 excess is due to chemical reactions.
Smith et al., 1997b provide an additional evidence of the non-atmospheric origin of the Greenland CO_2 signal, by measuring in parallel its stable carbon isotopic ratio. Two time slices of LGM and Holocene ice from the GISP2 core were measured: for LGM $\delta^{13}C$ was found too ^{13}C-enriched (varying from –4.45 to –3.70‰), while for the Holocene it was too depleted (-7.23 to –7.43‰) compared to Antarctic values. One could consider an acid-carbonate reaction occurring within the dust rich sections during the glacial period, the contaminant $\delta^{13}C$ being close to soil or marine carbonate signatures. For the Holocene, the CO_2 excess should originate from an isotopically depleted source, compared to the LGM; one possible candidate is isotopically-depleted organic compounds.

There exist three major pathways for the CO_2 excess observed in Greenland cores:

- the oxidation of organic carbon, through microbiological activity (Tschumi and Stauffer, 2000) or through chemical reaction (Campen et al., 2003)
- the reaction of carbonates with acid (Delmas, 1993; Anklin et al., 1995; Anklin et al., 1997; Smith et al., 1997a; Barnola, 1999)
- the snow melting -refreezing process (Neflel et al., 1983)

In the following the first two pathways will be commented:

II.4.2. In situ reactions of organic compounds (mainly oxidations)

II.4.2.1. Criteria

The chemicals relevant to this context should fulfil the following criteria: (1) the compound should combine certain physical-chemical properties that lead to its adsorption or snow deposition while its relative inertia is sufficient to survive the oxidative degradation within the surface snow; (2) the compound originating in the atmosphere is potentially capable of reacting with CO_2.

II.4.2.2. Known groups of interest

The main groups measured in snow and ice are (i) aldehyds (R^1-CHO), such as formaldehyde and acetaldehyde and (ii) mono- and di- carboxylic acids (R-COOH and HOOC-R-COOH), such as formic, acetic and oxalic acid (Kawamura et al., 2001; Guimbaud et al., 2002; Houdier et al., 2002). The above sub-groups constitute important oxidants of organics in ice. The simplest organic molecule is the hydroxide peroxide, H_2O_2 (Ahn et al., 2004).

II.4.2.3. Isotopic aspects

In Goldstein and Shaw, 2003 one can find a review of a wide range of **VOC**[2] identified in the atmosphere. What it will be encountered further on in this PhD study, deals with C3 and C4 plants influence in the atmospheric signal, the former having mean $\delta^{13}C$ values of -28‰, whereas C4 plants are more enriched (-11‰), (O'Leary, 1981). More ^{13}C-depleted atmospheric signatures, may thus be resulting from plant organic contamination.

II.4.3. In situ reactions of inorganic carbonate, $CaCO_3$, followed by reactions under acidic environment

This contamination source has been extensively discussed, as the majority of studies support this CO_2-production means.

The acid-carbonate reaction consists in the reaction of CO_3^{-2} with protons (H_3O^+or simply H^+), to form CO_2 in a two-stage acid-base reaction. The procedure can be visualized as follows:

$$CO_3^{2-} + H^+ \leftrightarrow HCO_3^- \quad (2\text{-}13)$$

$$HCO_3^- + H^+ \leftrightarrow CO_2 + H_2O \quad (2\text{-}14)$$

Both reactions are fully reversible and proceed until an equilibrium state is reached (Delmas, 1993), contrary to the case of organic contamination. Carbonate is mainly found in dust particles, associated with Ca^{2+} or Mg^{2+}, thus mostly being insoluble in pure water. In order the carbonate-acidity reaction to take place in the ice, both reactants must not neutralize each other before atmospheric deposition (Anklin et al., 1995). Smith et al., 1997a ; Smith et al., 1997b propose threshold $CaCO_3$ concentrations such as:

Case A: "low carbonate ice", with less than 5 ppb of Ca^{2+}. All Ca^{2+} reacts with H^+ before ice formation and the CO_2 content of the trapped air reflects ambient atmospheric values at the time of bubble formation.

[1] R stands for either a H atom or varying CHn chain
[2] Volatile Organic Compound

Case B: "high carbonate ice", with more than 70 ppb of Ca^{2+}. There is sufficient carbonate quantity to neutralize the existing H^+ without necessarily producing CO_2, thus no contamination for this case either. Still, the high $CaCO_3$ case may result in the opposite effect, *e.g.* CO_2 consumption, as under alkaline conditions the following reaction can take place:

$$CO_2 + H_2O + CO_3^{2-} \rightarrow 2HCO_3^- \qquad (2\text{-}15)$$

as introduced by Neftel et al., 1982 and discussed in Smith et al., 1997b.

Case C: "intermediate carbonate ice", with Ca^{2+} from 5-70 ppb, significant CO_2 amounts can be generated, as described in eq. 2-13; 2-14, thus contaminating the measuring signal.

In fig. 2-12 we try to directly compare Antarctic Ca^{+2} chemical composition with the Greenland one (Smith et al., 1997a). It shows that higher acidity and lower impurity levels (expressed as dust, Wolff et al., 1997 or here as Ca^{+2},) are found in the Antarctic ice, compared to the Greenland one (Stauffer et al., 1998), especially during the warm, interglacial periods where it belongs to case A.

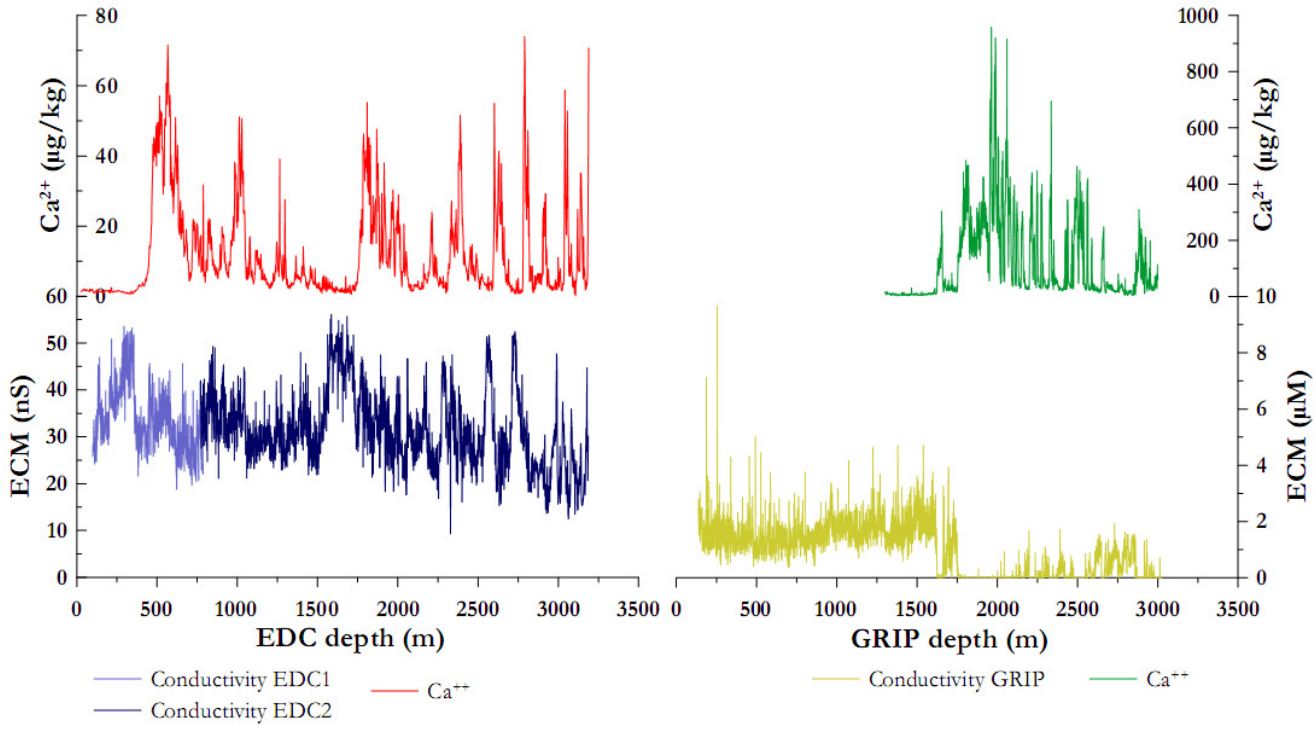

Fig. 2-12: *EDC (left panel) vs. GRIP (right panel) ECM and Ca^{2+} profiles plotted against depth; not the whole record can be represented for GRIP Ca^{+2}, since the signal was found below the detection limit during the Holocene. We observe* ***lower Ca^{+2}*** *concentration and* ***higher ECM*** *(ECM expressed in different units, since different measurements conditions) for the EDC core than GISP2 (Wolff et al., 2006; Stauffer et al., 2004 ; EPICA, 2004; Taylor et al., 1993; de Angelis et al., 1997; Fuhrer et al., 1993), implying weaker CO_2 contamination risk for the Antarctic site*

II.4.3.1. Origin and isotopic aspects

The main sources of carbonate transported to the ice sheets are the dry regions of the continents. Still, a small fraction originates from marine sea spray aerosols emitted from the open ocean, under the wind influence. In general, carbonate particles form the following three groups according to their formation or composition:

(i) carbonates originated from mechanical rocks crumbling, due to the glaciers action: *e.g.* marine limestone; this type is extended in European loess deposits during the ice ages. Marine carbonates $\delta^{13}C$ value is close to the mean oceanic isotopic composition, of ~0‰

(ii) limnic carbonates, formed by chemical soil or rocks weathering and the solutes are transported to lake basins; in terms of $\delta^{13}C$ values, dissolved inorganic carbon in rivers is more variable than marine carbonates, sometimes being even lighter (Mook, 2000)

(iii) pedogenic carbonates originated from semiarid soils and can be blown out after surface erosion, forced by the wind. The $\delta^{13}C$ values are mainly influenced from the vegetation type and range from –10 to 0‰ (Cerling et al., 1989).

The different origins of carbonate aerosols thus lead to potentially large isotopic composition variations of CO_2 produced by acid-carbonate reaction.

II.5. Extension of physical processes on gas age calculation challenge

The transformation of snow to ice is a slow process, when compared to the gas transfer within the firn column, being in the order of decades (Rommelaere et al., 1997). Therefore, the air occluded in bubbles is younger than the surrounding ice matrix. This difference is represented by the "Δage" notion and it depends principally on the firn densification rate and the examined climatic period. The above combined with gas diffusion in firn, render bubble air age as non-discrete, but instead it can be characterised by an "age distribution". As diffusion happens slowly, the air starts having a certain age due to the time needed for molecules to diffuse through the porous tortuosity linking the surface to the COD (Landais et al., 2006; Loulergue et al., 2007). The additional progressive pore close-off at the firn bottom adds another stronger attenuation of the atmospheric signal than that provoked by the molecular diffusion.

Δage is calculated when using firn densification models, based on site climatologic and meteorological parameters, such as (i) temperature fluctuations, (ii) accumulation rate, (iii) wind speed and (iv) insolation changes (mentioned in Loulergue, 2007). Air bubbles age can reach a probabilistic distribution of 300 years; this is the case for interglacial periods at EDC. It increases during glacial times, due to the lower accumulation rate. Loulergue et al., 2007 recently reported

the Δage in the EDC core, by providing 4 distinct scenarios, according to the site parameterizations. The estimations of the scenario no 4, now constituting the EPICA official EDC gas scale, EDC_gas_a, and has been used here (*cf. Ch. IV*).

II.6. Conclusions

From the atmosphere to the trapped bubble and then the ice core sample, CO_2 mixing and isotopic ratios can undergo several modifications due to physical or chemical processes. The physical processes in the firn include gravitational settling, molecular diffusion and thermal diffusion. They can be accounted for using equations best describing the phenomenon, and/or by quantifying each phenomenon using a dedicated tracer recorded in ice. The major bias is introduced by gravitational fractionation. Its effect on $\delta^{13}CO_2$ can reach max. 0.5‰ of enrichment.

In the ice, the physical process of clathrate formation (and then dissociation after ice core drilling) can fractionate mainly mixing and probably also isotopic ratios between the remaining bubbles and the formed hydrates. This is critical if the extraction procedure of trapped gases is not quantitative. This will be more specifically discussed in *Ch. III and V*.

Chemical reactions are known to occur in Greenland ice, affecting the CO_2 mixing and isotopic ratios. The artefact on the mixing ratio can reach ~50 ppmv. They involve two main mechanisms: oxidation of organic compounds and acid-carbonate reaction. In Antarctic ice such as EDC, the chemical composition of ice does not allow such reactions to occur, at the level of sensitivity of current experimental apparatus used in ice core laboratories. This, combined to the fact that the inner Antarctic site are more isolated from pollution sources, point to the choice of Antarctic ice cores in reconstructing past atmospheric CO_2 evolution.

Chapter III. Methods and instrumentation

III.1. Introduction

Chapter I raised the role of stable C isotopes on constraining the C budget. Chapter II exposed physical – chemical factors that influence the isotopic signal within the ice. In this chapter, experimental aspects on obtaining the atmospheric $\delta^{13}CO_2$ from ice cores are discussed. An overview is presented on the existing air extraction techniques from ice, their assets and handicaps. In the following, the reader gets acquainted with the applied experimental procedure during this 3 PhD-year work. The analytical protocol of in parallel CO_2 mixing ratio measurement with its stable isotopic ratios is provided and discussed for the first time. All corrections applied, other than those mentioned in Ch. II, are provided in order to obtain the final signal. This experimental protocol is then tested by various blank tests and validated by a number of known standard gas analysis, on a daily scale. The first applications on Vostok ice sample is presented here, permitting to further discuss the protocol accuracy and comment on corrections proposed elsewhere. More delicate calculation results from the two major sampling periods (TI and TII) are provided, in terms of standard gas evolution through time as well as analytical tendencies seen within the ice sample itself. The question of dry extraction technique efficiency on gas content quality, already raised in chapter II, is discussed with an intercomparison test on ice of different nature.

III.1.1. Analytical challenges related to quantified isotopic measurements

The quantification of isotopic composition of trace gases trapped in polar ice remains challenging in the environmental research for the following reasons:

- small available sample size: 1 kg of ice contains ~100cm^3 of air at standard pressure and temperature; *i.e.* 1 kg of ice contains from ~0.9 to ~0.6 μmoles of $^{12}CO_2$ and ~10.06 to ~6.5 *m*moles of $^{13}CO_2$, for Early Holocene, ***EH*** (280 ppmv) and Last Glacial Maximum, ***LGM*** (180 ppmv) conditions, respectively.
- high required precision for the results interpretation, considering that during TI $\delta^{13}C$ naturally oscillates by only 0.5‰. A difference of 0.1‰ between the carbon isotopic ratio of CO_2 in two LGM ice core samples translates into measuring a difference of 8.10^{-16} g of $^{13}CO_2$ per g of ice.

III.2. Overview of gas extraction methods on ice samples

Three main techniques exist for liberating the air trapped in the ice: the "wet extraction", the "dry extraction" and the "extraction by sublimation". All three methods are considered as "destructive" (Barnola et al., 1983), since they require sample loss for the sake of science.

III.2.1. Wet extraction or melt-refreezing method

III.2.1.1. Principle

The wet technique involves phase change of the sample from solid to liquid, and then back to solid. An ice sample is inserted into an extraction vessel, and then allowed to melt *in vacuo* to liberate the trapped gases (Sowers et al., 1997). The system is then slowly refreezed from bottom to top, aiming to expel most of the dissolved gas towards the free cell volume, and to keep the water vapour pressure in the air fraction at low levels (Chappellaz et al., 1990; Chappellaz et al., 1993).

III.2.1.2. Applications

This technique has been used to analyze constituents that are relatively insoluble and chemically stable in water, such as CH_4, O_2, N_2 and Ar (Sowers et al., 1997). CH_4 has been in the frontline for using this technique. An interesting application of the different behaviour of CO_2 towards the dry and wet method has been effectuated by Anklin et al., 1995 : by comparing the two techniques for CO_2 analysis they indirectly calculated the amount of carbonate contamination in the Greenland ice core (*cf. Ch. II*)! Kawamura et al., 2003 achieved in measuring CO_2 in the Dome Fuji ice with an updated wet technique. The extraction efficiency reached 100% of its capacity but was coped with problems of high water vapour levels.

III.2.1.3. Method advantages and drawbacks

The ~100% extraction efficiency (depending on how much dissolved gas is removed during re-freezing), as well as the relative simplicity of the melt-refreezing procedure, constitute the main advantages of this method (Stauffer et al., 1985).

The main drawback of this method is the presence of water, increasing the risk of contamination by *e.g.* microbiological production or consumption of CH_4 (Stauffer et al., 1985). Small artifacts resulting from gas desorption from the melting extraction system walls, should be also taken into account. The duration of the procedure (melting ~30min while refreezing ~1h30min) is also considered as a drawback. The wet method is regarded as unsuitable for CO_2 analysis (Zumbrunn et al., 1982 ; Oeschger et al., 1983), as (i) CO_2 molecule is extremely soluble in water, thus making almost impossible a quantitative CO_2 extraction via a melt/refreezing procedure (potential

underestimation of its mixing ratio) and (ii) there is an increased risk of *in situ* production of CO_2 if acidic aerosol species react with carbonate dust particles (Stauffer et al., 1985; Friedli et al., 1986; Fuchs et al., 1993; Sowers et al., 1997). As chemical reactions lead to isotopic fractionation, $\delta^{13}C$ analysis using a wet extraction technique is not adapted.

III.2.2. Dry extraction method

III.2.2.1. Principle

The dry extraction, based on a mechanical disintegration in solid phase of the ice core sample, has been considered as the conventional method of air extraction from ice for CO_2 measurements. There exist different disintegration techniques. In all cases, the ice sample (which could weight from 1g –case of *needle cracker* technique- to 1500g –case of *cheese grater*-) is placed into a stainless steel extraction vessel and is mechanically grinded (crushed, grated or milled) under vacuum to small grains or powder, while the escaping gas is either collected by expansion, compression or condensation or is flushed from the extraction cell using an inert (carrier) gas (*e.g.* He) (Fuchs et al., 1993; Sowers et al., 1997).

III.2.2.2. Applications

Needle cracker

Zumbrunn et al., 1982 and Neftel et al., 1982 established in Bern the needle cracker technique and applied it on CO_2 measurements upon cores from both hemispheres, for the last 40 ky. Tschumi and Stauffer, 2000 applied the same method in order to obtain a high spatial resolution record of the 'contaminated' Greenland ice core, while Indermühle et al., 1999 published a CO_2 over Holocene for TD core. Some time later, Monnin et al., 2001 produced the dataset-milestone of CO_2 from EDC core during TI. Leuenberger et al., 2003 presented an updated online technique for $\delta^{13}CO_2$ measurements, based on air dry extraction using a stainless steel needle cracker for very small ice samples (8g); they obtained in parallel $\delta^{18}O$ of CO_2 and CO_2 mixing ratio itself, either volumetrically or with an **IRLS**[1]. This technique has been applied for the first time on EDC samples during TI (Eyer, 2004).

Cheese grater

CSIRO[2] notably applied this method (Etheridge et al., 1996) and a dataset-milestone of CO_2 from Law Dome for the last 1000 years has been produced. The same extraction method is used

[1] Isotope Ratio Laser Spectroscopy
[2] Commonwealth Scientific and Industrial Research Organization

for determining $\delta^{13}CO_2$ in the same core for the same period by Francey et al., 1999, resulting in another dataset-milestone for atm. $\delta^{13}C$ during the last millennium (*cf. Ch. I; annex VI*).

Ice milling/grinding

LGGE principally applies this "dry" alternative, the measurement of the air content by Raynaud and Whillans, 1982 and the PhD thesis of Barnola, 1984 being the initial references. ~40g of ice is placed inside a stainless steel container with stainless steel ball bearings (fig. 3-1, *left panel*). After evacuation the container is shaken vertically and vigorously to crush the ice into a very fine powder (fig. 3-1, *right panel).* The released gas is then expanded into a sample loop and is injected into a Gas Chromatograph (**GC**) equipped with a Thermal Conductivity Detector (**TCD**) or a Flame Ionization Detector (**FID**) following methanation on a nickel catalyst (Barnola et al., 1983; Pépin, 2000; Bellier, 2004; Gallet, 2006).

Delmas et al., 1980 first applied the milling method to two Antarctic cores and discovered lower CO_2 values during LGM than today. Later on, Barnola et al., 1987 presented a CO_2 record from Vostok core over the last 160 ky. In Bern, a milling device similar to this of Grenoble was developed (Moor and Stauffer, 1984), but with more than 10-fold bigger sample size; this method, coupled with that of Friedli et al., 1984 was later used for determining in parallel CO_2 and $\delta^{13}C$ atmospheric signal, such as the first $\delta^{13}CO_2$ data between LGM and Holocene in Byrd core (Leuenberger et al., 1992) and a study on the S. Pole focused on the $\delta^{13}CO_2$ trend during the 13th century (Siegenthaler et al., 1988).

Fig. 3-1: (left panel)*: photos of ice mill before and after entering the sample with the dry extraction milling method;* ***right panel:*** *photos of ice mill after milling*

Micro-crusher

The micro-crusher constitutes the reference method in **SIO**[3], as described by Wahlen et al., 1991. Applications of this method are found in Smith et al., 1999 CO_2 and $\delta^{13}C$ first TD coupled CO_2 – $\delta^{13}C$ results for the last deglaciation, as well as in Indermühle et al., 1999, for the Holocene record.

III.2.2.3. Method advantages and drawbacks

The main advantage of the dry extraction method lies in the absence of liquid phase, avoiding any potential reaction (Stauffer et al., 1985). For the needle cracker case, the small size required and the fast procedure, permits a higher spatial resolution (Leuenberger et al., 2003; Eyer, 2004).

The major inconvenience of the milling technique involving stainless-steel particles friction, is the partial air release from the full sample (of ~60-80%). Non-crushed ice fragments remain at the end of the experimental procedure (Zumbrunn et al., 1982; Barnola et al., 1983; Barnola, 1984; Neftel et al., 1983; Stauffer et al., 1985; Gallet, 2006). Although Moor and Stauffer, 1984 mentioned that when grinding, it does not matter if the ice is crushed to fine or coarse chips or whether one starts with a single piece or several pieces of ice, it appeared since that two physical processes affect the relationship between extraction efficiency and the measured concentration: (i) the specific surface of crushed ice, susceptible to fractionate trace gases according to their affinity with the produced powder (Wilson and Long, 1997; Fuchs et al., 1993); (ii) the crushing process is less effective in releasing gases which have penetrated the ice matrix, implying that dry extraction techniques are efficient mainly on bubbles or 'young' ice. This efficiency depends on the type of dry extractor used, as the different types do not produce the same mesh of ice powder *(Cf. III.7.3.1 section).*

Another serious drawback of the dry extraction method is degassing from the ice mill material (stainless steel interior walls and/or balls). For *e.g.*, a three times more enriched CH_4 values have been measured with the LGGE crusher compared to what was initially expected (contamination of ~1900ppbv). Thus, the dry extraction way seems prohibited for at least CH_4 analysis (Güllük et al., 1998) (it is probably the case also for CO, *J. Chappellaz, pers. comm.*). Only when friction can be avoided, or degassing can be contained, can this method be extended to gases such as CH_4. Fuchs et al., 1993 and Etheridge et al., 1998 provide such advanced studies.

[3] Scripps Institute of Oceanography

III.2.3. Extraction by sublimation

III.2.3.1. Principle

The sublimation is based on IR irradiation of an ice sample, which is placed into a pre-evacuated glass container and maintained at temperatures below 0°C. IR rays sublimate the ice. The air liberated from the bubbles and the water vapour resulting from the heating are subsequently freezed by cold traps at –80 to –90°C, in order to remove the water vapour from the system, and liquid helium trap to condense the other gases (Wilson and Long, 1997; Güllük et al., 1998). The evaporation and re-condensation of ice in a closed system release all gaseous and solid components originally trapped in polar ice and allow quantitative analysis of the gases.

III.2.3.2. Applications

The air extraction by sublimation is relatively recent, compared to the dry and wet methods. First results are presented by Wilson and Long, 1997 on GISP2 data during the last glacial period (20-45 ky BP). Güllük et al., 1998 developed a technique for simultaneous determination of CO_2, CH_4, N_2O and CO in initial ice mass of 20-50g. Despite the high-blank results due to CO_2 adsorption/desorption from the system, they concluded sublimation to be the most efficient extraction technique. They also presented their first air results (from Siple) and ice results from Vostok, for the last 300 years. Siegenthaler et al., 2005 used this method for extraction intercomparison on the EDML Antarctic ice. They concluded to an agreement between the dry and sublimation technique results and the assumption that a fractionation of more than 5 ppmv for the former method is unlikely to occur.

Recently, within the EPICA gas consortium, AWI with the PhD student Jochen Schmitt achieved in designing a new apparatus based on the sublimation principle (Schmitt, 2006; Schmitt and Fischer, *to be subm.*). With this work, simultaneous measurements of CO_2 and $\delta^{13}CO_2$ can be performed on ice cores for the first time by sublimating the sample. Recent applications of this method concern Holocene investigation (Schmitt et al., 2007).

III.2.3.3. Method advantages and drawbacks

The main advantage over ice milling concerns the 100% extraction of the occluded air. It is not affected by the physical ice properties, *i.e.* the bubble/clathrate ratio. The glass used as sample container has smaller sorption properties than stainless steel and it allows visual monitoring of the experimental process, verifying that no liquid water forms in the system. The temperature and the speed of the procedure can be controlled by IR radiation. In addition to this, the method

provides an initial 'decontamination', by sublimating and discarding *e.g.* the outer 10% of the core, where impurities, fractures and drilling fluid traces may remain.

This method has still some drawbacks. Air extraction using the sublimation technique is a rather slow procedure. Wilson and Long, 1997 mention a 18h-procedure for analysing 3kg of ice while Güllük et al., 1998 need 30-45 min for sublimating only 50g of ice. The applied temperature is close to the ice melting point, thus risking contamination from potential chemical reactions taking place in the quasi-liquid layer of grain boundaries. Any potential impurity the natural sample contains, becomes more and more concentrated in the non-sublimated phase, increasing the risk of chemical reaction at the end of the sublimation process.

III.2.4. Intercomparison of the analytical system between 3 European laboratories (EPICA Consortium)

During this PhD study, the dry extraction method with the ball crusher was applied. Since LGGE belongs to the EPICA Consortium, with other 2 laboratories, all 3 trying to produce simultaneously CO_2 and $\delta^{13}C$ atmospheric data from polar ice, in table 3-1 major experimental items are exposed in order to comprehend major technical differences between them.

Property	UBern	LGGE-old	LGGE-new	AWI
Extr. Technique	Dry – needle cracker	Dry - milling	Dry - milling	Sublimation
Ice sample size	5-10g	40-50g	40-50g	~33g
Extraction efficiency	~70%	~70%	~70%	100%
Extraction temperature	-30°C	-65°C	-65°C	-28°C
CO_2 detection system	IRLS	GC-FID	GC	GC
Volume of air used for the analysis (STP)	0.5-1mL	4-5mL	4-5mL	~3.3mL
Standard gas used	CO_2=272, 322 and 342 ppmv; $\delta^{13}C$=-35 ‰;	CO_2=258 ppmv	CO_2=260.26 ppmv; $\delta^{13}C$=-6.4 ‰; $\delta^{18}O$=-7.75 ‰	CO_2=277.7 ppmv; $\delta^{13}C$=-2.75 ‰; $\delta^{18}O$=-14.72 ‰
Result extracted	CO_2; $\delta^{13}C$; $\delta^{18}O$	CO_2	CO_2; $\delta^{13}C$; $\delta^{18}O$	CO_2; $\delta^{13}C$; $\delta^{18}O$
on/off line coupling[4]	On-line	Off-line	Off-line	Off-line
Analytical precision	2.1 ppmv (CO_2); 0.13‰ ($\delta^{13}C$)	1.5ppmv (CO_2)	1.5ppmv (CO_2); 0.1‰ ($\delta^{13}C$)	1.5ppmv (CO_2); 0.06‰ ($\delta^{13}C$)
Number of replicates	3	3-5	3	5 (original version) 3 (latest version)
Total time (1 sample)	~6h	~6h	~7h	~24h*
Source	(Leuenberger et al., 2003; Eyer, 2004)	(Pépin, 2000; Bellier, 2004; Gallet, 2006);	(Lavric et al., in prep.); this study	(Schmitt, 2006; Schmitt and Fischer, to be submitted)

Table 3-1: *technical-based intercomparison of the 3 laboratories that belong to EPICA consortium and deal with atm. $\delta^{13}CO_2$ and CO_2 coupled measurements*

[4] off-line means the sample been treated separately from the extraction technique

III.3. General concept and layout of the experimental procedure

III.3.1. Overall

Our experimental procedure can be splitted into four steps:

- sample preparation
- air extraction
- gas transfer
- analysis of (i) CO_2; (ii) its stable isotopes

A part of the setup I will be mentioning (front line) was conceptualised by J. Chappellaz for an application on CH_4 carbon isotopes and installed at CEA/LSCE during the period 1995-1996 in collaboration with J. Jouzel and M. Stievenard. It was then brought back to LGGE when the mass spectrometer was installed in 1997, and improved during two PhD studies (Aballain, 2002; Bernard, 2004). The other part (back line) contains an extraction setup which was used for obtaining the Vostok CO_2 profile (Barnola et al., 1987). Jošt Valentin Lavrič, as a post-doc at LGGE in 2004-2006, modified the whole system to allow both CO_2 and CH_4 mixing and isotopic ratio analyses. The data presented in this PhD are the first produced with this new experimental design.

III.3.2. sample preparation

Fig. 3-2 presents the ice sample preparation:

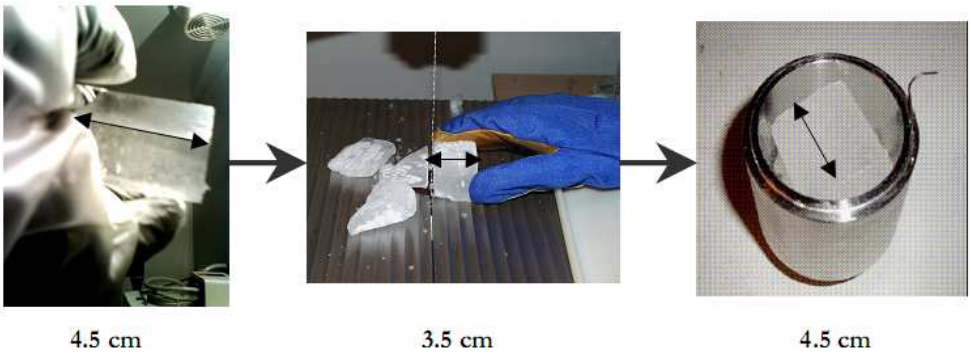

Fig. 3-2: *ice sample preparation; numbers beneath represent the scale shown in arrows*

The ice sample is cut in a cold room at -20°C with a pre-cleaned band saw. It has a cubic form, with dimensions of ~4cm for each side, equivalent to 40-50g of ice sample (corresponding to ~4-5cm^3 of occluded air). The external part of the ice core is removed during this process (by > 10

mm of thickness) to get rid of drilling fluid traces and of possible small fractures or cracks, both affecting the bubble composition. The sample is then put into a 150-cm^3 stainless steel ice mill. The ice mill is pre-cooled at –20°C for at least 1h30min before the sample introduction. It contains 8 stainless steel balls: 3 large ones (of 12 mm diameter), crushing the ice in smaller pieces, and 5 small ones (of 8 mm diameter) that reduce furthermore the sample in an ice powder (fig. 3-1). The ice mill is closed and tightened with 4 nuts (precisely turned with a manometric key), pressing an indium wire (1 mm thickness) between the cell and its cover. The mill and its valve are then immersed in a cold bath (~-65°C), prepared from an ethanol (95%) and (**LN2**[5]) mixture (see picture incorporated in table 3-3).

III.3.3. air extraction

The cooled sample system is connected to the analytical extraction line, consisting of stainless steel tubes and valves linked to a turbo-molecular pump and a primary oil pump. It is then evacuated during 45min, at a pressure below 10^{-3} mbar. The vacuum evolution is followed with a Pirani Gauge. Then the valve of the ice mill is closed, the mill is disconnected from the vacuum line and brought back in the cold room. It is then screwed to the vertical-motion ice crusher which is activated during 90sec, with two intervals of 15sec and two of 30sec (Barnola et al., 1983). Throughout this time, the ice mill should remain efficiently isolated from the atmospheric air. Due to the vertical motion, the indium seal between the mill and its cover may slightly flow away, thus requiring to check the screw tightness with a manometric key, between each interval of ice grinding. Once the milling is finished, the bath-cell system returns to the laboratory to be again connected to the vacuum line. The connection is then pumped for 20 minutes.

III.3.4. gas transfer

Fig 3-3 represents a simplified gas transfer scheme of the experimental protocol which will serve as model for the following discussion.

This experimental step contains the pre-concentration line, aiming at the sample contaminants clean-up (ex. water traces removal) and gas separation (*e.g.* of CO_2 from bulk[6] air constituents). It is divided into the following main parts: (1) the section under vacuum, (2) the high He-flow part and (3) the reduced He-flow part. A series of turbo molecular pumps, coupled with primary oil pumps, as well as different kinds of traps (*cf. below*) linked by Valco valves configure the above setting.

---

[5] LN2 stands for liquid N_2, extensively used during our analysis

[6] the bulk air consists of N_2, O_2, Ar and other atmospheric compounds which are not condensable at liquid nitrogen temperature (-196°C)

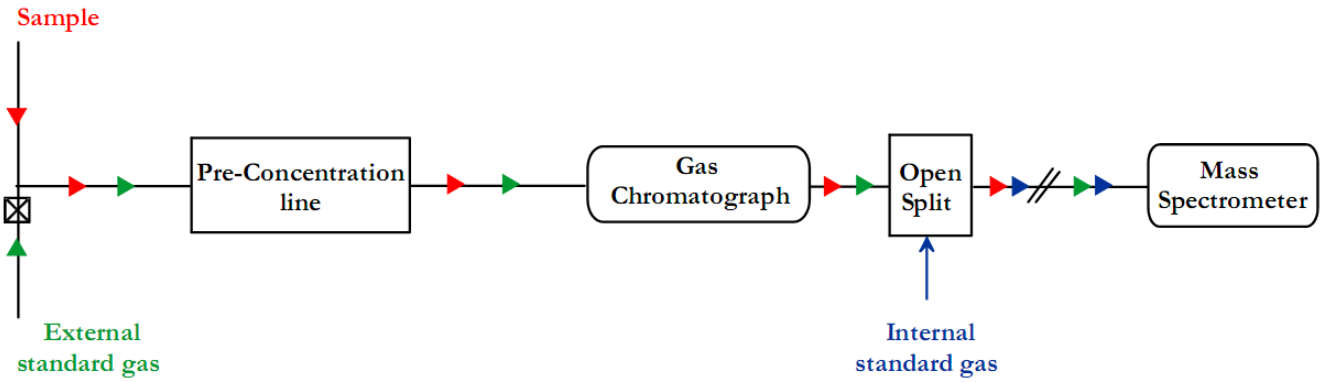

***Fig. 3-3**: simplified scheme on the analytical line system and the gas transfer process; red arrows represent air from crushed ice sample, which passes in alternance with the external standard gas (green arrows). In the open split section, the reference gas (internal standard gas, blue arrows) is coupled with either the st. gas or the sample air in the chromatogram once passed through the MS. The black valve in the front regulates the flowing of the st. gas or the sample over the gas transfer line. This figure is a simplification of **fig. 3-6** presented below*

Two different-sourced gas types circulate in our line: the standard gas and the air extracted from the ice. These two different transfers (represented with green and red arrows in the simplified fig. 3-3) are alternated. The following significant differences distinguish them:

- the CO_2 partial pressure from the sample in the ice mill is unknown (implying an unknown total pressure at the time of first expansion) whereas the standard gas pressure can be chosen ;
- the pressurized external standard gas flows through a flow-restriction valve, whereas the sample gas is expanded by opening an on/off valve ;
- The equilibration time of the gas in the sample loop is 1 min for the standard gas and 3 min for the sample gas.

Once the equilibration time is reached, the gas is carried through a sample loop (of 10 cm^3 for the case of CO_2 analysis) and a pre-concentration system, both parts being flushed by two different He fluxes. A water vapour trap (mixture of ethanol and LN2 at ~-80°C) is placed before the sample loop. This part of the line is maintained under high vacuum ($<5*10^{-4}$ mbar) during the line preparation and between the different steps of gas transfer. Once an ice core gas sample has been expanded in the sample loop, the valve of the ice mill is closed, thus keeping part of the sample gas into its dead volume for subsequent additional expansions. We usually perform three consecutive expansions of the same sample gas.

Downstream from the sample loop, the pre-concentration system contains the following parts:

- a heated glass trap (Pyrex, internal d: 1.8 mm), been dived into pure LN2; this trap aims at concentrating the sample and eliminating it from impurities or major air components, such as O_2, N_2, Ar. About half of the trap is immersed in LN2, whereas the upper part is wrapped by a heated tape and maintained at about 60°C. A He flux of 40 mL/min transfers the gas from the sample loop to the heated glass trap (*note*: in stand-by conditions, this flux is decreased to 9mL/min, to maintain the line clean and to save ultrapure He, *cf. III.4 section*)

- a Nafion tubular membrane, which permits residual water removal (to reduce the m/z 45 contamination provoked by the reaction of CO_2 with H_2O in the ionisation MS chamber, producing HCO_2^+ (Leckrone and Hayes, 1998)). The Nafion system maintains the whole system in a relatively dry condition, as verified by the m/z 18 (water vapour) signal. The sample passes through the membrane interior (λ=20 cm; internal d=1.8 mm), while the volume between the membrane and an external stainless steel ¼" tube is counter-flushed by an He flux; this allows to reach the same dew point in the sample as in the ultrapure He

- a cryofocus capillary immersed in LN2: it is made of uncoated silica and has an internal d of 0.32 mm (length: 1 m). It allows the CO_2 cryofocussing into a much smaller volume than the glass trap and thus to produce a sharp peak on the spectrogram once the capillary is warmed up. The cryofocus capillary is flushed with a smaller He flux than the heated glass trap (~3.5 mL/min vs. 40 mL/min), to accomodate the small flows required by the subsequent capillary column and transfer line to the mass spectrometer.

The cryofocused sample contains CO_2 but also other impurities, such as N_2O and traces of N_2 and O_2. Thus, once the cryofocused sample is removed from the capillary by warm-up, it then goes through a chromatographic column held in an oven. The principle of the GC lies in the differential adsorption of molecules as a function of their affinity with the stationary phase. The retention time of the molecules depends on their nature, on the stationary phase, on the column temperature and on the carrier gas flow rate. In our case, the used column is a **PLOT** (Porous Layer Open Tubular) GS-Q of melted Si with λ=30 m and internal d=0,32 mm, while the walls are covered with Porapak Q particles of a 10-μm size. The column is maintained at 70°C, and the He flow is ~3.5 ml/mn.

III.3.5. analysis of (i) CO_2; (ii) its stable isotopes

Once the sample has passed through the GC, it goes through another Nafion membrane belonging to **GC-IRMS**[7] interface part and then enters an open-split (fig. 3-3). The open-split is a glass tube open at one extremity. The capillary which transfers the sample is glued to the lower end. The tube is continuously flushed by a small flow ultrapure He, and the capillary linking the interface to the MS (internal d: 0.10 mm, λ: 1 m) is moved up and down in the glass tube to sample or not the eluents from the GC column. In the "down" position, the injection capillary to the MS gets into a "press-fit" connector, incorporated in the tube. The pure CO_2 reference gas (internal standard, *cf. III.6.2.1 section*) is also introduced to the MS via a second open-split system. In this case, the pure CO_2 stream is brought to the bottom dead-end of the glass tube, where the injection capillary leading to the MS (internal d: 0.075 mm, λ: 1 m) is permanently located.

III.3.5.1. Principle of MS

The principle of the mass spectrometer lies in separating ions according to their mass/charge (m/z) ratio. A MS is constituted by : (a) the source that generates, accelerates and collimates the ions; (b) the fly tube, inside which strong electric/magnetic fields are used to separate the ions into different beams and (c) the collector, where the different ion beams are electronically counted (fig. 3-4). The whole procedure takes place within four steps:

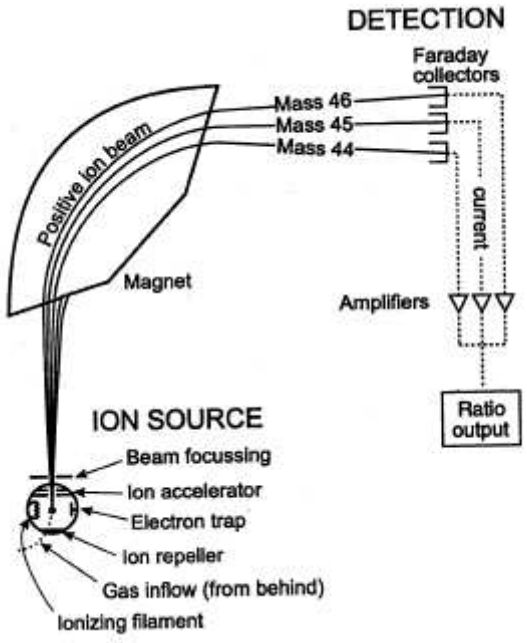

Fig. 3-4: *different parts of a Mass Spectrometer*

[7] IRMS for Isotope Ration Mass Spectrometer, sometimes summarized as « **MS** »

Ionisation: the gas of interest is first converted into ions inside a high vacuum chamber (3.10^{-6} to 10^{-7} mbar). Electrons produced by a heated (2000°C) tungsten filament 'bombard' the gas, which is then positively charged.

Acceleration: the ions are accelerated with a maximum energy of 10 keV through a high voltage setup, while collimating plates and electronic lenses are employed to focus the ions into a narrow beam (<1mm diameter).

Separation: the charged, energetic beam is passed through a strong magnetic field (of ~1 Tesla), which serves as a 'prism' in that it resolves the single collimated beam into several distinct ones. For *e.g.*, each beam is composed of ions that have a common characteristic, such as momentum, velocity or energy; this should differ from another beam's ions common property. Then, the beam leaves the magnetic sector, according to their different ratios m/z.

Detection: the spectrogram, constituted by counts of the individual beams as a function of time is electronically produced and compared between beams to finally be translated into relative abundances. This is done by the collectors, placed at the end of the ion path. In our case several detectors, the collectors **MEMCO** (Multi Element Multi Collector) are Faraday cups precisely aligned for measuring the m/z ratios 28, 29, 32, 34, 44, 45 and 46, permitting the simultaneous measurements of two or more isotope ratios from a stationary beam condition. The weak ionic currents (a few nA) are amplified by a dedicated electronic under vacuum, their ratio providing us with the isotopic ratios.

Sample injection to the MS

The sample introduction into the source of an IRMS can be achieved with two different techniques: (1) dual-inlet and (2) continuous flow (CF).

Dual inlet system: description – applications – advantages – drawbacks

The dual-inlet system, introduced by Urey in 1948 and described by McKinney et al., 1950 constitutes the breakthrough in classical IRMS (Werner et al., 2001b). It requires sample introduction into an internal variable volume of the MS, next to another variable volume with a standard gas, whose isotopic composition is known. The unknown and standard gas volumes are tuned to reach the same internal pressure, and are coupled with the MS source through two capillary tubes, leaking the gas at the same flow and permitting statistical comparison by alternating sample flow and reference flow.

Several studies have used this method for ice core $\delta^{13}CO_2$ research, such as Friedli et al., 1984; Friedli et al., 1986; Siegenthaler et al., 1988; Leuenberger et al., 1992; Indermühle et al., 1999; Smith et al., 1999.

A high precision can be achieved with this MS configuration (better than 0.01‰ for $\delta^{13}CO_2$), due to the repeated measurements and to identical conditions for the sample and the standard. Francey et al., 1999 set as minimum scatter goal for ice samples 0.015‰. Ciais et al., 1995a ; Fisher et al., 2005 report high precisions for the case of atmospheric $\delta^{13}C$ samples, of 0.03‰, while Werner et al., 2001b even higher, of 0.01‰.

Some of the above studies reported problems caused by isobaric interferences from organic impurities and N_2O which are not well removed by off-line sample preparation. These organic contaminants can originate either from the drilling fluid, the laboratory air (*e.g.* organic solvents used in cold traps and cooling systems) or even from organic impurities contained in the ice *(cf. Ch. II)*. The dual-inlet has the additional drawback of large sample requirement (of up to 1 kg), since only a small fraction (<1%) of the sample enters the MS ion source, and a pressure of several tens of mbar is required in the variable volume to drive gas flow through the capillary. Some "cross-contamination" incidences have been testimonied with the dual-inlet procedure due to the sometimes insufficient 'idle time' intervening between two measurements. This 'idle time' is necessary for adequate gas removal from the ion source (Werner et al., 2001b).

Continuous Flow system - description

A more recent and promising sample injection method is the Continuous Flow (**CF**). It allows an on-line transfer of the sample, with GC separation of CO_2 from impurities under a continuous He flow (accompanied with a slight decreased ionization MS efficiency). In a typical CF application, CO_2 is transferred and purified within small diameter capillaries using a pressurized He carrier. The sample is then inserted into the MS ion source via the open split device. In that case, 30% of the sample enters to the IRMS at once, thus permitting a reduction of sample size by two orders of magnitude compared to the dual-inlet technique. The precision is not as high as for the dual-inlet case, due to the absence of statistical tests on a single measurement, but the reproducibility can reach 0.1‰ or better due to a combination of reasons: (i) there is a markedly lowered memory effect due to uninterrupted gas flow through the ion source, (ii) limited adsorption/desorption processes occur on internal surfaces and the single inlet capillary, avoiding problems of sample or reference inlet paths asymmetrical behaviours (Leuenberger et al., 2000) and (iii) CF coupled to IRMS permits N_2O-CO_2 chromatographic separation and it provides both

the mixing ratio and isotopic ratio measurements on CO_2 (Ferretti et al., 2000; Ribas-Carbo et al., 2002).

Continuous Flow - Applications

A pioneering work in applying this technique for measuring $\delta^{13}CO_2$ on ice was presented by Leuenberger et al., 2003, who connected an improved needle cracker version of that applied from Monnin et al., 2001 to a newly developed CF system. Although theoretically possible, Leuenberger et al., 2003 did not couple the whole system with a GC. An application of this experimental setup is the PhD work of Eyer, 2004.

The mass spectrometer used at LGGE is a MAT 252 Finnigan model, run under Continuous Flow. It is equipped with a triple MEMCO system, having three Faraday cups associated with amplifiers. These cups receive the ratios m/z 44, 45 and 46, used for measuring the isotopic $\delta^{13}CO_2$ and $\delta^{18}O$-CO_2 signals. The measured tension (voltage) is generated from the continuous ion currents in the Faraday cups, using resistors with $3*10^8$ Ω for m/z 44, $3*10^{10}$ Ω for m/z 45 and $1*10^{11}$ Ω for m/z 46. The MS software ISODAT 2.0. converts the measured ion current into a voltage amplitude over the Ohm's Law:

$$V = R \times I \qquad (3\text{-}1)$$

$\boldsymbol{V}$ being the voltage (Volts); $\boldsymbol{R}$ the resistance (in Ohm or Ω); $\boldsymbol{I}$ the current intensity (in A).

The R of cup 44 being of $3*10^8$ Ω means that for a 1-Volt amplitude the ion current should be of 3.33 *n*A. For *e.g.*, during TI-measurements, the ion current varied from 2.35 to 15 *n*A (corresponding to 0.7-4.5 V).

The IRMS was tuned for maximum sensitivity with the focusing lenses. The VISC window above the source, affecting the residence time of the sample gas into the source, is nearly fully open. This decreases the MS sensitivity (typically 3000 CO_2 molecules per ion produced), but provides sharper CO_2 peaks, and thus a better peak definition with respect to background ion counts. The obtained peak amplitude is measured in Volt, while the peak area is in Volt*sec. An integration time of 0.25 s was selected as sampling rate for the three m/z traces. A threshold on the signal slope of 0.2 mV/s for the peak start and 2.0 mV/s for its ending have been defined. The minimum peak height had been defined at 50 mV, the peak resolution at 50%, while the maximum peak width is set to 180s. The exiting chromatogram, out of the above configurations, is presented in fig. 3-5.

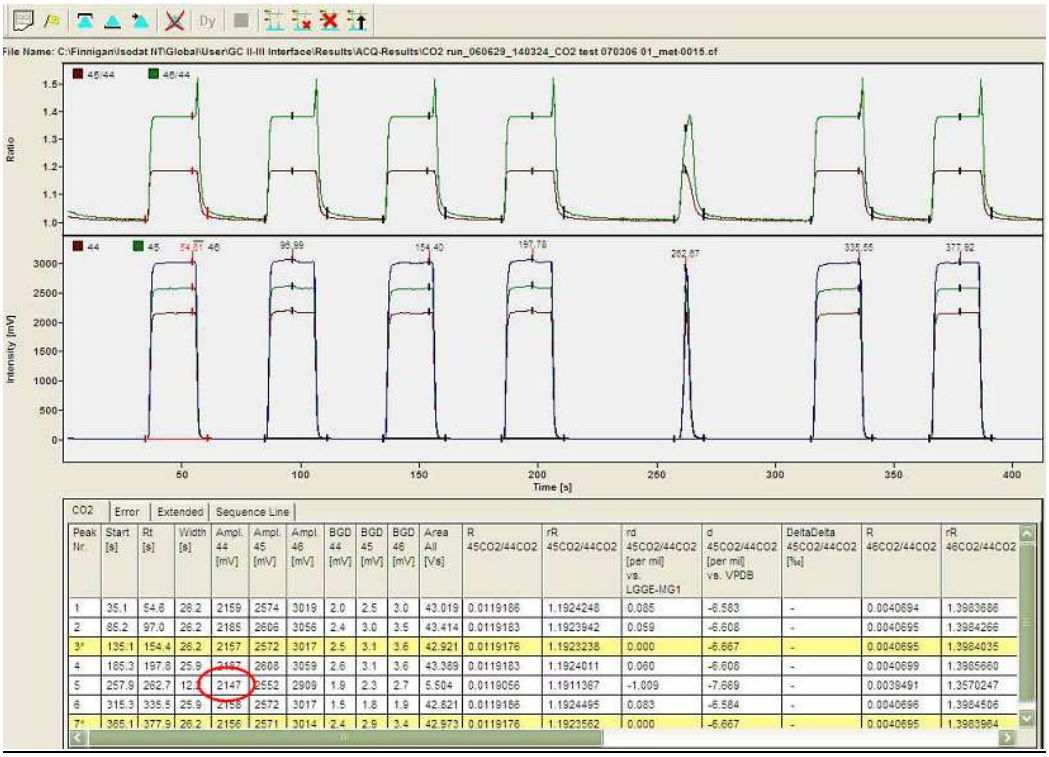

Peak Nr.	Start [s]	Rt [s]	Width [s]	Ampl. 44 [mV]	Ampl. 45 [mV]	Ampl. 46 [mV]	BGD 44 [mV]	BGD 45 [mV]	BGD 46 [mV]	Area All [Vs]	R 45CO2/44CO2	rR 45CO2/44CO2	rd 45CO2/44CO2 [per mil] vs. LGGE-IMG1	d 45CO2/44CO2 [per mil] vs. VPDB	DeltaDelta 45CO2/44CO2 [‰]	R 46CO2/44CO2	rR 46CO2/44CO2
1	35.1	54.6	26.2	2159	2574	3019	2.0	2.5	3.0	43.019	0.0119186	1.1924248	0.085	-6.583	-	0.0040694	1.3983686
2	86.2	97.0	26.2	2185	2606	3056	2.4	3.0	3.5	43.414	0.0119183	1.1923942	0.059	-6.608	-	0.0040695	1.3984266
3*	136.1	154.4	26.2	2157	2572	3017	2.5	3.1	3.6	42.921	0.0119176	1.1923238	0.000	-6.667	-	0.0040695	1.3984035
4	186.3	197.8	25.9	2167	2608	3059	2.6	3.1	3.6	43.389	0.0119183	1.1924011	0.060	-6.608	-	0.0040699	1.3985660
5	257.9	282.7	12.5	2147	2552	2909	1.9	2.3	2.7	5.504	0.0119056	1.1911367	-1.009	-7.689	-	0.0039491	1.3570247
6	315.3	335.5	25.9	2158	2572	3017	1.5	1.8	1.9	42.821	0.0119186	1.1924495	0.083	-6.584	-	0.0040696	1.3984506
7*	365.1	377.9	26.2	2156	2571	3014	2.4	2.9	3.4	42.973	0.0119176	1.1923562	0.000	-6.667	-	0.0040695	1.3983964

***Fig. 3-5**: chromatogram coming out of the CF-IRMS, with ISODAT 2.0 software*

III.4. Description of the analytical procedure

In the following, our daily procedure including standard gas and sample analysis, as well as their interaction in terms of timing will be discussed, combined with the sample, baths and standard gas bottle preparation. The ensemble of different sub-procedures synchronization is a prerequisite in order to avoid any time loss and to obtain fully comparable results during the integrated sampling period.

III.4.1. preparative steps before analysis

III.4.1.1. system line conception

Fig. 3-6 illustrates the line system, as conceived by J.-V. Lavric.

All system description conducted on the next paragraphs, are based on this figure.

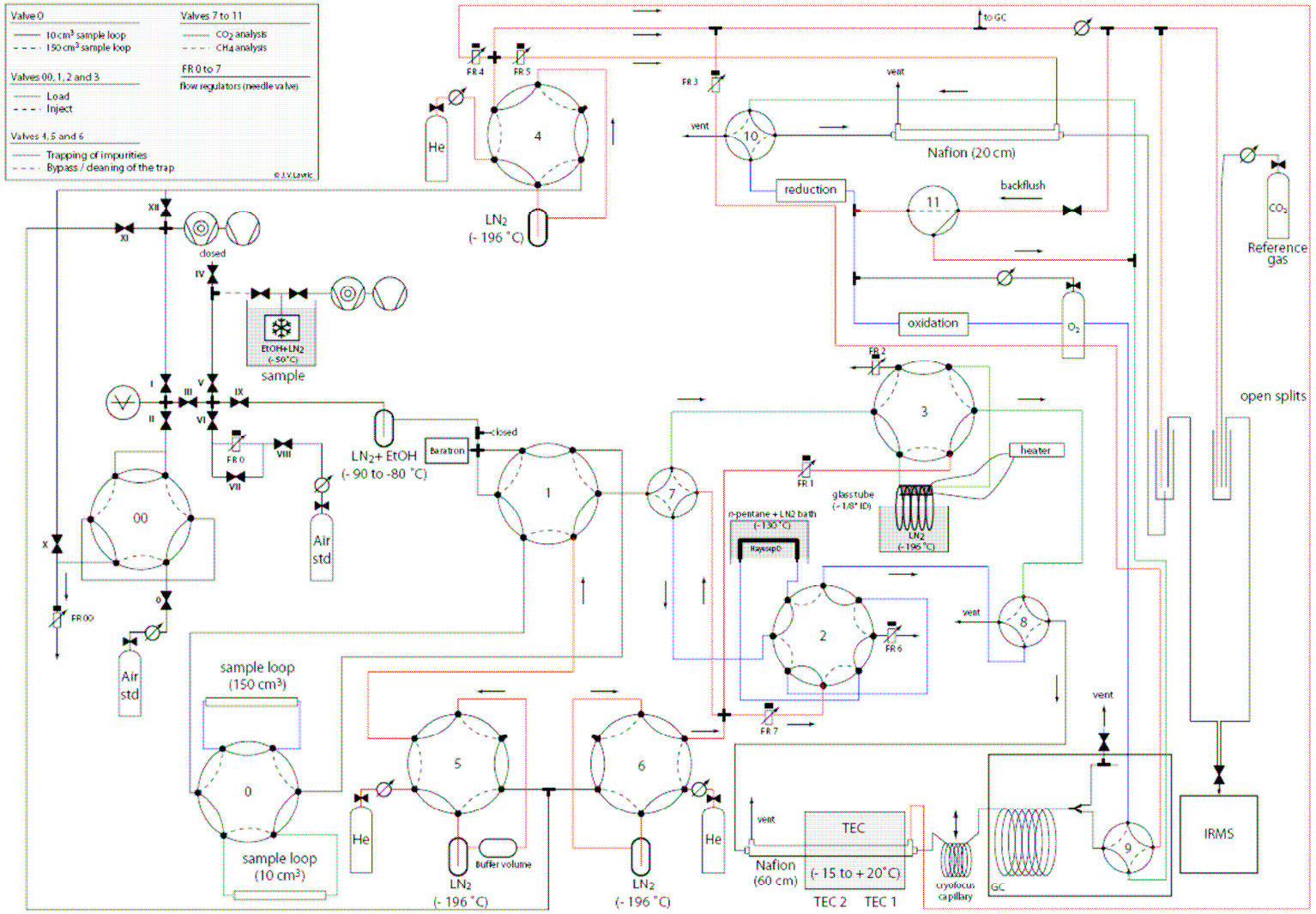

***Fig. 3-6**: ensemble of the experimental set-up, a simplified version provided in fig. 3-3; grey line corresponds to the high vacuumed sample loop area; red line: He flux throughout the system; green line: sample transect for CO_2 analysis; blue line: sample transect for CH_4 analysis*

III.4.1.2. He bottles

Since the analysis part is based on the Continuous Flow principle (*cf. above*), the use of pure He as (1) system 'scavenger' and (2) carrier gas, is requisite. Therefore, three bottles (4, 5 and 6) of ultrapure He (99,9999%, "He 2" AIR LIQUIDE, all remaining trace gases totalling 1 ppmv) are used. He4 is set to 2.7 bars, He5 at 2 bars, while He6 at 3 bars. He5 having the largest flow in the system is additionally purified with a chemical trap online.

Final purification of the He carrier lines (for the pre-concentration, the capillary and GC lines, and the interface / open-split) takes place through three traps cooled at LN2 temperature during measurements. Overnight, these three traps are removed from the main streams (using three bypass valves). Turbo pumps are put in stand-by mode (75% of max speed) to reduce their load. The vacuum lines are kept in "static", *i.e.* with all valves closed to isolate the different volumes from oil vapor in case one of the pumps accidentally shuts down.

Table 3-2 describes the scavenging steps of He bottles used at moments off-analysis

n° He bottle	**Main destination (protocol)**	**scavenging steps (bypass mode)**
4	GC/C - IRMS	*FR4* → Nafion → vent *FR3* → *9* → oxyd. → red. → *10* → vent Backflush (on) → *11* → *9* → vent Backflush (off) → *9* → GC Open split for sample Open split for reference gas *FR5* → Nafion → vent
5	Sample loop	*1* → *7* → *3* → *FR2*
6	Pre-conc.	7 → *2* → *FR6* *FR1* → *3* → *8* → Nafion → cryofocus capillary *FR7* → *2* → *8* → vent

Table 3-2: *scavenging parts when He traps are on 'bypass' mode; numbers denote valves seen in fig. 3-6*

III.4.1.3. entering the lab/ system cleaning

The turbo pumps are set to full speed and then the valves XI and XII (connecting the He traps to the pumps) are opened. This allows the cleaning of the He traps. Opening valve I allows to check the pressure with the Pirani gauge. The He traps pumping lasts at least for 1h30min, until the Pirani gauge reaches its detection limit ($<5*10^{-4}$ mbar). The He traps are then immersed in LN2 and put back in series in the He carrier lines, by closing valves XI and XII and switching the bypass valves to the "trap" status.

III.4.1.4. last steps before analysis

By opening the valves III and IX, the pumping of the line under vacuum (I→ III→ IX→ water vapour trap → {1} → sample loop {0} → {1}) starts. Meanwhile, the FR2 flow is increased from ~9mL/min to 40mL/min and the glass trap connected to the valve 3 is heated (80V applied to the heating wire). The upstream pressure of the reference gas (in the **GC/C**[8] interface) is adjusted to 1.3 bar, in order to have comparable first day signals. The upstream He pressure of the GC/C interface remains unchanged at 1 bar. Daily cleaning of the external reference gas line is performed while cold baths are prepared (table 3-3); valves VI and VIII are left open for pumping (during the opening of the standard gas bottle, valve IX remains closed, for security reasons). Flushing of the entire reference gas line takes place three times. The CSIRO tank is then kept fully open during analysis. The changeover valve of the IRMS is activated to shift into CF mode into the source. The emission of the IRMS source is set to maximum (1.48 mA, whereas it is kept at 0.1 mA overnight to save on filament lifetime) and the signals m/z 40 (Ar→ leak indicator), 18 (water vapour) and 44-45-46 ($^{12}CO_2$, $^{13}CO_2$, ^{18}O-CO_2) are measured with the resistance at $3*10^{10}$ Ω. The main analytical protocol can then start.

bath purpose	components	temperature
He trap	LN2	-196°C
water vapor trap	C_2H_5OH + LN2	~-80°C
heated glass trap	LN2	-196°C
cryofocus capillary	LN2	-196°C
sample bath	C_2H_5OH + LN2	~-65°C

Table 3-3: *baths prepared for analytical protocol;, including a picture of introducing LN2 in C_2H_5OH bath*

III.4.2. Strictly time-dependent procedure

In order to minimize the degrees of freedom in the analytical procedure, the steps below are followed with a chronometer. This is particularly critical regarding the time spent between ionization of consecutive samples/standards, as there can be small memory effects associated with the GC column and the slow degassing of the interface capillaries.

[8] Gas Chromatograph/Combustion interface, the latter used for CH_4 analysis (*cf. fig. 3-6*)

III.4.2.1. External standard gas and blank procedure

Table 3-4 shows the time-dependent evolution of the (external) standard gas, while this of the blank differentiates in omitting the step of any gas introduction to the system (underlined parts)

Time (min:s)	step	comments
0:00	Close valves III and I	Gas equilibration in the closed sample loop-*1* system over 1 min
	Inject st. gas to the line/ <u>omit</u>	
	P stabilized in baratron/ <u>omit</u>	
0:10 (max)	Plunge heated glass trap in LN2	
1:00	v. *1*→ inject	He 5 transfers the air from the sample loop to the glass trap
	Open valves III and I	
2:00	Submerge cryofocus capillary in LN2	
3:00	v.*3*→ inject and v.*1*→ load	He 5 cleans the vacuum line; He 6 goes through the glass trap
3:15	Withdraw LN2 from heated trap	He 6 carries sample through the cryofocus capillary
	Pre-concentration lasts >12min	
9:20 (max)	Adjust reference gas pressure vs. expected amplitude 44	
17:30	Launch ISODAT sequence	
18:20	Withdraw LN2 from cryofocus capillary and v.*3*→ load mode	
18:40	ISODAT sequence start-up	
~22:40	St. gas peak elutes in the spectrogram	
~25:40	End of sequence	

Table 3-4: *time-dependent st. gas injection and evolution through time; blank test included*

III.4.2.2. Ice sample

The acquisition procedure of the ice sample expanded to the pre-concentration line is identical to this for the st. gas, with the exception of the initial equilibration time. Table 3-5 highlights this difference of the air sample treatment, always based on the general fig. 3-6 scheme.

Time (min:s)	step
0:00	Close valve VI
	Close valves III and I
	Stop pumping on the ice mill line
	Open valve V
	Open ice mill valve → sample gas expansion
	P stabilized in sample loop over 3 mn
2:10 (max)	Plunge heated glass trap in LN2
3:00	v.*1*→ inject
	close valve V
	Close ice mill valve
	Open valves III and I
	Open valve connecting ice mill to pump
4:00 …	Submerge cryofocus capillary in LN2….

Table 3-5: *time-dependent protocol for sample treatment (main differences from st. gas)*

III.4.2.3. Synthesis

The daily procedure consists of the combination of the above separate processes. Table 3-6 represents the case of analyzing one ice sample.

min	procedure	related section	duration
	Pumping He-traps (front line) Pumping sample (back) line LN2 tank and traps refilling Ice sample selection	*III.4.1.3*	1h 30 min
90	He-carrier contaminants trapping Opening st. gas Changing He fluxes, adjusting ref. gas Cold baths preparation Opening and checking MS signal	*III.4.1.3;* *III. 4.1.4*	60 min
150	Blank1 Sample preparation in cold room	*III.4.2.1* *III.3.2*	26 min
176	St. gas 1 Cooled sample connected online Pumping on sample cell	*III.4.2.1* *III.3.4*	26 min
202	St. gas 2	*III.4.2.1*	26 min
228	St. gas 3	*III.4.2.1*	26 min
254	St. gas 4 Disconnecting ice mill Ice grinding	*III.4.2.1* *III.3.3*	26 min
280	St. gas 5 Re-connect cooled sample online Pumping on connection	*III.4.2.1* *III.3.3*	26 min
306	1st sample expansion	*III.4.2.2*	28 min
334	2nd sample expansion	*III.4.2.2*	28 min
362	St. gas 6	*III.4.2.1*	26 min
388	3rd sample expansion	*III.4.2.2*	28 min
416	St. gas 7	*III.4.2.1*	26 min
442	Blank 2	*III.4.2.1*	26 min
468	end		

Table 3-6: *Synthesis of the daily protocol schedule; case of one ice sampling*

We proceeded to 5 standard gas injections (of different amounts, *i.e.* different pressure reading with the Baratron, from ~7 to ~16 mbar, translating into 0.8 to 1.9 nmol of CO_2 in air) in order to plot the calibration curve used to calculate the sample CO_2 mixing ratios. The amount of standard gas introduced for each calibration point does not always follow the same order, to avoid systematic biases.

The full processing of a standard gas injection takes 26 min, and 28 min for the sample. But preparation of the next standard or sample can take place while the ISODAT sequence of the

current standard or sample is running, thus saving a few minutes. Therefore, the total time-span for measuring one ice core sample (of 7.8h) given in table 3-6 is slightly less in reality, which permits in some cases to proceed to a second sample analysis during the same day *(cf. next section & Ch. V)*.

III.4.3. Protocol changes through time (2006 vs. 2007-8)

- during the first PhD year, the flow-restriction valve was manipulated manually. Therefore, care was taken in order to inject gas with a reproducible flux, independently from the gas amount, to avoid fractionation biases. Being aware of the sensitivity of this valve, in 2007 we proceeded to a different system structure, by maintaining the flow-restriction valve in a fixed position implying a fixed flow rate, while the total amount of injected gas was controlled by the adjacent on/off valves (difference illustrated in fig. 3-7)

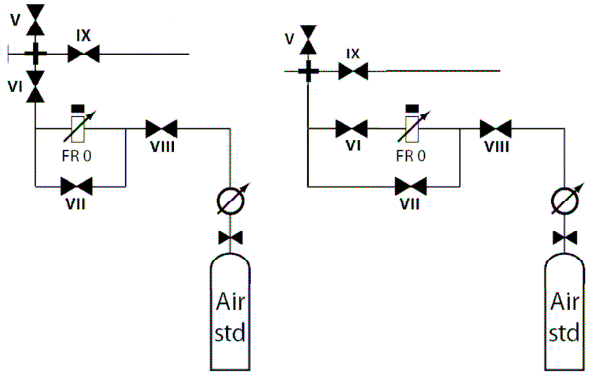

Fig. 3-7: *simple figure of the difference between 2006 (left) and 2008 (right) configurations on st. gas injection to the line*

- valves XI and XII that connect the pump with He trap, were reduced to only valve XII in 2008
- alteration of fixation axis from the ice crusher, potentially affecting the miling efficiency throughout 2008
- re-configuration of the MS tuning, leading to slightly better sensitivity
- in 2008, the pumping on He-traps was done overnight, in order to save time for more sample analysis (*vs.* the 1.5h spent in 2006); effectively, in 2008 measurements of two samples per day were systematically accomplished, whereas in 2006 only 1 sample/day was analyzed.
- ISODAT sequence configuration: the pure CO_2 reference gas coming out 30 s after the standard/sample peak elutes together with the GC eluents and corresponding

background ("backflush off), whereas in 2006 it eluted in "backflush on" mode (background corresponding only to the He from the interface).

III.4.3.1. Direct applications

The above protocol changes may be depicted in the analytical results. Below, a first intercomparison between the two major sampling periods will be exposed.

Peak amplitude and areas as a function of standard gas pressure

Fig. 3-8 represents the relationship between injected pressure of standard gas and the obtained amplitude (mV) and area (V*sec) for the two major analytical periods (*cf.* table 3-7 for calendar details)

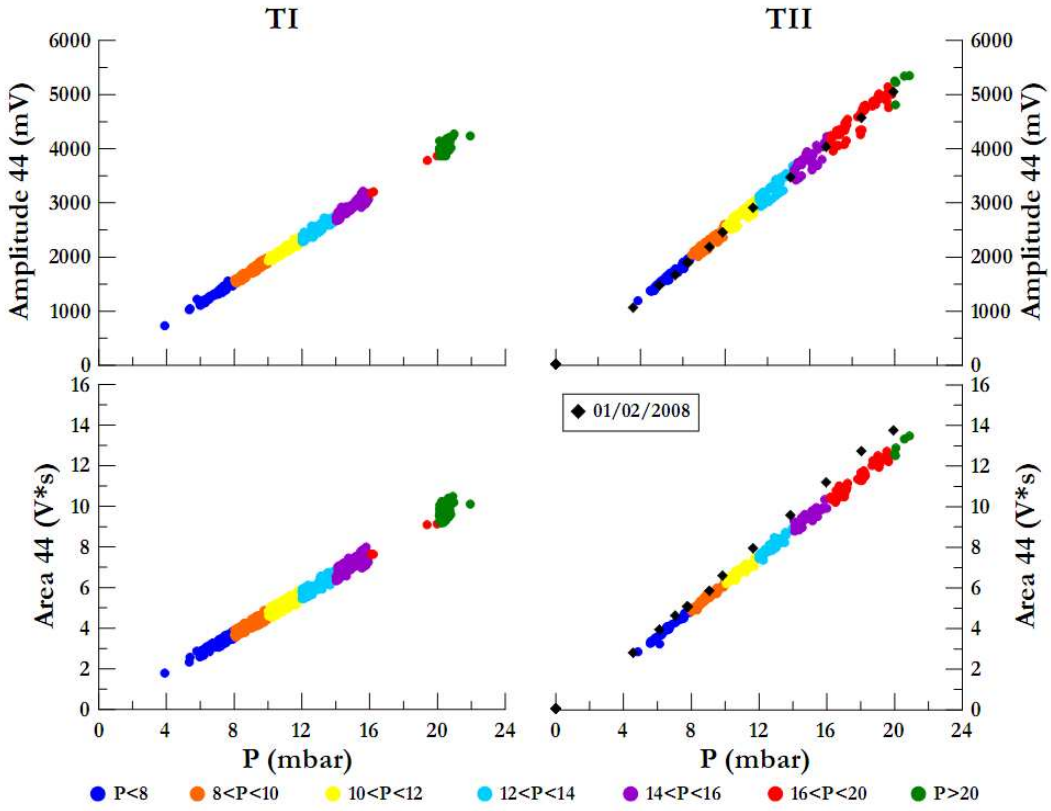

Fig. 3-8: *P of injected st. gas vs Amplitude (upper plots) and Area (lower plots) for all st. gas injections throughout TI (left panel) and TII (right panel); an exceptional day with a great P amplitude (**01/02/2008**) is superposed to the equivalent sampling period*

For both periods, a nice linear relationship shows up. Some differences can still be detected:

- P against amplitude is better correlated for TI, while for TII, area correlates better with the injected P than TI. Still, amplitude-deduced calibrations were better for both sampling

periods (R^2=0.999), thus permitting in calculating CO_2 mixing ratio for both cases in exactly the same way *(cf. below)*

- The slope of both peak amplitude and area as a function of P is larger for TII analyses than TI (Δamplitude of 4V for TI against 4.5V for TII, Δarea of 8V*sec for TI against 12V*sec for TII).

A possible explanation for this difference lies in the MS tuning for better sensitivity in 2008.

CO_2 concentration measurements

The MS response to given CO_2 peaks provides CO_2 mixing ratios, using two approaches:

- based on the sample m/z 44 area (Ferretti et al., 2000; Ribas-Carbo et al., 2002; Kawamura et al., 2003; Schnyder et al., 2004)
- based on the sample m/z 44 amplitude (Leuenberger et al., 2003; Eyer, 2004)

CO_2 is calculated by applying the following equation:

$$CO_{2,sample} = \frac{pCO_{2,sample}}{P_{sample}} \tag{3-2}$$

with

$$pCO_{2,sample} = \frac{i_{sample} \times P_{st.gas}}{i_{st.gas}} \times [CO_2]_{st.gas} \tag{3-3}$$

so

$$CO_{2,sample} = \frac{i_{sample} \times P_{st.gas}}{P_{sample} \times i_{st.gas}} \times CO_{2,st.gas} \tag{3-4}$$

$\boldsymbol{CO_{2,\,sample}}$ and $\boldsymbol{CO_{2,\,st.gas}}$ denoting the respective CO_2 mixing ratios (ppmv) of the ice sample and the standard gas; $\boldsymbol{i_{sample}}$ and $\boldsymbol{i_{st.\,gas}}$ the respective ion current amplitudes of m/z 44 for the sample and standard gas; $\boldsymbol{P_{sample}}$ and $\boldsymbol{P_{st.\,gas}}$ the pressure reading of the expanded air with the baratron gauge

An equivalent equation was applied for measuring CO_2 against area, by replacing i (amplitude) with A (Area). The results for both kinds of calculations are presented in fig. 3-9 for the two main sampling periods.

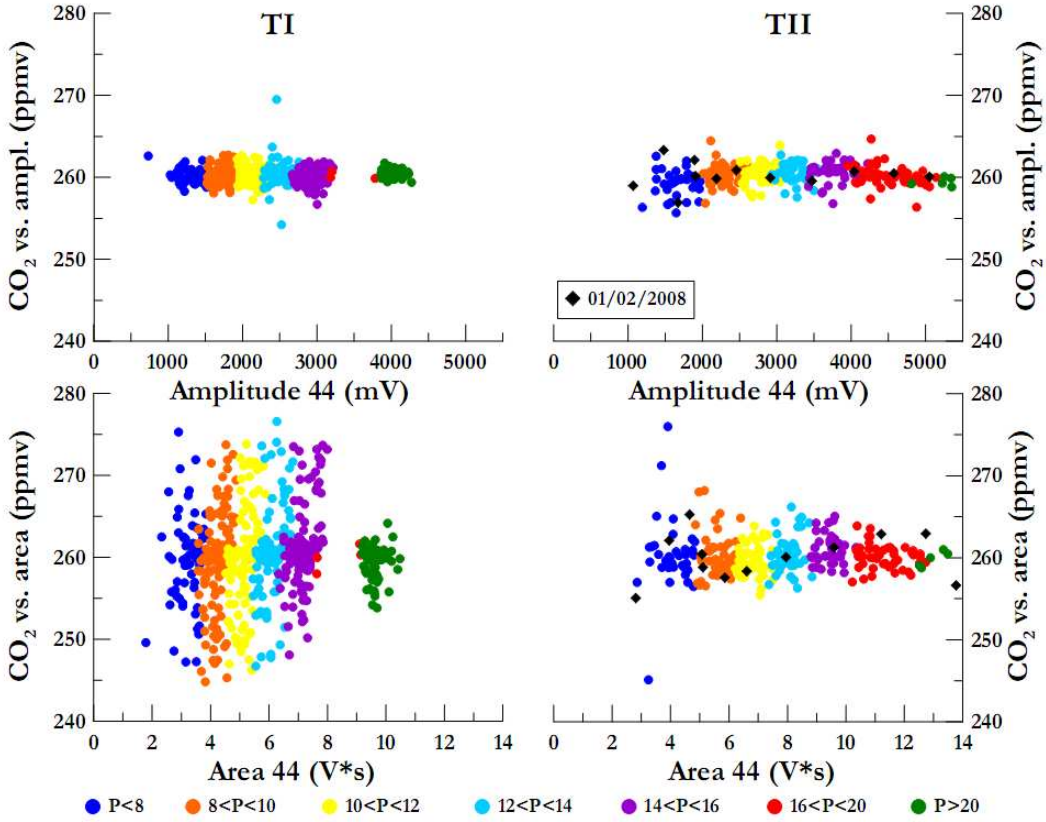

Fig. 3-9: *calculated st. gas CO_2 vs amplitude (upper plots) and area (lower plots) for all st. gas injections throughout TI (left panel) and TII (right panel); an exceptional day with a great P amplitude (**01/02/2008**) is superposed to the equivalent sampling period*

From the Fig. 3-9 it appears that during the TI analytical period CO_2 calculated vs. Area is highly scattered compared with CO_2 vs. Amplitude, and this difference disappears during the TII analytical period, which is also attributed to the updated MS tuning.

III.5. Corrections applied

III.5.1. Corrections by the IRMS software

In order to internationally derive referenced $\delta^{13}C$ values from the three ion current signals m/z 44, m/z 45 and m/z 46, two basic steps are required:

- background correction from the ion currents
- $\delta^{17}O$ correction

The above steps are performed using the Finnigan software package ISODAT NT 2.0, with which the CF-IRMS system is operated. As long as the isotope ratios are at natural abundance, the ^{13}C trace always tracks the ^{12}C at a level of 1.1%, irrespective of the source of the CO_2, be it due to samples, artefacts or chemical noise from column bleed. But the m/z ratios show a

prominent S-shaped signal for each peak. The m/z 45 and m/z 46 signals precede the m/z 44 one by roughly 100ms (depending on GC flow rate, temperature, column state *etc.*), because of preferential absorption of the light isotopologue on the column stationary phase. Thus, the maxima of the three m/z traces is shifted by the software to align them and to avoid bias in the delta calculation due to different peak start and end for the three traces.

III.5.1.1. background correction from the ion currents

The background m/z signal needed to calculate each peak amplitude and area is considered as "individual background" for the subsequent peak : the minimum running average of five points among the 20 points preceding peak detection gives the corresponding background value.

III.5.1.2. $\delta^{17}O$ correction:

The precise measurement of isotope ratios is often hampered by interfering ion currents from other species also hitting the Faraday cup detectors. The prominent case in our application is the contribution of isobaric $^{12}C^{16}O^{17}O^{+\cdot}$ ion current at m/z 45, constituting an isobaric interference for $^{13}CO_2$. In our case, the Santrock et al., 1985 correction is applied.

III.5.2. Other corrections

III.5.2.1. drift corrections

Drifts as a function of time are variations observed within an experimental day, on time scales from minutes to hours, affecting the isotopic measurements. Drifts can have multiple causes, such as (i) room temperature and pressure changes; (ii) the isotope change of a reference gas during an analysis sequence; (iii) build-up of water or other contaminants, such as ice accumulation in the cold trap or water vapour condensation on the tubing surface; (iv) surface desorption and absorption processes (memory effects); (v) changing conditions of mass spectrometer and more unknown events (Werner and Brand, 2001a; Huber et al., 2003).

Such drifts are corrected linearly between two standard measurements; therefore, frequent standard measurements improve accuracy. Still, multiple standard peaks allow for a more efficient drift correction and more importantly, evaluation of the quality of a single measurement (Brand, 1996). In the laboratory, air conditioning is set to ~20°C in order to reduce drifts. Still, in the course of a sample run, small temperature rise of (i) the room, (ii) the water vapour trap and (iii) the sample bath, coincide with an increased signal of m/z 18 (water vapour) which could be a potential daily drifts generator.

Analyses of equal amounts of standard gas at the beginning and at the end of the full experimental procedure shows no obvious trend. The bracketing of sample aliquots with standard gas aliquots reduces the effect of any instrumental drift that may occur during the analysis period.

III.5.2.2. linearity corrections

A second feature encountered in IRMS applications is the isotopic ratio dependence from the peak intensity, *i.e.* the amount of introduced gas in the ion source. This is generally called "linearity" effect. It is more properly called as "amount dependency effect" (J. Schmitt, *pers. comm.*), since the relation of $\delta^{13}C$ with peak intensity is exponential (Hall et al., 1999).

A weak trend towards more ^{13}C- and ^{18}O- depleted values was systematically observed when introducing smaller standard gas amounts to the sample loop (*i.e.* decreasing gas pressure, *cf. fig. 3-10 left panel*). Until 2 V (corresponding to ~10mbar of introduced gas) there is no visual linearity effect; below 2 V, though, (and down to 1V *i.e.* ~5 mbar of st. gas), this effect becomes significant and corrections should be applied. The standard gas amplitude ranges from ~750 mV (introduced P≈ 3.6 mbar) to ~4300 mV (for a P of ~21 mbar).

In our protocol, we considered non-linearity biases and corrected every sample peak against a standard gas peak of a similar amplitude, injected immediately after the sample.

Another correction strategy for linearity effect, was proposed by Hall et al., 1999, who defined a logarithmic relationship between the $\delta^{13}C$ value and the peak amplitude (intensity of m/z 44):

$$\delta^{13}C_{corr} = \delta^{13}C_{raw} - m \times \ln(i_{44}) + c \qquad (3\text{-}5)$$

with $\boldsymbol{\delta^{13}C_{corr}}$ the corrected $\delta^{13}C$ values, $\boldsymbol{\delta^{13}C_{raw}}$ the raw values from IRMS, $\boldsymbol{m}$ and $\boldsymbol{c}$ the polynomial coefficients, while $\boldsymbol{I_{44}}$ the peak intensity (maximum amplitude in mV).

When applying this second correction to the ensemble of our standard gas results for the TI sampling period[9], the decreasing trend for both isotopes vanishes (Fig. 3-10 *right panel*).

Therefore, an application of both "amount-dependent corrections" was proceeded to a limited number of samples. The small population tested showed the unanimous ameliorated $\delta^{13}C$ sigma – of max. 0.2‰- for the standard gases, when the eq. 3-5 was applied (as the right panel of fig. 3-10 proposed). Still, the complete application of both corrections to the obtained sample values gave no major differences between the two correction types. This correction intercomparison has been additionally applied for the first results from Vostok ice and is shown in table 3-8 of III.7-2

[9] to be more precise, we applied the correction to the total mean value, as calculated from the ensemble of the injections

section. No general amelioration of the obtained sigma was observed for the proposed correction of Hall et al., 1999, while the mean values (over the three expansions) remain in the same level.

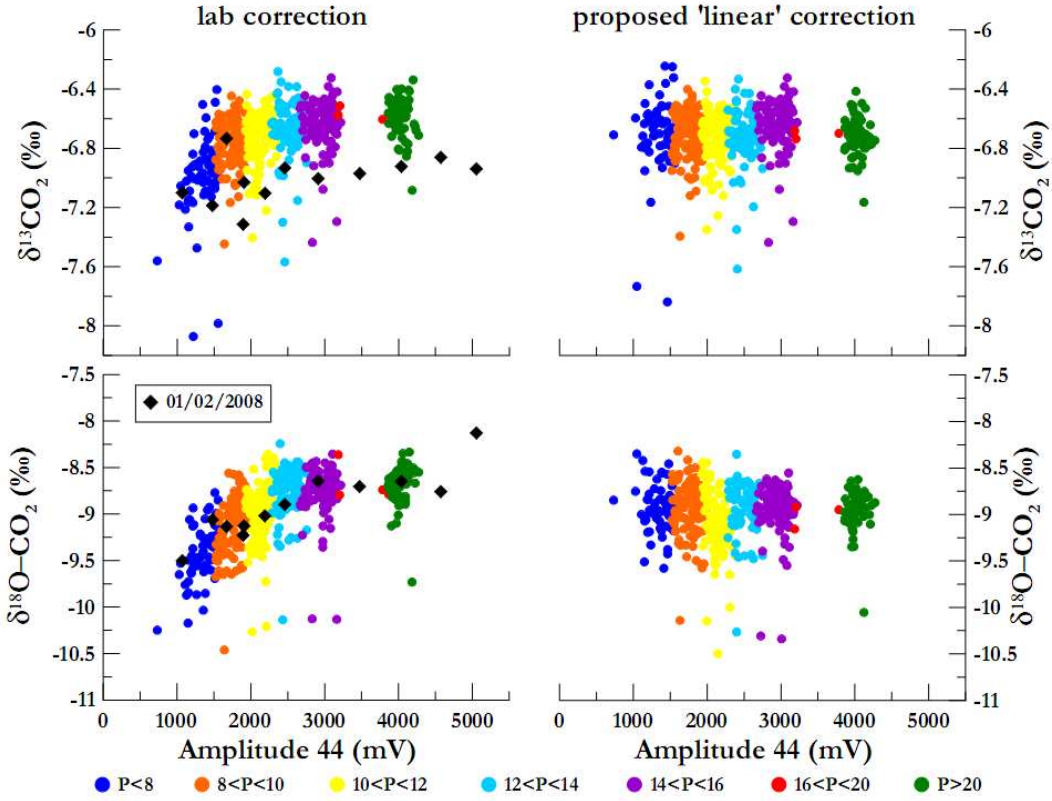

Fig. 3-10: *evolution of st. gas $\delta^{13}CO_2$ (upper plots) and $\delta^{18}O$-CO_2 (lower plots) against amplitude 44, for the ensemble of TI sampling period. For intercomparison reasons, results from a single day, belonging to TII, are superposed. Both sets of plots are juxtaposed by the proposed linear correction from Hall et al., 1999*

The above points to the validity of the linearity correction applied in the first place in LGGE.

III.5.2.3. N_2O correction

N_2O is isobaric to CO_2. Within the ion source of IRMS m/z of 44, 45 and 46 are also produced for the case of N_2O, but with different isotopic ratios than CO_2. This requires a specific correction based on the expected concentration of N_2O, the ratio of CO_2/N_2O ionization efficiency in the MS, and the expected N_2O isotopic ratio. Eyer, 2004 reported a constant value for EDML data during Holocene of ~0.23‰.

Ghosh and Brand, 2003 highlighted the efficiency of using coupled GC-IRMS in separating CO_2 from N_2O in case of requiring quantification of the stable isotopes of CO_2, which was first applied by Ferretti et al., 2000. The CO_2 peak entering the ion source has almost a Gaussian shape and N_2O resides on the tail of the much larger (of 1000 times) CO_2 peak; in our case, the use of a long Poparak-Q column, and a small He flow of 3 mL/min, seem to resolve the separation problem. Therefore no N_2O correction is applied to our measurements.

III.6. Procedure validation with blank tests and reference gas standards

III.6.1. Laboratory calendar

Table 3-7 exposes the calendar with the main sampling periods, the majority of which will be provided in this study.

Time period	Measuring period	People involved	Days after 15-03-2006
Vostok sample test	March 2006	Jost + Anna	0-10
TI	April – November 2006	Anna	20 - 233
EPICA Gas intercomparison	September 2007	Anna + Hinrich	539 - 557
Last 1000 years	October 2007 – February 2008	Hinrich + Anna	566 - 690
AIM 12 *part I*	February 2008	Anna	691 - 704
AIM 12 *part II*	March – June 2008	Hinrich	718 - 827
EPICA Ice intercomparison			
TII	(3 points in November 2006) February – May 2008	Anna	(205 – 207) 705 - 785

Table 3-7*: time-related overview of performed analysisthroughout this PhD*

III.6.2. Results from standard gases

In order to evaluate the new experimental procedure, the following parameters are considered of primary importance: (a) the reproducibility of repeated measurements on a given standard gas, (b) the absolute accuracy or deviation of the measured values against the expected one, (c) the blank tests of the overall procedure on artificial bubble-free ice (**BFI**).

III.6.2.1. Standard gases-protocol reproducibility and accuracy

In our measuring procedure two standard gases are involved: the internal pure CO_2 standard gas and the external standard gas (CO_2 in air).

The **internal standard gas** (*reference* or *working* gas) is an ATMO MESSER pure CO_2 standard with $\delta^{13}C$ value of -6.475±0.1‰ versus V-PDB[10]. The working gas is directly injected into the open split, without following the whole pre-concentration trajectory.

[10] value determined by comparison with GS-19 and GS-20 pure CO_2 standards, through dual-inlet measurements at LGGE by J.V. Lavric

The chromatogram exited from the MS and already shown in fig. 3-5, explains the sequence of internal standard gas introduction, interrupted by the sample or external standard gas peak. The $^{13}C/^{12}C$ ratio of the fourth internal standard gas peak is considered as the reference for δ calculations, as it immediately leads the peak of interest, with the same background conditions. Its attributed value is –6.475‰ (internal standard value), and is very close to the external standard gas value (-6.40‰). Still, in case the 4th internal standard gas peak provides a weird value, we then choose another reference peak or eventually two peaks (fig. 3-5, lower panel when we considered the 3rd and 7th peak as reference peaks). This concerns only 5% of the overall measurements.

The **external standard gas** –named CSIRO 1677- (referred to as *standard gas* or *Keeling standard*) was prepared at CSIRO, Australia in spring 1995 (Haan, 1996), and checked at CSIRO over a period of five years for any possible drift, before being shipped to LGGE. Its final CO_2 value is 260.26 ± 0.2 ppmv (on the **WMO**[11] CO_2 mole fraction scale) and $\delta^{13}CO_2$= –6.40±0.03 ‰ versus VPDB (CG92 scale). It is used for daily system calibrations and for blank tests.

During the 3-year PhD interval, both standard gases remained unchanged; this allows for a time-based evaluation of (i) CO_2-against amplitude- values, (ii) CO_2-against area- values, (iii) $\delta^{13}CO_2$ and (iv) $\delta^{18}O$-CO_2, with respect to the assigned external standard gas values. Such an application on TI and TII periods is exposed in fig. 3-11 with blue and green points, respectively.

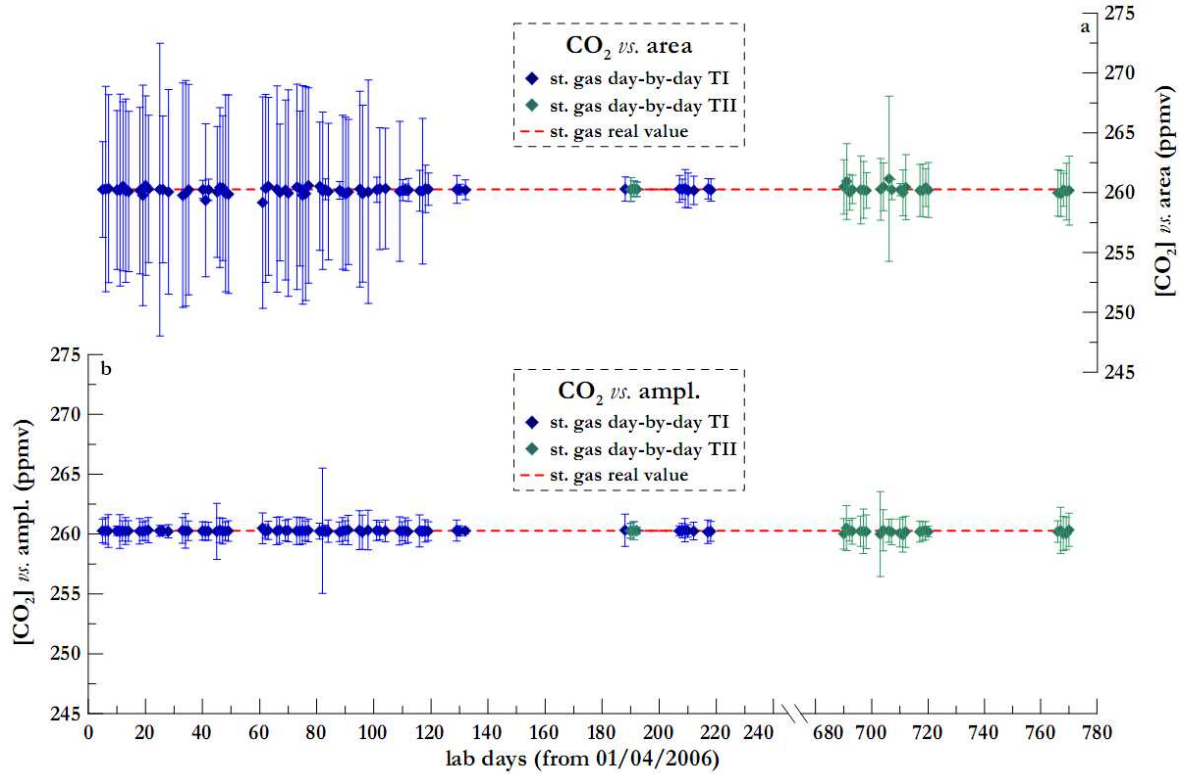

[11] World Meteorological Organization

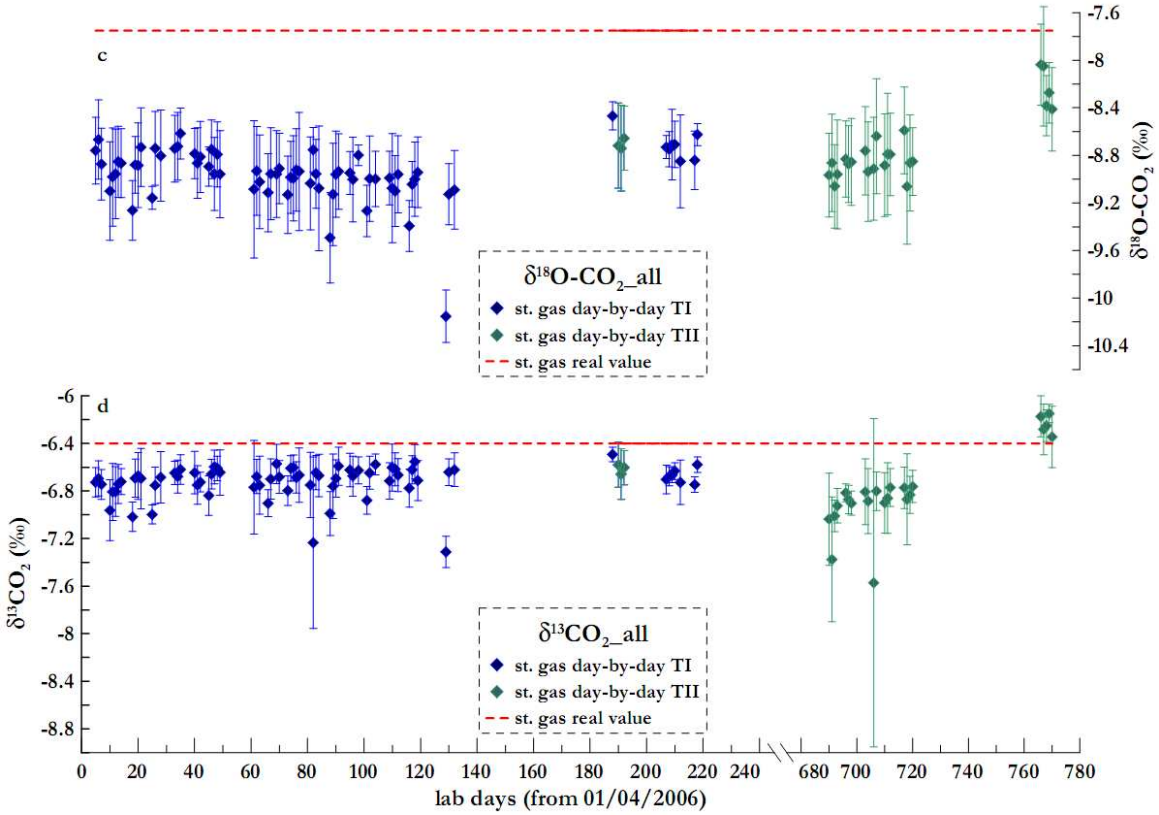

Fig. 3-11: *day-to-day evolution for the st. gas for TI (blue) and TII (green) sampling periods on a. CO_2 vs.area; b. CO_2 vs.amplitude; c. $\delta^{18}O$-CO_2 and d. $\delta^{13}CO_2$.*

The following problematic days were detected for TI: (1) on day 82, CO_2-vs.-amplitude mean value being coincident to the true one, the standard deviation is more than 5-fold higher than usually; the same day $\delta^{13}C$ was found depleted by -0.835‰ vs. the real standard gas value. The reason lies in the liquid nitrogen He trap damage during the experimental procedure; still, $\delta^{18}O$ curiously experiences very reproducible values, being closer than the rest to the "real" $\delta^{18}O$ values.(2) on day 129, both isotope values are found very depleted (by 0.913 and 2.402 ‰, for $\delta^{13}C$ and $\delta^{18}O$ respectively; this was most probably the effect of a summer week off, leaving the MS on static state; the following day values returned to their 'normal' levels. We consider having sufficiently corrected for the sample values, as the 'unknown' isotope values were also found negative compared to adjacent samples. The worst experimental day for TII was the day 706, where the upper limits of area-deduced CO_2 mixing ratio enrichment was simultaneously found more ^{13}C-depleted, in parallel with a greatest σ for area-deduced CO_2 and $\delta^{13}C$. A logical explanation on terms of analytical procedure cannot be provided, as nothing weird occurred this day; we conclude to the human-dependence of our protocol to be the potential reason, since the previous day another experimentalist was measuring in the lab

Termination I

At a glance, we deduce that :

- the variance around the mean CO_2 mixing ratio is more than 5-fold larger when using the area instead of the amplitude of the external standard peaks,
- a negative shift is observed for the case of isotopic ratios, with a mean deviation of –0.31‰ and –1.19‰ for $\delta^{13}C$ and $\delta^{18}O$, respectively

- no obvious trend throughout the 8-month analysis period is observed for the two isotopic ratios, nor for the variance of CO_2 mixing ratio, implying no analytical setup shift.

Termination II

Some differences took place in the analytical procedure and tuning, compared to 2006 (*cf. section III.4.3).* A main difference from 2006 is that in 2008 two samples per day were analyzed, as the 90min initial pumping was conducted during the previous night. Moreover, water vapour and blank signals were found elevated in 2008 compared to 2006 *(cf. section III.6.3.1.).* This is coherent with the more important sample through-put, reducing the time for the system to get back to background vacuum and trace concentrations in the vacuum and helium lines. Here we discuss the protocol change imprint on the st. gas evolution throughout the main sampling periods, considering their 2 years time-lap:

- the most eye-catching difference concerns the decreased variance of standard gas CO_2 calculations based on peak area, compared with 2006 (fig. 3-11a). The σ-scatter decreases by a factor of ~2.5. The opposite is observed for the amplitude-effect, as the σ increases by a factor of ~1.3 against the 2006 result (fig. 3-11b). This results from MS tuning changes.

- the isotopes of the standard gas during TII present some differences in behaviour when compared to the TI-period results. A trend towards more ^{13}C- and ^{18}O-enriched values is detected at the end of the analysis period, after a month pause (fig. 3-11c;d).

- the mean σ for both isotopes gets higher in 2008 (by 0.09‰ for ^{13}C and 0.08‰ for ^{18}O), when compared to 2006; an initial 0.53‰-^{13}C (fig. 3-11d) and 1.11‰-^{18}O (fig. 3-11c) depletion during the first analysis time-slice (*defined above*) is observed, followed by a 0.16‰ enrichment of ^{13}C and a 0.48‰ of ^{18}O.

III.6.3. Results from blank measurements

The following 'blank tests' were conducted throughout the analysis days at irregular intervals in order to detect potential problems on different experimental parts:

III.6.3.1. no gas injection in the line ($P_{initial}$=0)

We proceeded to this blank type (*cf.* table 3-4) in order to detect any leak or contamination in the pre-concentration and analysis part, by omitting any gas introduction in the system.

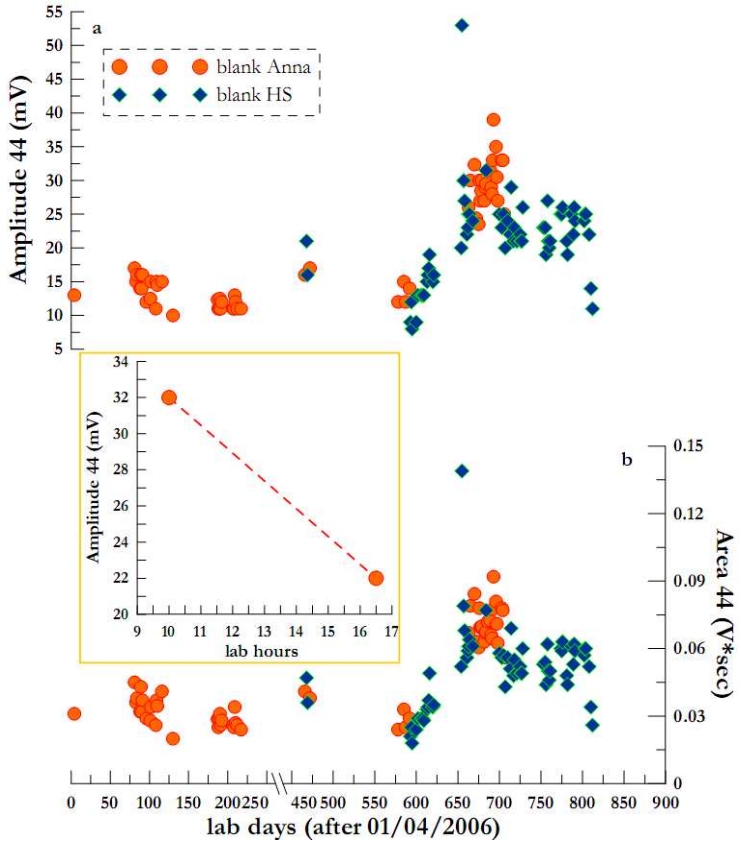

Fig. 3-12: *day-to-day blank (P=0) evolution of (a) amplitude; (b) area 44 during the PhD thesis; Anna and HS's manipulations represented differently. Yellow framed case in-between graphs: signal reduction throughout time during the same sampling day, showing the system amelioration*

Fig. 3-12 presents (a) the amplitude and (b) area *m/z* 44 results for the years 2006-2008. A signal increase occurred around day 650; deterioration throughout time is therefore observed, possibly due to the increase sample through-put, or increased sensitivity of the MS. The background stays at quite low levels, representing 0.48 to 2.2% of the max and min Ampl.44 values of typical external standard and sample injections (corresponding to P of 21 and 5 mbar), compared to 0.33 to 1.7% for the 2006 period. Additionally, when measuring a blank twice a day –often in 2008-, a signal lessening is observed, implying that the contamination is decreased by sample processing throughout the analytical line *(yellow frame in fig. 3-12)*. Werner and Brand, 2001a applied a mass balance equation, involving the average peak area (V*sec) and δ-value (‰) of the blank measurement for quantification and correction of blank contribution:

$$\delta^{13}C_{total} \times area_{total} = \delta^{13}C_{sample} \times area_{sample} + \delta^{13}C_{blank} \times area_{blank} \quad (3\text{-}6)$$

They deduce that this correction is very small. No such correction was applied in this study, as the significance of a $\delta^{13}C$ value obtained on such blank is hampered by the non-linearity of the

MS and the uncertainty due to signal amplitude lies well inside the shot-noise limit of the Faraday cups.

III.6.3.2. using ext. standard gas as unknown

This kind of test was effectuated in order to check for fractionation sources in the front part of the pre-concentration line. Moreover, this test permits us to verify the real external standard gas value through our system, by linearly correcting the 'unknown' gas (*cf.* III.5.2.2). The results are presented in the fig. 3-13, conducted by 2 different experimentalists (as different colours):

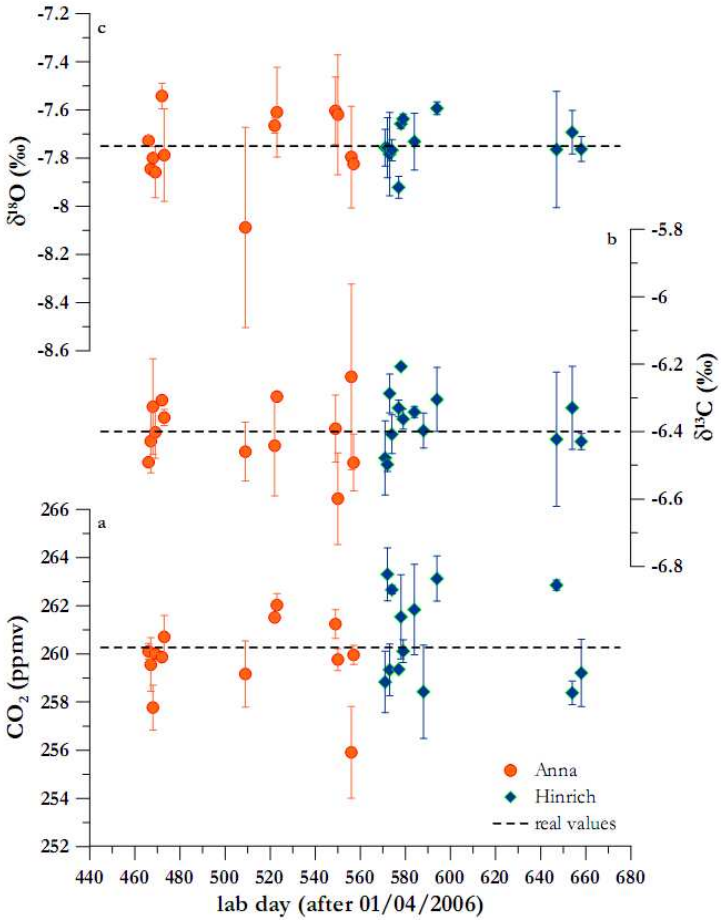

Fig. 3-13: *results from the test when the "standard gas = unknown" (Anna and HS)*

From the above figure, the results are rather satisfying for the following two reasons: (i) the mean values are close to the real mean value (within the error bars) for most of the cases and (ii) no obvious trend exists throughout the sampling period. From the above, we deduce that the correction linearily applied erased any fractionation trends one sees in the raw st. gas values.

III.6.3.3. using an empty cell/ ice mill

Results provided by an empty cell were furthermore tested, maintained at similar temperatures as our sample, into which a known amount of standard gas (in terms of pressure) is introduced. The

whole system does not undergo grinding. Thus it differs from the real sample treatment. Still, this test allows to quantify any possible fractionation when expanding a known gas from the cold cell to the sample loop. Fig. 3-14 shows results from this test. Despite the small test number (n=5), we can still conclude on the absence of trend for all examined variables.

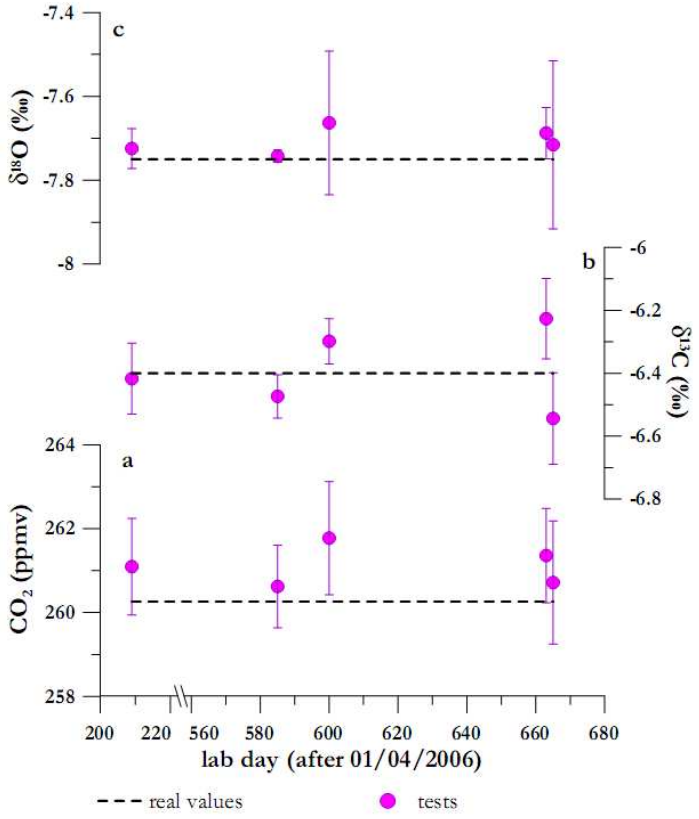

Fig. 3-14: *empty cell 'test' results on (a) CO_2; (b) $\delta^{13}CO_2$ and (c) $\delta^{18}O$-CO_2*

note for the superstitious:

Throughout the sampling period, five ice mills were available for analysis; we consciously preferred a specific ice mill among the five: the #5. Fig. 3-15 shows an intercomparison test performed between empty #5 (of our preference) and #1 mills. These results, combined to our initial results in April 2006 (where those provided from mill #1 were systematically more scattered than those of mill #5), adequately justify our preference for the above-mentioned one and only #5.

This kind of ice mill efficiency discrepancy has been mentioned before (Barnola et al., 1987). This is clearly attributed to some details of the mill manufacturing. We speculate that it has to do with the thread of the plug fitted to the mill cover. This thread is more or less loose from one mill to another, and the efficiency of pumping on the small volume of air located around the thread may thus vary, and thus may let a variable and very small amount of ambient air contaminants in the dead volume. This air would then be released in the dead volume when the ice mill (and thus the thread) is put under strain during grinding,

thus contaminating with a varying amplitude the signal out of the ice core sample.

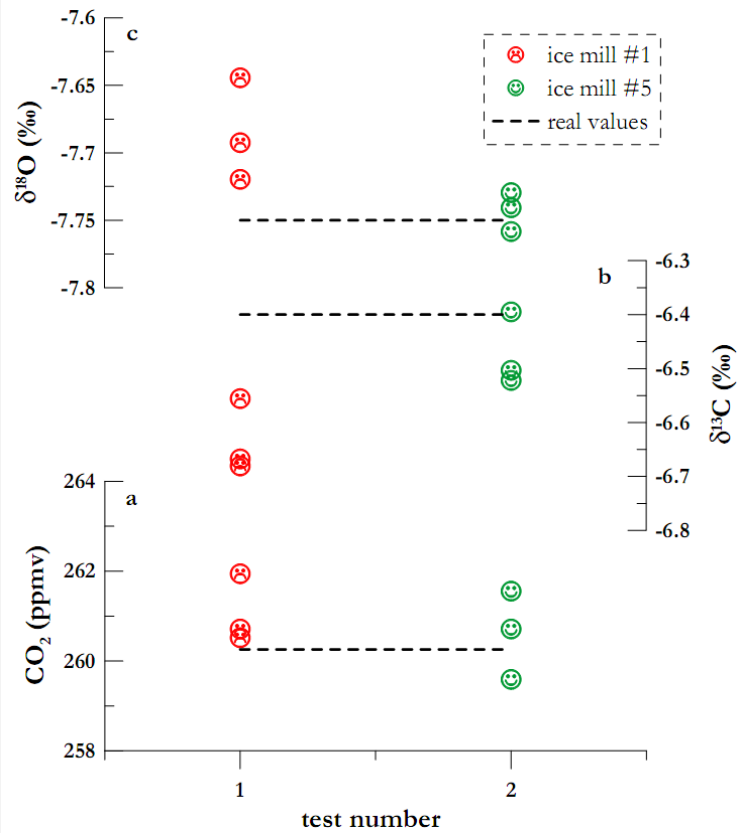

Fig. 3-15: *different #ice mill test results from 06/11/07 on (a) CO_2; (b) $\delta^{13}CO_2$ and (c) $\delta^{18}O$-CO_2*

The above graph shows the intercomparison results between the two ice mills, used under similar lab conditions (handled on the same day, 06-11-2007). While no considerable differences are observed in terms of data scatter, results for both CO_2 and its stable isotopes are closer to the real value for the case of mill #5. The above observation gives more confidence for the ice mill #5 over the #1.

III.6.3.4. tests on bubble-free ice (BFI)

The principle of this test consists in including a gas-free single crystal ice of identical size and weight as a natural ice core sample in the ice mill, additionally to the previous test. Known standard gas quantity is transferred to the ice mill and either the ice is ground or not, the standard gas gets subsequently expanded and measured. This test allows the quantification of possible fractionation coming from ice surface / standard gas interactions or from the presence of water vapour in the ice mill for the non-grinding case, while the grinding version surrounds all possible real sample fractionations, except for the linking of air with ice matrix (which can be very crucial, *e.g.* in bubble against clathrates). Different experimentalists proceeded in this kind of tests; the combined results are presented in fig. 3-16:

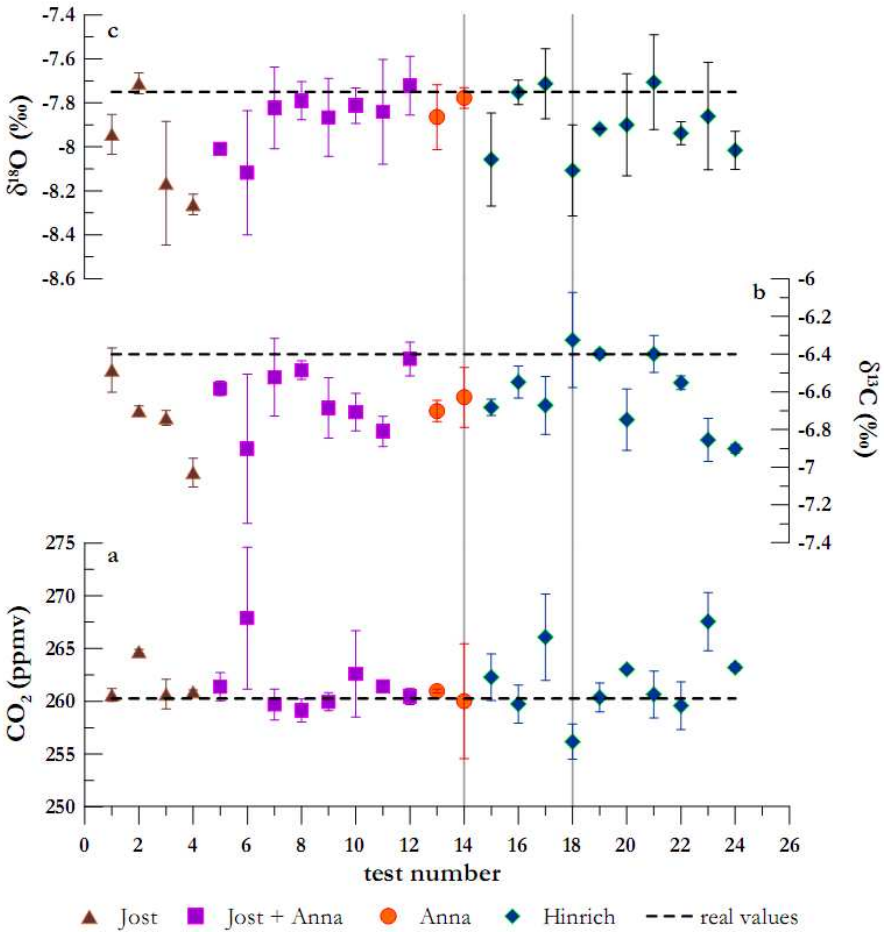

Fig. 3-16: *BFI 'test' results with the contribution of different experimentalists; dotted lines are the real values of the st. gas, while grey vertical lines are the limit points for the three PhD years ie. 1-14: 2006, 14-18:2007 and 18-26: 2008*

As was also the main conclusion for the standard gas case, no fractionation for the CO_2 mixing ratio was encountered, but for the case of isotopes more depleted values than the 'real' ones were observed (of an order of -0.25‰ for $\delta^{13}CO_2$). No differences were deduced out of the –limited-number of milling against the non-miling study cases. Still the way of realizing the whole experiment may produce fractionations other than those who may take place during the real extractions. This, combined with the limited tests number, justifies the non-applying of such correction, until more statistical-robust results of similar tests will come out in the future.

III.7. Analytical observations on ice core measurements

Three main axis will be discussed in the following:

- the behaviour of the gas extracted from the ice sample against time, for each of the examined variables;

- application on Vostok data to test the reproducibility of the analytical method;
- tests on the extraction efficiency of our method, by proceeding to two comparisons:

  (a) bubble ice with ice from transition bubble-clathrate zone

  (b) bubble and clathrated ice

III.7.1. CO_2 and isotopic ratio trends with expansion

Since each gas sample is expanded several times into the sample loop and subsequently measured, we can evaluate possible trends between these expansions. These trends are statistically robust as they rely on a large number of measurements. The different expansions trends deduced for CO_2, $\delta^{13}CO_2$ and $\delta^{18}O$-CO_2 for TI and TII are examined below, in forms of histograms[12].

III.7.1.1. CO_2 results

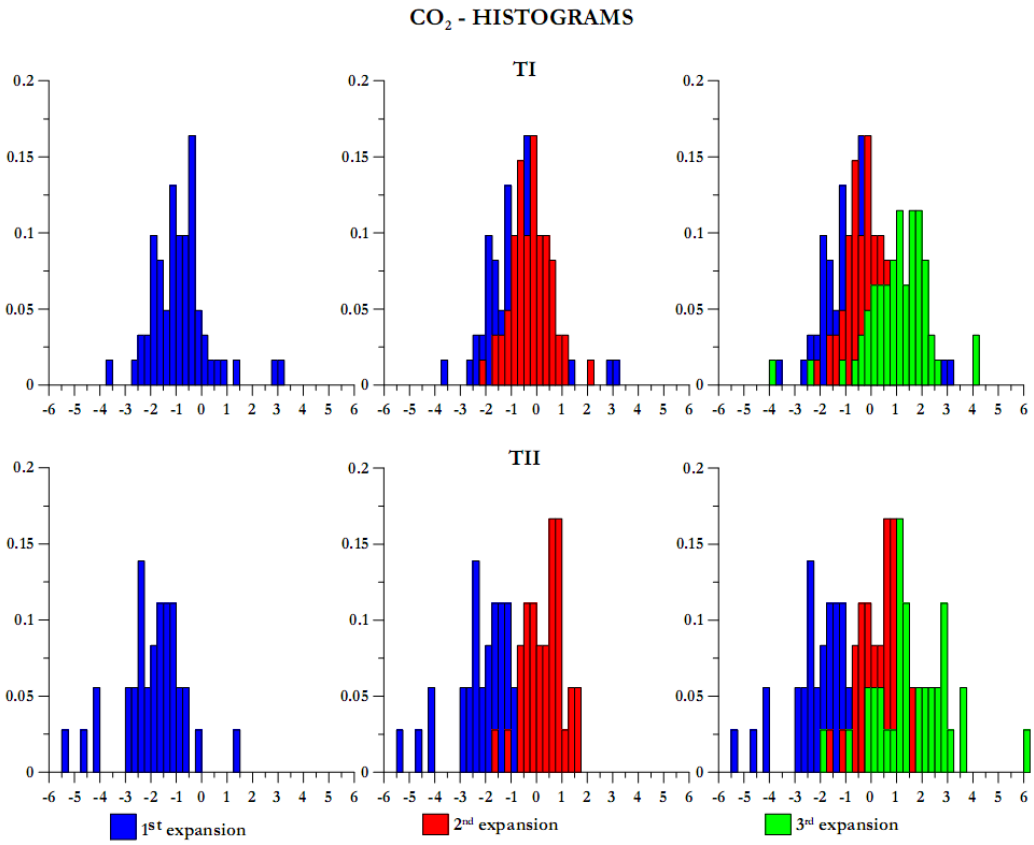

Fig. 3-17: *different expansions tendency for CO_2– **histogram** of both TI and TII periods, "zero" being the average value of the 3 expansions*

[12] the "offset" seen for different expansions is calculated by subtracting the single expansion-value from the 3-expansions mean outcome, *cf* annex IV.

Fig. 3-17 shows a clear drift towards higher values throughout the consecutive expansions. On average, the difference between the 1st and the 3rd expansion amount to 1.91 ppmv (TI) to 3.53 ppmv (TII).

III.7.1.2. $\delta^{13}CO_2$ results

A small drift towards more ^{13}C-depleted values from expansion 1 to expansion 3 is observed in fig. 3-18. Its amplitude is of the order of 0.1‰ (0.107‰ -TI- *vs.* 0.070‰ -TII-). As the isotopic ratio is calculated against a standard gas peak having a similar amplitude, this drift cannot be attributed to the non-linearity of the MS, as discussed earlier in the chapter. It is related with the gas evolution in the ice mill between consecutive expansions.

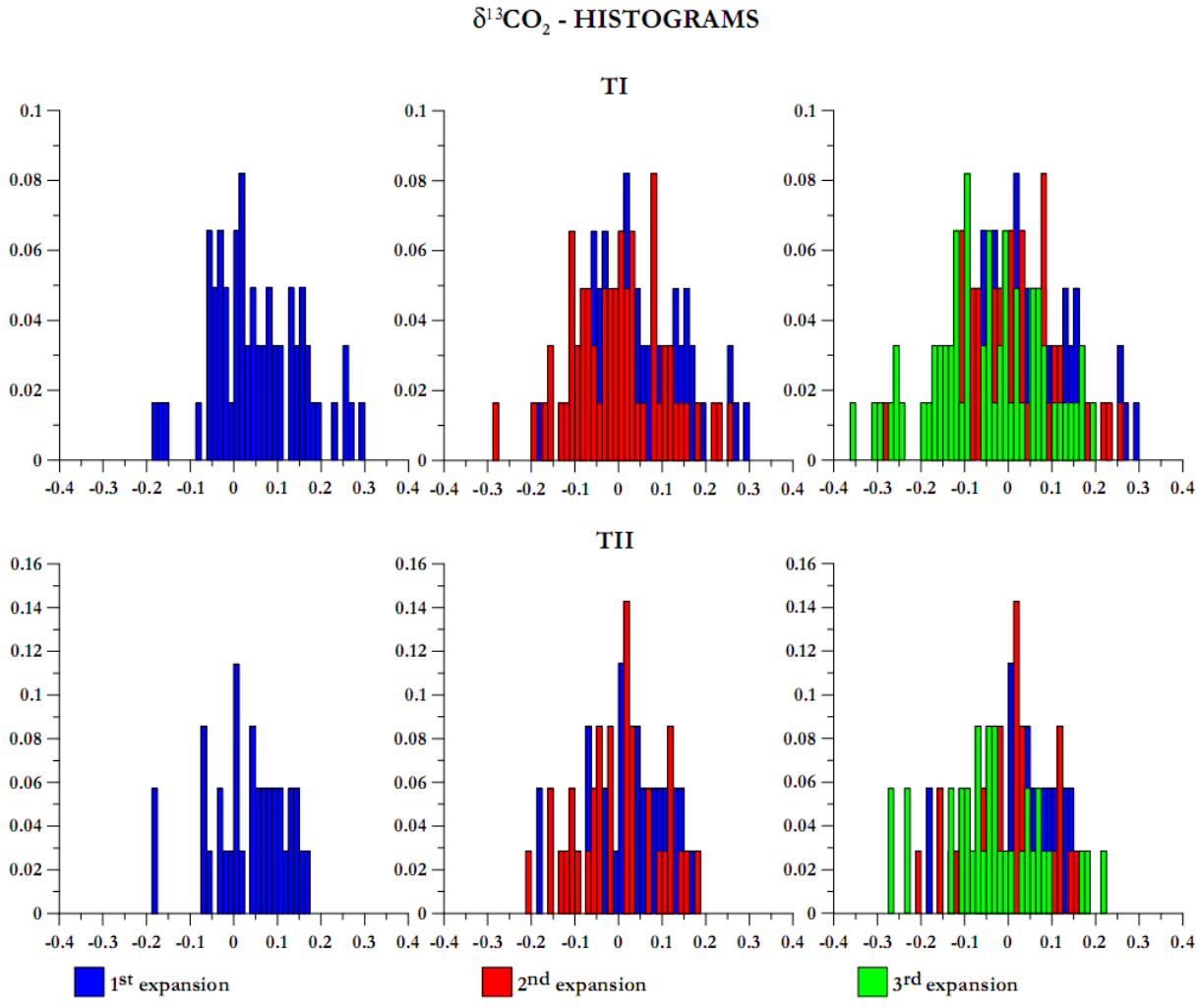

Fig. 3-18: *histogram of different expansions trends of $\delta^{13}CO_2$ over time, for both TI and TII periods*

III.7.1.3. $\delta^{18}O$-CO_2 results

Fig. 3-19 witnesses a large positive $\delta^{18}O$ drift from expansion 1 to expansion 3, by 1.507‰ for TI and 0.878‰ for TII.

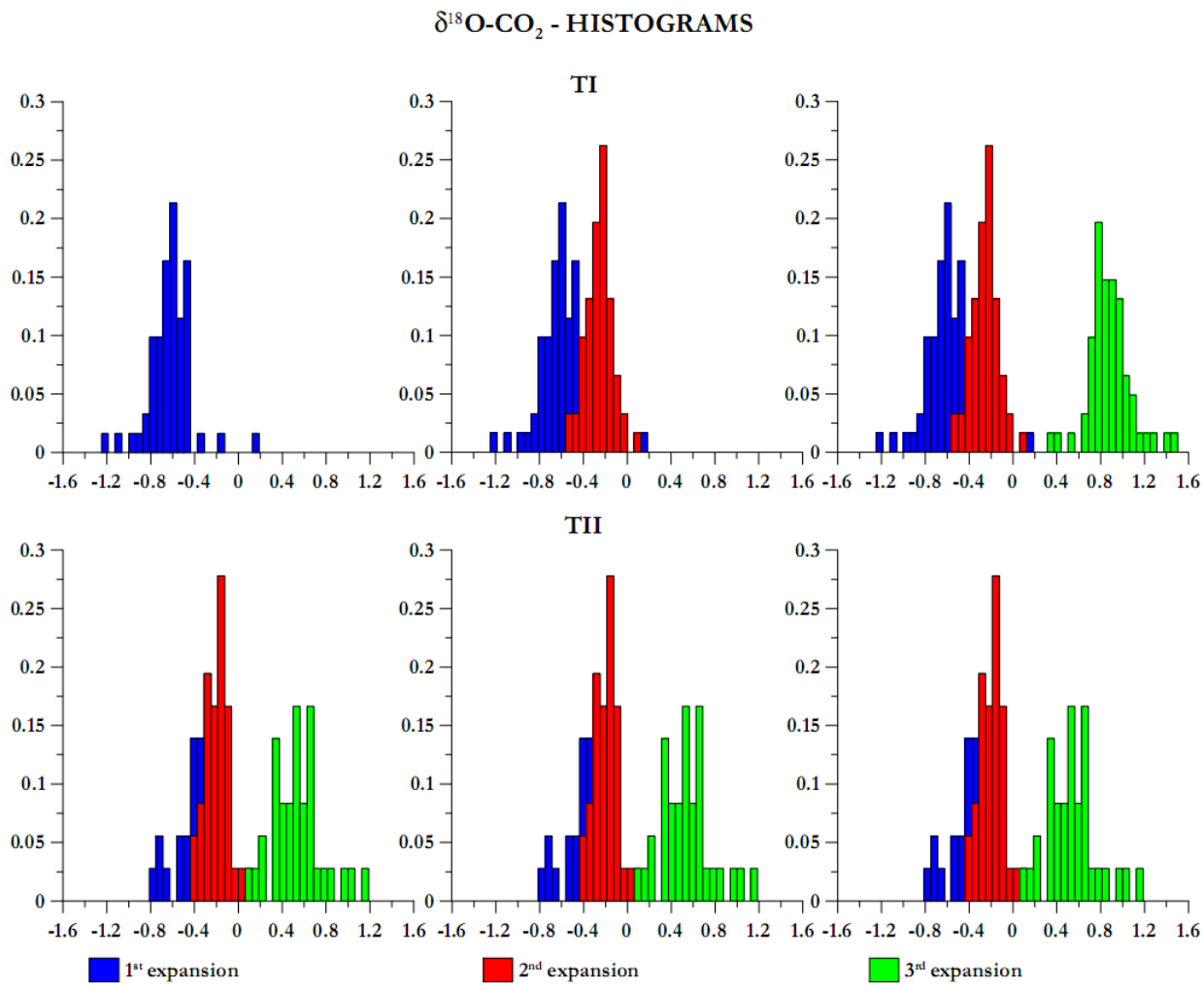

Fig. 3-19: *histogram of different expansions trends of $\delta^{18}O$-CO_2 vs. time - for both TI and TII periods*

III.7.1.4. Potential drift generators

Desorption processes occurring between the stainless-steel-ice interface within the ice mill constitute the major candidates for the positive CO_2 drift observed for the majority of the sample expansions. Leaned on the principle that desorbed CO_2 has similar signature to C sources used for the mill fabrication (i.e. having a signature of ~-25‰), this phenomenon seems to justify the more ^{13}C-depleted tendency through time.

The increasing water vapour quantity (from ~50-mV in the beginning of the experiment to ~250 at the very end of it), coupled with higher temperatures in the lab, line and various mixed baths could play a role to the $\delta^{18}O$ drifts, since the equilibration between CO_2 and H_2O is directly depicted to the stable oxygen isotope (*cf. annex III*).

Thermal diffusion influence cannot be neglected either, when taking into account the >3-min equilibration occurring with the ice mill valve open; still this time is small when compared to the 28-min experimental duration.

The "diffusion pump" effect, as introduced by J.-M. Barnola, would be an interesting explanation for both CO_2 and $\delta^{18}O$-CO_2 trends: the expanded gas of the very first expansion partially returns to the ice mill, leaving slightly depleted the residual CO_2 in the expansion line. Therefore, the following expansions have as initial CO_2 the enriched amount residing in the ice mill.

III.7.1.5. Outliers definition

From the above histograms, the mean σ value can be calculated and according to the desired confidence level for our data, the values >3σ (at least) are excluded. With this way, combined with the consideration of technical problems during the analytical procedure, the "bad data" were rejected (cf. annex IV for formulae and more histograms, for TI and TII).

III.7.2. Reproducibility on numerous replicates of Vostok ice core

In March 2006, just before starting the TI measurements, the reproducibility of the protocol was tested using a Vostok ice core sample, named BH7#161, corresponding to ~3080 y BP for the age of the trapped gas and containing CO_2 at 271.12 ± 7.75 ppmv. This sample was splitted into 8 sub-samples. With the method of >3σ rejection of the histograms *(cf. annex IV)*, one sub-sample *(D1)* was excluded. The accepted results, are presented in fig. 3-20 and are not corrected for gravitation as the purpose of the experiment was only to evaluate the protocol reproducibility.

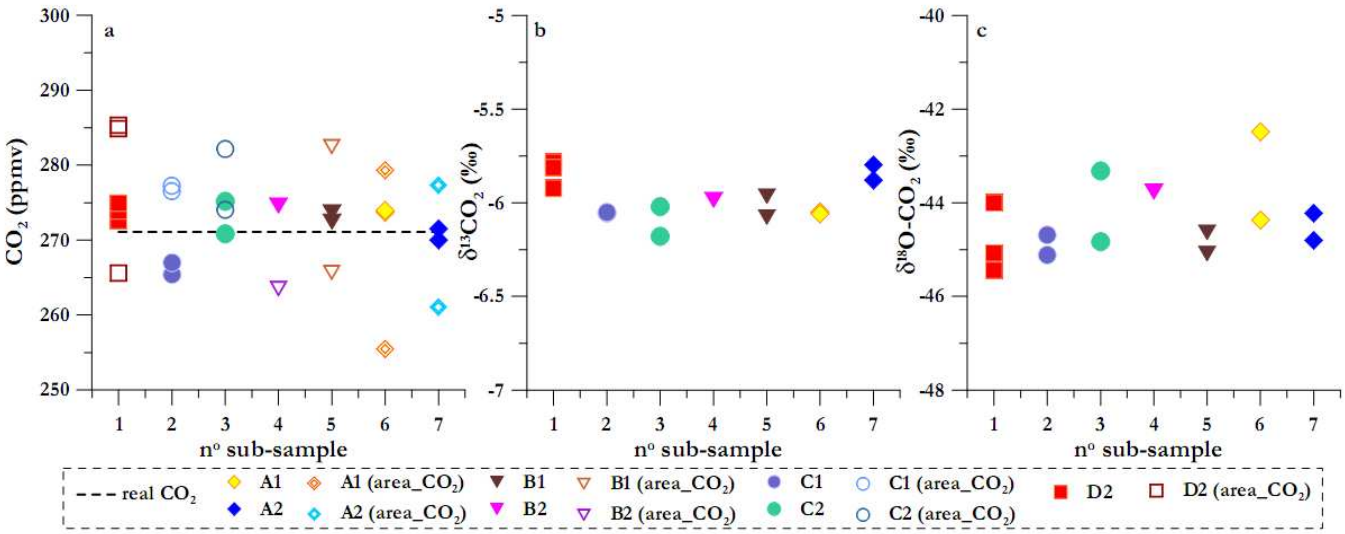

Fig. 3-20: *Vostok results: (a) amplitude- and area- deduced CO_2; (b) $\delta^{13}CO_2$; (c) $\delta^{18}O$-CO_2 against nº of sample examined; dotted line shows the interpolated value from the atmospheric signal of Barnola et al., 1987*

BH7# 161	A			B			C			D		
	CO_2	$\delta^{13}C$	$\delta^{18}O$	CO_2	$\delta^{13}C$	$\delta^{18}O$	CO_2	$\delta^{13}C$	$\delta^{18}O$	CO_2	$\delta^{13}C$	$\delta^{18}O$
Raw data	272.31	-5.95	-43.97	273.61	-6.01	-44.49	269.62	-6.08	-44.49	273.82	-5.84	-44.84
	(1.88)	(0.13)	(1.02)	(1.09)	(0.06)	(0.67)	(4.35)	(0.07)	(0.80)	(1.18)	(0.07)	(0.75)
Linear corr 1		-5.82	-43.82		-5.90	-44.48		-6.02	-44.54		-5.94	-45.00
		(0.17)	(1.08)		(0.12)	(0.66)		(0.06)	(0.81)		(0.04)	(0.82)
Linear corr 2		-5.84	-43.94		-5.95	-44.58		-6.10	-44.69		-5.97	-45.07
		(0.19)	(0.99)		(0.11)	(0.59)		(0.06)	(0.78)		(0.11)	(0.65)

total	Raw	Corr 1	Corr 2
$\delta^{13}C$	-5.97	-5.92	-5.96
	(0.12)	(0.13)	(0.13)
$\delta^{18}O$	-44.42	-44.42	-44.53
	(0.81)	(0.88)	(0.82)

Table 3-8: *comparison of raw data to linearity-corrected (two versions) ones, as proposed in III.5.2.2 section; here only amplitude-deduced CO_2 calculations are presented in contrast to fig. 3-20 which presents both calculated CO_2 results*

The above first ice results were encouraging, for the following reasons: (i) both area- and amplitude-deduced (fig. 3-20a) CO_2 values are close to the expected one, as calculated out of the results of Barnola et al., 1987[13]; (ii) both ^{13}C and ^{18}O values are reproducible within 2,95 ppmv, 0.12‰ and 0.81‰ for CO_2, $\delta^{13}C$ and $\delta^{18}O$, respectively (n=14), fig. 3-20; table 3-8).

III.7.3. Extraction efficiency - bubble against clathrate ice

In Ch. II, the physical - chemical principles related to the formation of air hydrates within the ice matrix were discussed, while in section III.2.2 the extraction efficiency constraint against the dry method was introduced. Smith et al., 1999 mention that the accuracy of $\delta^{13}CO_2$ measurements performed on BFI may be affected by the presence of clathrates, while Eyer, 2004 found reduced CO_2 mixing ratios accompanied by ^{13}C-depleted isotopic values when measuring clathrate ice[14]. Still, the depths measured by Eyer, 2004 belong to the bubble- clathrate transition zone, which is considered more unstable than the pure clathrated one (*cf. Ch. II*).

[13] BH7 data used to find the CO_2 value for the used sample were of depths 124.6 and 173.1m taking into account that Vostok cores are of 1 m-length); the CO_2 values calculated in 1987 were 274.5 ± 5 ppmv and 270.0 ± 10.5 ppmv, respectively

[14] ^{13}C-depleted values were encountered only in his article version, not the PhD-one (*cf. Ch. I*)

The combined measurement of CO_2 with its stable isotopic ratio, provided an opportunitity to test the above assumptions throughout this PhD. Therefore, a strategic analytical scenario was established, involving the comparison of two ice cores and taking the worst case scenario, *i.e.* the one core belonging to the bubble zone and the other to the transition bubble-clathrate zone and compare their mixing and isotopic ratios. If no fractionation is viewed, then we can proceed to a second comparison of a purely clathrated zone with a bubble zone of the same core, to further test air extraction efficiency differences.

These tests aim to better comprehend the extraction method used and the limitations it provides against the analyzed ice core state.

Focus on EDC

At the Concordia site, where the mean annual temperature is –54.5°C, the formation of N_2 and O_2 clathrate is theoretically possible at depth as shallow as 400 m and at even shallower depths for CO_2, due to its low dissociation partial pressure (Price, 1995; Ikeda et al., 1999). Nevertheless, microscopic observations show that the first 580 m of the EDC core, covering in particular the TI-period, is free of clathrates *(V. Lipenkov, pers. comm.)*. On the other hand, TII samples include fully clathrated gases. In between, a transition zone exists where bubbles and clathrates co-exist due to the slow dynamic of clathrate formation (limited by diffusion of water molecules from the bubble walls).

III.7.3.1. Clathrate bias with the LGGE extraction setup: EDC versus Berkner

A comparison between EDC ice and ice from the Berkner Island drilling was set in 2008. Both selected core sections belong to the same time-frame (40-50 ky BP) called Antarctic Isotope Maxima (**AIM**) 12 or A2 (according to EDML or Byrd nomenclature, respectively). AIM 12 was accompanied by a CO_2 peak of ~15-20 ppmv amplitude (Stauffer et al., 1988; Ahn et al., 2004; Ahn and Brook, 2007). EDC ice (of depths 800-860 m) belongs to the transition ("brittle") zone, while Berkner ice (depths between 730-760 m) is in bubble form. To our knowledge, such analytical attempt is the first of its kind. The EDC ice bags were effectively of poor quality, with lots of fractures and cracks. The best shaped parts of each bag were chosen in order to obtain unbiased information. In fig. 3-21, the state of the art of corresponding gas records is presented, superimposing 3 different ice cores –Berkner island, Byrd and Vostok – on their (a) CH_4 and (b) CO_2 content.

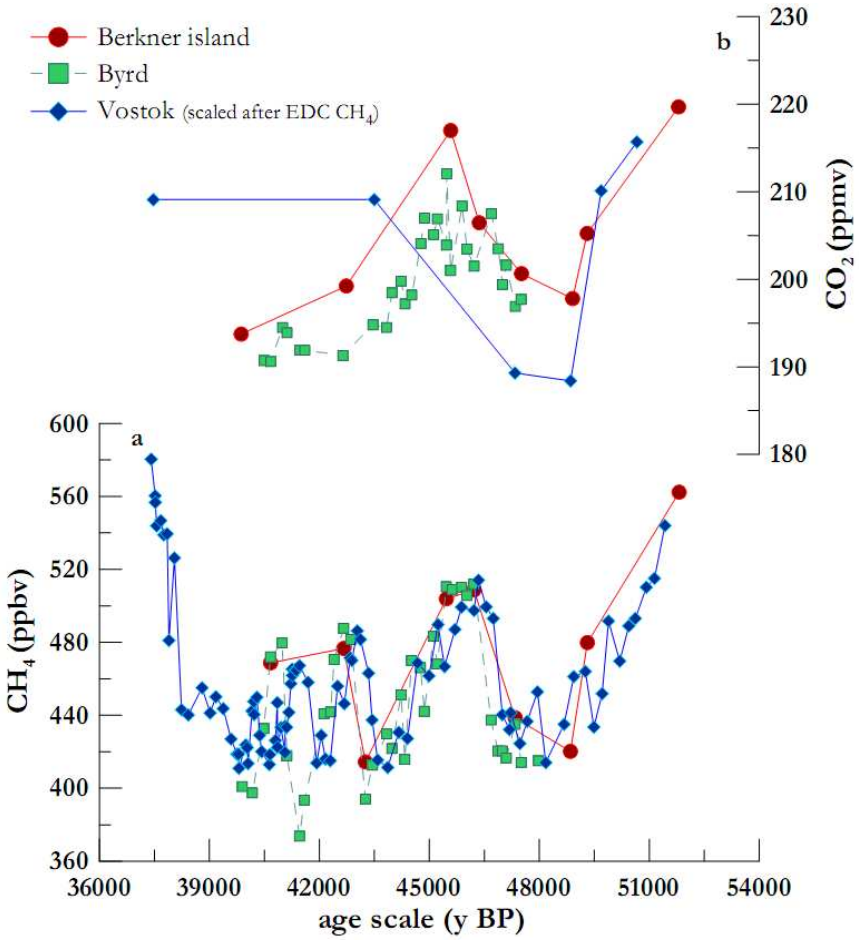

Fig. 3-21: *state-of-the –art of ice cores reconstructing AIM12: Berkner Island (red circles); Byrd (green squares); Vostok (blue diamonds); data from Neftel et al., 1988; Blunier and Brook, 2001; J.-M. Barnola and Martine LeFloch, pers. comm.; Vostok has been synchronized to EDC3_gas_a scale (Lüthi et al., 2008)*

Berkner Island and Byrd cores in fig. 3-21 capture the CO_2 peak associated with AIM events (at ~46 ky BP), which reflect the connection of SH warming to reduced oceanic heat transport into the N. Atlantic during stadials first defined in EPICA, 2006. The Vostok core however, (here synchronized vs. EDC), suggests CO_2-depleted values (yet at low-resolution). Byrd core also suggests a CO_2-depletion, when compared to Berkner[15]. No synchronization issues can be provided as explanation, since their CH_4 reconstructions coincide.

[15] A recent study providing a new series of CO_2 measurements for Byrd core, shows elevated CO_2 values for the studied period, reaching the ones from Berkner core Ahn J. and Brook E. J. (2008) Atmospheric CO_2 and Climate on Millennial Time Scales During the Last Glacial Period. *Science* **322**, 83-85.

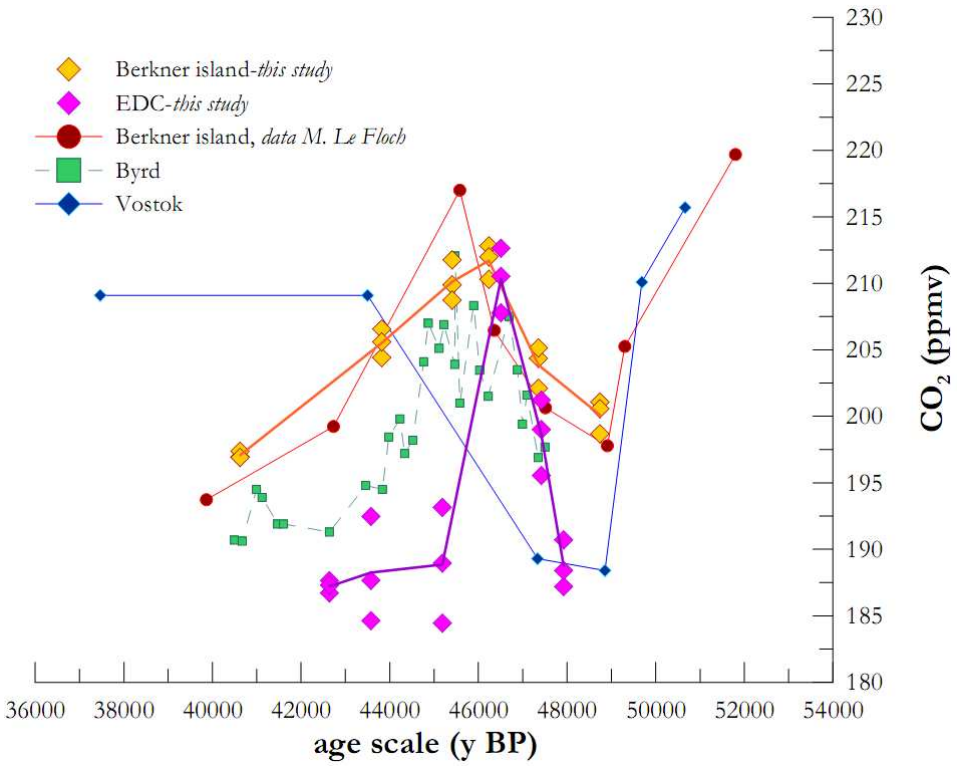

Fig. 3-22: *presentation of CO_2 mixing ratio data intercomparison from Berkner (yellow diamonds) and EDC (magenta diamonds); the three expansions are exposed, as well as the line that links the mean value*

Fig. 3-22 illustrates the contribution of this study to the Berkner – EDC cores intercomparison. We deduce the following points: (i) our Berkner CO_2 signal is comparable to the one previously obtained at LGGE with the same ice mill but with GC-FID analysis; the fit is good both in terms of trend and magnitude, with the exception of the peak point shown in the previous Berkner data, being enriched by 5 ppmv *vs.* our CO_2 peak (which is attributed in the different depth levels measurement, as well as the low resolution of both datasets); (ii) a "time shift" of the characteristic AIM 12 CO_2 peaks appears between EDC and previous Berkner Island datasets, even though both cores are synchronized through CH_4 tie-points signals (fig. 3-21a); this shift disappears with the actual Berkner CO_2 data; (iii) while the new data provided from this study, show a concomitant and of similar absolute value CO_2 peak for EDC and Berkner Island datasets, this is not the case for the boundary time-limits of the AIM 12 event; there, an average difference of 12 ppmv is found between the two cores, EDC being more depleted; (iv) the inhomogeneous combination of bubbles and hydrates at the different depth levels of these EDC samples may justify the higher scatter one finds for the CO_2 mixing ratio compared to Berkner (2.6 ppmv and 1.2 ppmv, repectively).

Fig. 3-23 puts together (a) CO_2 mixing ratio, (b) $\delta^{13}C$ for EDC and Berkner cores.

This brings the following observations:

- although the EDC CO_2 mixing ratios appear generally depleted compared to Berkner Island, this is not the case for $\delta^{13}C$: the data obtained from both cores are of the same average absolute value –6.25‰
- while the CO_2 standard deviation over the 3 consecutive expansions is higher in EDC than in Berkner Island ice, this is not observed for the isotopes measurements for the average of samples (valid if we exclude the 3rd expansion of the older EDC sample below)

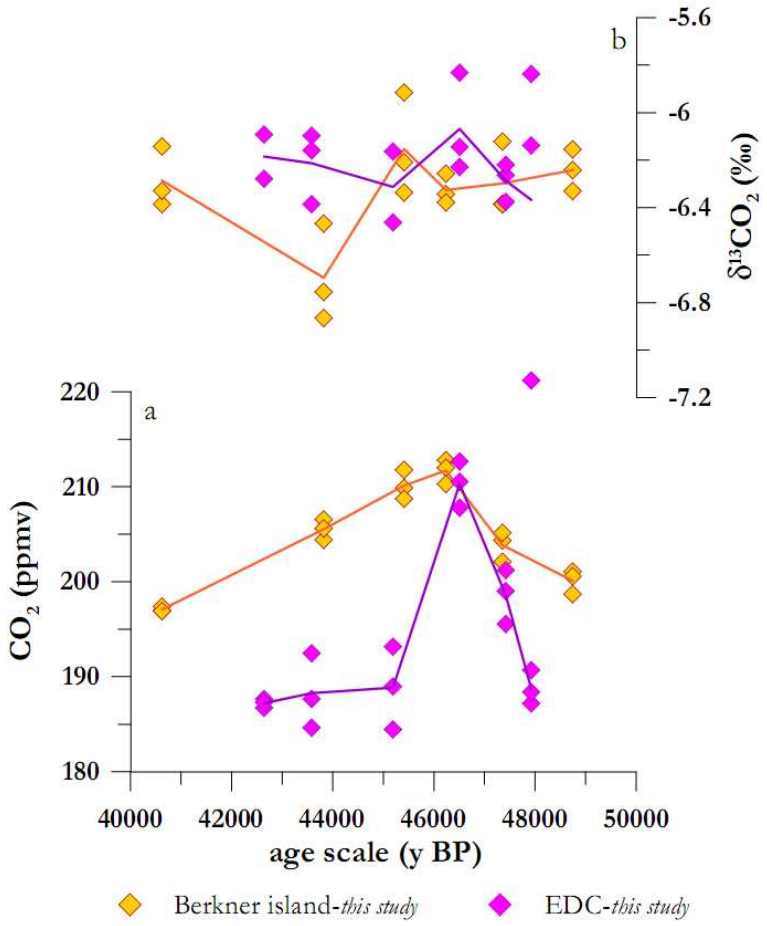

***Fig. 3-23** : intercomparison of Berkner core (yellow diamonds) and EDC core (magenta diamonds) on (a) mixing ratio; (b) $\delta^{13}C$. All (3) expansions are provided, as well as the averaged line*

A major conclusion can be drawn out of these 2 points: the transition from bubbles to gas hydrates is accompanied by partial fractionations of the CO_2 mixing ratio which affect the results obtained with the LGGE ball mill, while the stable C isotopes outcome appears not influenced.

Based on the observation that the clathrate/bubble coexistency does not seem to affect the CO_2 isotopic ratio, it permitted me to investigate an older termination (TII), where all gases are in

clathrate form (more stable than the bimodal state encountered in the AIM 12 EDC core, Ikeda et al., 1999). Results from this exercise on the grinding efficiency are presented below.

III.7.3.2. Air extraction efficiency between TI and TII sampling periods

TI and TII periods differ in the ice properties, the former been represented by bubble ice and the latter clathrate ice. The clathrate formation is due to the increased hydrostatic pressure with depth, rendering gases in air-bubbles no longer stable separately from water molecules with increasing depth (Ikeda et al., 1999). As clathrates have a more stable structure than bubbles, their decomposition through dry crushing becomes a problem and can generate artifacts in the measurements (Wilson and Long, 1997; Anklin et al., 1997; Schmitt, 2006).

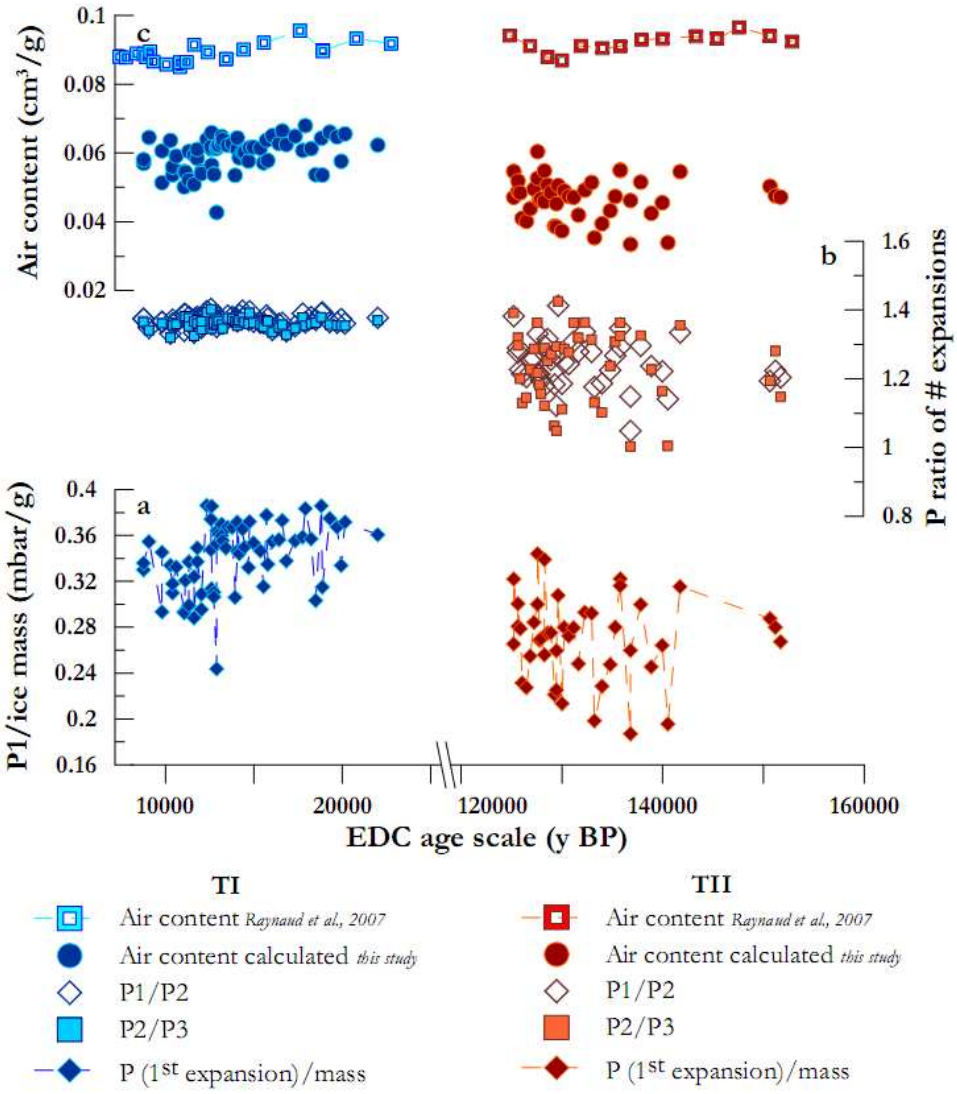

Fig. 3-24 *: technical aspects for the two major sampling periods (a) 1st expansion pressure P/ice sample mass ratio; (b) P1/P2 & P3/P2 ratios and (c) calculated air content, as deduced from formulae found in annex V, against air content data from Raynaud et al., 2007*

Fig. 3-24 shows two ratios aiming at evaluating the extraction efficiency: the 1st expansion pressure to ice mass ratio, and the ratio between 1st (2nd) and 2nd (3rd) expansions. The first ratio is influenced by two factors: (i) the air content of ice core samples, (ii) the grinding efficiency, related with the ice structure and the sample size. The second ratio indicates whether water vapour is present in abnormally large amounts during one expansion, thus affecting the P reading, or whether some gas is still released from the grinded powder and uncrushed ice pieces in the mill between two consecutive expansions.

From fig. 3-24a;b, it is clear that the TII sample series show smaller and more scattered ratios than TI series. As the average sample size did not change between the two series, and as the air content variations between the two Terminations lie within the same range (fig. 3-24c, *upper curve*), this favors a reduced efficiency and reproducibility of the ice mill on fully clathrated ice (TII) compared with bubble ice (TI). Regarding the ratios between consecutive expansions, similar mean values are observed when comparing the two ratios P1/P2 and P2/P3, thus suggesting no specific problem with increasing water vapor in the expanded gas due to the slow warming of the mill bath with time. On the other hand, the increased scatter of the TII series combined with its overall lower ratio, and with the P2/P3 ratio often lower than the P1/P2 ratio for the samples showing the lowest ratios overall, clearly indicate that some additional sample gas can be released from the grinded powder and/or uncrushed ice pieces, during the time separating two consecutive expansions. This very probably relates with the slow kinetic of clathrate dissociation. The air content calculated result (fig. 3-24c) further supports the above assumptions (calculations can be found in annex V). Air content was found lower during TII than TI (0.047 cm^3/g on average during TII vs. 0.060 cm^3/g of TI), whereas published data do not support such statement. The problem we encountered with the ball crusher in the cold room in 2008 (*cf. III.4.3*) could give the answer. Still, the 3 measurements of MIS 6 accomplished in November 2006 gave the same results as 2008 *(cf. Ch. V)*. The upper points to real ice state changes, adequately seen throughout our experimental protocol.

The considerable temperature gradient between the core original site and the storage cold rooms (in our case there is a 30°C-ΔT between Dome Concordia site and the Fontanil or LGGE storage cold rooms) can cause a slow clathrate relaxation and reappearance of small bubbles in the ice core (Ikeda et al., 1999). However, considering visual differences between the cores of TI and TII, as well as the above-mentioned physical differences, one concludes to the main existence of clathrates for samples representing TII. Concerning data exploitation, this is discussed in Ch. V.

The combined studies from *i.* Güllük et al., 1998 – who found similar gas results on clathrated Vostok ice, by comparing a dry extraction and sublimation technique – and *ii.* Eyer, 2004 who

presented lower CO_2 values but no depletion in his isotope data[16], provide some first support on the inadequate extraction efficiency of the clathrated ice with our method but without affecting the isotopic composition of the obtained result. For the unstable brittle zone, CO_2 mixing ratio may fractionate but this is not the case for its stable isotopes.

III.8. Conclusion

Here we present a new analytical protocol, developed just before the start-up of this PhD study and evaluated throughout this 3-year period. This method leans on the ice sample destruction by crushing (milling), otherwise called 'dry extraction technique' and it allows the concomitant analysis of the CO_2 mixing ratio and its stable isotopic ratios. A detailed description of the ensemble of processes an ice sample undergoes is provided, from its crushing up to the analysis of the desired gas content. The various blank tests applied, validated the performance and the efficiency in reconstructing a real atmospheric signal. A ~0.25‰ ^{13}C-depletion is encountered during bubble-free ice tests, independently of the ice crushing interval. Deviations of the standard gas throughout time were also studied, being particularly interested in the two major sampling periods which will be exposed in Ch. IV and V. Major signal drifts with time were attributed to the MS parameters shift. A first exercise on Vostok ice revealed reproducible results. A similar behaviour was encountered for ice sample from the main sampling periods, showing comparable drifts over time with comparable st. deviations, thus assuring for the measurements quality. An experiment took place on the response of this new method towards ice of different physical properties, which revealed lowered grinding efficiency for clathrate ice and reduced air content vs. known values, validating previous assumptions on the default of such technique towards clathrate ice. Still, a further intercomparison of bubble ice and the brittle zone, demonstrated absence of fractionation for the stable carbon isotope, giving confidence on further applications on older ice.

In the following, more applications of this protocol will be exposed on sample series covering a whole deglaciation, as well as some scientific-based discussion on the obtained signal.

Perspectives:

On ameliorated gas extraction techniques:

An idealized method would be an extraction by continuous ice melting, rapidly decoupling the CO_2 from the liquid phase, in order to avoid carbon acid reactions.

[16] for the PhD version

A more sophisticated idea could be the application of a non-destructive method (*e.g.* optical analysis), in order to avoid any interaction with the ice matrix.

On BFI tests:

The use of artificial ice contained with air of a known isotopic composition, would be highly desirable for future applications.

On comparing ice with different physical properties:

Such comparison should be extended over a depth range where EDC ice is fully clathrated whereas Berkner Island still holds a concomitant gas composition in bubbly ice (since the "brittle zone" is very unstable and thus not directly comparable with the older, clathrated zone).

Chapter IV. Termination I

IV.1. Introduction

In this chapter, the first data produced with the protocol presented in Chapter III, will be exposed and discussed. The period in question is called Termination I (***TI***), covering the transition from MIS 2 (Last Glacial Maximum, ***LGM***) to MIS 1 (Holocene), *i.e.* the time frame from ~20 ky BP to ~10 ky BP. The reasons for selecting this period over others, as well as the main climatic events encountered throughout the ~10 ky time frame are provided in section 2. Paleoceanographic proxies that contributed in interpreting our signal are exposed in section 2, as well. In section 3 the main coupled atmospheric CO_2 and $\delta^{13}CO_2$ results are presented, accompanied by a model-based interpretation in an article form submitted to Science. In section 4, a more detailed discussion on the causes of the deglacial CO_2 rise takes place, considering the new constraints our isotopic signal affords, as well as the outputs of other models compared to our simulated results. Section 5 presents additional data measured for the E. Holocene and superpose them to previous ones, while section 6 deals with the delicate aspect of records synchronization, by showing some representative exercises accomplished. Chapter IV ends with a final intercomparison of our data series over other data produced for the same period within the EPICA consortium that has been well-discussed throughout this PhD study.

IV.2. State of the art

IV.2.1. Reasons for studying this transition in EDC core

- TI is accessible using various environmental tools: marine organisms found in sediments from different water depths (planktonic and benthic), tree rings (for the end of TI), corals, speleothems, lake sediments (including pollen records), ice cores.. TI constitutes, therefore, a well-referenced period with good data intercomparison

- A series of important rapid events, occurring at both hemispheres, are documented : Heinrich 1 event, Bølling-Allerød, Antarctic Cold Reversal and Younger Dryas; all events are related with inter-hemispheric anti-phase connections and show the dynamic character of our period of interest (further discussed in the next section);

- The abrupt climatic events mentioned above are associated with changes in ocean circulation patterns, which can be highly relevant with respect to carbon/climate interactions;

- EDC core at the corresponding depth range only includes gases in the form of bubbles, thus avoiding experimental challenges involved in terms of air extraction on clathrated ice (*cf. Ch. III*); in addition, the thinning of ice layers is less than 20%, so a relatively high time resolution is obtained;

- EDC core has been the reference core for two previous studies: one on CO_2 mixing ratio (Monnin et al., 2001) and one on CO_2 and its stable isotopes (Eyer, 2004); this permits a direct intercomparison and discussion, without having to deal with synchronization challenges;

- TI has been extensively studied through climate and climate-carbon modeling exercises ; therefore, mathematical applications already exist for the interpretation of our dataset (Brovkin et al., 2002; Köhler et al., 2005)

IV.2.2. Rapid climate changes presentation

IV.2.2.1. Heinrich 1

Introduction on Heinrich events

Heinrich (**H**) events are oceanic cold events. They are characterized by large accumulation of ice-rafted debris (**IRD**) carried along by armadas of icebergs and found notably in N. Atlantic marine sediments between 40 and 60°N (Heinrich, 1988). The origin of these iceberg melting events can be precisely determined by mineralogical, geochemical and physical properties of the IRD sediment contents. The Hudson Bay lobe of the Laurentide ice sheet in Canada has been in the frontline of candidates (MacAyeal, 1993; Hemming, 2004). This huge ice sheet surged into the N. Atlantic, entraining fine grains eroded from the underlying rocks, sediments. Other potential protagonists lie in either the European Ice Sheets -Iceland, Fennoscandia and British Isles- (Grousset et al., 2001) or even the S. Hemisphere and the West Antarctic Ice Sheet (Hulbe et al., 2004), the latter bringing iceberg armadas in the austral ocean. The freshwater input leads to a reduction in **NADW**[1] production, and thus in a slowing-down of the **THC**[2] (Siani et al., 2001).

[1] Recall: North Atlantic Deep Waters
[2] Recall: thermohaline circulation

N. Atlantic subtropical regions get also influenced by cooling and advection of low-salinity Arctic water masses that accompany H events (Bard et al., 2000); the induced cooling is considered as the most intense of the last ice age (Hemming, 2004). Their oceanic character is correlated with atmospheric phenomena (cold stadials in between D/O warm events), the cold, oceanic signal leading over the atmospheric one (Bard, 2002; Labeyrie et al., 2004).

Focus on last deglaciation

Heinrich 1 (**H1**) event has been considered as the equivalent of "Oldest Dryas" cooling in Europe (Keigwin and Lehman, 1994) ; it has been recorded in the N. Atlantic and localized with a corresponding wide time-frame: 17-16 ky (Lagerklint and Wright, 1999); 17.5 – 14.5 ky (Levi et al., 2007); 17.2-17.6 ky (McCabe and Clark, 1998); ~17-14.7 ky BP (Schulz et al., 2001); 15-14.3 ky (Keigwin and Lehman, 1994); 16.8 ky (Hemming, 2004).

IV.2.2.2. B/A + ACR

The Bølling/Allerød (**B/A**) was an interstadial that intervened between the Oldest and Younger Dryas. It is mentioned also as *D/O 0*. It consists of two separate warm periods, the dominant Bølling (named after a Danish lake) and the Allerød (called after a Danish municipality). B/A, during which THC strengthens to equivalent modern values (Rahmstorf, 2002), is well registered in both ice cores (through water isotopes and CH_4 records) and N. Atlantic marine sediments. B/A is thought to have been the direct result of the meltwater pulse 1A (**MWP-1A**) (Weaver et al., 2003). Parallel to this warm event of the N. Hemisphere (**NH**), S. Hemisphere (**SH**) reveals an opposite pattern. Thus, while NH warmed, the SH slightly cooled down or entered a period of constant temperature, marking the Antarctic Cold Reversal (**ACR**) episode. This is well depicted by the Antarctic δD record (Jouzel et al., 2007).

IV.2.2.3. Younger Dryas (**YD**)

The YD stadial constitutes another millennium-long cold snap that punctuated TI; it was a brief (1300±70y) period (Fairbanks, 1990), which followed the B/A interstadial. Current theories attribute the YD to a catastrophic release of fresh water stored in the proglacial Lake Agassiz (Teller et al., 2002), initiated by either an opening of the Laurentide ice sheet, flooding the Great Lakes region, or a delayed response to the MWP-1A –the latter being a subject of controversy (Sima et al., 2004)-. Firestone et al., 2007 even found in carbon-rich black layer sediment profiles an extraterrestrial origin for this Laurentide sheet destabilization! The fresh water release is thought to have been accomplished over the course of a single year, a quantity that would match today's annual net fresh water input to the Atlantic northern from 45°N!

Linking H and YD events

YD event has been linked with the drainage of Lake Agassiz (Teller et al., 2002), which added significant freshwater into the N. Atlantic (Fairbanks, 1989), while Heinrich events are associated with iceberg surges throughout the N. Atlantic. Although the triggers of both events are substantially different, one could assume that they exhibited similar climate-carbon cycle responses. In addition to this, both events are linked to a reduction of THC (Keigwin and Lehman, 1994; Broecker, 2003), with differences in relative magnitudes (Rahmstorf, 2002). As with H events and their atmospheric counterpart through stadials in-between D/O events, YD cold stadial had a strong imprint in the atmosphere and therefore is well registered in ice cores. YD is frequently called "H0 event" (Skinner and Shackleton, 2006).

IV.2.2.4. Bipolar seesaw events throughout TI

Since we deal with the interpretation of a global atmospheric signal, the interplay between the NH and SH should be taken into account. During the NH cold periods of H1 and YD, the SH was warming up, while in the ocean a redistribution took place: NADW weakened and became shallower, forming the LGM-like "**GNAIW**[3]" structure, while AABW –or **AAIW**[4]- got enhanced, flushing the Atlantic basin up to 60°N (Duplessy et al., 1988; Fichefet et al., 1994; Marchitto et al., 1998; Elliot et al., 2002; Rickaby and Elderfield, 2005). The opposite is encountered for the B/A warm episode in the NH, whose Southern counterpart was the ACR. Broecker, 1998 introduced the concept of "bipolar seesaw" to explain the differing north-south patterns. He proposed a system modulation by the varying inter-hemispheric heat transport associated with the THC. Robinson et al., 2005 by measuring $\Delta^{14}C$ in various deep ocean areas, support this idea. The anti-correlated NH and SH deep water formation interplays can be reconstructed using oceanic proxies capable of differentiating the two major water masses. Since NADW are nutrient-depleted compared to AABW ones, indicators such as PO_4^{3-}, Cd/Ca or benthic $\delta^{13}C$ (if the air-sea component of the latter is excluded) can be used to visualize the bipolar seesaw. Fig. 4-1 shows the Holocene – LGM difference of a. PO_4 and b. $\delta^{13}C$ in the Atlantic sector.

[3] Glacial North Atlantic Intermediate Waters
[4] Antarctic Intermediate Waters

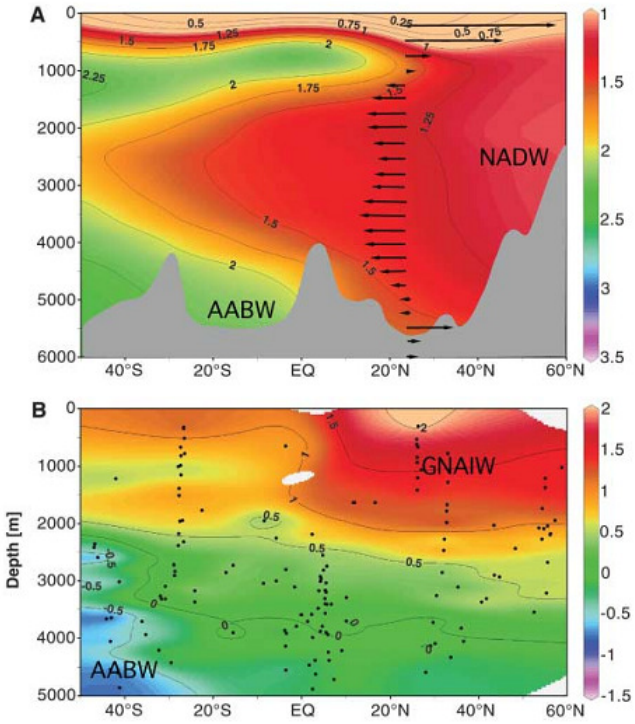

***Fig. 4-1**: visualization of the bipolar seesaw in the Atlantic sector and the different signatures in (i) nutrient content –here expressed as PO_4^{3-}- (upper curve, during IG) and $\delta^{13}C$ (lower curve, during G period. From both plots we deduce (a) the difference in relative intensity of bottom water formation between G-IG periods, seen from the nutrient proxies and (b) the lower nutrient content of NH deep waters (expressed equally as more enriched ^{13}C values, attention nutrient upper scale is reversed), relative to the AABW, implying older age of the latter (cf. Ch. I). Data compilation and presentation by Lynch-Stieglitz et al., 2007*

IV.2.3. Paleoceanographic proxies used to interpret the data

IV.2.3.1. $^{231}Pa/^{230}Th$ ratio

The ratio between the two isotopologues Protactinium-231 (^{231}Pa) and Thorium-230 (^{230}Th) constitutes an important indicator of paleo-oceanic circulation intensity (McManus et al., 2004). They are produced from the radioactive decay of Uranium-235 and 234 (^{235}U, ^{234}U), respectively. The residence time of U in the ocean being much higher than the oceanic mixing time (450 vs. 1.5 ky (Chen et al., 1986; Broecker and Peng, 1982)), permits its homogeneous distribution within the water column. The two isotopologues are produced with a constant seawater ratio of 0.093 (Yu et al., 1996). ^{231}Pa and ^{230}Th are removed from seawater by adsorption on settling particles, which then sink to the ocean floor. When measuring the $^{231}Pa/^{230}Th$ ratio in sediments, one finds varying values, reflecting either different speed or mechanisms of removal from the water column or different strengths in the transfer from the surface ocean to the sediment. ^{231}Pa has a residence time of 100-200 y in the water column, close to the transit time of surface waters to the deep ocean in the modern Atlantic (Broecker et al., 1985). As a result, ~50% of the ^{231}Pa produced in

Atlantic deep water is exported into the S. Ocean via the NADW. ^{230}Th, on the contrary, has a shorter residence time (of ~30y) which minimizes its transport from the Atlantic to the S. Ocean. Therefore, higher ^{231}Pa/^{230}Th ratios (with a max of 0.093) means high sedimentation rate or slow deep water transport towards the S. Ocean, *i.e.* weak NADW formation. The opposite is valid for the case of low ^{231}Pa/^{230}Th ratios (Gherardi, 2006).

IV.2.3.2. Oceanic (sedimentary) δ^{13}C data

The δ^{13}C signature of major water masses and its origin has been described in *Ch. I*. In this section, more details are provided on the δ^{13}C data specifically used to interpret our signal.

- Benthic data

Waters are constantly moving and mixing with other water masses, thus combining their water mass characteristics, in proportion to their relative fluxes. For the case of the Atlantic ocean, NADW and AABW waters have opposite signatures, the former being young, nutrient-depleted[5] and δ^{13}C-enriched and the latter being old, nutrient-enriched and δ^{13}C-depleted. The "cold" TI sub-periods of TI (H1 and YD), are supposed to be accompanied by a reduction in the strength of NADW and an enhancement of the AABW intensity. Therefore, when measuring benthic foraminifera in the N. Atlantic, one can visualize the balance of fluxes from these two water masses. During H1 and YD, the AABW signal will dominate and an overall δ^{13}C depletion is witnessed in the deep Atlantic. This is evidenced in the dataset of Rickaby and Elderfield, 2005 here exposed in the draft below. Still, the same pattern has been encountered in a series of other studies such as: Keigwin and Lehman, 1994; Elliot et al., 2002; Labeyrie et al., 2005; Waelbroeck et al., 2006; Skinner and Shackleton, 2006.

- Planktonic data

Planktonic foraminifera mainly bear the signature of local processes in surface waters. However a concomitant δ^{13}C decreasing signal appears in different oceanic regions (Indo-Pacific, sub-Antarctic and S. Atlantic) at the beginning of the deglaciation, suggesting a common mechanism affecting this proxy in different S. Ocean-connected basins (Ninnemann and Charles, 1997; Spero and Lea, 2002). This negative shift could potentially result from the overall re-organization of the water column. For instance, since sea ice disappears and air-sea exchange becomes stronger, the

[5] There exists an anti-correlation between nutrient and δ^{13}C oceanic content, as is explained in Broecker W. S. (2005) *The Role of the Ocean in Climate Yesterday, Today and Tomorrow*., the nutrient content being frequently expressed by the ratio Cd/Ca, as provided in Marchitto J. T. M., Curry W. B. and Oppo D. W. (1998) Millennial-scale changes in North Atlantic circulation since the last glaciation. *Nature* **393**, 557-561.

old C in the deep ocean (rich in CO_2 and depleted in ^{13}C) could get to the atmosphere and leave a signature in the surface waters as well.

IV.2.3.3. $\Delta^{14}C$ data

Radiocarbon activity in intermediate waters informs us on circulation patterns. ^{14}C is produced cosmogenically. Its radioactive decay depletes the $^{14}C/^{12}C$ ratio by 1% every 80y in C-bearing compounds. In any given sea water sample, the strength of this depletion depends on the duration of water isolation from the atmosphere (Broecker, 2005). The opposite effect is observed for the atmospheric ^{14}C value. Therefore, deep Atlantic waters are more ^{14}C-enriched than deep S. Ocean waters. Recently, Marchitto et al., 2007 measured $\Delta^{14}C$ in N.E. tropical Pacific sediments covering TI and suggested in particular a strengthening of the transfer of "old" waters originating from the S. Ocean (having a depleted $\Delta^{14}C$ signature) and reaching the N.E. tropical Pacific during H1 and the YD.

IV.3. CO_2 and $\delta^{13}CO_2$ results over TI from the EDC core

IV.3.1. Laboratory brief calendar

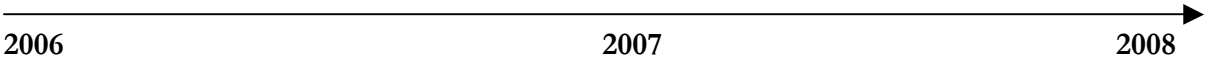

69 samples

A detailed table on the days dedicated for sampling period TI measurement is exposed in annex I. Raw data are given in annex II, while the equivalent $\delta^{18}O$ dataset is provided in annex III.

In the following two sections, the main draft as well as the supplementary material as submitted to Science journal, are disposed:

IV.3.2. Main draft

(pages 111-122)

IV.3.3. Supplementary material

(pages 123-137)

IV.3.2. A detailed carbon isotopic constraint on the causes of the deglacial CO_2 increase

Anna Lourantou[1*], Jošt V. Lavrič[1,†], Peter Köhler[2], Jean-Marc Barnola[1], Elisabeth Michel[3], Didier Paillard[3], Dominique Raynaud[1] and Jérôme Chappellaz[1]

[1] Laboratoire de Glaciologie et Géophysique de l'Environnement (LGGE, CNRS, Université Joseph Fourier- Grenoble), St Martin d'Hères, France

[2] Alfred Wegener Institute for Polar and Marine Research, Bremerhaven, Germany

[3] Laboratoire des Sciences du Climat et de l'Environnement (IPSL/CEA, CNRS, Université Versailles-St Quentin), Gif-Sur-Yvette, France

† Now at [3]

* To whom correspondence should be addressed: lourantou@lgge.obs.ujf-grenoble.fr

A new high-resolution ice-core record of the CO_2 stable carbon isotopic ratio casts light on the causes of the 40% carbon dioxide increase over the last deglaciation

Abstract

The causes of the ~80 ppmv increase of atmospheric carbon dioxide mixing ratio (CO_2) during the last glacial-interglacial climatic transition remain highly debated. Using the EPICA Dome C Antarctic ice core, we analysed in detail the concomitant evolution of CO_2 and its stable carbon isotopic ratio ($\delta^{13}CO_2$). Agreeing well with the existing record from the Taylor Dome ice core, our better resolved data reveal two negative $\delta^{13}CO_2$ excursions, concomitant with the Heinrich 1 and Younger Dryas events, and a positive $\delta^{13}CO_2$ peak during the Bølling/Allerød warm period. A comparison with outputs of two carbon cycle box models suggests that the CO_2 rise, accompanied by a $\delta^{13}CO_2$ decrease at the start of the deglaciation, is generated by the Southern Ocean stratification breakdown and decline of marine productivity. The $\delta^{13}CO_2$ peak potentially results from rapid vegetation buildup. The youngest $\delta^{13}CO_2$ minimum combines opposite effects of oceanic and terrestrial contributions.

Atmospheric CO_2 is the most important human-induced greenhouse gas and a large contributor to the actual global warming[1]. Knowing the evolution of its stable carbon isotopic ratio ($\delta^{13}CO_2$)[2] is essential for the identification of biogeochemical processes driving the observed variations in CO_2. Former studies[3;4] gave further evidence for the man-made origin of the CO_2 rise during the last 200 years, based on a decline of $\delta^{13}CO_2$ (of ~1.5 ‰) to its modern value of –7.8‰. This

decrease is related to the ^{13}C-depleted signature of the major anthropogenic CO_2 sources, fossil fuel burning and deforestation (~-30‰ and -25‰, respectively).

In contrast, natural changes in CO_2, such as the 80-ppmv rise over Termination I (hereafter TI), *i.e.* the transition from the Last Glacial Maximum (LGM ~20 ky BP[5]) to the Early Holocene (EH, ~10 ky BP), are still not well understood. Modelling studies[6;7] attribute it to various oceanic processes, but without consensus on their relative importance[8;9]. More constraints from paleoatmospheric $\delta^{13}CO_2$ data are thus needed. So far, a unique record of atmospheric $\delta^{13}CO_2$ through TI (including ~15 measurements) has been obtained from the Taylor Dome (TD) ice core[10], filling the time jigsaw between LGM and EH first produced from the Byrd core[11].

In this study we: (1) present a new highly-resolved record of CO_2 and $\delta^{13}CO_2$ across TI from the EPICA Dome C (EDC) ice core, (2) compare it with previously published data (EDC for CO_2 and TD for $\delta^{13}CO_2$)[10;12] and (3) employ two C-cycle models for hypotheses testing and record interpretation[13;14].

All samples originate from the EDC ice core drilled at Concordia Station in Antarctica (75°06'S, 123°21'E; 3233m. a.s.l) during the field season 1997-98. 63 samples were measured with a new analytical system[15], from 50 different depth intervals (345 to 580 m of depth) covering the time period from 9 to 22 ky BP and providing a mean time resolution of 220 y through the transition. Each data point corresponds to the average value of 3 replicate measurements on the same extracted gas; the pooled standard deviation on these replicates is 0.98 ppmv for CO_2 and 0.098 ‰ for $\delta^{13}CO_2$. Duplicate analyses of 13 samples from neighbouring depths yielded a similar reproducibility (1σ) of 0.99 ppmv and 0.104 ‰, respectively. Measurements were performed on clathrate-free ice samples shallower than 600 m.

The new CO_2 and $\delta^{13}CO_2$ datasets are plotted with previously published data (CO_2, δD and CH_4) from EDC[12;16;17] and TD[10;18] in *Fig. 1*. The agreement between the two CO_2 records from the same EDC core[12] is remarkable *($R^2 = 0.996$, Fig. 1c)*. Their high temporal resolution allows the division of TI into four sub-periods (SP-I to SP-IV)[12], characterized by different rates of CO_2 change. With 40 measurements throughout TI, the data resolution is improved by more than a factor of two compared with the existing TD record[10] *(Fig. 1c;d)*. Overall, the EDC and TD $\delta^{13}CO_2$ show similar mean values and trends in the course of TI, with 75% of the TD data falling within the 1σ EDC uncertainty (taking into account dating errors in the comparison). On the other hand, the TD CO_2 data are more scattered than the EDC ones. Both EDC and TD $\delta^{13}CO_2$

records reveal a W-shape through TI, with maximum amplitude of change of ~0.5‰. The better time resolution of the EDC profile reveals a more structured signal within the ~0.10‰ experimental uncertainty, permitting for the first time a detailed comparison with the CO_2 slope changes.

This comparison, visualized in *Fig. 1c;d* reveals a much different behaviour between CO_2 and $\delta^{13}CO_2$: while CO_2 mostly shows linear trends within each SP, $\delta^{13}CO_2$ exposes a more dynamic pattern during the SPs II to IV, with spikes and troughs superimposed on relatively stable boundary values. The evolution of both CO_2 and $\delta^{13}CO_2$, with respect to Northern and Southern Hemisphere (*hereafter NH and SH, respectively*) climatic events, can be summarized as follows: subsequent to the late LGM (20-17.6 ky BP) with average levels of 188±1.3 ppmv for CO_2 and –6.57±0.14 ‰ for $\delta^{13}CO_2$ (n=10), the early part of TI (SP-I, from 17.6 to 16.2 ky BP) is associated with a 25-ppmv rise of CO_2 and a 0.32-‰ fall of $\delta^{13}CO_2$. SP-II (16.2 to 14.7 ky BP), during which the Heinrich 1 (H1) event ends, reveals a two-step CO_2 rise; the first occurs until 15 ky with a progressive 14-ppmv increase and the second with a 12-ppmv rise within only 300 y. Meanwhile, $\delta^{13}CO_2$ experiences an oscillation of ~0.20-‰ amplitude and reaches a minimum of –7.01±0.10 ‰ at about 15.5 ky BP. The abrupt CO_2 rise at the end of SP-II is accompanied by a 0.15 ‰ decline of $\delta^{13}CO_2$. SP-III (from 14.7 to 12.8 ky BP), coincident with the Antarctic Cold Reversal (ACR) in the SH and the Bølling/Allerød (B/A) warm event in the NH, is marked by a progressive 3-ppmv decrease of CO_2, while a positive excursion up to a level of –6.54±0.15 ‰ is observed for $\delta^{13}CO_2$ during the mid-SP-III (~14.1 ky BP). Another $\delta^{13}CO_2$ spike, sharper and of higher amplitude than the first one, appears 1 ky later at the end of SP-III, but we are unsure about its significance. Duplicate measurements confirmed the elevated $\delta^{13}CO_2$ value, but neighbouring ice samples were not available to check if the spike results from a local artefact related with the ice core quality or if it corresponds to a real atmospheric signal. SP-IV (between 12.8 and 11.6 ky BP), during which the Younger Dryas (YD) cold event in the NH and the post-ACR warming in the SH took place, reveals similar patterns for both CO_2 and $\delta^{13}CO_2$ as for SP-II. Thus, a progressive 13-ppmv CO_2 increase is observed until 12 ky, while a more abrupt rise of 10 ppmv is seen during the last 300 y. In the meantime, $\delta^{13}CO_2$ experiences a negative excursion down to –6.98±0.13 ‰ (n=6) around 12.2 ky BP, during the first part of SP-IV, whereas during the last 300 y it rises by 0.24‰. The opposite $\delta^{13}CO_2$ trends observed during the abrupt CO_2 rise at the end of SPs II and IV, may imply different forcing mechanisms for these two time-periods.

The EH (11.6 to 9 ky BP) $\delta^{13}CO_2$ mean level amounts to -6.75±0.10‰ (n=14), being more ^{13}C-depleted than at the end of LGM (-6.57±0.14‰, n=10). In contrast, previous studies concluded

to heavier $\delta^{13}CO_2$ values (by 0.16‰[10] to 0.19±0.18‰[11]) during the Holocene than at the LGM. They were based on measurements performed on older LGM ice, when CO_2 was more variable[10] *(Fig. 1c)*, while Holocene data covered a different time window (from 8 to 7 ky BP, GICC05 agescale[19]) than considered here. In addition, the Holocene $\delta^{13}CO_2$ level may be subject to significant fluctuations[10]. When comparing our EH and LGM $\delta^{13}CO_2$ to the few TD values available at similar ages, we indeed find the same decreasing trend[10] *(Fig. 1d)*.

Overall, the main $\delta^{13}CO_2$ variations seem coincident with fluctuations of the CO_2 rate of change, implying major reorganizations in the atmosphere-ocean-biosphere carbon exchanges. A comparison with C-cycle related tracers in the ocean (*Fig. 2*) suggests some potential major players: the North Atlantic Deep Waters (NADW) reduction during H1 and YD (*Fig. 2b*), deduced from $^{231}Pa/^{230}Th$ changes in the N. Atlantic[20]), is accompanied by a flushing of deep waters from the Southern Ocean (SO) into the N. Atlantic. These nutrient-enriched and $\delta^{13}C$-depleted waters, (opposed to those associated with NADW), are registered in N. Atlantic marine sediments[21] *(Fig. 2c)*, witnessing two negative $\delta^{13}C$-excursions during H1 and YD. Recently, a detailed $\Delta^{14}C$ record from N. Pacific intermediate waters was obtained through TI, showing two negative excursions of more than 200‰ during the same periods. They were interpreted as the transfer of old Antarctic Bottom Waters (AABW) into the N. Pacific, associated with the SO stratification breakdown, releasing sequestered and ^{13}C-depleted carbon into the atmosphere[22] (*Fig. 2d*). The latter is also witnessed in a low-resolution equatorial Pacific surface waters signal, where a significant ^{13}C-depletion is observed during the early deglaciation[23] *(Fig. 2e)*. This significant SO reconfiguration should have generated concomitant negative excursions in atmospheric $\delta^{13}CO_2$ and resumption of the signal in-between, a feature that we indeed observe in the EDC $\delta^{13}CO_2$ profile. This points oceanic circulation changes as potential drivers of our atmospheric signal throughout TI. Nevertheless, the $\delta^{13}CO_2$ maximum during the B/A, associated with the CH_4 maximum of TI *(Fig. 1b)* partly attributed to wetland emission increases[24], suggests a non-negligible role of the continental biosphere on the CO_2 signal during SP-III.

In order to further quantify the relative role of different mechanisms in the CO_2 and $\delta^{13}CO_2$ trends, we use two C-cycle box models: a coupled atmosphere/ocean/sediment/biosphere model applied in a transient mode and forced with time-dependent boundary conditions over TI ("BICYCLE")[13] *(see Fig. S2 in [19])* and a conceptual ocean/atmosphere model run under equilibrium ("BOXKIT")[14]. *Fig. 3* illustrates the imprint of individual time-dependent processes simulated with BICYCLE, on atmospheric *(a)* CO_2 and *(b)* $\delta^{13}CO_2$. The proxies used to represent

the time evolution of each process, as well as the modifications brought to BICYCLE versus the original version[13] are provided in [19] *(Figs. S3; S4)*. The sequence of simulated CO_2 and $\delta^{13}CO_2$ changes bearing similarities with the EDC observations can be summarized as follows: the initial CO_2 rise and $\delta^{13}CO_2$ decrease are principally forced by SO changes, explaining the observed correlation between CO_2 and the Antarctic plateau isotopic profiles[12;16] *(Fig. 1a;c)* or the SO Sea Surface Temperature (SST)[25]; the reduction of SO biological productivity (due to the onset of Fe-limitation[26]), combined with SO stratification breakdown[23] (related to sea-ice retreat and to decreasing salinity[7;27]) provoke a 15 and 22-ppmv CO_2-rise and a 0.20 and 0.32 ‰ $\delta^{13}CO_2$ decline, respectively. During the NH cold events (H1 and YD), NADW weakens[20], dampening the CO_2 increase and $\delta^{13}CO_2$ decrease related to AABW enhancement (+4.5 ppmv; -0.04‰)[21] (*Fig. S4 in* [19]); NADW (AABW) strengthening (weakening) at the end of SP-II and SP-IV, combined with stronger SO water mixing at the end of YD, lead to a CO_2 outgassing of 10 and 7 ppmv, respectively[12]. Neither carbonate compensation[28] nor sea level rise[29] processes leave a significant imprint on $\delta^{13}CO_2$ within the SPs (while the former generates a positive $\delta^{13}CO_2$ trend of +0.08‰ throughout TI, and the latter significantly affects CO_2 during the ACR, by provoking a 3-ppmv reduction). In contrast, vegetation growth, lagging SO warming[30] and forced by CO_2 fertilization and NH warming[19], starts affecting $\delta^{13}CO_2$ during SP-II and becomes a major driver of this signal during SP-III and SP-IV. The rise-and-fall of total biospheric carbon by 200PgC during SP-III and SP-IV respectively[13], lead to a 15-ppmv decrease and a 17-ppmv rise of CO_2, also causing a +0.35‰ and -0.40‰ $\delta^{13}CO_2$ anomaly.

The integrated signal from all these processes can be compared both for its timing and magnitude with our data, as seen in *Fig. 3*, (c) for CO_2, (d) for $\delta^{13}CO_2$. Overall, the patterns within the increasing CO_2 trend, as well as the $\delta^{13}CO_2$ W-shaped curve throughout TI, are well captured and the data/model agreement is improved with our recent BICYCLE simulation compared to the original version[13], although the timing (for both signals) can differ between observations and model outputs. In particular, the EDC $\delta^{13}CO_2$ peak of SP-III and the minimum of SP-IV appear delayed with respect to the BICYCLE output. Both $\delta^{13}CO_2$ features result from the terrestrial component in BICYCLE, itself mainly driven by NH temperature. As both EDC $\delta^{13}CO_2$ and the biosphere imprint in BICYCLE are on a common time scale, the shift cannot be attributed to dating errors. One explanation lies in the time response of biospheric components to climate change in BICYCLE, being possibly underestimated. We are equally aware that the model parameterisations bear other uncertainties and potential biases, such as: (i) the relative dating of the various input signals and their synchronization with ice cores, (ii) the pertinence of

the proxies used for each process (*e.g.* the magnitude of oceanic fluxes throughout TI), (iii) the coarse spatial resolution of low-latitudes, limiting investigations of the role of equatorial regions on our atmospheric signal. Still, the good resemblance between the BICYCLE and EDC trends gives some credibility to the sequence of processes involved in our interpretation of the combined CO_2 and $\delta^{13}CO_2$ trends over TI in the model.

Fig. 3c;d also incorporates the BOXKIT model outputs, permitting a direct comparison between the two box models. When BOXKIT is parameterized with similar forcings as BICYCLE, similar overall trends both for CO_2 and $\delta^{13}CO_2$ are obtained. However, the $\delta^{13}CO_2$ spike and trough of SP-III and SP-IV is not reproduced by BOXKIT. This model does not include a terrestrial reservoir, opposite to BICYCLE. On the other hand, it permits an easier modification of oceanic variables, as it is run in steady state. We conducted sensitivity tests in an attempt to reproduce the CO_2 and $\delta^{13}CO_2$ trends of SP-III with an oceanic scenario only and thus without considering a changing terrestrial biosphere. Increasing tropical SSTs by 3°C (instead of 0.5°C), concomitantly with NH warming, allows BOXKIT to reproduce the $\delta^{13}CO_2$ increase of SP-III with a lower magnitude than observed in the EDC core, while the CO_2 model output agrees well with our data.

In summary, our new record of $\delta^{13}CO_2$ from the EDC ice core over the last deglaciation, reveals sharp fluctuations mostly associated with variations in the CO_2 rate of change. Two C-cycle box models, applied for signal interpretation, jointly conclude towards the dominant role of oceanic processes (principally in the SO, such as marine productivity and SO stratification decline) during the early part of the deglaciation. Oceanic processes drive the CO_2 trend until the B/A period, when the terrestrial biosphere begins to strongly imprint the $\delta^{13}CO_2$ signal and to affect the CO_2 level. The YD $\delta^{13}CO_2$ minimum followed by the increase to EH values results from opposite contributions from the terrestrial biosphere and the ocean. Still, although the terrestrial biosphere appears as the main driver of $\delta^{13}CO_2$ after the start of the B/A, further sensitivity tests suggest that other mechanisms involving *e.g.* the equatorial ocean may also have partly contributed to the observed trend. More sophisticated approaches using coupled carbon-climate Earth system models will be needed in the future to better disentangle the contribution of each process, with their direct parameterisations in the models instead of the use of proxies. Our detailed EDC profile clearly highlights the need for fine time resolution in producing future $\delta^{13}CO_2$ records throughout major climatic events.

References:

1. IPCC, Climate Change 2007: The Physical Science Basis. Contribution of Working Group I to the Fourth Assessment Report of the Intergovernmental Panel on Climate Change (Solomon, S., D. Qin, M. Manning, Z. Chen, M. Marquis, K.B. Averyt, M. Tignor and H.L. Miller (eds.)). Cambridge University Press, Cambridge, United Kingdom and New York, NY, USA, 2007, 996 pp.
2. $\delta^{13}CO_2$ is reported in standard δ (delta) notation as the per mil (‰) difference between the stable carbon isotope composition of the sample and the standard Vienna Pee-Dee Belemnite (VPDB) :
$$\delta^{13}CO_2 = \left[\frac{\left({}^{13}CO_2 / {}^{12}CO_2 \right)_{sample}}{\left({}^{13}CO_2 / {}^{12}CO_2 \right)_{VPDB}} - 1 \right]$$
3. Francey, R.J., et al., A 1000-year high precision record of $\delta^{13}C$ in atmospheric CO_2. Tellus B, 1999. **51**(2): p. 170–193.
4. Friedli, H., et al., Ice core record of the $^{13}C/^{12}C$ ratio of atmospheric CO_2 in the past two centuries. Nature, 1986. **324**(6094): p. 237-238.
5. BP means Before Present, the present being defined at 1950 Anno Domini AD; ky for kilo (10^3) years
6. Broecker, W.S. and T.H. Peng, Carbon cycle: 1985 glacial to interglacial changes in the operation of the global carbon cycle. Radiocarbon, 1986. **28**(2A): p. 309-327.
7. Watson, A.J. and A.C. Naveira Garabato, The role of Southern Ocean mixing and upwelling in glacial-interglacial atmospheric CO_2 change. Tellus B, 2006. **58**(1): p. 73-87.
8. Archer, D., et al., What caused the glacial/interglacial atmospheric pCO_2 cycles? Reviews of Geophysics, 2000. **38**(2): p. 159-190.
9. Sigman, D. and E. Boyle, Glacial/interglacial variations in atmospheric carbon dioxide. Nature, 2000. **407**(6806): p. 859-869.
10. Smith, H.J., et al., Dual modes of the carbon cycle since the Last Glacial Maximum. Nature, 1999. **400**(6741): p. 248-250.
11. Leuenberger, M., U. Siegenthaler, and C. Langway, Carbon isotope composition of atmospheric CO_2 during the last ice age from an Antarctic ice core. Nature, 1992. **357**(6378): p. 488 - 490.
12. Monnin, E., et al., Atmospheric CO_2 Concentrations over the Last Glacial Termination. Science, 2001. **291**(5501): p. 112 - 114.
13. Köhler, P., et al., Quantitative interpretation of atmospheric carbon records over the last glacial termination. Global Biogeochemical Cycles, 2005. **19**: GB4020.
14. Paillard, D., M. Ghil, and H.L. Treut, Dissolved organic mater and the glacial-interglacial pCO_2 problem. Global Biogeochemical Cycles, 1993. **7**(4): p. 901-914.
15. Lavric, J.V., et al., Measurement of carbon isotope composition and mixing ratio of CO_2 in ancient air from ice core samples. in prep.
16. Jouzel, J., et al., Orbital and Millennial Antarctic Climate Variability over the Past 800,000 Years. Science, 2007. **317**(5839): p. 793 - 796.
17. Loulergue, L., et al., Orbital and millennial-scale features of atmospheric CH_4 over the past 800,000 years. Nature, 2008. **453**(7193): p. 383-386.
18. Brook, E.J., et al., On the Origin and Timing of Rapid Changes in Atmospheric Methane During the Last Glacial Period. Global Biogeochemical Cycles, 2000. **14**(2): p. 559–572.
19. See supplementary material.
20. McManus, J.F., et al., Collapse and rapid resumption of Atlantic meridional circulation linked to deglacial climate changes. Nature, 2004. **428**(6985): p. 834-837
21. Rickaby, R.E.M. and H. Elderfield, Evidence from the high-latitude North Atlantic for variations in Antarctic Intermediate water flow during the last deglaciation. Geochemistry Geophysics Geosystems, 2005. **6**: Q05001.
22. Marchitto, T.M., et al., Marine Radiocarbon Evidence for the Mechanism of Deglacial Atmospheric CO_2 Rise. Science, 2007. **316**(5830): p. 1456 - 1459.
23. Spero, H.J. and D.W. Lea, The Cause of Carbon Isotope Minimum Events on Glacial Terminations. Science, 2002. **296**(5567): p. 522-525.
24. Fischer, H., et al., Changing boreal methane sources and constant biomass burning during the last termination. Nature, 2008. **452**(7189): p. 864-867.
25. Bianchi, C. and R. Gersonde, Climate evolution at the last deglaciation: the role of the Southern Ocean. Earth and Planetary Science Letters, 2004. **228**(3-4): p. 407-424.
26. Martin, J.H., R.M. Gordon, and S.E. Fitzwater, Iron in Antarctic waters. Nature, 1990. **345**(6271): p. 156 -

158.
27. Stephens, B.B. and R.F. Keeling, The influence of Antarctic sea ice on glacial-interglacial CO_2 variations. Nature, 2000. **404**(6774): p. 171-174.
28. Archer, D. and E. Maier-Reimer, Effect of deep-sea sedimentary calcite preservation on atmospheric CO_2 concentration. Nature, 1994. **367**(6460): p. 260 - 263.
29. Fairbanks, R.G., A 17,000-year glacio-eustatic sea level record: influence of glacial melting rates on the Younger Dryas event and deep-ocean circulation. Nature, 1989. **342**(6250): p. 637 - 642
30. Hughen, K.A., et al., Abrupt Tropical Vegetation Response to Rapid Climate Changes. Science, 2004. **304**(5679): p. 1955 - 1959.
31. EPICA Community Members, One-to-one coupling of glacial climate variability in Greenland and Antarctica. Nature, 2006. **444**(7116): p. 195-198.

Acknowledgements *: no acknowledgments within review process*

Figure captions:

Figure 1.

CO_2 and $\delta^{13}CO_2$ evolution during the last deglaciation from the EPICA Dome C (EDC) ice core: (a) δD of ice in EDC averaged over 500y *(grey line)*[16], (b) atmospheric CH_4 mixing ratio *(red line and triangles: EDC*[17]*; green dots : TD*[18]*)*, (c) atmospheric CO_2 mixing ratio (*red line and dots: EDC measurements*[12]*; blue line and diamonds: this study; green dots: TD*[10]); and (d) $\delta^{13}CO_2$ data *(blue line and diamonds: this study; green dots : TD*[10]*)*. When duplicate measurements were performed, the line runs through the mean. The dotted lines for our CO_2 and $\delta^{13}CO_2$ data correspond to the 1σ uncertainty envelope.

All gas records are plotted versus the Greenland GICC05 age scale (details in [19]). The upper x-axis represents the EDC depth for the gas records. δD is plotted on a chronology combining the CH_4 fit to GICC05 and the EDC3 delta-age[31].

The vertical dotted lines correspond to boundaries between different CO_2 rates of change during the deglaciation, as defined by[12]. The time periods in-between are noted SP-I to SP-IV. YD: Younger Dryas; B/A: Bølling/Allerød; ACR: Antarctica Cold Reversal; H1: Heinrich 1.

Figure 2.

Comparison between atm. $\delta^{13}CO_2$ and paleoceanographic tracers during TI: **(a)** atmospheric $\delta^{13}CO_2$, from *this study*; **(b)** $^{231}Pa/^{230}Th$ in the subtropical N. Atlantic, a tracer of North Atlantic Deep Waters formation strength[20]; **(c)** benthic $\delta^{13}C$ in N. Atlantic intermediate waters, reflecting the relative strength between NADW and Antarctic intermediate waters throughout TI[21]; **(d)** $\Delta^{14}C$ data of intermediate waters in N. Pacific, a proxy for Southern Ocean overturning strength[22]; **(e)** low-resolution planktonic $\delta^{13}C$ in the Eastern Equatorial Pacific, associated with SO stratification strength[23]. Atmospheric $\delta^{13}CO_2$ is plotted versus the Greenland GICC05 age scale, while the oceanic proxies are on their original time scale.

Figure 3.

Comparison between EDC CO_2 and $\delta^{13}CO_2$ data and box-model simulations.

Left panels:

Imprint of individual C-cycle processes on atmospheric (a) CO_2 and (b) $\delta^{13}CO_2$, simulated with the BICYCLE model (description in [19]). All curves express an anomaly ΔpCO_2 and $\Delta\delta^{13}CO_2$ versus a "zero" point representing the boundary EH conditions. Processes are indicated epigrammatically (more details in [19]):

(1) SO mixing; (2) marine productivity; (3) sea ice; (4) NADW combined with AABW; (5) sea level; (6) carbonate compensation; (7) ocean temperature and (8) terrestrial biosphere.

Right panels:

Superposition of the BICYCLE simulation integrating all individual processes of the left panels (*grey line*) with our data (*deep blue line and diamonds*). The equilibrium-state BOXKIT model outputs, using similar boundary conditions as BICYCLE for each time period *(red triangles)* are also plotted for (c) CO_2 and (d) $\delta^{13}CO_2$. Red squares correspond to BOXKIT simulations using higher equatorial SST magnitudes. All series are plotted versus GICC05 age scale.

Figures

Figure 1

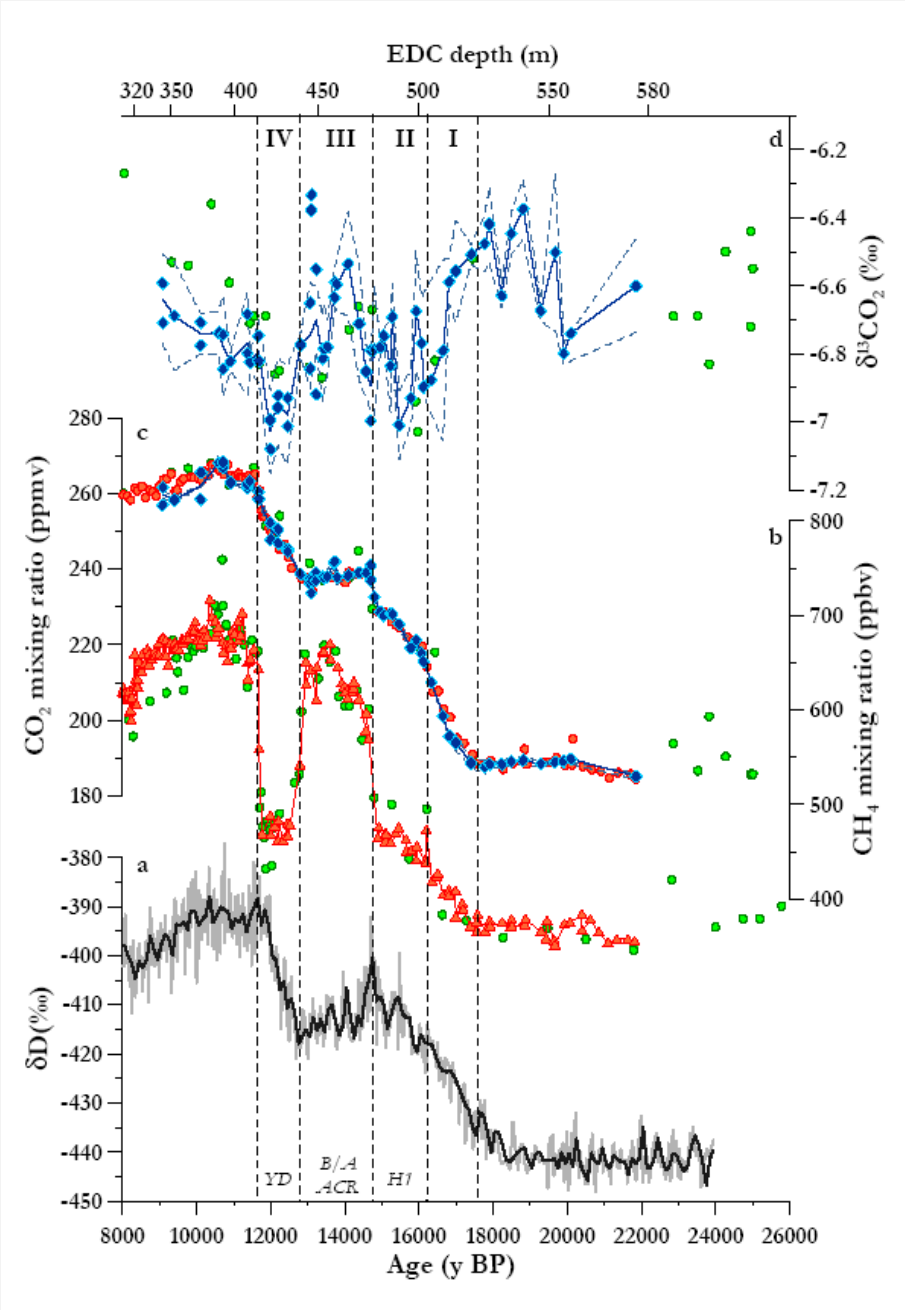

Figure 2

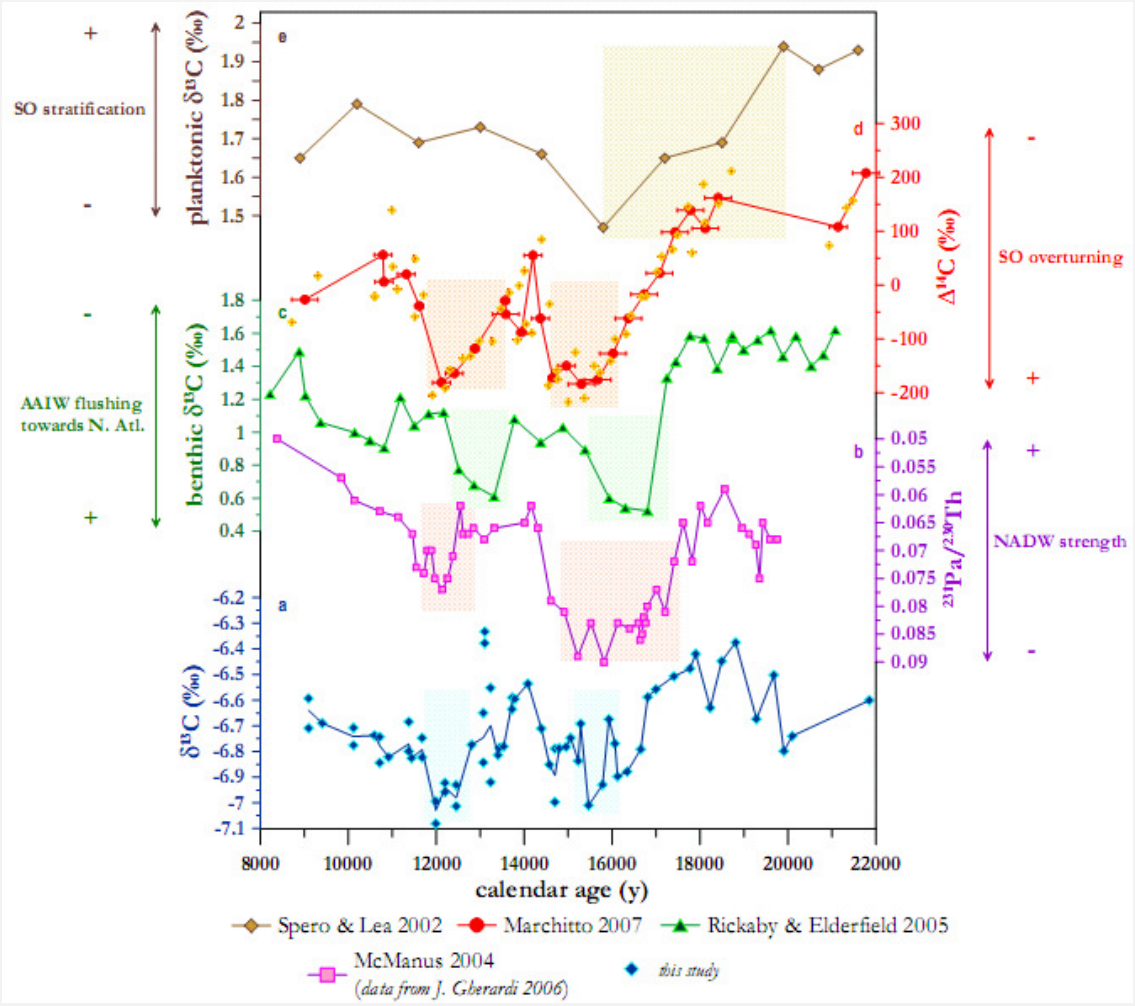
SO stratification
+
-
planktonic δ13C (‰)
e
d
SO overturning
Δ14C (‰)
AAIW flushing
towards N. Atl.
benthic δ13C (‰)
c
b
NADW strength
231Pa/230Th
a
δ13C (‰)
calendar age (y)
Spero & Lea 2002
Marchitto 2007
Rickaby & Elderfield 2005
McManus 2004
(data from J. Gherardi 2006)
this study

Figure 3

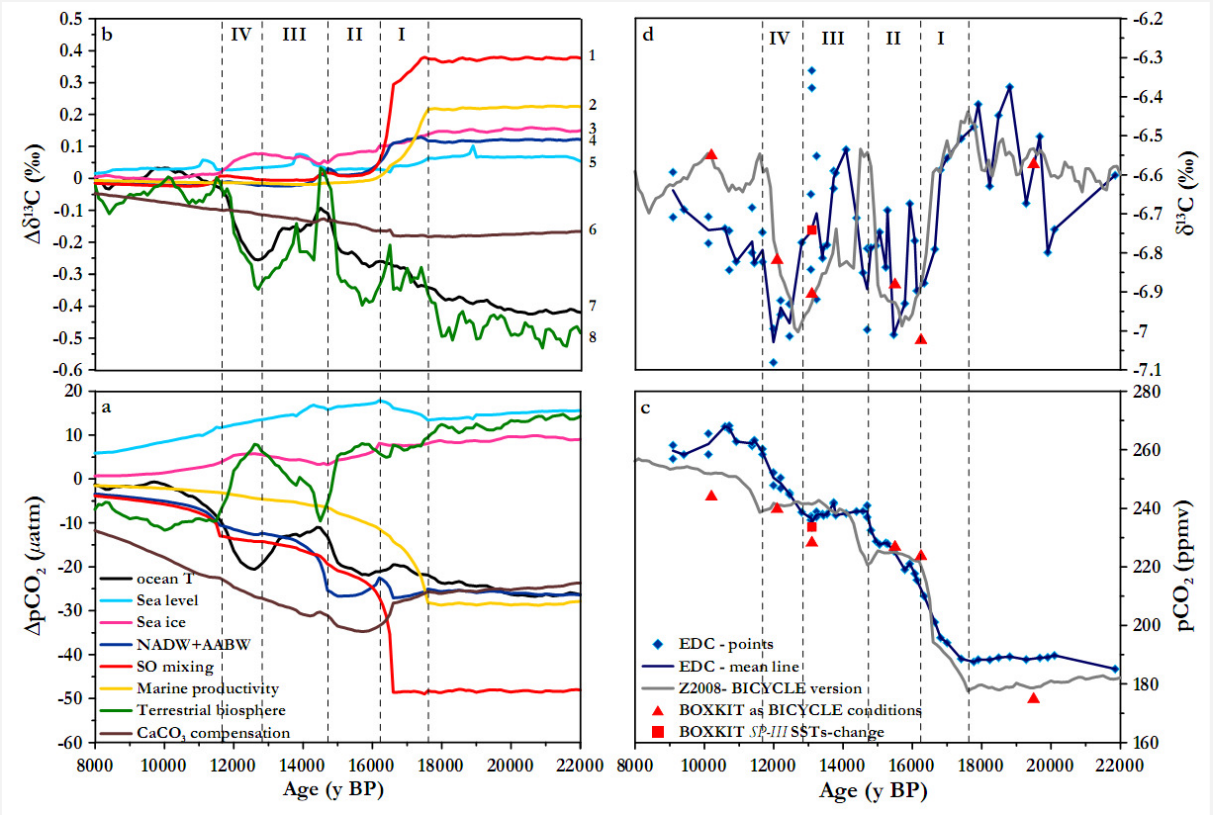
b
IV
III
II
I
Δδ13C (‰)
1
2
3
4
5
6
7
8
d
δ13C (‰)
a
ΔpCO2 (μatm)
ocean T
Sea level
Sea ice
NADW+AABW
SO mixing
Marine productivity
Terrestrial biosphere
CaCO3 compensation
c
pCO2 (ppmv)
EDC - points
EDC - mean line
Z2008- BICYCLE version
BOXKIT as BICYCLE conditions
BOXKIT S3-III SSTs-change
Age (y BP)
Age (y BP)

IV.3.3. Supplementary material

1) $\delta^{13}CO_2$ analysis/ corrections applied

A detailed description of extraction methods, isotope analysis and experimental tests will be provided elsewhere[1]. In short, 40-50 g of ice are sealed in a stainless steel ball mill, evacuated and crushed to fine powder. The gas liberated from the bubbles is expanded over a -80°C ethanol/liquid nitrogen (LN) water trap onto an evacuated 10 cm^3 sample loop. From there it is flushed by a ultrapure helium stream through a glass trap where the CO_2 is frozen out at LN temperature (-196°C). The trapped CO_2 is then transferred into another ultrapure helium stream, to be cryofocused on a small volume uncoated glass capillary tubing at LN temperature. The subsequent warming of the capillary allows the gas transfer into a gas chromatograph to separate the CO_2 from residual impurities (e.g. N_2O[2]) and its introduction via an open split to the isotope ratio mass spectrometer (IRMS, Finnigan MAT 252). The sample introduction in the IRMS is bracketed with injections of a pure CO_2 standard reference gas (ATMO MESSER, $\delta^{13}C$ = -6.475±0.1‰ versus VPDB) through another open split, to correct for instrumental drift at the scale of a few minutes.

On a daily basis, the correction of the carbon isotopic ratios obtained for ice samples is based on an external air standard (prepared at CSIRO, Australia: CO_2 = 260.26 ± 0.2 ppmv ; $\delta^{13}CO_2$= –6.40±0.03 ‰ versus VPDB), which is preconcentrated and transferred identically to ice-core gas samples. This is done several times before the sample, in-between the three expansions of the sample, and after the sample. On average, the deviation from the attributed CSIRO values over the whole EDC measurement period is no more than –0.30‰ for these daily standard measurements. The deviation observed on each day is applied to the samples measured on the same day. CO_2 in the ice samples is deduced from a linear regression between the pressure of the introduced standard gas and the CO_2 peak amplitude measured by the IRMS. The m/z 44 peak height of the pure CO_2 standard injected with each gas sample is fitted as closely as possible to the expected CO_2 peak height from the ice-core gas sample or CSIRO standard. The amount of standard gas processed before each ice-core gas sample expansion is also adjusted to the expected gas sample peak height. Blank runs are conducted by carrying out the gas transfer procedure without introducing any gas in the sample loop, as well as with artificial bubble-free ice. Results show no contamination of the whole setup for the former case and a slight negative shift for the latter one (-0.30±0.08‰, n=3). Due to the small number of bubble-free ice tests, and due to some doubts about their representativity of extraction conditions for real samples (*e.g.* possible isotopic fractionation of the standard gas when expanded from the vacuum line into the ball mill before crushing), we decided not to apply such correction to our measurements. Our

results can thus safely be compared qualitatively, but the absolute values may be subject to future additional small corrections.

Correction for diffusion processes in the firn column

Gravitational correction was calculated using $\delta^{15}N$ data of air from the EDC core[3] and modelled $\delta^{15}N$ data from an empirically derived relationship:

$$\delta^{15}N = 0.0020032 \times \delta D + 1.2969$$

Gravitational correction was applied for both CO_2 and $\delta^{13}CO_2$. The divergence between measured and modelled $\delta^{15}N$ data can be seen in Fig. S1.

Considering measured and calculated values, modelled $\delta^{15}N$ is lower than the measured one by a maximum of ~0.05‰ for LGM (n=2) and EH (n=3) while a good fit between both series is found throughout the deglaciation. When considering both series extrapolated to our depths, the difference is reduced to max. 0.03-0.04 ‰. Our $\delta^{13}CO_2$ data were corrected using the modelled $\delta^{15}N$ data because the availability of measured $\delta^{15}N$ data (interpolated at the depths of our samples) was restricted over the full depth range, and because the application of the measured value would introduce its analytical noise in the correction. The gravitational effect on $\delta^{13}CO_2$ being identical to $\delta^{15}N$ (1 atomic mass unit difference in both cases), the correction for our depths amounts between -0.41 and -0.55 ‰, following the δD trends throughout TI(Fig. S1).

The CO_2 mixing ratio was also corrected for gravitational fractionation, using the equation[4]:

$$[CO_2]_{corr} = [CO_2]_{meas} - \left[\left(M_{CO_2} - M_{air}\right) \times \delta^{15}N \times [CO_{2meas}]\right] = [CO_{2meas}] \times \left(1 - \frac{\delta^{15}N \times 15.2}{1000}\right)$$

M= molecular mass

In this case, the gravitational correction amounts between 1.16 and 2.20 ppmv.

Note that the gravitational correction was not applied for previous EDC CO_2 records[5].

The difference of the diffusion coefficient in air between $^{12}CO_2$ and $^{13}CO_2$ generates changes in the $\delta^{13}CO_2$ signal in firn air and trapped bubbles, whenever CO_2 varies in the atmosphere, and even if atmospheric $\delta^{13}CO_2$ does not change. The magnitude of this effect can be calculated with firn air diffusion models[6]. Under present-day conditions when CO_2 increases by about 2 ppmv/y, the

diffusion correction on firn air and trapped bubbles composition amounts to about 0.10‰ on a 70-m thick firn column[6]. As the correction is at first order proportional to the CO_2 rate of change, and as the largest observed CO_2 rate of change during TI is about 20 times smaller than the present-day rate of increase[7], the correction would amount to less than 0.01‰ on the EDC $\delta^{13}CO_2$ profile, and is thus neglected here.

Age scale

All EDC records are originally dated on the EDC3beta6[8] and EDC3_gas_a[9] age scales for ice and gas data, respectively. However, in order to compare our EDC data with data from other cores (of marine or polar origin) and with box-model simulations using NH datasets as proxies for some C-cycle processes, we synchronised both EDC and TD, using CH_4 as a time marker, to the newest Greenland chronology GICC05[10], applying the Analyseries software[11]. The tie-points for each core are presented in *table 1*. The synchronised TD chronology is less constrained than the EDC one, due to the poorer time resolution of its data[12]. The ice chronology (for δD in *Fig. 1* of the main text) is obtained by a combination of the CH_4 age fit on the GICC05 time scale and the Δ-age calculated with the EDC3beta6 chronology.

2) Data interpretation

Model BICYCLE

The model consists of a well-mixed atmospheric box interacting with a 10-box ocean reservoir and the terrestrial biosphere, which is sub-divided into 7 compartments[12]. The ocean further communicates with a sediment and a rock reservoir *(Fig. S2a)*. Mass balance equations are solved for the carbon stocks of the biospheric compartments, for Dissolved Inorganic Carbon, Total Alkalinity, PO_4 and O_2 in the 10 oceanic reservoirs, for CO_2 in the atmosphere and for the carbon isotopes in all reservoirs. We chose this box model for the following reasons: (a) it considers the major reservoirs (atmosphere, ocean, terrestrial biosphere), including a scheme for the carbonate compensation mechanism, which should not be ignored at these time scales[13]; (b) its typical time frame of simulations is relevant to our study; (c) it allows one to calculate transient carbon states for each reservoir; (d) it has been recently validated against present-day constraints and applied on interpreting the CO_2 and $\delta^{13}CO_2$ TD data during TI, as well $\Delta^{14}C$[14-16].

We use the model version, where terrestrial net primary productivity is more influenced by climate

(notably temperature) change than by CO_2 fertilization. This version is labelled "TB2" in former applications[17] (from now on called "GBC2005-version"). Here an update of this version is presented ("Z2008").

Model outputs are given in atmospheric partial pressure (pCO_2) in µatm units, which, only in dry air and at standard pressure conditions are identical to ice core nomenclature (ppmv); here an equality between the two is assumed, neglecting a relatively constant offset between both quantities of a few ppmv.

Parameterizations

Process variables were represented by proxy records or were parameterized as follows:

1) Sea level rises by ~110m between 22 and 8 kyr BP based on reconstructions of coral reef terraces[18] (*Fig. S3A*). This leads to changes in the salinity, in the concentrations of all oceanic tracers and in the volumes and surface areas of the oceanic boxes.

2) Temperature of all oceanic boxes is prescribed for present day from [19]. It changes over time according to oceanic proxy evidences for equatorial SST[20] (*Fig S3C*) and deep ocean temperature[21] (*F S3C*). High latitudinal changes are represented by ice core isotopic profiles (North Atlantic and North Pacific: $\delta^{18}O$ on GICC05 age scale from NorthGRIP[22;23], *Fig. S3B*; Southern Ocean: δD (corrected for the effect of sea level rise) from EDC[8;24] synchronised to GICC05[10;22], *Fig S3D*. Both ice core records are scaled to provide a ΔT of 4 K between the minimum glacial values and the present-day.

3) Marine productivity in the SO is scaled (if allowed by macro-nutrient availability) on dust input to the SO as approximated by the non sea-salt-dust record measured in EDC[25] (*Fig S3E*).

4) Ocean circulation between the 10 boxes for present conditions is parameterized with data from the World Ocean Circulation Experiment WOCE[26] (*Fig S2*). Compared to the initial application of BICYCLE[12], it was slightly modified to get a better agreement between simulated and reconstructed oceanic ^{13}C[27]. About 30% of the upwelled waters in the SO are immediately redistributed to the intermediate equatorial Atlantic Ocean, the residence of these (upwelled) waters being too small for the gas exchange to come to equilibrium.

5) The temporal changes in the ocean circulation (*Fig. S3F*) concern four distinct flow patterns :

   - NADW and the subsequent southward flow of deep waters in the Atlantic, their upwelling in

the Southern Ocean, and their northward surface flow, again in the Atlantic Ocean. The strength of NADW is assumed to be about 40% weaker[28] during the LGM than at present day (10 versus 16 Sv) with an even larger reduction to 2 Sv during H1 and a slight decrease of 5 Sv (versus EH value) during the YD[29].

- Changes in AABW which penetrate both the deep Atlantic (AABW_A) and deep Pacific (AABW_P). Based on the N-S anticorrelation during the abrupt climatic changes of TI, we considered a strengthening of these ocean flows in parallel with the weakening of NADW (*i.e.* during H1 and YD) and vice versa (for B/Å)[30;31]. In this study, we considered the EH AABW overall flux of 15 Sv (being partitioned between 6 SV for the Atlantic section and 9 Sv for the Pacific one) to be equal with the LGM configuration. During the cold NH events, each section were strengthened by 3 Sv.

- Vertical mixing in the SO (SOX). Based on various proxy evidence (e.g. $\delta^{13}C$ data from[32;33]), we propose that the glacial SO was highly stratified. We thus configured a 0 Sv for SOX during LGM, while at the beginning of TI, it was strengthened by 15 Sv. The end of YD also coincides with a further 5 Sv-enhancement.

- Changes in the terrestrial biosphere carbon pool are driven by a global temperature anomaly, which is calculated from the NorthGRIP $\delta^{18}O$ and EDC δD records, by applying a weighting function giving ¾ to NorthGRIP and ¼ to EDC, reflecting the latitudinal distribution of land outside of Antarctica. The glacial/interglacial amplitude of temperature change is considered as 8 K in the North and 5 K in the South. The parameterization of net primary productivity due to CO_2 fertilisation directly depends on the model calculated atmospheric CO_2 values. More details on the terrestrial biosphere module can be found in [17].

All ice core records (isotopic temperature proxies and nss-dust) were implemented as 500-year running means in the different parameterizations.

Modifications in oceanic variables

Compared with the GBC2005 version of BICYCLE, we modified some parameterizations for the new (Z2008) simulations, as follows :

(a) Carbonate compensation is represented by a relaxation function, which brings deep ocean carbonate ion concentration, CO_3^{2-}, back to initial values after every perturbation. This relaxation operates with a time delay (e-folding time) of τ = 1.5 kyr to account for the relatively slow

processes in the sediments. This value of τ was chosen based on reconstructed deep ocean carbonate ion dynamics[34]. Details of the approach are described in [14].

As far as ocean circulation changes (*Fig. S2b* for a general ocean circulation flow scheme and *Fig. S4a; b* for detailed changes) are concerned, we assumed a reduction of NADW by 8 Sv during H1, instead of the complete shutdown initially proposed. We also changed AABW in antiphase with NH deep waters, in order to better represent the bipolar seesaw in the simulations. Furthermore, 30% of upwelling fluxes in the SO are directly redistributed to the Atlantic intermediate waters (mentioned above)

Comparison between the GBC2005 and Z2008 BICYCLE simulations

Fig. S4 illustrates the effect of modified parameterizations for three processes in Z2008 on (a) CO_2; (b) $\delta^{13}CO_2$ (expressed as Δ with respect to a "zero" point corresponding to the EH). *Fig. S4c and Fig. S4d* represent the integrated output of both BICYCLE versions for CO_2 and $\delta^{13}CO_2$, respectively. Comparing the steady-state values for GBC2005 version, a higher/lower CO_2 (+10/-10ppmv) and $\delta^{13}CO_2$ (+0.18/-0.21‰) model output for the EH and LGM, respectively, is observed (*Fig. S4c;d*). When introducing a sediment response time to ocean CO_3^{-2} changes as mentioned above, the model/data CO_2 discrepancies are attenuated *(fig S4a;c)*. Concerning $\delta^{13}CO_2$, changes in the sediment e-folding time also gives better agreement between the model output and our data for the EH, while a NADW reduction instead of a shut-down during H1 generates a more positive modelled LGM output *(fig S4b; d)*.

Furthermore, we examined in detail the role of AABW, being anticorrelated with the NADW evolution throughout TI, by increasing its flow by 3 Sv during SP-II and SP-IV (*Fig. S3F)*. This leads to a 5-ppmv rise and a 0.04-‰ decrease for the two sub-periods, improving the data/model agreement *(fig S4 a;b)*. The opposed AABW-NADW modelled trends for both CO_2 and $\delta^{13}CO_2$ (*Fig. S4a*), reflect the bipolar seesaw imprint on the C-cycle towards the atmospheric reservoir *(Fig.2c;d in main text)*.

This new version of BICYCLE simulations (Z2008) leads to the following improvements:

1. LGM and EH boundary values are more consistent with our data

2. The timing and trend of the early deglaciation are better reconstructed, due to updated runs using the most recent age scale GICC05. Still, inconsistencies exist for the last two SPs of TI, as for the

case of TB2; the model trends lead the data.

3. The magnitudes of both CO_2 and $\delta^{13}CO_2$ changes throughout the different SPs are more consistent with our data.

The largest discrepancy between our data and BICYCLE new version lies in the EH. It could be explained by inadequate ocean circulation parameterisation: for instance AABW gets stable in BICYCLE simulations at the end of YD, whereas it should have been enhanced at that time, as for NADW

Model BOXKIT

This model provides an alternative to BICYCLE, to evaluate the magnitude of CO_2 and $\delta^{13}CO_2$ changes due to oceanic processes. Its ocean configuration is set to 10 boxes, similarly to BICYCLE; it includes a well-mixed atmospheric box, but not the terrestrial biosphere. The model solves the mass balance equations for PO_4, DIC, TAlk, O_2, as well as the isotopes ^{13}C and ^{14}C of DIC in all model boxes. Biological productivity in surface boxes is parameterized as a function of PO_4 using a standard Michaelis-Menton formula and constant Redfield ratios. The remineralization in the intermediate and deep ocean is represented as a constant fraction of the falling biological particulate flux. In contrast to BICYCLE, the terrestrial biosphere is not explicitly represented and there is no exchange with the sediment interface (no carbonate compensation): all tracers are therefore fully conservative in the ocean-atmosphere system. The model is highly configurable and allows for many sensitivity experiments. It is run under different equilibrium regimes[35]. Boundary conditions and input parameters were the same as in the BICYCLE experiments, allowing for a direct comparison between model outputs. Minor deviations between the models were further tested *(ex. ratio change)* and several sensitivity tests were performed, as described in the main text and visualised in *Fig. 3c;d.*

I.1.1. Supplementary - references

1. Lavric, J.V., et al., Measurement of carbon isotope composition and mixing ratio of CO_2 in ancient air from ice core samples. in prep.
2. Ferretti, D.F., et al., A new gas chromatograph-isotope ratio mass spectrometry technique for high-precision, N_2O-free analysis of $\delta^{13}C$ and $\delta^{18}O$ in atmospheric CO_2 from small air samples. Journal of Geophysical Research, 2000. **105**(D5): p. 6709–6718.
3. Dreyfus, G., PhD manuscript, in prep.
4. Etheridge, D.M., et al., Natural and anthropogenic changes in atmospheric CO_2 over the last 1000 years from air in Antarctic ice and firn. Journal of Geophysical Research, 1996. **101**(D2): p. 4115–4128.
5. Monnin, E., et al., Atmospheric CO_2 Concentrations over the Last Glacial Termination. Science, 2001. **291**(5501): p. 112 - 114.
6. Trudinger, C.M., et al., Modeling air movement and bubble trapping in firn. Journal of Geophysical Research, 1997. **102**(D6): p. 6747–6763.
7. Joos, F. and R. Spahni, Rates of change in natural and anthropogenic radiative forcing over the past 20,000 years. PNAS, 2008. **105**(5): p. 1425-1430.

8. Parrenin, F., et al., The EDC3 chronology for the EPICA Dome C ice core. Clim. Past, 2007. **3**(3): p. 485-497.
9. Loulergue, L., et al., New constraints on the gas age-ice age difference along the EPICA ice cores, 0–50 kyr. Clim. Past 2007. **3**(3): p. 527-540.
10. EPICA Community Members, One-to-one coupling of glacial climate variability in Greenland and Antarctica. Nature, 2006. **444**(7116): p. 195-198.
11. Paillard, D., L. Labeyrie, and P. Yiou, Macintosh program performs time-series analysis. EOS, transactions American Geophysical Union, 1996. **77**(39).
12. Köhler, P., et al., Quantitative interpretation of atmospheric carbon records over the last glacial termination. Global Biogeochemical Cycles, 2005. **19**: GB4020.
13. Broecker, W.S. and T.-H. Peng, The Role of $CaCO_3$ Compensation in the Glacial to Interglacial Atmospheric CO_2 Change. Global Biogeochemical Cycles, 1987. **1**(1): p. 15-29.
14. Köhler, P. and H. Fischer, Simulating low frequency changes in atmospheric CO_2 during the last 740 000 years. Clim. Past 2006. **2**(1): p. 57-78.
15. Köhler, P., et al., On the application and interpretation of Keeling plots in paleo climate research – deciphering $\delta^{13}C$ of atmospheric CO_2 measured in ice cores. Biogeosciences, 2006. **3**: p. 539-556.
16. Köhler, P., R. Muscheler, and H. Fischer, A model-based interpretation of low-frequency changes in the carbon cycle during the last 120,000 years and its implications for the reconstruction of atmospheric $\Delta^{14}C$. Geochemistry Geophysics Geosystems, 2006. **7**: Q11N06.
17. Köhler, P. and H. Fischer, Simulating changes in the terrestrial biosphere during the last glacial/interglacial transition. Global and Planetary Change, 2004. **43**(1-2): p. 33-55.
18. Fairbanks, R.G., The Age and Origin of the "Younger Dryas Climate Event" in Greenland Ice Cores. Paleoceanography, 1990. **5**(6): p. 937-948.
19. Levitus and Boyer, World Ocean Atlas Vol 4: Temperature. 1994.
20. Visser, K., R. Thunell, and L. Stott, Magnitude and timing of temperature change in the Indo-Pacific warm pool during deglaciation. Nature, 2003. **421**(6919): p. 152-155.
21. Labeyrie, L.D., J.C. Duplessy, and P.L. Blanc, Variations in mode of formation and temperature of oceanic deep waters over the past 125,000 years. Nature, 1987. **327**(6122): p. 477-482.
22. Andersen, K.K., et al., The Greenland Ice Core Chronology 2005, 15–42 ka. Part 1: constructing the time scale. Quaternary Science Reviews, 2007. **25**(23-24): p. 3246-3257
23. NGRIP, M., High-resolution record of Northern Hemisphere climate extending into the last interglacial period. Nature, 2004. **431**(7005): p. 147-151.
24. Jouzel, J., et al., A New 27 Ky High Resolution East Antarctic Climate Record. Geophysical Research Letters, 2001. **28**(16): p. 3199-3202.
25. Roethlisberger, R., et al., Dust and sea salt variability in central East Antarctica (Dome C) over the last 45 kyrs and its implications for southern high-latitude climate Geophysical Research Letters, 2002. **29**(20) pp. 24-1, Cite ID 1963
26. Ganachaud, A. and C. Wunsch, Improved estimates of global ocean circulation, heat transport and mixing from hydrographic data. Nature, 2000. **408**(6811): p. 453-457.
27. Köhler, P. et al., submitted to Global Biogeochemical Cycles.
28. Meissner, K.J., et al., Ventilation of the North Atlantic Ocean during the Last Glacial Maximum: A comparison between simulated and observed radiocarbon ages. Paleoceanography, 2003. **18**(2), Cite ID 1023
29. McManus, J.F., et al., Collapse and rapid resumption of Atlantic meridional circulation linked to deglacial climate changes. Nature, 2004. **428**(6985): p. 834-837
30. Broecker, W.S., Paleocean Circulation during the Last Deglaciation: A Bipolar Seesaw? Paleoceanography, 1998. **13**(2): p. 119-121.
31. Rickaby, R.E.M. and H. Elderfield, Evidence from the high-latitude North Atlantic for variations in Antarctic Intermediate water flow during the last deglaciation. Geochemistry Geophysics Geosystems, 2005. **6**: Q05001.
32. Hodell, D.A., et al., Pleistocene vertical carbon isotope and carbonate gradients in the South Atlantic sector of the Southern Ocean. Geochemistry, Geophysics, Geosystems, 2003. **4**(1), Cite ID 1004
33. Spero, H.J. and D.W. Lea, The Cause of Carbon Isotope Minimum Events on Glacial Terminations. Science, 2002. **296**(5567): p. 522-525.
34. Marchitto, T.M., J. Lynch-Stieglitz, and S.R. Hemming, Deep Pacific $CaCO_3$ compensation and glacial–interglacial atmospheric CO_2. Earth and Planetary Science Letters, 2005. **231**(3-4): p. 317-336.
35. Paillard, D., M. Ghil, and H.L. Treut, Dissolved organic mater and the glacial-interglacial pCO_2 problem. Global Biogeochemical Cycles, 1993. **7**(4): p. 901-914.
36. Brook, E.J., et al., On the Origin and Timing of Rapid Changes in Atmospheric Methane During the Last Glacial Period. Global Biogeochemical Cycles, 2000. **14**(2): p. 559–572.

Supplementary figures

Figure S1

Gravitational correction applied to our data.

(a) EDC $\delta^{15}N$ values during TI, measured in the trapped gases[3] (blue circles and line) or calculated from an empirical equation between δD and $\delta^{15}N$ (pink line). Corrections are applied both for (b) (CO_2) and (c) $\delta^{13}CO_2$. The different curves are plotted here versus EDC3_gas_a scale[9].

Figure S2

Sketch of the "Box model of the Isotopic Carbon cYCLE" (BICYCLE).

(a) Overall model setup.

Compartments in the terrestrial biosphere distinguish different primary production schemes for grasses (C3, C4), non woody (NW) and woody (W) biomas of tree, detritus (D) and fast and slow (FS, SS) decomposing soils.

(b) Close-up on the definition of ocean boxes and the circulation scheme. Fluxes are given in Sverdrup ($1Sv = 10^6\ m^3/s$)

Figure S3

Proxy data sets used to force BICYCLE forward in time. Shadings highlight the definition of sub-periods given in the main text.

A: Coral reef terraces as indicator for sea level rise[18].

B: NorthGRIP $\delta^{18}O$ as northern high latitude temperature proxy[23].

C: Changes in equatoral SST[20] and deep ocean temperature in different oceanic compartments[21].

D: EDC δD as southern high latitude temperature proxy[24].

E: EDC nonseasalt (nss) dust as proxy of aeolian iron input into the Southern Ocean[25].

F: Assumed changes in ocean circulation fields.

B, D, E: these data show large short term fluctuations; therefore, the original records are overlayed by

a 500-year running mean which is used in the simulations.

All ice core records (B, D, E) are plotted versus the GICC05 age scale.

Figure S4

left panel:

Comparison of process imprints with BICYCLE GBC2005 and Z2008 versions, on (a) CO_2 and (b) $\delta^{13}CO_2$ (expressed as a difference, Δ, with respect to the initial Early Holocene steady state or "zero" point)

The GBC2005 version[12] is represented by dotted lines while Z2008 is plotted as straight lines.

The concerned processes are:

deep water formation changes (blue line) : influence solely of NADW in GBC2005 (dotted line); NADW and AABW (being anticorrelated) together in Z2008 (straight line).

The AABW evolution in Z2008 is represented by the straight orange line

$CaCO_3$ compensation mechanism (dark brown) : the GBC2005 version corresponds to an immediate sediment reaction to changes (dotted line), whereas the new Z2008 version reflects the introduction of an e-folding time for this response (straight line).

right panel:

Comparison of both model versions (black lines) to our dataset (blue diamonds). The dotted line corresponds to the initial BICYCLE (GBC2005) simulation throughout TI, as described in [12]. The straight line corresponds to our modified BICYCLE Z2008-configuration. The four plots are on the Greenland GICC05 age scale

Supplementary tables

Table S1: Tie-points between the EDC EDC3_gas_a[9] and GICC05 time scales[10;22;23]

EDC3_gas-a age (y BP)	GICC05 gas age (y BP)	CH_4 value (ppbv)	event description
7890	8240	590	CH_4 minimum during Holocene
11330	11680	560	CH_4 mid-rise / ending of YD
11920	12330	460	CH_4 YD minimum
12340	12790	540	CH_4 mid decrease / ending of B/A
13070	13600	670	B/A CH_4 peak
14010	14640	570	CH_4 mid-rise / towards B/A
15870	16200	470	CH_4 peak
17790	17800	370	CH_4 drop
19690	19670	350	CH_4 drop
21220	21100	350	CH_4 drop during LGM

The TD-core was initially plotted versus GISP2 age scale[36]. GISP2 is almost synchronous to GICC05; still, for the LGM time-period, GISP2 had to be rescaled :

TD gas age (y BP)	GICC05 gas age (y BP)	CH_4 value (ppbv)	event description
8300	8290	570	CH_4 minimum during Holocene
11690	11660	660	CH_4 peak after YD
11890	11860	430	CH_4 YD minimum
12910	12830	600	CH_4 mid decrease / ending of B/A
13570	13430	670	B/A CH_4 peak
14880	14790	510	Just before the B/A CH_4 rise
16770	16200	500	CH_4 peak before B/A
26470	22810	420	CH_4 peak during LGM

Figures

Figure S1

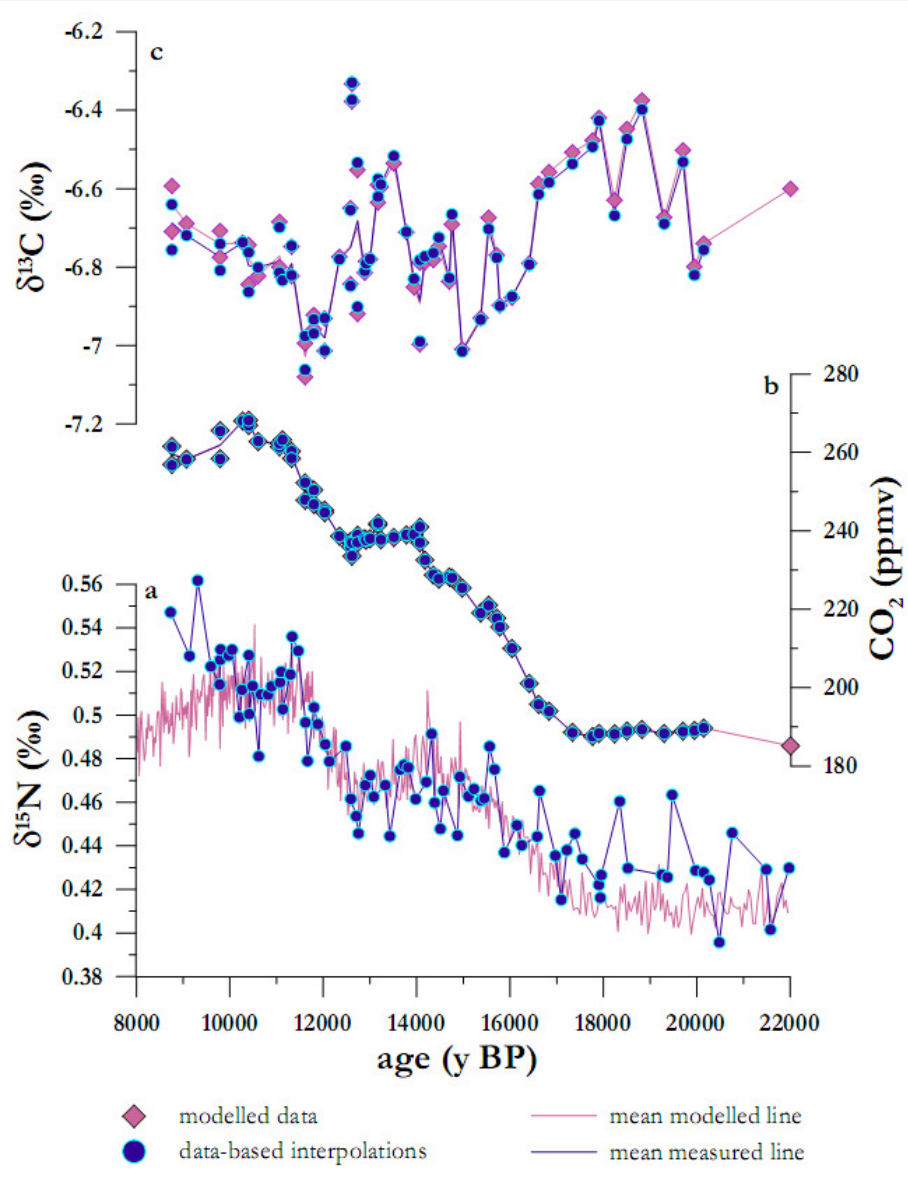

Figure S2

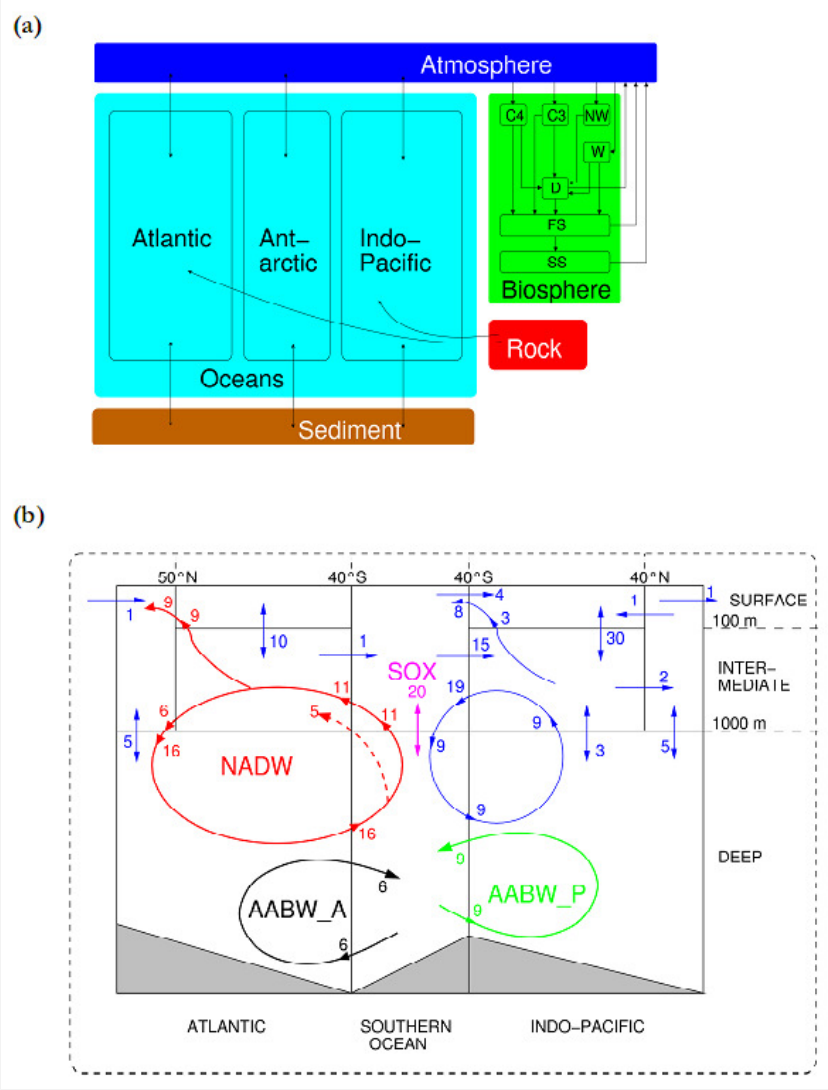
(a)
Atmosphere
Atlantic
Ant–
arctic
Indo–
Pacific
Oceans
Sediment
C4
C3
NW
W
D
FS
SS
Biosphere
Rock
(b)
50°N
40°S
40°S
40°N
SURFACE
100 m
INTER–
MEDIATE
1000 m
DEEP
SOX
20
NADW
AABW_A
AABW_P
ATLANTIC
SOUTHERN
OCEAN
INDO–PACIFIC

Figure S3

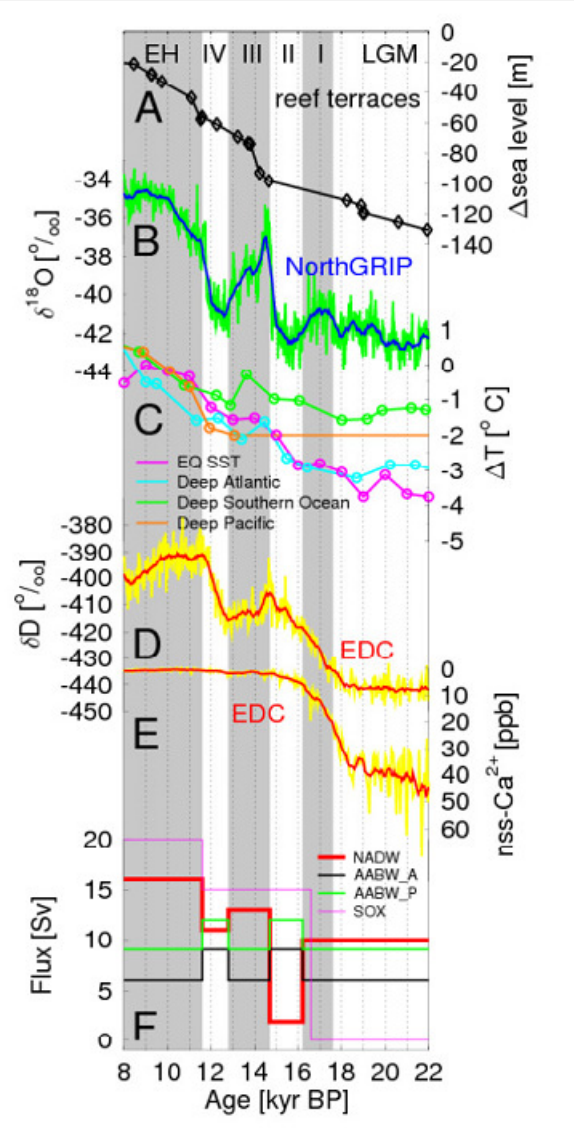
EH
IV
III
II
I
LGM
A
reef terraces
Δsea level [m]
B
NorthGRIP
δ18O [‰]
C
EQ SST
Deep Atlantic
Deep Southern Ocean
Deep Pacific
ΔT [°C]
D
EDC
δD [‰]
E
EDC
nss-Ca2+ [ppb]
NADW
AABW_A
AABW_P
SOX
F
Flux [Sv]
Age [kyr BP]

Figure S4

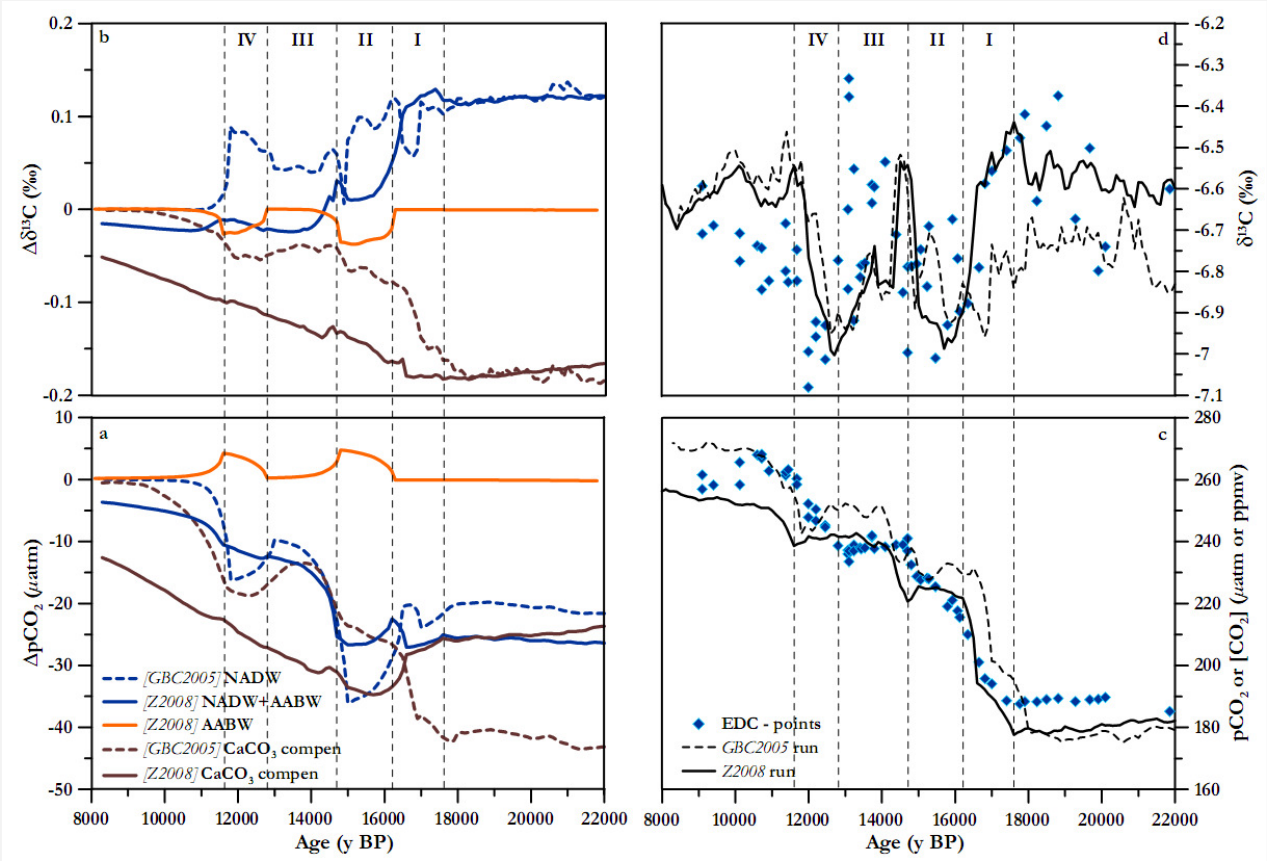
b
IV
III
II
I
ΔδC (‰)
a
ΔpCO2 (µatm)
[GBC2005] NADW
[Z2008] NADW+AABW
[Z2008] AABW
[GBC2005] CaCO3 compen
[Z2008] CaCO3 compen
Age (y BP)
d
δ13C (‰)
c
EDC - points
GBC2005 run
Z2008 run
pCO2 or [CO2] (µatm or ppmv)
Age (y BP)

IV.4. Discussion - On the causes of CO_2 deglacial evolution

In this section some main theories on the causes of the G-IG CO_2 rise will be exposed. The potential protagonists, their impact on CO_2 and $\delta^{13}C$, when available, and their strengths and caveats will be discussed, based (i) on literature research and (ii) on our own simulated results by either BICYCLE (most of which are already provided in IV.3.2 draft or BOXKIT (sensitivity tests).

IV.4.1. Sea Surface Temperature

CO_2 is more soluble in cold water (Henry's law). Consequently, the ocean has a tendency in absorbing CO_2 during cold periods and out-gassing CO_2 during warm periods[1]. There are some limitations on the reconstructions of SSTs throughout the TI for different oceanic regions or depths, dealing with the physical water properties (knowing that salty water freezes at –2°C), the oceanographic indicators (alkenones against Mg/Ca ratio, *see Bard, 2002 for more*) or the ventilation conditions. Despite the above constraints, SST changes have been long considered as primordial on exerting control upon both CO_2 and $\delta^{13}C$ on G-IG timescales. Both box model and **GCM**[2] results reveal a range of 14-23 ppmv rise for CO_2 (Broecker and Peng, 1986; Heinze et al., 1991; Toggweiler, 1999; Ridgwell, 2001; Köhler et al., 2005), the latter concluded in a 32-ppmv increase when SST is examined separately *(cf. IV.3.2)*. The impact of SST on $\delta^{13}C$ involves additional parameters, such as reservoir changing sizes of oceanic and atmospheric pools and the air-sea exchange isotopic fractionation, being itself also dependent on temperature. Ridgwell, 2001 calculates a 0.19‰ increase for $\delta^{13}C$ between G and IG, while Köhler et al., 2005 simulate the doubled value. Tests with the BOXKIT model, having a similar ocean configuration to BICYCLE (*cf. annex VIII*), agree with pre-mentioned assumptions on sign and magnitudes for both variables. If a 3°C rise is applied to separate surface boxes, an overall CO_2 rise of ~18.5 ppmv is simulated, accompanied by a $\delta^{13}CO_2$ enrichment by ~0.3‰. These calculations critically depend on the input LGM parameters: for instance Ridgwell, 2001 by introducing a 2°C additional cooling to the **CLIMAP**[3] equatorial SST reconstructions during LGM, resulted in an additional G-IG CO_2 rise by ~+13-ppmv and ~+0.14‰ for $\delta^{13}CO_2$. Increased sensibility of polar regions concerning CO_2 with box models, is validated in BOXKIT simulations, the S.

[1] As already exposed in Ch. I, CO_2 is more soluble in saline waters, as well (principle of THC); the interplay of temperature and salinity is therefore crucial in quantifying the effect of solubility to atmospheric CO_2. Enhanced evaporation or ice sheet formation render water more saline

[2] General Circulation Models

[3] Climate: Long-Range Investigation, Mapping, and Prediction

Ocean box being at least twice as sensible as the rest of the compartments, the N. Atlantic one following.

Focus on equatorial regions

Box models are not sensible enough on SST changes from equatorial regions. Still, these regions are thought to contribute to G-IG CO_2 changes either in a direct way, through heat exchange with the atmosphere, or indirectly, through their influence on the hydrological cycle, since they are major sources of latent heat and water vapor to the atmosphere.

When consulting the relevant tropical-equatorial literature (some representative data seen in fig. 4-2, left panel), one finds contradictory SST signals: (i) those exhibiting the same pattern and timing as Antarctic SST (Levi et al., 2007; Visser et al., 2003; Lea et al., 2000; Rühlemann et al., 1999; Koutavas et al., 2002 and (ii) SST records representing the same oscillations as the NH temperature signals (Bard et al., 1997; Kienast et al., 2001; Lea et al., 2003; Hughen et al., 2004; Kienast et al., 2006). In the first case, where equatorial regions lead over NH warming, changes in THC could be responsible for this asynchrony (Rühlemann et al., 1999) and has been considered to our model input forcings. On the opposite case of synchronicity between low latitudes and NH changes, other driving factors have been proposed as responsible for inter-hemispheric climatic connections leading to synchronous global atmospheric changes (*e.g.* water vapour, Bard et al., 1997).

On the right panel of fig. 4-2, we expose a run test using SSTs belonging to these different categories[4]. A correlation with the phase, the sign and less the magnitude of our $\delta^{13}CO_2$ signal is best simulated when considering equatorial SST data being in phase with the NH (Lea et al., 2003). A similar output was concluded with the BOXKIT model for the SP-III (*cf. IV.3.2*).

The coarse resolution of both box models used cannot provide additional information on the role of equatorial regions. Still, here we provide some first evidence that should be further searched in the future.

[4] simulation test conducted in AWI from P. Köhler in July 2007

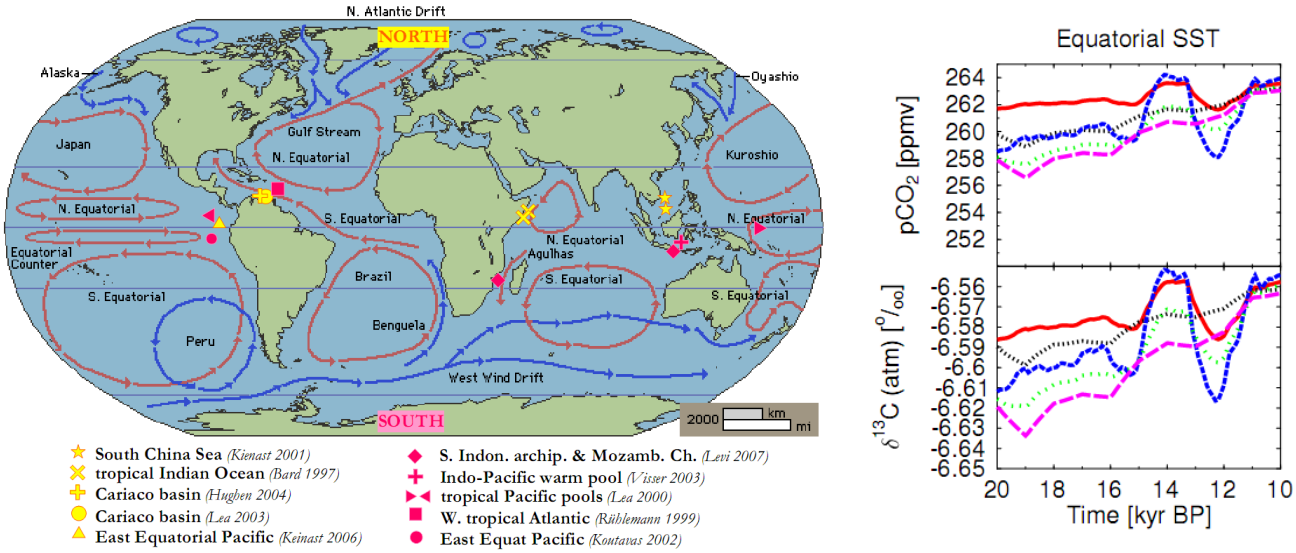

Fig. 4-2: (left panel) *Low latitudes trend during TI, been in pace with either NH (yellow signs) or SH (magenta signs) trends.* ***(Right panel)*** *model simulations considering the following scenarios: SSTs of Visser et al., 2003 seen as (i) black line –for equat. Pacific only - (ii) magenta line –for the whole equat. Ocean-. SSTs from Lea et al., 2003 seen as (iii) red line for the equat. Atlantic only- and (iv) blue for the whole equat. ocean. The green line couples the data from Visser et al., 2003 and that from Lea et al., 2003 for the corresponding area. The scenario used in Köhler et al., 2005 was the (ii) with the magenta line.*

IV.4.2. Sea level

Sea level rises up to ~120m throughout G-IG transitions, as a response of the waxing and waning of ice sheets. Proxy sea level indicators are mainly coral reef terraces (Fairbanks, 1989) and transgressions of shallow marine environments (Yokoyama et al., 2000). In an alternative way, sea level (and global ice volume) can be reconstructed from oxygen isotopic composition of benthic (and sometimes planktic) foraminifera, after making strong assumptions on local hydrological, temperature or salinity patterns (Lea et al., 2002; Waelbroeck et al., 2008). In principle, sea level change throughout TI should have provoked a decline in CO_2, opposite to that observed in ice cores, the main reasons lying in :

- a rise in hydrostatic pressure at deep-sea sediments surface, leading to reduced $CaCO_3$ preservation in the deep ocean, which then leads to an input of DIC and TAlk, driving CO_2 to lower values
- a "dilution" of C-cycle elements, such as DIC or TAlk and nutrients,
- a lower salinity : during G periods, ice sheets formation let more salt in the oceans, while during IG their melting lowers ocean salinity by 3% (Toggweiler and Samuels, 1995)

In the literature, a ~13 ppmv decrease has been reported for CO_2 (Broecker and Peng, 1986; Ridgwell, 2001; Köhler et al., 2005; Brovkin et al., 2007), the latter study finding it halved when combined with other scenarios. Sea level changes do not impact $\delta^{13}CO_2$ (<0.02‰, (Ridgwell, 2001; Köhler et al., 2005)). When rising sea level similarly to Köhler et al., 2005 in our BOXKIT simulation, a ~9 ppmv decrease revealed, accompanied by almost no atm. $\delta^{13}CO_2$ change, in accordance with what was simulated in the draft attached.

IV.4.3. Sea ice extent

Sea ice extent changes are closely related to gas exchange rates. Recent LGM reconstructions suggest that ice cover was much more extensive than today, especially during the winter period (Gersonde et al., 2005). Since NH acts as a sink and the SH as a source of CO_2 on **PI**[5] conditions, and since the sea ice acts as a barrier between air and ocean at LGM, this would lead to a strong hemisphere-dependence for both atmospheric CO_2 and $\delta^{13}CO_2$ signals. Concretely, a CO_2 enhancement is expected for the SH and decline for the NH during the G-IG transition. Stephens and Keeling, 2000, in a modelling approach, found that G-IG variability in S. Ocean sea ice coverage had a considerable effect on both the CO_2 concentration and its stable carbon isotopic composition. They achieved in simulating a 67-ppmv CO_2 G-IG rise and a 0.9‰ decline in $\delta^{13}CO_2$, by enhancing the air-sea exchange south of the **APF**[6] and by reducing deep DIC concentration. Other modelling studies did not reach such elevated values. The differences from this widely-referenced study were primarily attributed to the box model resolution, while their surface pCO_2 distribution, together with a possible overestimate of LGM sea-ice coverage had been questioned. Morales-Maqueda and Rahmstorf, 2002 conclude to only a 15-50% sea ice influence on the total G-IG CO_2 trend. Ridgwell, 2001 report a ~12 ppmv G-IG CO_2 decline for the NH and a ~7.5 ppmv rise for the SH. The net CO_2 decline was accompanied by an overall ~0.37‰ $\delta^{13}CO_2$ G-IG decline (Ridgwell, 2001), with a ~80% contribution from the SH, due to the larger surface area. The isotopic results were compatible with the outputs from Broecker and Peng, 1986. Köhler et al., 2006 by applying extreme sea ice cover conditions (reducing gas exchange rates to zero), yield to a 35-ppmv drop for NH and a 15-ppmv rise for SH, while for both cases $\delta^{13}CO_2$ declined by 0.04 and 1‰, respectively. Overall, the evaluation of the sea ice effect on CO_2 G-IG changes has been considered model-dependent (Archer et al., 2003). In our case presented in the draft, model resolution is coarse, thus not permitting on a clear distinction between NH and SH. We therefore observe a small decreasing CO_2 trend simulated out of the

[5] Rappel: Pre-Industrial
[6] Antarctic Polar Front

sea ice extent. Further tests with BOXKIT agree well with BICYCLE; separate tests on surface ocean boxes revealed a higher CO_2 depletion for the NH, while no major differences are seen for $\delta^{13}CO_2$. Another factor which should not be neglected deals with the efficiency of gases to diffuse across sea-ice, which is far from zero (Zemmelink et al., 2006). The majority of studies provide different magnitudes for both CO_2 and $\delta^{13}CO_2$ simulated signals, when compared to Stephens and Keeling, 2000 study. For this reason the latter study is sometimes excluded from data compilations (*e.g.* in fig. 4-4).

IV.4.4. Ocean circulation

Changes in the strength of THC or in wind-driven equatorial upwelling rates and their impact on both solubility and biological pumps have been long considered as a key driving force behind G-IG atmospheric CO_2 variations (Siegenthaler and Wenk, 1984; Sarmiento and Toggweiler, 1984; Howard and Prell, 1994; Toggweiler, 1999). Increased surface stratification is considered as an important driver, as well (François et al., 1997). Below I attempt to separate oceanic circulation branches and quantify their influence against our atmospheric signal.

IV.4.4.1. THC

Ocean circulation patterns in the Atlantic sector are already discussed in the general framework of the bipolar seesaw (*cf. IV.2.2.4 section*). In the literature, one finds variable model outputs, depending mainly on the input conditions in terms of oceanic fluxes. Toggweiler, 1999 report a ~20-ppmv CO_2 rise from only deep water ventilation G-IG reconfigurations, while Ridgwell, 2001 finds a small ~6-ppmv increase, accompanied by no alterations in $\delta^{13}CO_2$ (<0.03‰) in a THC variability test based only on end-member advective fields. Köhler et al., 2006 find the opposite modeled trends for CO_2 than the previous studies, by regarding a close link of THC weakening with upwelling reduction (thus leading to a 10 ppmv- CO_2 drop and a $\delta^{13}CO_2$ rise by 0.05‰ during the cold NH periods). Köhler and Fischer, 2006 remind that any oceanic circulation effect, combined with the sea ice effect, during the periods of the bipolar seesaw throughout TI, would provoke an in-phase response from both hemispheres towards the atmospheric CO_2 signal. For e.g., a NADW reduction during the cold NH periods (H1 and YD), would lead to a CO_2 rise, considering a concomitant NH sea ice increase and the "CO_2 sink" character of the N. Atlantic. Furthermore, the combination of the "CO_2 source" behavior of the S. Ocean, with a SH sea ice melting and an enhancement of AABW during the same cold NH sub-periods, would also lead to an increase in atmospheric CO_2. Fischer et al., 2003 rule out a leading THC influence on the CO_2 signal, by recalling the close correlation of CO_2 with Antarctic temperature and the absence of any rapid NH event (*i.e.* D/O) in the CO_2 signal. But such

qualitative assessment cannot lead to any substantiated conclusion. Deglacial scenarios of THC changes have to be integrated in carbon-cycle models to quantify their impact on CO_2.

THC changes, as explained in paleoceanographic data (Marchitto et al., 1998; McManus et al., 2004; Rickaby and Elderfield, 2005) during the NH cold periods of TI (SP-II with H1 and SP-IV with YD) are depicted onto the CO_2 signal, with an abrupt rise at the end of these periods (Monnin et al., 2001). Effectively, these CO_2 increasing patterns are observed through both model processes (BICYCLE, *cf. IV.3.2* and BOXKIT). A NADW enhancement at the end of SP-II and SP-IV led to $\delta^{13}CO_2$ trends opposed to our atmospheric signal, though. In addition to this, model results during the cold NH periods on the anti-phased signal of NADW and AABW are provided in the *IV.3.3 section*, where we see the dominance of the AABW over NADW to our atmospheric signal.

IV.4.4.2. Vertical mixing and ocean stratification reconfigurations

Vertical mixing G-IG changes and their impact on atmospheric values have been linked with the S. Ocean (François et al., 1997). It has been hypothesized that during G periods, the increase in sea ice cover, reducing air-sea exchange, kept stored in the deep ocean high CO_2 concentrations. With the onset of the deglaciation, SH temperature rose and the ice sheet melted, leading to a S. Ocean stratification breakdown, thus liberating the stored DIC in the deep ocean towards the atmosphere (accompanied by a ^{13}C-depleted signal). The above mechanism has been widely investigated and validated through a number of marine data (Hodell et al., 2003; François et al., 1997; Adkins et al., 2002) and model outputs (Gildor et al., 2002 ; Watson and Garabato, 2006). Köhler et al., 2005 report a ~30ppmv rise (in accordance with Schmittner et al., 2007) and a ~0.25‰ G-IG decline (*cf. IV.3.2 section*). BOXKIT reconstructs the same tendencies but of reduced amplitude.

IV.4.5. Wind speed

Wind speed paleo-reconstructions have been contradictory to the past, back to the LGM. While GCM model results[7] suggest no serious wind strength difference between LGM and Holocene, ice proxies, such as sodium rates, provide evidence of at least 50% higher winds during glacial periods (Keir, 1993). Ridgwell, 2001 finds a 4.5 ppmv rise accompanying a 0.16‰ rise, related to lower G-IG wind strength. In fig. 4-3, we provide a test on winds strength change conducted in AWI with P. Köhler, by changing in an anti-phased manner polar and equatorial winds:

[7] from BRIDGE simulations provided in the http://www.paleo.bris.ac.uk/ummodel/users/guest/index.html

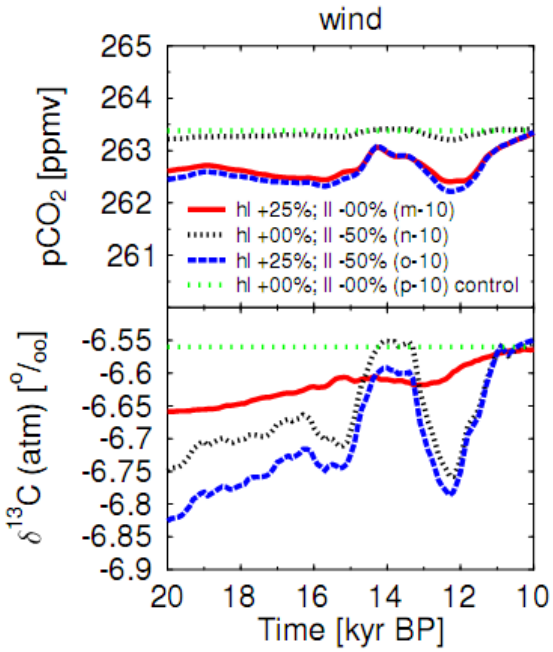

Fig. 4-3: *BICYCLE simulations for various combined scenarios of wind strength concerning hl =high latitudes and ll =low latitudes during LGM. Red line shows the case of enhancing winds of hl by 25% during LGM, black line shows the case of reducing ll winds by 50% during LGM and the blue line exposes the combined result of the upper two cases.*

We deduce that the best case scenario leading towards our atm. $\delta^{13}CO_2$ signal consists of either a 50% wind G-IG enhancement in equatorial regions, leading to an El Niño-like pattern at G state, or a combined weakening of polar winds (by 25%), accompanied by the same 50% equatorial winds enhancement. Still, in BICYCLE simulations, winds were temperature-dependent; this, combined to the opposed opinion on the winds forcing on a G-IG scale, we did not include such simulation in the combined proposed scenario in *IV.3.2 section.*

IV.4.6. Coral reef hypothesis

G-IG sea level rise provoked flooding of the continental shelves, implying a fourfold increase of shallow areas availability for coral reef growth. This led to enhanced carbonate deposition, resulting in principle in a CO_2 increase (Berger, 1982). Ridgwell, 2001, adapting the parameterizations of Munhoven and François, 1996, simulated a ~46 ppmv G-IG CO_2 rise from this mechanism, while the isotopic signal is not much influenced (<0.02‰). The "coral reef hypothesis", initially proposed by Archer and Maier-Reimer, 1994 as protagonist on the G-IG CO_2 rise, has been questioned, due to relative timing aspects: ice core data reveal that CO_2 rises much before sea level rise (Vecsei and Berger, 2004). Still, this theory remains a possible important player for subsequent CO_2 changes during IG (*e.g.* during Holocene). Taking the above timing constraint into consideration, Köhler et al., 2005 simulated a 1-3 ppmv CO_2 rise on a G-

IG scale; this number could be higher in case of $CaCO_3$ accumulation from means other than coral reefs.

IV.4.7. Carbonate compensation

Ocean carbon chemistry is strictly defined by a number of equilibria, being largely pH-dependent. Any imbalance occurring in either C sources (*e.g.* terrestrial weathering) or C sinks (*e.g.* sediment deposition) of the main chemical protagonist, $CaCO_3$, will alter the balance of ocean carbonate ion, CO_3^{2-}. This defines the ocean capacity for "carbonate compensation". Below, a qualitative example is exposed for G-IG transitions:

The forest ecosystem expansion towards higher latitudes, as well as the productivity stimulation by CO_2 fertilization, accompanying deglaciations, increase the C content of the terrestrial biosphere. This C has been taken out of the ocean/atmosphere reservoirs. The CO_2 removal from the ocean leads to an increase in pH and CO_3^{2-} concentration. The latter enhances $CaCO_3$ precipitation, further increasing the release of CO_2 in the atmosphere .

Carbonate compensation dynamics is characterized by an e-folding time function (τ), describing the temporal delay of the sediment response to deep ocean changes in CO_3^{2-} concentration. e-folding time estimates vary in the literature: Ridgwell, 2001 suggests a 9ky-e-folding time, while Köhler and Fischer, 2006 had applied a much faster response of 1.5 and 6 ky, based on previous modelling studies (*e.g.* Archer et al., 1998, suggesting a 6ky-value and paleoceanic reconstructions of Marchitto et al., 2005, proposing a delay of 1.5ky). Carbonate compensation itself constitutes only a response process to all other C-cycle changes. It is thus model-dependent. This mechanism lacks in explaining the correlation between CO_2 and Antarctic δD (Fischer et al., 2003). Köhler and Fischer, 2006 report a 15-ppmv maximum rise due to the oceanic response through the last 5 terminations, while an upper estimate being ~35 ppmv of TI, related to no time-delayed response of $CaCO_3$ chemistry. This upper limit has been equally simulated by Toggweiler, 1999 and Brovkin et al., 2007, being related to ocean flux reconfigurations. In the draft attached, a τ of 1.5 ky was applied to finally observe a max. 15 ppmv CO_2 rise due to this process. No variations were observed for the isotopic signal.

IV.4.8. Rain ratio change

Chapter I introduced the two biological oceanic pumps: the organic and counter carbonate, dealing with particulate organic carbon (**POC**) and $CaCO_3$, respectively. The change of the relative flux of $CaCO_3$ against, POC ($CaCO_3$/POC), called rain ratio, **RR**, has been suggested to

be a potential responsible for G-IG CO_2 rise. The principle lies on a RR increase (enhanced biogenic $CaCO_3$ production or a reduced pelagic POC one) during the transition, directly propagating to the sea floor (Archer and Maier-Reimer, 1994). This RR shift would be tightly related with ecosystem changes. Coccolithophorid phytoplankton (and the equivalent zooplankton, foraminifera) are the main species who contribute to $CaCO_3$ export. They compete against diatoms (algae producing opal shells, POC). This competition is basically dependent on SST changes and silicate acid, H_4SiO_4, availability. Sigman and Boyle, 2000 suggest a 55-ppmv rise with a doubling of RR, while Brovkin et al., 2007 in a recent modeling study, report a potential G-IG CO_2 rise of 12 ppmv from this RR change. Still, this theory gets in conflict with i. 'unexpected' results on the lysocline or carbonate compensation depth (**CCD**) reconstructions[8] (Sigman et al., 1998); ii. "ballasting" minerals which tend to change the analogy between euphotic and sedimentary RR[9] (Ridgwell, 2003). Therefore, model simulations sometimes do not incorporate RR changes (Köhler et al., 2005). A change of RR within a BOXKIT test from 0.14 to 0.17 leads to a ~7 ppmv rise accompanied by a small $\delta^{13}CO_2$ decrease (~0.05 ‰).

IV.4.9. Fe fertilization hypothesis

The S. Ocean, the equatorial Pacific and the N. Pacific are **HNLC**[10] regions. In these areas, iron (Fe), a micro-element, limits primary production, *i.e.* the uptake of NO_3^- and PO_4^{3-} in surface waters. G conditions were more arid and dusty than today. The evidence that Fe was more abundant during G periods, established the Fe fertilization hypothesis (Martin et al., 1990), suggesting an increased export production in times of high aeolian Fe input. Fe is reconstructed from ice core chemical indicators, such as, dust, nss-Ca^{2+} or from direct Fe measurements (Wolff et al., 2006 ; Gaspari et al., 2006) and used in numerical approaches (Ridgwell, 2001; Köhler et al., 2005; Köhler and Fischer, 2006). Both proxies and model studies suggest this mechanism to having acted on the deglaciation startup. The model outputs of Köhler et al., 2005 suggest a contribution of ~20ppmv to the G-IG CO_2 rise, in accordance with the <30-ppmv model result from Bopp et al., 2003 and with the dust proxies estimate from Röthlisberger et al., 2004. On the contrary, earlier model outputs from Ridgwell, 2001 found a 52 ppmv G-IG CO_2 rise, in

[8] lysocline and CCD are the oceanic "boundary points", closely related to the carbonate saturation levels; lysocline being the depth below which $CaCO_3$ dissolution strongly increases and CCD, being the depth of equilibrium between $CaCO_3$ precipitation and dissolution. Any $CaCO_3$ input (mainly from rivers) or burial (removal in sediments and coral reefs) rate changes impose changes in the above depth levels. The RR change hypothesis does not fit the proposed depths shift on a deglaciation timescale, in magnitude terms.

[9] Any change in the RR of either carbonate or biogenic carbon produced in the ocean surface, is supposed to be communicated to the ocean sediments; recent research on POC transport controls to sediments is not depicted in ocean sediments, due to the presence of minerals, affecting the $CaCO_3$/ POC proportion

[10] Rappel: High Nutrient Low Chlorophyll

agreement with Brovkin et al., 2007, who simulated almost two-fold higher CO_2 values. In between stands the reasoning of Kohfeld et al., 2005, who proposed that Fe fertilization and mechanisms intervening to be responsible for half of the observed G-IG CO_2 rise. Despite this inconsistency, models simulating different CO_2 magnitude changes reveal a 0.15-0.20 ‰ $\delta^{13}CO_2$ decline (Ridgwell, 2001; Köhler et al., 2005). Our BOXKIT simulation revealed a ~20 ppmv rise together with a ~0.27‰ $\delta^{13}CO_2$ decline.

IV.4.10. Role of terrestrial biosphere

G-IG transition equals vegetation expansion replacing ice sheets, deserts shrinking, grasslands (tundra) to tropical (boreal) forests conversion. The C storage in terrestrial ecosystems can be reconstructed from either terrestrial proxies (Adams et al., 1990), by the means of climate vegetation models (Prentice and Fung, 1990), or by determining changes in the average $\delta^{13}C$ of the world oceans (Duplessy et al., 1988). All methods conclude to a higher terrestrial C storage during IG conditions, ranging from 600 to 1300 PgC[11] (see references in Ridgwell and Zeebe, 2005). Köhler and Fischer, 2004 compiled available data to sum up to a G-IG terrestrial change of 300-700 PgC, mainly based on Bird et al., 1994. The detailed amplitude and time dependence of the influence of the terrestrial biosphere at such timescales has been highly debated, without reaching any consensus up to date. But overall, if an averaged 500 PgC were transferred from the ocean/atmosphere to the biosphere throughout the G-IG transition, CO_2 should have declined, opposite to the trend observed in the ice core records. So it has been simulated, but with varying magnitudes: e.g. Ridgwell, 2001 found a decline by 25 ppmv, being slightly higher than other studies in the 12-17 ppmv-range (Archer et al., 2000; Broecker and Peng, 1986; Köhler and Fischer, 2006; Brovkin et al., 2007). Thus, more than 100 ppmv of CO_2 rise have to be explained by oceanic processes when taking into account the terrestrial biosphere G-IG evolution. This deglacial CO_2 decrease would have been accompanied by a C isotopic rise of ~0.31‰ (Ridgwell, 2001; Köhler et al., 2005). The model study of Köhler and Fischer, 2004 discusses on the influence of terrestrial biosphere on both CO_2 and $\delta^{13}CO_2$. A first suggestion on the potential decoupling between the two C cycle variables is exposed, due to their differentiated origin (CO_2 linked to the ocean whereas $\delta^{13}CO_2$ fluxes linked to terrestrial biosphere), which is partly supported in section *IV.3.2* with our data interpretation. Brovkin et al., 2002 used marine photosynthesis fractionation data in their model to conclude that the marine and terrestrial isotopic signatures cannot be separated and thus, interpreted in the integrated atmospheric signal.

[11] PgC equals to 10^{15}g C or Gigatons of C

IV.4.11. Synopsis

Evaluating the relative importance of each mechanism listed above leads to no current consensus. Probably each of them played a role of variable importance as a function of time. Fig. 4-4 presents a synthesis of the possible amplitude of G-IG CO_2 change associated with each mechanism, plotted against its level of scientific understanding, first synthesized by Ridgwell and Kohfeld, 2006.

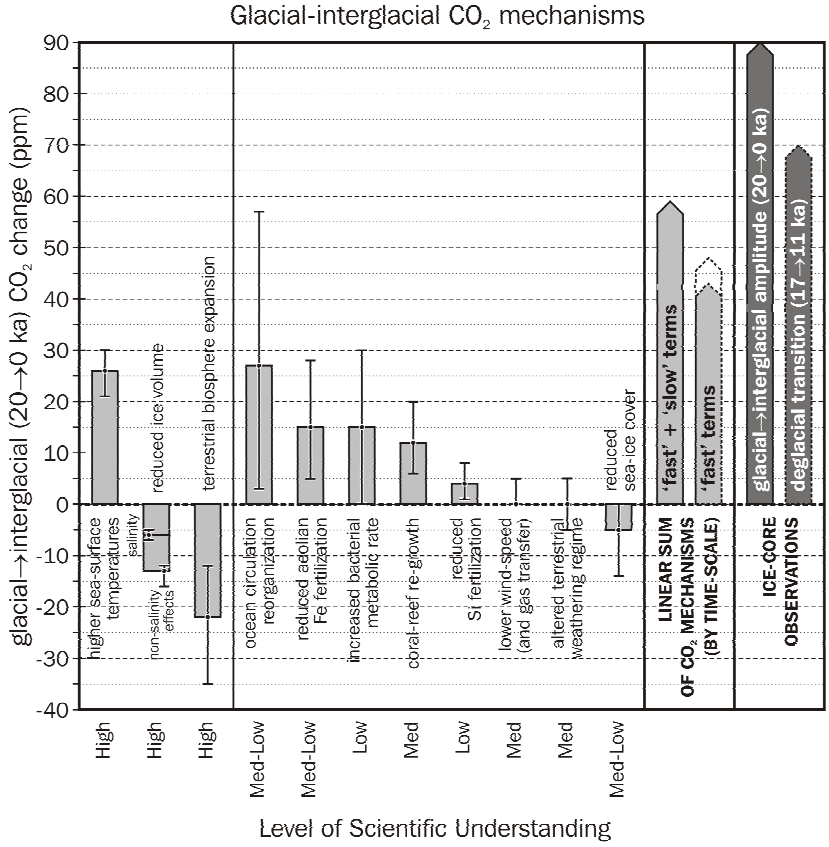

Fig. 4-4: *different G-IG hypothesis on the causes of the deglacial CO_2 rise compiled together against the level of scientific understanding, provided by Andy Ridgwell, (pers. comm.) and it will soon appear in Kohfeld, in preparation. Some additional forcing parameters are given, other than discussed in the text, such as the increased bacterial metabolic rate (Matsumoto et al., 2007), the reduced Si fertilization (Archer et al., 2000; Ridgwell et al., 2002), and the altered terrestrial weathering regime (Munhoven and François, 1996; Brovkin et al., 2007)*

IV.4.11.1. Focus on the S. Ocean

The Southern ocean is considered as a key area for triggering the G-IG CO_2 increase, primarily due to the correlation of its temperature (assumed to mimic δD in Antarctica) with CO_2 (Monnin et al., 2001) and secondly through a number of mechanisms, such as : a. biological productivity decline (Knox and McElroy, 1984; Sarmiento and Toggweiler, 1984); b. increased vertical mixing rates (François et al., 1997); c. decreased sea ice cover (Broecker and Peng, 1986; Stephens and Keeling, 2000). The leading role of the S. Ocean over CO_2 changes during TI, was

deduced in the first place by the correlation of deuterium data of the EDC core (Jouzel et al., 2007) and our CO_2, as shown in the attached draft, in agreement with previous studies (Monnin et al., 2001; Bianchi and Gersonde, 2004).

IV.5. Additional "young" points to our dataset

Three late Holocene $\delta^{13}CO_2$ measurements were performed on the EDC core, but not included in the manuscript as they did not bring information relevant to the paper conclusions. Fig. 4-5 shows the full dataset including these three depth levels :

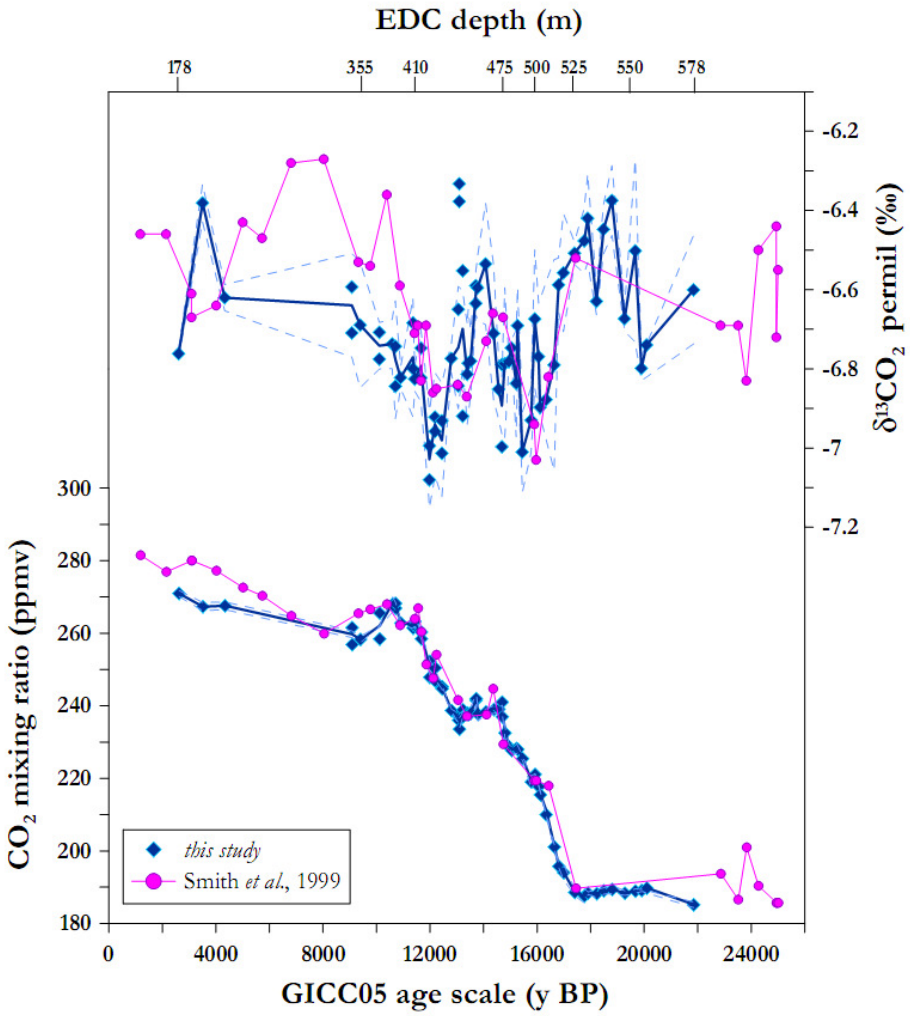

***Fig. 4-5**: Fig. 1of draft (section IV.3.2) if 3 Holocene data-points were included*

When these 3 points are considered, the mean 1σ of our $\delta^{13}C$ measurements is improved. The time-gap between 5 and 8 ky (period not covered by our measurements) does not allow us to carry any additional detailed comparison with the TD results. Still, both datasets agree reasonably well during the period of concomitant data availability in the late Holocene. We did not include

these 3 points in the manuscript, because it could evolve more discussion in the LGM- Holocene differences, which was not the focus topic of this study, even though it would provide more evidence in the validity of the previous published dataset.

IV.6. Synchronization issues

Loulergue et al., 2007 constructed four different scenarios for the age of trapped gases in EDC during TI, as shown in Fig. 4-6 when applied to our CO_2 profile.

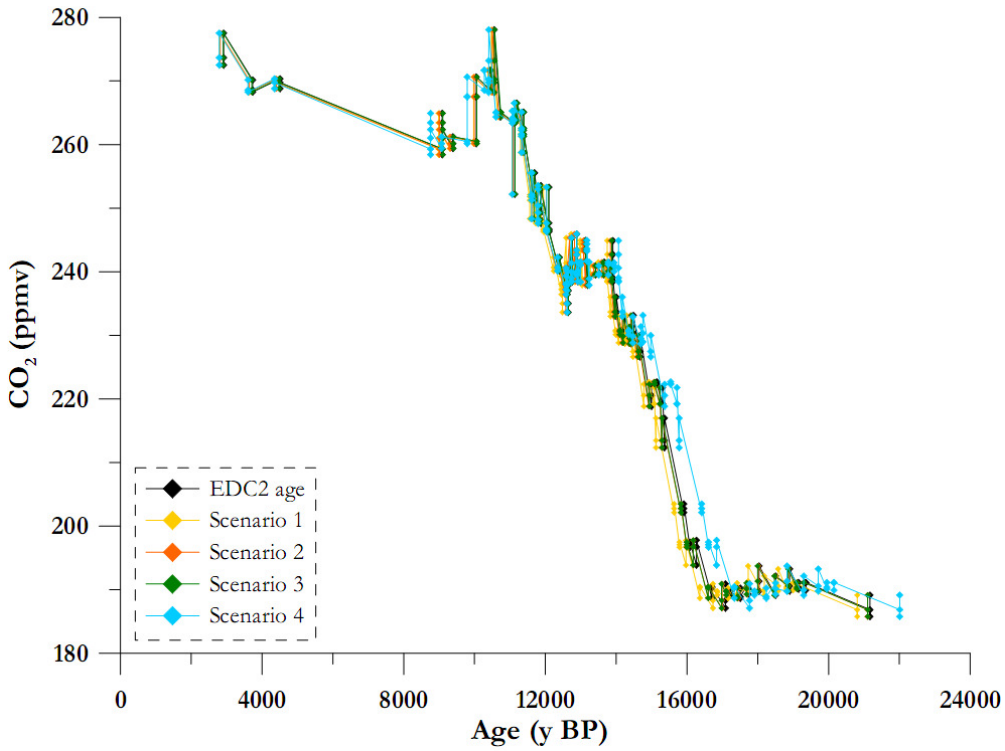

***Fig. 4-6**: our CO_2 plotted against the 4 gas age scenarios proposed by Loulergue et al., 2007*

The fourth scenario (named EDC3_gas_a), is the actual official EPICA gas age as it provides the best fit between gas chronologies of the two EPICA cores (EDC and EDML). However we have reconsidered this gas chronology for the following reasons :

- The TD data (Smith et al., 1999) were originally dated against the GISP2 age scale, using the gas CH_4 as synchronization tool (Brook et al., 2000). It has to be brought on a coherent timescale with the one used for EDC

- As our dataset is compared with N. Hemisphere proxies from *e.g.* N. Atlantic marine records, we needed to build a chronology compatible with such dating approach

- the final "reference" time scale for our interpretation should be as accurate as possible; up to now, the most precise glaciological age scale is the GICC05 built for Greenland ice cores, GISP, GISP2 and NGRIP (Andersen et al., 2007) based on annual layers counting

In order to synchronize these different records, the program *Analyseries* was applied (Paillard et al., 1996), to fit the ensemble of data (published and new ones) to this GICC05 age scale. The whole exercise is based on the CH_4 synchronization. Table 4-1 provides the CH_4 tie-points for the case of TI, while in fig. 4-7, the comparison of the TD and EDC CH_4 profiles with the Greenland one, before and after synchronization, is presented.

SP	n	EDC99 (z)	CH4	EDC3_gas_a	GICC05
LGM	25	528.24	384	17543	17579
I	14	506.28	473	15870	16198.9
II	15-16	479.43→474.04	465→569	14289→14010	14894→14644
III	22	443.13	542	12338	12793.9
IV	12-13	418.02→415.08	643→665	11325→11216	11676.15→11547.83

***Table 4-1**: Synchronization issues from EDC3_gas_a to GICC05, using CH_4 for tie-points; data from Loulergue et al., 2008 and synchronization program from Paillard et al., 1996*

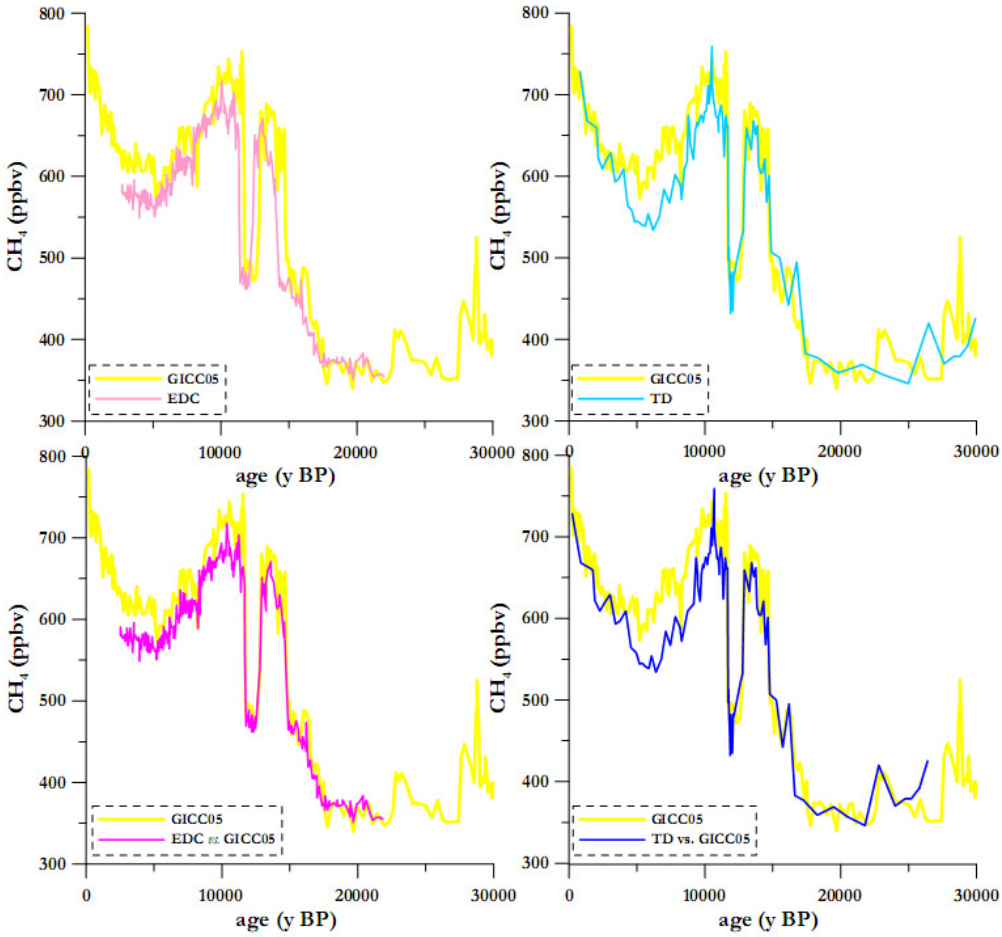

***Fig. 4-7**: plots of CH_4 vs. time for three cores: EDC, TD and GICC05. The upper plots provide the superposition of (left) EDC and (right) TD with GICC05. The lower plots provide the result of synchronization using the Analyseries software (Paillard et al., 1996). Data from Brook et al., 2000; Blunier et al., 2007; Loulergue et al., 2008*

IV.7. Comparison with unpublished $\delta^{13}CO_2$ data

IV.7.1. UBern

The EDC ice core had already been analyzed for $\delta^{13}CO_2$ over the same time period by a PhD student at the University of Bern (Eyer, 2004). In the following, the two datasets are compared. Fig. 4-8 provides their superposition against EDC depth.

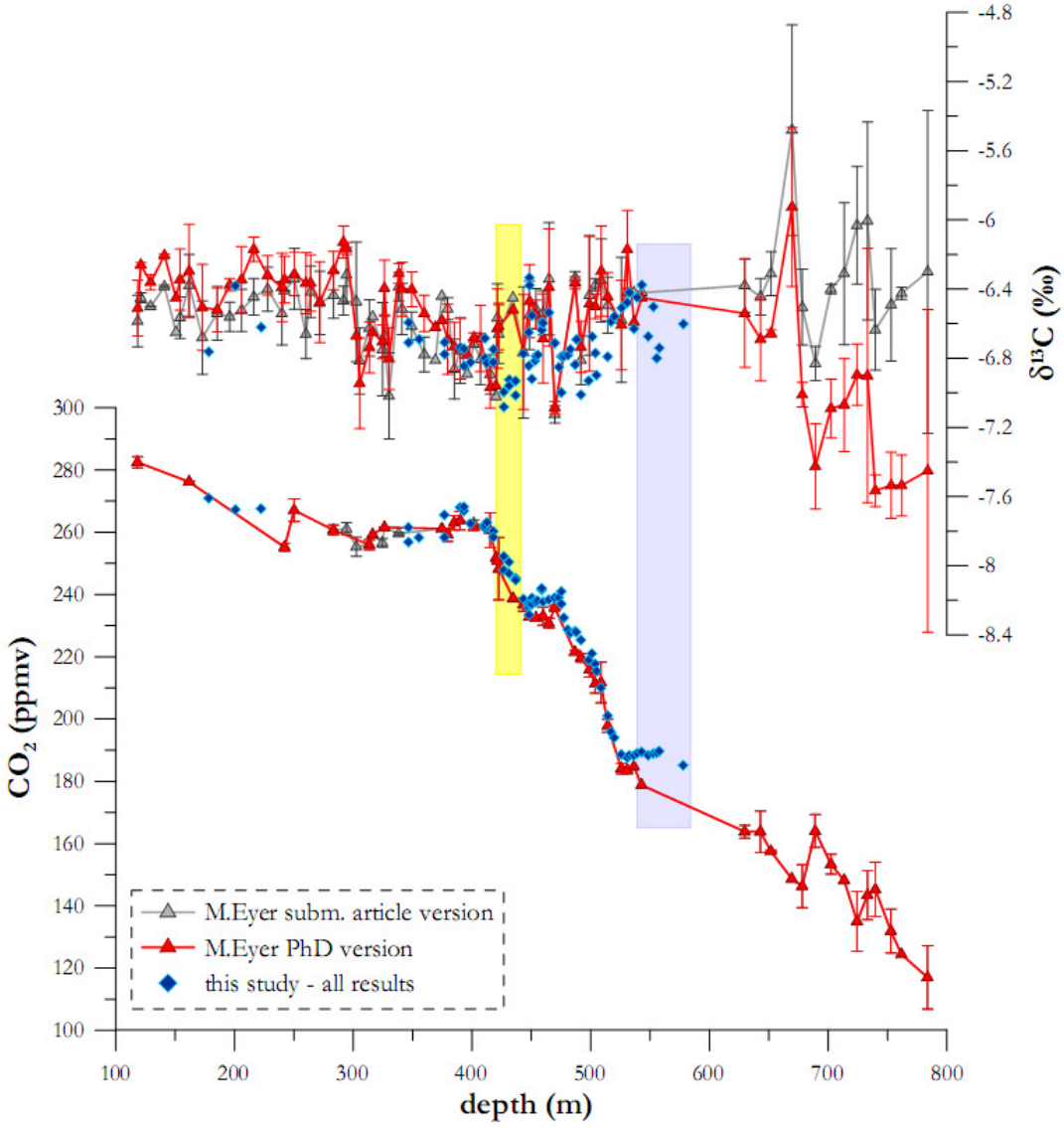

***Fig. 4-8**: Intercomparison UBern - LGGE*

There are two versions of the UBern dataset: one from a submitted article and one from the PhD manuscript of Eyer, 2004. Both versions differ in the Holocene part, as well as in the clathrated part of the EDC core (LGM period). The article version is considered as more valid *(M. Leuenberger, pers. comm.)*. The CO_2 mixing ratio was not measured on every sample. The published UBern CO_2 profile from Monnin et al. (2001) has been obtained with a different analytical protocol.

Overall, the two datasets follow the same general pattern; still UBern data are more scattered by 0.09 ‰ than ours. The two datasets mainly disagree over the yellow-marked period. It concerns a single depth level from UBern, measured only once (no 1σ available), whereas our dataset over the same period includes 6 depth levels, 5 of which had been analyzed twice. This period corresponds to the second minimum of our dataset coinciding with the YD.

As N_2O is not separated from CO_2 with the UBern experimental setup, we speculate that part of the scattering and discrepancy between their dataset and ours comes from the large variability of N_2O at small depth scale in the core, due to *in situ* production mechanisms and real atmospheric changes. Overall, the reproducibility of our analytical system over three consecutive expansions on the same ice core sample is better than obtained by UBern through their multiple expansion of the same transferred gas sample. No direct comparison can be accomplished for the LGM period (starting from the blue-framed area and going downwards the core); at the LGM-area where we obtained some points, there are no equivalent UBern ones. Still, the clathrate-effect (more in particular the increased instability of the brittle zone), clearly visualized for the UBern case, was also tested in our laboratory for another time period (*cf. Ch. III*). Whereas UBern found a ~50 ppmv negative shift for CO_2 and no fractionation for the $\delta^{13}CO_2$ during MIS2 (article version considered), our AIM 12 results showed no more than a 12-ppmv negative fractionation for CO_2 (but equally no apparent fractionation for the carbon isotope).

IV.7.2. AWI

Jochen Schmitt at AWI measured seven EDC samples chosen for the depth range of 400-500m, using his sublimation technique. The results are presented in fig. 4-9.

Although the limited number of measurements does not allow us to draw firm conclusions, we observe that AWI results confirm the lower $\delta^{13}CO_2$ during the YD compared with the B/A and the Early Holocene, although a difference appear on the absolute values (which could result from differences in the standard gas scale, or in the blank of each extraction system). The majority of these results measured by Jochen are within the error bars of our data. Two results are different

(in fig. 4-9 been colored) and particularly ^{13}C-depleted, whereas their CO_2 value is comparable to our adjacent value for the yellow-colored one and significantly different for the green-colored one. The latter could thus have been affected by an experimental artifact. More of such intercomparison exercises are required in the future.

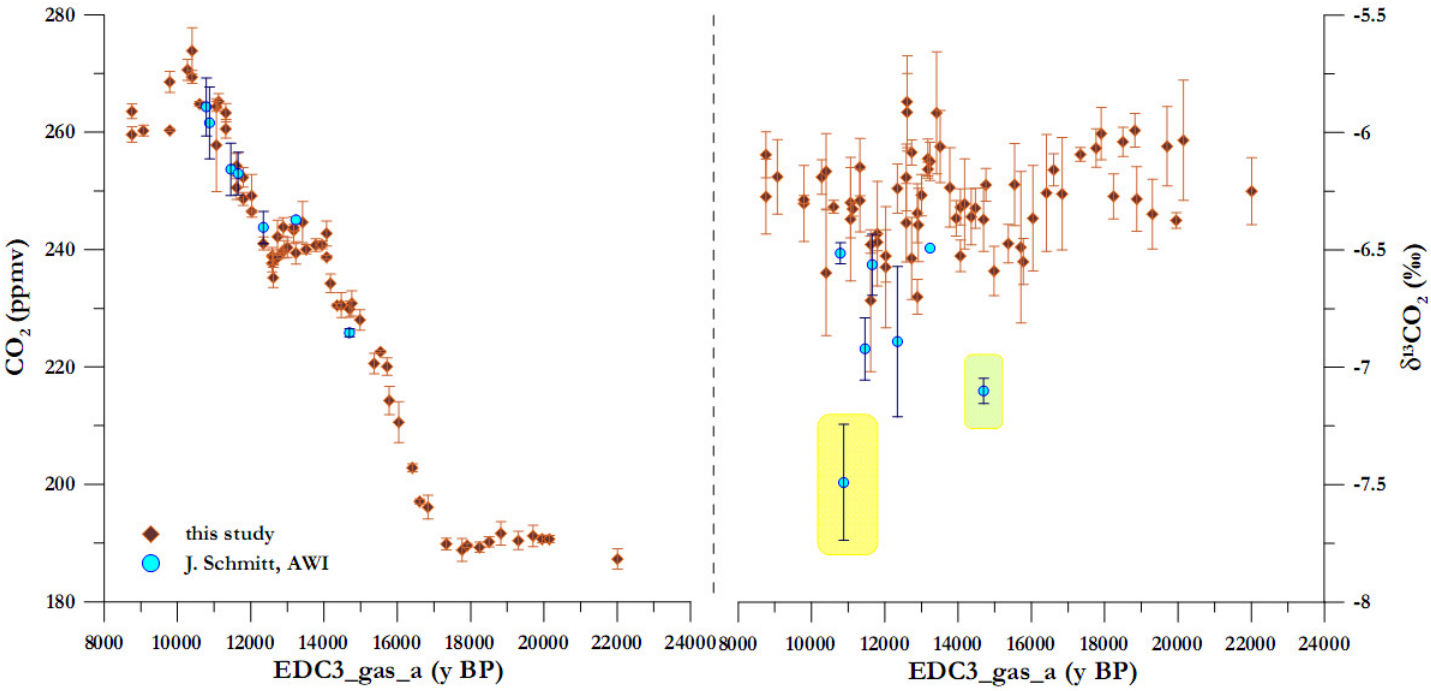

***Fig. 4-9**: Intercomparison LGGE-AWI*

IV.8. Conclusion

Within this chapter, we presented a new CO_2 and $\delta^{13}CO_2$ dataset over TI for the EDC core and we conducted a first interpretation based on a comparison with C-cycle proxies in the ocean and on two C-cycle box models. There are several lines of evidence arguing in favor of the significance of our new dataset:

The new analytical technique developed at LGGE (*cf. Ch III*) has undergone a large number of tests showing that the results can be interpreted within a 0.10‰ 1σ uncertainty envelope. The new results agree well with previously published datasets from the EDC and TD cores. Furthermore, we expose evidence arguing for the validity of our data against the one measured by UBern, by discussing the inconsistent points from an analytical point of view, as well as by the intermediate of a third series accomplished by the AWI EPICA partner.

We equally expose some representative exercise on synchronization issues between different ice cores, highlighting the importance in well-phasing records of different origin. The newest age scale GICC05 was mainly used for intercomparison reasons.

The application of two C-cycle box models, showed that combined scenarios of various C-cycle mechanisms originating mainly in the ocean are able to explain our data. The role of terrestrial biosphere should nevertheless not be ignored..

We conclude that changes in Southern Ocean stratification were probably the main Earth system internal driver of the CO_2 and $\delta^{13}CO_2$ trends over the last deglaciation, with additional contributions from the decrease in Fe fertilization during the first part of the TI. The buildup and decay of the terrestrial biosphere started influencing the C cycle atmospheric variables in the course of the B/A and YD events.

This exercise, initiated us on the potential mechanisms a deglaciation undergoes. This encouraged us in proceeding on additional exploration, in order to validate the above proposed mechanisms upon earlier historical age scales. We therefore proceeded to a second deglaciation examination.

Chapter V. Termination II

V.1. Introduction

Ch. IV presented the combined CO_2- $\delta^{13}CO_2$ dataset for the last deglaciation and discussed to which extent these data can be used to constrain some important forcing hypotheses on the causes of the ~80 ppmv CO_2 increase. In this chapter we extend our interest to the transition period from MIS 6 to MIS 5, which covers the time scale from ~155 to ~125 ky BP and leads to the Eemian period in Europe, *i.e.* the penultimate interglacial.

Very few data document CO_2 mixing ratios during Termination II from ice cores. There exist no ice core $\delta^{13}CO_2$ record reported for this particular period. Understanding the forcing mechanisms dominating deglaciations, requires to put in perspective the well-known TI against an earlier glacial termination. TII is the natural candidate for this purpose, since it precedes TI and still has a good time resolution in the EDC core. In addition, it leads to warmer peak interglacial temperature in Antarctica (Jouzel et al., 2007) and higher CO_2 mixing ratios (Petit et al., 1999) compared with the early Holocene, thus bringing questions on the causes of such peculiar conditions. In this chapter, the first EDC CO_2 and $\delta^{13}CO_2$ data are presented for TII and are compared to TI. A potential flaw in this comparison arises from the difference between the bubbly TI ice and the clathrated TII ice, which will be discussed in the chapter.

In the following section, the general context for studying the TII is given, as well as the known climatic conditions during TII. In section 3 the new measurements of CO_2 and $\delta^{13}CO_2$ are presented. In section 4 these data are compared with already existing ones in ice cores and marine sediment records. In Section 5, TI and TII are compared, regarding all available evidence from ice and marine data can provide against our data, to suggest a deglacial scenario supported from this new dataset in (6). Finally, a special section (7) deals with the analytical importance and challenges accompanying these new data. Due to the limited time available since the production of these new data, the chapter will provide a more qualitative discussion than for TI.

V.2. State of the art

V.2.1. Why studying TII period on EDC ice core

- TII is the next deglaciation one encounters in history (preceding TI). It is poorly studied, though, due to lack of adequately resolved sedimentary records and stratigraphic uncertainties. Data acquisition from different natural means will help filling this gap. Ice

cores in particular are considered as one of the best paleo-information, due to good age constraining methods provided by ice flow and accumulation models (Waelbroeck et al., 2008).

- TII is known to be as one of the most rapid and abrupt terminations in the late Quaternary (Broecker and van_Donk, 1970), leading to a warmer interglacial than the Holocene in the SH by 2-5°C (Bianchi and Gersonde, 2002; Jouzel et al., 2007) and in the Arctic region by 4-5°C in summer (CAPE, 2006). The last interglacial has been considered as an analogue of the anticipated future GHG-induced warming, with a more elevated sea level by 4-6 m than present and a reduced Greenland Ice Sheet (Carlson et al., 2008). Although there could be some common mechanisms between the two periods (notably the ice sheet response to radiative forcing), these two periods largely differ in their insolation characteristics. Furthermore, average climatic conditions during MIS 5e are still not well established (Cortijo et al., 1994; Field et al., 1994; Adkins et al., 1997; Oppo et al., 1997; Lototskaya et al., 1998; Cortijo et al., 1999; Bauch et al., 2000; Bauch and Kandiano, 2007). Examining the glacial termination can provide hints into the sequence of events and mechanisms leading to a warmer interglacial
- The EDC ice core allow us to directly compare with TI, with limited bias on *i.* dating challenges (same ice core and same gas age scenario applied); *ii.* experimental challenges (use of the same analytical protocol); *iii.* artifacts (same chemical composition of the core between the two Terminations; analysis conducted by the same person)
- Abrupt climatic events took place during TII, as for TI, but with different time sequences and magnitudes; the evolution of the stable carbon isotopic composition of atmospheric CO_2 could shed light on the impact of these events on the carbon cycle, especially when compared with other paleo-data (oceanographic, pollen, corals, terrestrial biosphere).
- The depth range including TII in the EDC ice belongs to the fully clathrated region. Dealing with TII sample analysis will provide further hints on one of the technical questions raised in *Ch. III*, on the effect of pure bubble, bubble-clathrate, and pure clathrate zones in terms of grinding efficiency and possible bias on the mixing and isotopic ratios of CO_2.

V.2.2. Main abrupt climatic changes during TII

V.2.2.1. TII Younger Dryas-like standstill

Similarly to TI, TII took place in two phases of drastic change, interrupted by more 'stable' conditions, thus defining a Younger Dryas-like event. Such a standstill possibly occurs during

every deglaciation (Sarnthein and Tiedemann, 1990; Sima et al., 2004; Cortese et al., 2007). For TII, this YD-like event is recorded in pollen, marine & lacustrine sediments and terrestrial records both in the NH (Seidenkrantz et al., 1996; Gouzy et al., 2004) as well as in the SH (Bianchi and Gersonde, 2002), but it is of a weaker amplitude than the YD encountered during TI. There is an oscillation enclosing the TII standstill event which has been called the "Zeifen/Kattegat" (Seidenkrantz et al., 1996), analogous to Allerød/Dryas transition in TI. The reasons for this interruption seen in the N. Atlantic can be either "regional" (*i.e.* due to water mass circulation changes) or "global" (*i.e.* due to an interruption in polar ice sheet melting (Gouzy et al., 2004; Cannariato and Kennett, 2005; Lototskaya and Ganssen, 1999)). Still, its absence in the water isotopic records from Antarctic ice cores, as well as in the CH_4 signal suggests that the effect of such event was limited to a relatively narrow regional scale.

V.2.2.2. Heinrich event during TII: existing challenges

TII, as TI, also exhibits a Heinrich event. The IRD deposit seen during TII, has been named as layer 11 (Heinrich, 1988), or H11 by Robinson et al., 1995, while Broecker, 1994 named it H7 and van Kreveld et al., 1996 as h7. In this study it is presented as H11. As discussed in *Ch. IV*, Heinrich events are localized in the N. Atlantic and are primarily considered as an oceanic phenomenon, having a counterpart in the atmosphere through long-lasting cold conditions. It is not yet clear if H11 left an imprint in the ice core record, since it is of lower intensity than H1. Dating uncertainties are very large for this event, for the ensemble of marine and stalagmite records, placing H11 on a broad time frame of 128-131 ky (Adkins et al., 1997; van Kreveld et al., 1996; Müller and Kukla, 2004; Skinner and Shackleton, 2006). In addition to this, there are studies who contradict on the relative time location of H11 against the YD-like pause during TII (Lototskaya and Ganssen, 1999; Pahnke and Zahn, 2005), the former placing H11 after the standstill *(cf. V.4.7 section)*.

V.2.3. Absence of proxies from NH ice cores

GRIP and GISP2 ice cores, located at Summit, Greenland, reveal coeval signals for both the last deglaciation and the last glacial period. Still, large differences are observed at depths larger than 2750 m and ages older than 105-110 ky (*i.e.* 10% of the signal). Large water isotopic shifts were found in the GRIP core (Dansgaard et al., 1993), that were not encountered in the GISP2 core (Taylor et al., 1993). Since the two drill sites are only 28 km apart, the water isotopic difference encountered cannot be attributed to climatic conditions. The most possible explanation lies on stratigraphic disturbances, linked to ice flow processes (Grootes et al., 1993). Such disturbances have since been confirmed by ice core chemistry (Legrand et al., 1997), Beryllium-10

measurements (Yiou et al., 1997), texture (Thorsteinsson, 1996) and gas composition (Souchez et al., 1995; Chappellaz et al., 1997). The bottom GRIP part seems to be the problematic one, as revealed from the intercomparison with the Vostok record (Fuchs and Leuenberger, 1996) or with marine sediments (McManus et al., 1994; Keigwin et al., 1994; Bianchi and Gersonde, 2002). Still, lake pollen records (Field et al., 1994) or Mediterranean speleothems (Frumkin et al., 2000) show rapid climatic events during the Eemian, supporting the GRIP oscillations. Landais et al., 2003 tried to retrace the disturbed GRIP part, but without being able to reconstruct the whole penultimate glacial transition.

Since we cannot compare our CO_2 record with the NH one (discussed in *Ch. II*) we are thus restricted to Antarctic ice core signals covering the time period of interest. Additionally, due to the absence of highly-resolved age scales such as GICC05 (not extended until MIS 6), our record is compared to N. Atlantic marine sediments or records from other regions, considering serious chronological limitations covering the various archives.

V.3. Results

V.3.1. Laboratory brief calendar

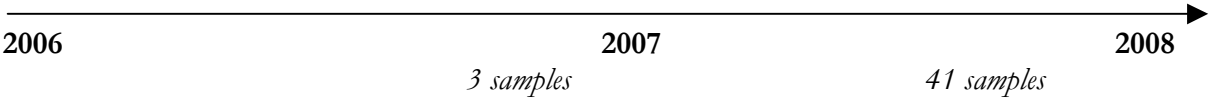

Annex I presents the analytical calendar table for the time dedicated for TII sample measurements, as well as the calendar-based differences with TI.

V.3.2. Data processing

We analyzed a total of 37 depth levels from which 7 were duplicated. Protocol changes between the two major sampling periods are discussed in *Ch. III*. 5 results were rejected because the dispersion between the three consecutive expansions over-passed the 3σ threshold for data acceptance, as deduced from the histograms presented in C*h. III (more in annex IV)*. Rejected values are more frequent than for TI (sampling period 2006), during which laboratory problems were limited (*cf. Ch. III*). The physical status of trapped gases (clathrated ice) could have contributed to some of the abnormal scattering (*e.g.* CO_2 constantly rising with time and the opposite trends for its stable isotopes). Unfortunately, this data rejection criterion coincided with the majority of duplicates. Therefore, statistical numbers provided in table 5-1 correspond only to two duplicated samples

	CO_2 (ppmv)	$\delta^{13}C$ (‰)
Precision (1σ)	1.87	0.102
Reproducibility (1σ)	1.94	0.128

***Table 5-1**: statistical numbers i.e. precision -means of reproducibility between three expansions for the ensemble of samples- and reproducibility means between duplicates of the same sample*

V.3.3. CO_2 and $\delta^{13}CO_2$ time evolution

Figure 5-1 presents the CO_2 and $\delta^{13}C$ data after rejection of the 5 samples which provided abnormal scattering through the three expansions, and after correction for gravitational fractionation (Ch. II). Raw data are given in annex II, the graphs on their gradient evolution can be found in annex IV while the equivalent $\delta^{18}O$ dataset is provided in annex III.

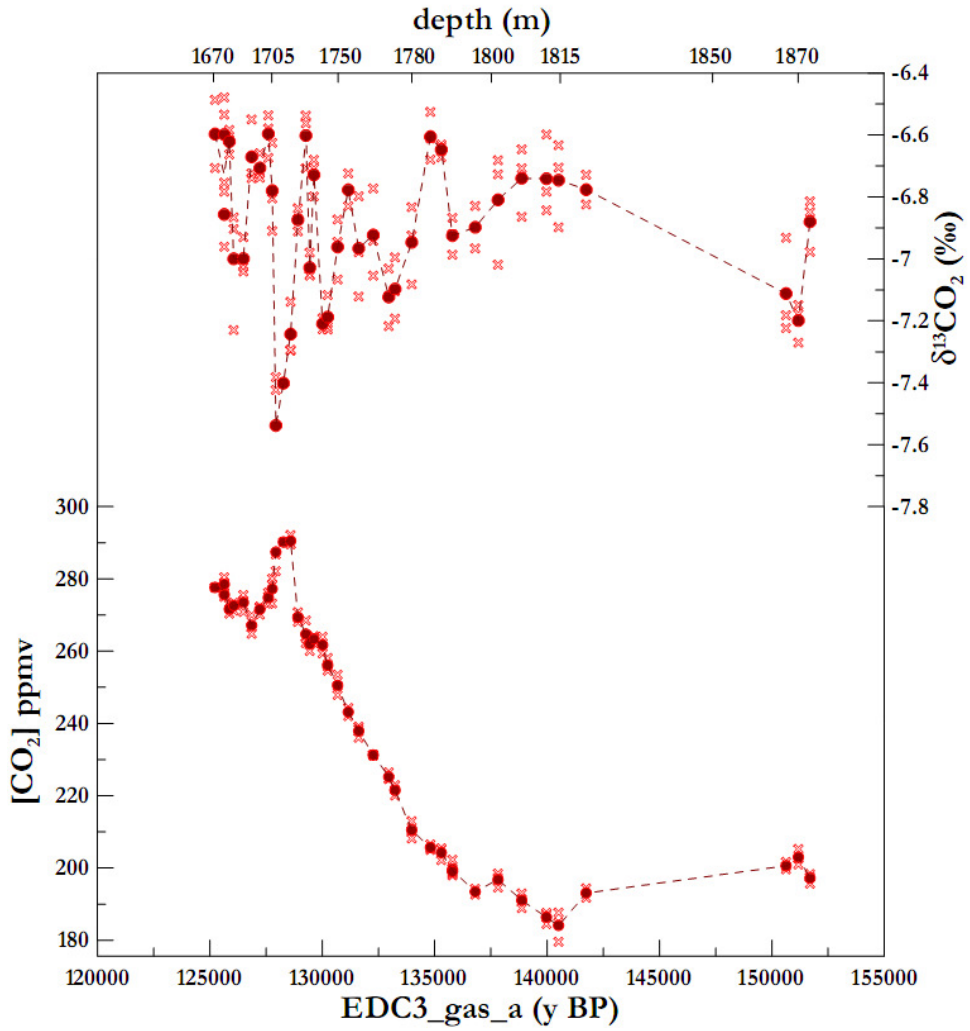

***Figure 5-1**: EDC CO_2 and $\delta^{13}CO_2$ over TII vs. depth (upper x axis); b. EDC3_gas_a age (lower x axis), after gravitational correction. Red crosses represent all results, while red circles the values deduced from the mean of all expansions and the dotted line links all mean (duplicates included) values*

The co-evolution of CO_2 and $\delta^{13}CO_2$ can be described as follows, through the full TII and then in more details through changes in the CO_2 growth rate :

- The comparison of glacial and interglacial boundary conditions gives *i.* a 77.0±2.2 ppmv and a 0.38±0.16‰ rise for CO_2 and $\delta^{13}CO_2$, respectively, when including the 3 MIS6 values with the MIS5e ones covering the CO_2 plateau from 151.2±0.5 to 125.5±0.2 ky, and *ii.* a 105.1±0.9 ppmv increase and a 0.58±0.06 ‰ decline, if values from the start of TII and the ones from the CO_2 optimum from 140.2±0.4 to 128.4±0.2 ky are taken into account
- Although the time resolution of the record does not yet provide details on this specific trend, a ~16.2 ppm decrease and a 0.32‰ rise seem to accompany the transition from MIS6 to the beginning of TII
- From 141 to 134 ky, CO_2 increases slowly by 26.4 ppmv while $\delta^{13}CO_2$ declines by about 0.20‰; the end of this period shows a ~0.31‰ positive peak within ~1.8 ky
- The following ~4 ky (from 134 to 130 ky) are characterized by a more rapid 51.2 ppmv regular CO_2 rise accompanied by another positive $\delta^{13}CO_2$, peak of up to ~0.38‰, superimposed on a slightly lower $\delta^{13}CO_2$ background compared with the previous period
- An overview of the first 10.5 ky of the deglaciation (140.5 to 130 ky) reveals a 77.6 ppmv rise accompanied by a net 0.46‰ decline
- Between 130 and 128.9 ky, the CO_2 mixing ratio barely increases by 7.7 ppmv (60% of this increase occurring within the last 350 y). $\delta^{13}CO_2$ shows a strong positive peak of 0.60‰
- The following ~1.0 ky are first marked by an abrupt CO_2 increase (21.1 ppmv) taking place within 335 y. The corresponding rate of increase, of 0.06 ppmv/y, is 2 to 3 times larger than the rapid increases observed during TI, at the beginning of the Bølling-Allerød, and at the end of the Younger Dryas[1]. The rapid increase is followed by a CO_2 plateau at 289.4±1.7 ppmv, extending from 128.6 ka to 127.9 ka, at a level significantly larger than the maximum CO_2 level observed during the pre-industrial Holocene. The rapid increase and the subsequent plateau are accompanied by a strong negative $\delta^{13}CO_2$ excursion of 0.66‰, reaching the most negative values observed throughout the Termination, *i.e.* –7.54‰, corresponding to an overall ~0.79‰ decline since the beginning of the deglaciation

[1] We found a ~21ppmv increase within 335y, whereas for TI the end of SP-II is marked by an abrupt 8 ppmv increase for a period of 300 y and at the end of SP-IV a 6 ppmv increase equivalent to 200y Monnin E., Indermühle A., Dällenbach A., Flückiger J., Stauffer B., Stocker T. F., Raynaud D. and Barnola J.-M. (2001) Atmospheric CO_2 Concentrations over the Last Glacial Termination. *Science* **291**, 112 - 114.

- From 127.9 to 126.9 ky, CO_2 reveals a 20.3±2.9 ppmv decline, taking place in two steps : a first rapid decline of 10.2 ppmv within 160 y, followed by a slower one of 10.1 ppmv within 917 y. The rapid decline is accompanied by a very large $\delta^{13}CO_2$ increase of 0.76±0.19‰, back to the maximum level observed during other time periods during the Termination
- The last ~1.6 ky of our record show a slow 10.5±1.5 ppmv rise and a $\delta^{13}CO_2$ increase of 0.33±0.08‰.

According to these different trends of CO_2 with time, we decided to sub-divide TII and the early part of MIS 5e covered by our record into Sub-Periods, **SP** (Fig 5-2), as for TI (Monnin et al., 2001), each period corresponding to a different rate of CO_2 change.

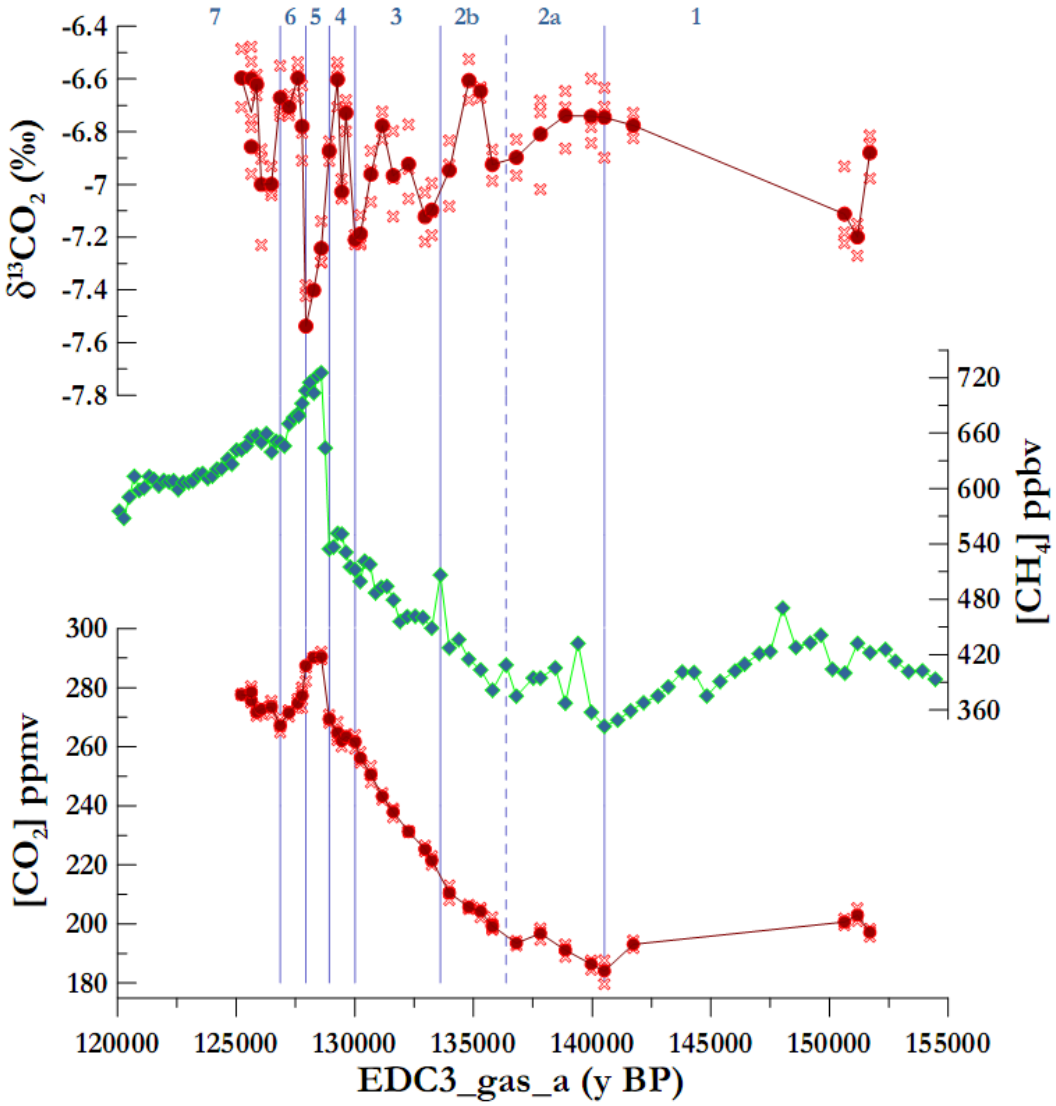

***Figure 5-2**: TII divided in SPs based on different CO_2 gradients (for this termination, changes in CO_2 gradients coincide with changes in CH_4 gradients, as well, see main text)*

SP 2 could be further divided into two time frames, *a* and *b*, as the CO_2 trend suggests a slightly different slope between both, and as $\delta^{13}CO_2$ exhibits a positive peak during the second time frame.

Table 5-2 summarizes the rate of increase for CO_2, and provides qualitative trends for its stable carbon isotope ratio and for CH_4.

N° of Sub-period	CO_2 (ppmv/ky)	$\delta^{13}C$	CH_4	Probable event
1 (Δt=11.2 ky; n=5)	↓ (1.2)	↑	↓	MIS6→ TII
2 (Δt= 4.1 ky; n=5) (Δt= 2.8 ky; n=5)	a. ↑ (2.3) b. ↑ (6.2)	a. ↓ b. peaks	a. ↑ highly oscillating b. ↑	TII onset
3 (Δt= 3.6 ky; n=9)	↑ (14.2)	↓ experiences a peak at mid-3	↑ but for a ~950-y interval it stays cst* *(456-460 ppbv)* and at the end it seems also cst	YD-like pause? (CH_4 version)
4 (Δt= 1.1 ky; n=5)	~↑(max. 7.0)	↑ peaks	↑	YD--like pause? (CO_2 version) H11 ?
5 (Δt= ~1 ky; n=4)	↑↑ (18.4; max 63.0 !)	↓↓	↑↑ (beginning of the rise and optimum in phase with CO_2)	H11? Climatic optimum MIS5e onset
6 (Δt= 1.1 ky; n=5)	↓↓ (18.8 ; max 63.4 !)	↑↑	↓	Post-MIS5e peak
7 (Δt= 1.63 ky; n=7)	↑ (6.4)	↔ showing a trough at mid-7	~↔	Towards MIS 5d

***Table 5-2**: SPs gradients for CO_2 only; tendencies for $\delta^{13}CO_2$ and CH_4 SPs characteristics vs. our data*

Overall, changes in $\delta^{13}CO_2$ are associated with changes in the CO_2 rate of increase, with mainly anti-phased gradients, as was equally found for TI case.

V.4. Comparisons with other TII data in ice

Fig 5-3 shows a first plot series superposing our data against the EDC deuterium/hydrogen isotopic ratio, Vostok CO_2, EDC and Vostok CH_4 and EDC deuterium excess. The most recent EDC scales, EDC3 for deuterium/hydrogen and deuterium excess, and EDC3_gas_a for the trapped gases, are used.

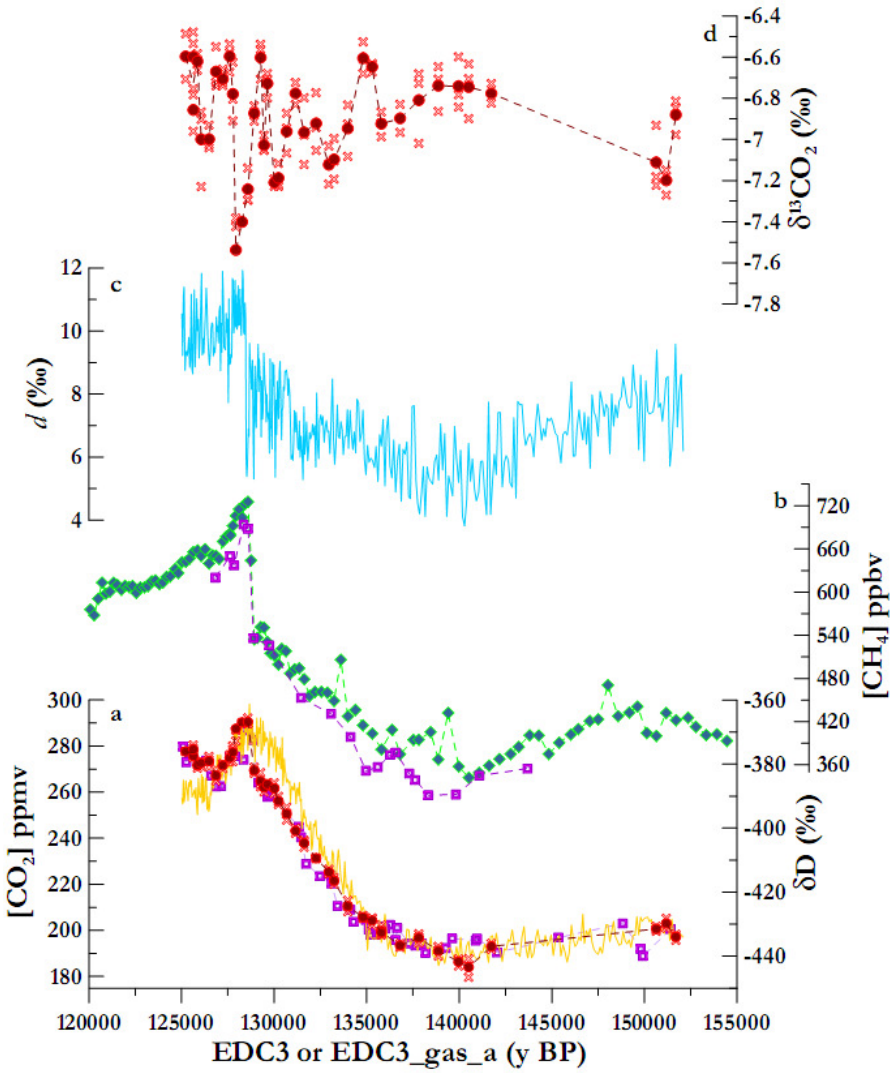

***Figure 5-3**: our data compared to other (ice core) data : a. CO_2 from this study (deep red circles) and Vostok (purple squares) (Petit et al., 1999; Pépin, 2000); both in EDC3_gas_a age scale; deuterium from EDC (orange line) (Jouzel et al., 2007); b. EDC CH_4 (Loulergue et al., 2008) superposed with Vostok CH_4 (Chappellaz et al., 1990), the latter in the EDC3_gas_a scale; c. deuterium excess (V. Masson-Delmotte, pers. comm.); d. $\delta^{13}CO_2$ from this study*

V.4.1. Deuterium

Overall fig. 5-3a suggests a coeval increase in deuterium and CO_2 throughout TII[2]. This in-parallel evolution lasts almost 10 ky. Between 131.4 – 130.9 ky, the temperature-proxy seems to stabilize. This occurs 1 ky before CO_2 shows a similar 'pause', just before the optimum. Then, deuterium and CO_2 differentiate in their rising trends, the former increasing gradually within ~2 ky, while the latter experiences an abrupt rise at ~128.9 ky. Still, both reach their optimum of

[2] Fischer H., Wahlen M., Smith J., Mastroianni D. and Deck B. (1999) Ice Core Records of Atmospheric CO_2 Around the Last Three Glacial Terminations. Ibid. **283**, 1712-1714. had given an estimated deuterium lead of 600±400 y over CO_2; still their data were scattered and were focused on the early deglacial changes and not the entire transitions

MIS 5e at almost the same time, ~128.6 ky. After the optimum, the relative phasing between CO_2 and δD becomes more complicated, since CO_2 reaches a minimum either after 0.5 ky of an initial δD trough or 0.4 ky before the δD minimum of this period. Antarctic temperature reconstruction out of deuterium, as provided by Jouzel et al., 2007 gives an identical evolution throughout TII. Due to the uncertainties in Δage calculations, we cannot draw firmer conclusions on the phasing between the two signals.

V.4.2. Vostok CO_2

Fig. 5-3a shows a second data series provided by Petit et al., 1999; Pépin, 2000 ; Pépin et al., 2001, synchronized against the newest EDC3_gas_a scale by Lüthi et al., 2008.

EDC data presented in this study have been gravitationally corrected, whereas Vostok data have not. The major inconsistency between the two CO_2 datasets lies from 139.6 to 141 ky. During this 500-y period, the 3 Vostok points included, appear more enriched by 10 ppmv than the 2 EDC points presented here. This could partly result from the difficulty of synchronization between the two cores. Still, small analytical differences between Vostok and EDC measurements cannot be excluded, especially when taking into account the generally poorer condition of Vostok ice compared to EDC in the depth range of interest. This seems confirmed when considering some possible outliers existing in the Vostok record, such as at ~128.9 ky, just before the climatic CO_2 optimum, or at ~128.3 ky when Vostok CO_2 declines abruptly to rise back again, something not observed in our EDC data.

However as a whole, the available EDC and Vostok CO_2 datasets are well correlated (**R^2=0.98)**.

Fischer et al., 1999 measured CO_2 at high resolution on the Vostok ice core over TII. Their data show an initial dip of CO_2 at 135 ky before the start of the TII increase. The CO_2 optimum reaches 290 ppmv and is dated at 128ky with the Vostok GT4 time scale. Similar trends are observed in our EDC data, but the timing differs: we locate the above events 5 and 0.5 ky, respectively, earlier. An interpolation exercise on CH_4, validated the well synchronization between Vostok and EDC core at this time frame (fig. 5-3b), also proved by the previous intercomparison with data from Petit et al., 1999; Pépin et al., 2001. If we proceed to the same exercise with the data from Fischer et al., 1999, the dating inconsistencies on CO_2 persist. Fig. 5-4 zooms this problem in for the ensemble of Vostok CO_2 results, superimposed with the EDC deuterium data. From the above, we conclude that the timing inconsistency between Fischer et al., 1999 and our data does not originate on used time scale (rescaling vs. EDC of the ameliorated Vostok scale from Parrenin et al., 2004), but on an artifact in some of Fischer et al., 1999 measurements. This, combined with the higher scatter of Fischer et al., 1999 data against those measured in LGGE, lead us in excluding this dataset from any comparison to our data from now on.

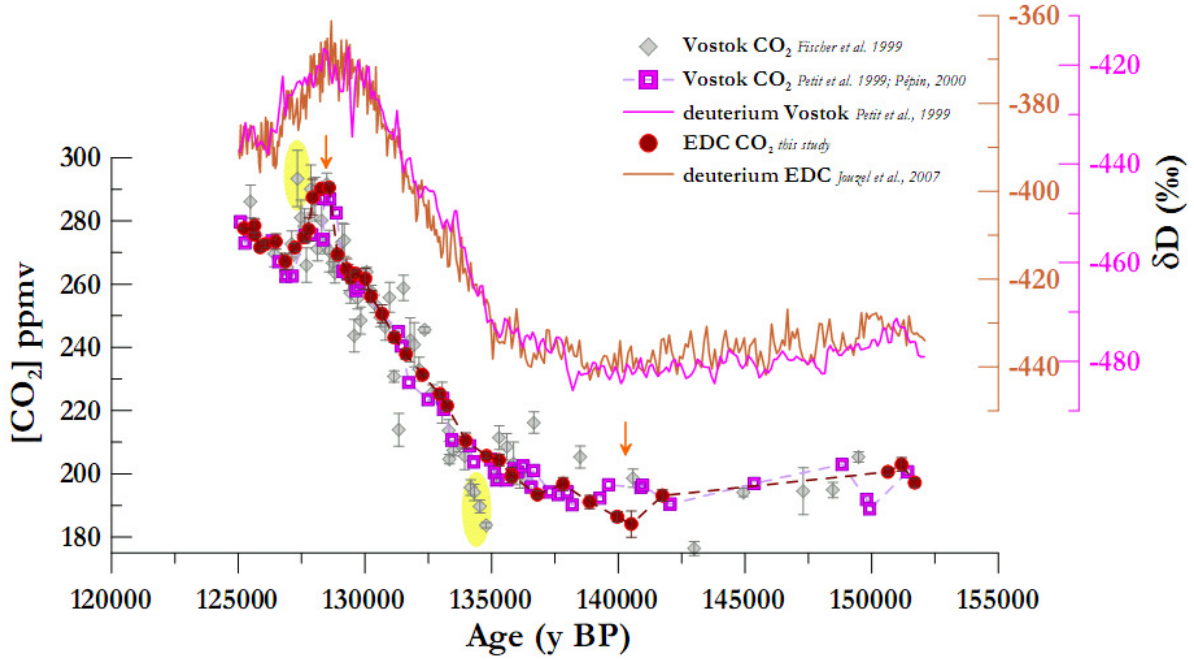

***Figure 5-4**: Zoom-in of the superposition of CO_2 data from the EDC core (this study) with two series of datasets from the Vostok core (data from Fischer et al., 1999 added here, in grey). While our data agree well with those from previously produced in LGGE and provided in the EDC3_gas_a scale by Lüthi et al., 2008, this is not the case for the Fischer et al., 1999, the latter being far more scattered than our dataset. Vostok deuterium data as provided by Petit et al., 1999 are superimposed to EDC data (Jouzel et al., 2007) to show timing consistencies between the two core. Yellow frames highlight the dating inconsistency between Fischer's data and the 2nd Vostok dataset, while orange arrows show the corresponding points of this study*

V.4.3. CH_4

Fig. 5-3b shows the EDC CH_4 and CO_2 datasets. Obtained on the same ice core, they allow for a direct intercomparison. We deduce the following:

- As a whole, both datasets show parallel changes in their rate of increase; evidence lies in table 5-2, where one realizes the same phase sign for each perturbation, as well as in fig. 5-2, where every single sub-period definition (based on solely CO_2 gradient changes) is accompanied by evident CH_4 profile changes
- At ~140.5ky they both reveal a minimum
- They both seem to stabilize just before their abrupt rising of MIS 5e from ~128.9 to ~128.6 ky BP (which occurs also concomitantly), while afterwards they show a very slow decreasing pattern; still CH_4 starts to decrease faster slightly earlier than CO_2; this difference is significant, since the data resolution for both gases is high enough.
- A minimum is observed in both datasets at ~127 ky

V.4.4. Deuterium excess

Deuterium excess (*d*) represents the deviation of δD with respect to its standard linear relationship with $\delta^{18}O$ observed in precipitations. It is defined by the following equation:

$$d = \delta D - 8 \times \delta^{18} O \quad (5\text{-}1)$$

Deuterium excess depends on temperature conditions, humidity and wind strength that prevail at the water source region (Merlivat and Jouzel, 1979). It can trace the precipitation origin, being particularly sensitive to the seasonal variations (Ciais et al., 1995b). EDC core, being located on a plateau, is considered to receive moisture from rather distant sources, situated at subtropical latitudes in the Indian Ocean. These moisture sources vary with time and climate, affecting the deuterium excess. For instance, during glacial intervals, the expanded sea ice cover around Antarctica in winter time limits the moisture contribution from cold high latitudes. In this case, the precipitation source is located at lower, warmer latitudes and the opposite happens during IG periods (Masson-Delmotte et al., 2005). Cortese et al., 2007, by comparing ΔTsource at Vostok and at a site in S. Ocean, suggest a connection in terms of moisture exchange, between the subantarctic ocean and the Antarctic continent.

Fig. 5-3c shows the deuterium excess evolution in the EDC core during TII. A well-marked shift takes place in parallel with the abrupt CO_2 and CH_4 rise at the end of TII, implying a rapid shift in moisture source. The parallel evolution with CH_4 suggests a causal link through a possible shift in the **ITCZ**[3] location, provoking changes in atmospheric circulation patterns and humidity transport both at low and high latitudes. The enhanced low latitude SST reconstructions during the optimum MIS5e (Lea et al., 2000; Lea et al., 2002), also support rise in atmospheric circulation.

Fig 5-5 shows a second data comparison series, between our data and the EDC dust information from nss[4]-Ca^{2+} and Fe fluxes, as well as ss-Na^{+} data from marine origin (Wolff et al., 2006). All plots are against the most recent EDC scales, as mentioned before. The following chemistry data are less resolved than the previously mentioned ones, but they are unique in providing timing constraints on the processes they represent against our data.

[3] Inter-tropical Convergence Zone
[4] nss for non sea salt, *i.e.* deprived from the oceanic influence. The opposite for ss (sea salt)

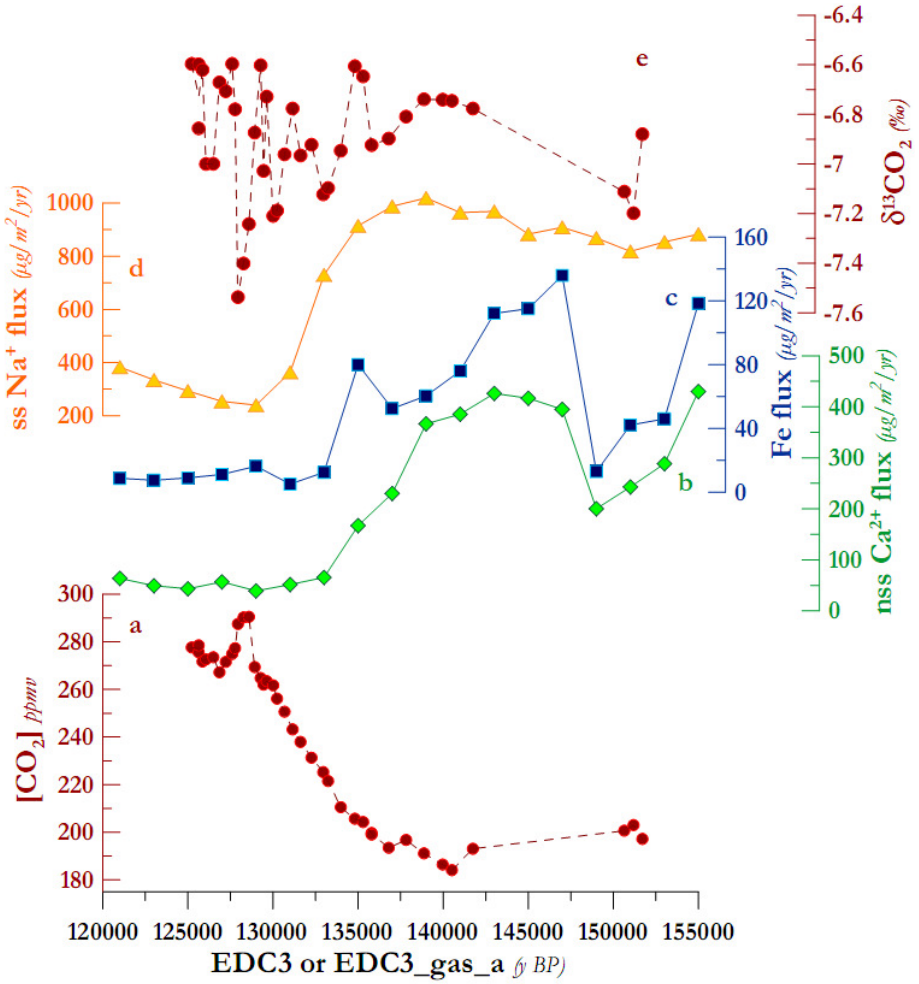

***Figure 5-5**: (a) CO_2 and (e) $\delta^{13}CO_2$ from this study, compared to a second ice core data series: b. nss-Ca^{+2} data; c. Fe flux data and d. ss-Na^{+}; the first two constituting a proxy for continental deposition whereas the ss-Na^{+} is a marine source proxy, notably of sea ice extension. Data from Wolff et al., 2006*

V.4.5. nss-Ca^{+2} and Fe fluxes in EDC core

Calcium, Ca, constitutes mainly the proxy for terrestrial sources, having nevertheless a marine signature, as well. Fe (iron) is a microelement originating from continental sources. It is closely related with HNLC regions, such as the S. Ocean and the role of dust deposition against marine productivity. When extracting the marine influence from the calcium record, we obtain the nss-Ca^{+2} and is provided in fig. 5-5b. A very good correlation is then expected from the corrected nss-Ca^{+2} record with the Fe fluxes one. Effectively, fig. 5-5c verifies this concordance, by showing Fe fluxes from EDC core. We have therefore at our disposal two separate records, representative of the Fe fertilisation activity in the S. Ocean, linked with the dust influence, notably the S. America (Patagonia). Direct Fe flux curve is more representative when dealing with Fe fertilization theory timing. Still, both reconstructions can be considered adequately reliable. In our case, they show a steep decreasing trend throughout the major part of TII. At 133 ky BP,

both nss-Ca^{+2} and Fe fluxes show a change in this trend. From then, both datasets seem to oscillate around a stable value, until the end of the record. In particular, nss-Ca^{+2} reconstruction shows a minimum just before the abrupt CO_2 MIS 5e rise, at 129 ky BP. For the Fe case, the lowest flux value is found 2 ky earlier. Taking into account the low resolution of the data, as well as the higher scatter of Fe flux dataset, one cannot assume firmly on the exact timing of dust deposition or Fe fertilization cessation. Still, the fact of dust influence throughout the major deglaciation part (during a mean ~15 ky period) is well considered as a major forcing factor for TII.

A Fe flux peak is registered at 135 ky BP. During this time frame, CO_2 was rather constant, while the atmospheric $\delta^{13}CO_2$ experienced a maximum peak. These 3 atmospheric variables could have been inter-correlated at this period, via a productivity maximum, pumping away CO_2 from the atmosphere while enriching the atmospheric $\delta^{13}CO_2$ signal.

V.4.6. ss-Na^+ flux in EDC core

Sodium, Na, contrary to Ca, originates mainly from the marine realm. Na signal contains some continental dust imprint, which, when reduced from the integral Na signal, in a similar way as the reduction of the marine influence in the continental nss-Ca^{2+} data, it provides the ss-Na^+, shown in fig. 5-5d for the EDC core. ss-Na^+ is an indicator of winter sea ice extent in the Indian sector of the S. Ocean (Wolff et al., 2006). Fig. 5-5d reveals a smooth increasing trend, *i.e.* sea ice expansion, from MIS 6 until 139 ky. By this time, CO_2 has already started rising (by ~1.5 ky before). This is in pace with previous assumptions on the CO_2 leading of sea ice extent and global ice volume (Broecker and Henderson, 1998; Sowers et al., 1991; Mudelsee, 2001). From 139 ky, ss-Na^+ undergoes a steep decline, reaching a minimum 10 ky later. This sea ice minimum coincides with the onset of the abrupt CO_2 rise of MIS 5e. From the above, sea ice extent change could be considered as a major protagonist for this deglaciation, mainly related with air sea exchange enhancement (as was equally proposed for TI). Still, after 129 ky, a smooth increase is observed for the ss-Na^+, spanning the rest of the MIS 5 record we dispose in fig. 5-5d , *i.e.*, even after the CO_2 big decrease following MIS 5e optimum. This means that additional forcings should be solicited to explain the post MIS 5e CO_2 and $\delta^{13}CO_2$ behaviour, while, in the following, the questions raised by the sea ice behaviour will be examined with oceanic circulation parameters.

V.4.7. paleo-oceanographic data over TII

Difficulties in precisely dating marine records with respect to each other and to ice records over TII, combined with the generally poorer resolution they dispose, lead to less robust assessment

about the overall timing and phasing of paleoceanographic changes through the period of interest. However some basic features can be extracted from the available records:

V.4.7.1. SST and NADW strength

SSTs seem to have been colder and the NADW weakened throughout TII when compared to TI. Lower benthic $\delta^{13}C$ values are registered in N. Atlantic sediment cores during TII (Duplessy and Shackleton, 1985; Sarnthein and Tiedemann, 1990). The generally more ^{13}C-depleted values seen in the oceanic signal, may imply weakened NADW flux throughout TII and an equivalent compensation from Southern-sourced waters (Oppo et al., 1997; Lototskaya and Ganssen, 1999). This lowering might have been also propagated towards the atmospheric signal.

V.4.7.2. Millennial-scale oscillations

Despite their overall weakened state, NADW oscillated according to the bipolar seesaw principle, imposed by cold and warm periods successions, always in anticorrelation with AABW (or AAIW) (Bianchi and Gersonde, 2002). Periods with ^{13}C-depleted incursions in the N. Atlantic are principally attributed to cold events (*e.g.* YD-like, Sarnthein and Tiedemann, 1990) or H11 (Skinner and Shackleton, 2006), associated with deep water re-organizations (Adkins et al., 1997) and coinciding with low $\delta^{18}O$ incursions of S. Ocean origin, as seen during TI (Labeyrie et al., 2005). A challenge exists on the relative timings of the cold SP during TII and their location to the ice core record. Fig. 5-6 illustrates two examples of synchronization tentative of YD-like and H11 events in our record. A point differing the two deglaciations, lies to the absence of the "B/A" warm analogue for TII (seen later on fig. 5-8b; 5-10c).

Climatic "pause"

Our data may agree with the two-step deglaciation hypothesis, and studies placing the "YD-like standstill" between 128-130 ky. In our record, this "pause" could have been evidenced by the concomitant reduced increasing rate of both GHGs just before the MIS 5e optimum.

H11- synchronization questions

Even though the possibility of a difference in origin, duration and intensity of Heinrich events during the Quaternary cannot be ruled out (Lototskaya et al., 1998), still at the ensemble of marine N. Atlantic records, these events are accompanied by negative $\delta^{13}C$ incursions.

A Northern NH study localizes H11 event at 129 ky BP (Carlson et al., 2008).

(i) If the dating is correct, H11 occurs just before the temperature optimum. If we place H11 just between the "pause" and the optimum, $\delta^{13}C$ declines, as observed during TI and proposed by marine sediments (fig. 5-6); this, combined with the hypothesis that H11 lags the 'standstill' (contrary to TI and shown in fig. 5-6), the W-shape pattern observed for $\delta^{13}CO_2$ during TI is also

reproduced for TII. However, these authors superimpose EDC CH_4 values, which are much delayed when compared to our time scale.

(ii) If we consider correct the relative timing between H11 and CH_4, and we place CH_4 in the EDC3_gas_a scale, then H11 occurs very early to our record (~133ky), coinciding with one $\delta^{13}C$ negative incursion. Then, a $\delta^{13}CO_2$ pattern equivalent to TI and considering the same relative timing as TI occurs

(iii) If finally, we compare with TI events sequence, as provided by the same study, 'our' H events are localized 2 ky later than Carlson et al., 2008; if we apply the same as them, H11 is placed at ~127 ky BP, *i.e.* just after the climatic optimum, coinciding with the post-minimum $\delta^{13}C$ value.

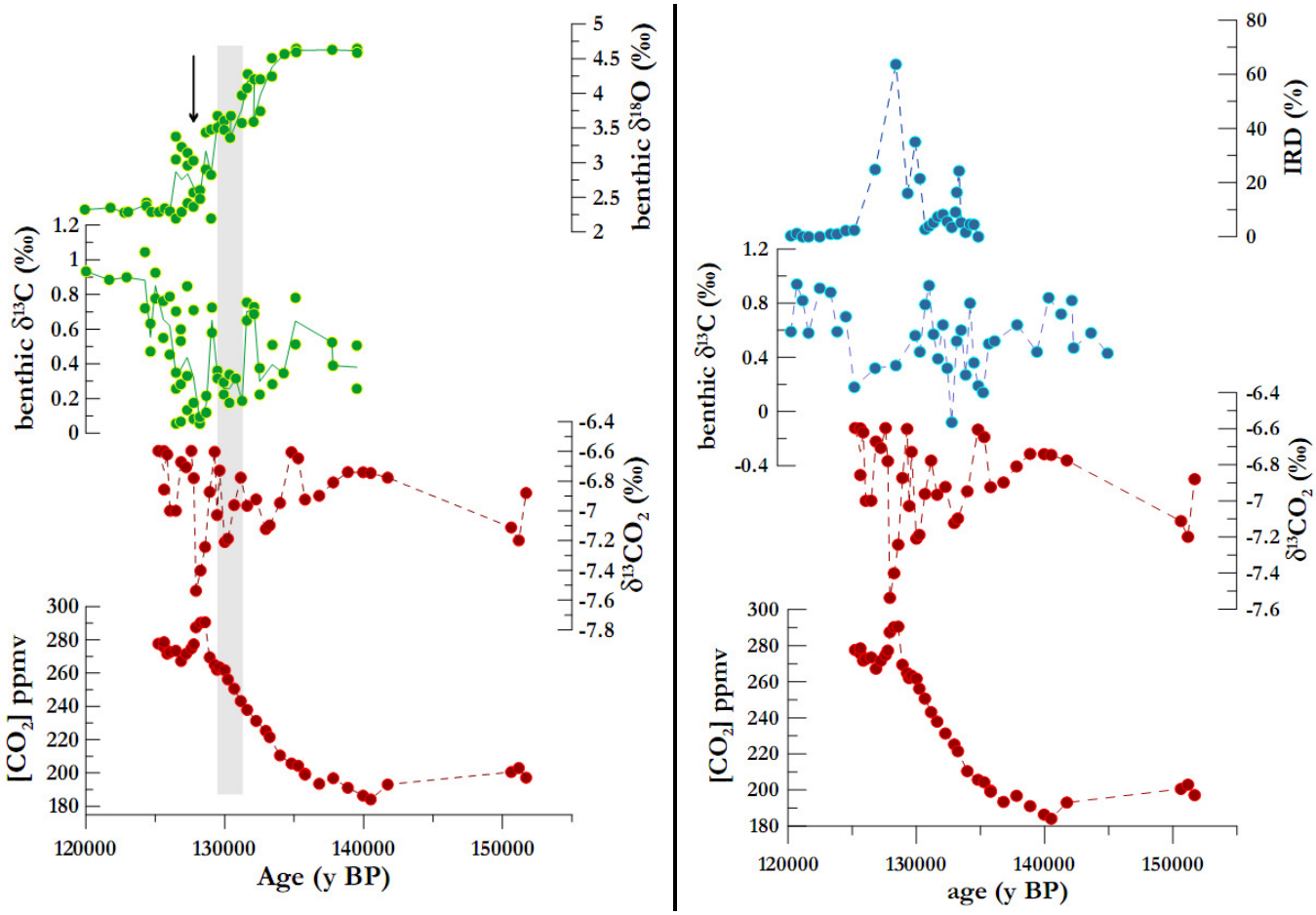

Figure 5-6: *our data (red circles) compared to oceanic data to disentangle timing problems* ***(left panel)****: data from a N. Atlantic core (45°N; 25°W) of Lototskaya and Ganssen, 1999, green circles. The high resolution permitted them to localize the different abrupt climatic events within TII: here in the grey frame the "pause" is depicted, while the black arrow shows the time position of H11; $\delta^{18}O$ values of the same benthic species are equally plotted to facilitate synchronization issues;* ***(right panel)*** *data from another N. Atlantic site (55°N; 15°W) from Oppo et al., 2001, blue circles, where IRD maximum coincides with benthic $\delta^{13}C$ trough in the marine record. Both cores were plotted against their original time scales. Both studies provide evidence that cold deglaciation periods are accompanied by negative δ^{13} excursions, as for TI, while they agree on the timing of H11 event occurrence just after the climatic optimum*

V.4.7.3. S. Ocean vertical mixing

As for TI, planktic $\delta^{13}C$ data reveal a re-organization of the S. Ocean vertical mixing changes, potentially affecting the atmospheric signal, as well (*cf. Ch. IV*, one of the main conclusions on the deglaciation start-up). Fig. 5-7 illustrates data from Spero and Lea, 2002 for TII, accompanied by the equivalent $\delta^{18}O$ record. The authors find a ^{13}C-depletion during TII, with a minimum value at ~129 ky, suggesting similar mechanisms as for TI. Indeed, our results fit well with the planktic signal; still a question arises as to whether the S. Ocean stratification breakdown happens much later than for TI. The answer lies in the sea ice retreat, exposed before, in fig. 5-5d that localized the ss-Na^+ minimum value just before the climatic optimum, in excellent accordance with what this planktic signal provides.

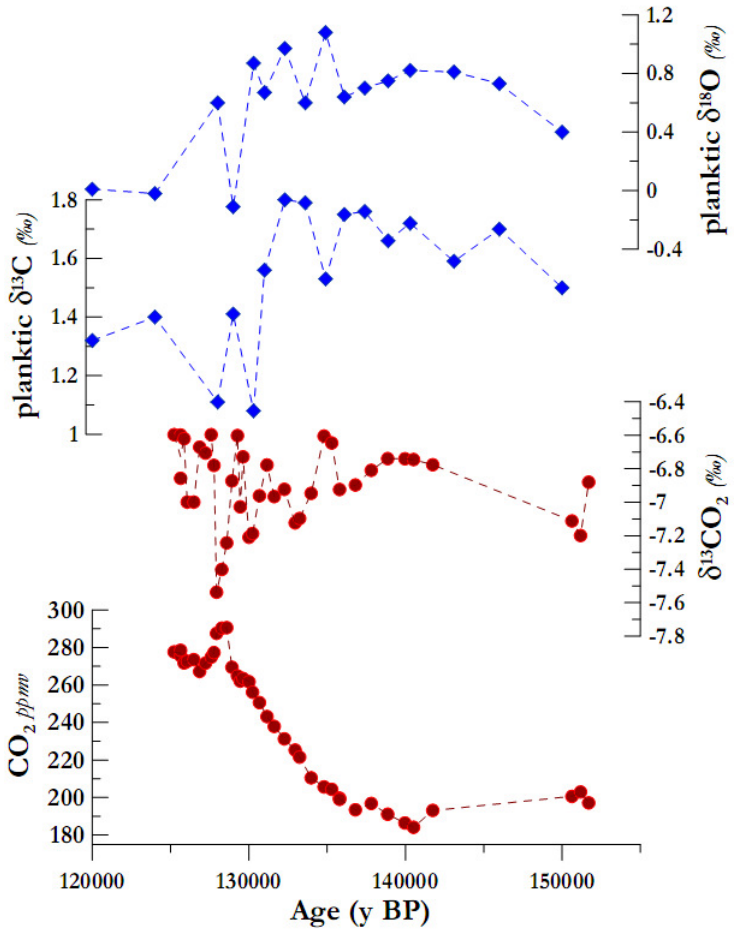

Figure 5-7: *our data (red circles) compared to intermediate water-dwelled planktonic data of East Equatorial Pacific showing a depletion during the deglaciation, potentially meaning S. Ocean stratification breakdown in the deglaciation set-up (blue diamonds, the same dataset shown for TI on Ch. IV). Data plotted against the original age scale, as provided by Spero and Lea, 2002*

V.4.7.4. MIS 5e

Marine records further validate the concomitant NH and SH warming at the climatic optimum: Duplessy et al., 2007 superimpose $\delta^{18}O$ benthic records from the N. Atlantic and S. Ocean, showing a decline at ~130 ky. If this is combined with the concomitant rise of CO_2 and CH_4 at MIS 5e, one should therefore think of a mechanism linking both hemispheres towards warmer conditions on a very short time scale. MIS 5e is equally connected with increasing vegetation in Western Europe, linked with higher temperatures (Sánchez-Goñi et al., 2005).
According to Adkins et al., 1997, the climatic optimum (registered in their core at ~129 ky) is accompanied by a strong NADW flux, which is subsequently weakened, in phase with both GHGs decline. This reminds of the MWPs during TI (at the end of SP-II and SP-IV) where an abrupt increase in MOC[5] was strongly related to an enhancement of both CO_2 and CH_4

V.4.7.5. Challenge on selecting the appropriate core

Selection of any given sediment core for comparison with our globally significant atmospheric record from EDC must take into account possible regional influences. Both the interpretation of benthic $\delta^{13}C$ record, in terms of intermediate/deep water mass ventilation, and the exact synchronization of the records for different oceanic cores can be problematic. However, $\delta^{13}C$ of benthic marine organisms reveal oceanic circulation patterns related to the bipolar seesaw mechanism (Broecker, 1998). A common pattern observed through time periods, is a N. Atlantic benthic $\delta^{13}C$ drop simultaneous with an enhanced IRD signal in marine sediments, while higher SSTs are found in the S.H. together with benthic $\delta^{13}C$ peak in the S.W. Pacific (Chapman and Shackleton, 1999; Pahnke and Zahn, 2005). The above $\delta^{13}C$ configurations are representative of sluggish NADW and enhanced AAIW formation. However an increased SST is seen from another core in the S. Ocean next to S. Africa, at a site affected by the Agulhas current (Cortese et al., 2007)) but associated with a minimum in benthic $\delta^{13}C$; this minimum corresponds to regional changes, such as weaker **CDW**[6] in the Atlantic, opposed to the enhanced AAIW in the Pacific. Therefore, a decoupling between deep and intermediate waters impacts during cold N. Atlantic periods is suggested (Cortese et al., 2007; Molyneux et al., 2007). This reflects the importance of selecting the right core locations in interpreting our atmospheric signal.

[5] Meridional Oceanic Circulation
[6] Circumpolar Deep Water

V.5. Comparison between TI and TII

In this section an intercomparison between the first two deglaciations will be accomplished, based on the data provided from this study, with support from ice core and oceanic proxies exposed in the following figures (fig. 5-8 to 5-10).

Fig. 5-8 shows a direct intercomparison of the evolution of CO_2 and $\delta^{13}CO_2$ for the two deglaciations, provided from this study, together with CH_4, deuterium and its excess, *d*.

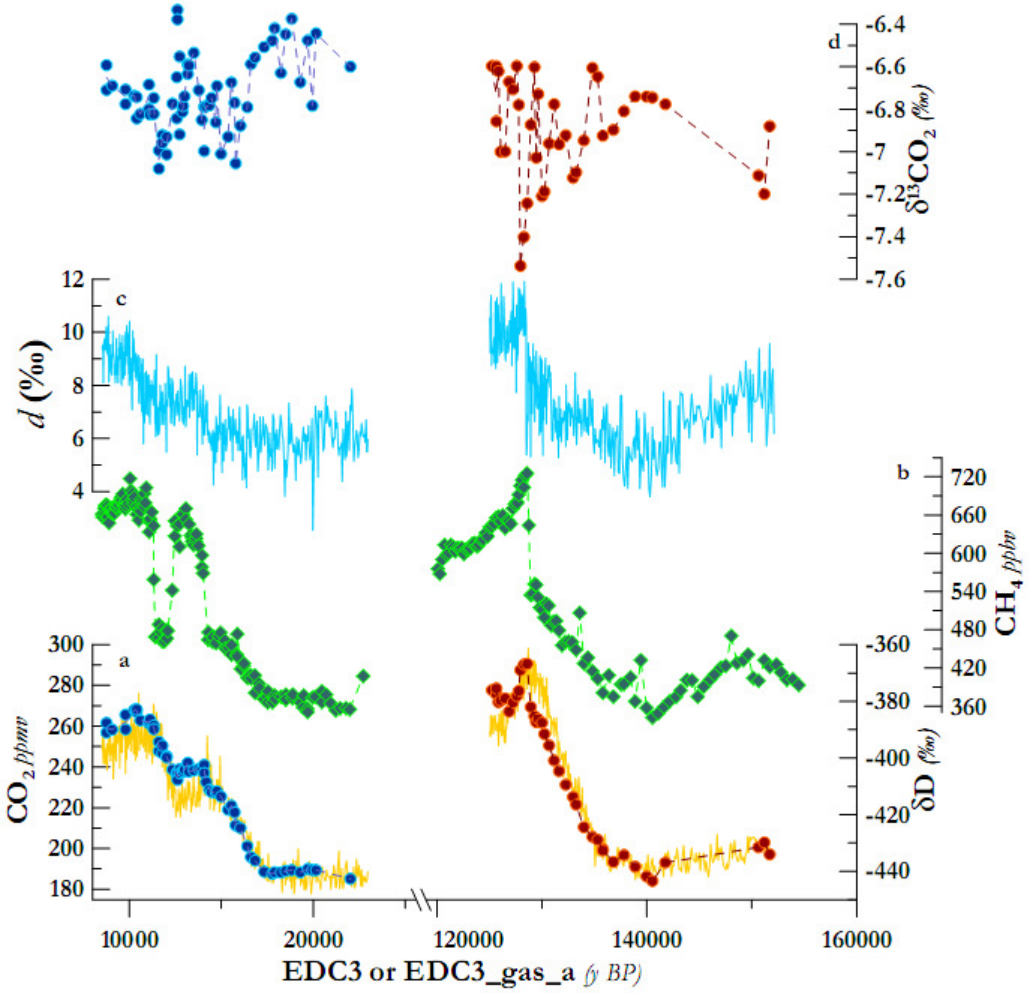

***Figure 5-8**: TI - TII intercomparison on the following variables : (a) CO_2 from this study, superposed with deuterium from Jouzel et al., 2007; (b) CH_4 data from Loulergue et al., 2008; deuterium excess, d, (V. Masson-Delmotte, pers. comm.) and (d) $\delta^{13}CO_2$ from this study. All variables are exposed against the newest age scales for either the ice or the gas occluded within*

In fig. 5-9, another intercomparison series is exposed, analogously to fig. 5-5 for both deglaciations.

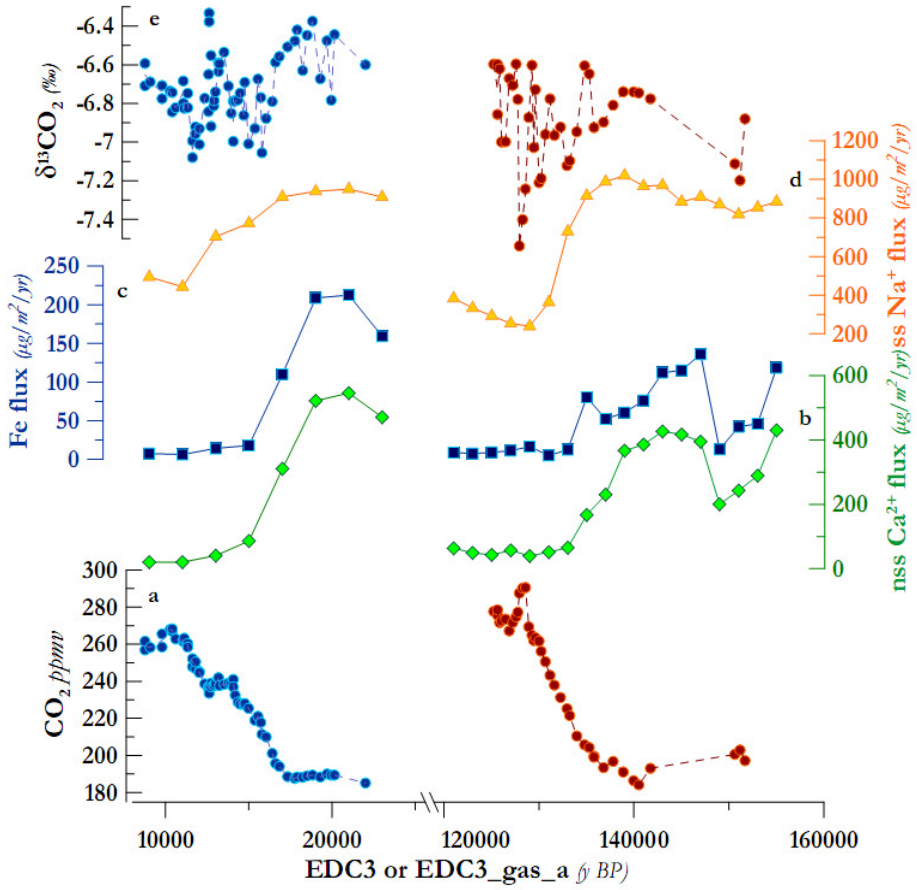

***Figure 5-9**: TI - TII intercomparison of the following variables: (a) CO_2; (b) nss-Ca^{+2} data; (c) Fe flux data; (d) ss-Na^{+} and (e) $\delta^{13}CO_2$. (a) and (e) being from this study, while the rest of chemistry data from Wolff et al., 2006*

Fig. 5-10 shows the superposition of our atmospheric data with benthic and planktic $\delta^{13}C$:

Overall, TI is better dated than TII, as a result from the more abundant and well-resolved datasets obtained for TI. A synchronization exercise of different marine records can be found in Cannariato and Kennett, 2005. Still, in the ice cores domain it should be stated that the newest gas age (EDC3_gas_a) needs updating, mainly in the TI time frame (F. Parennin; C. Waelbroeck, *pers. comm.*).

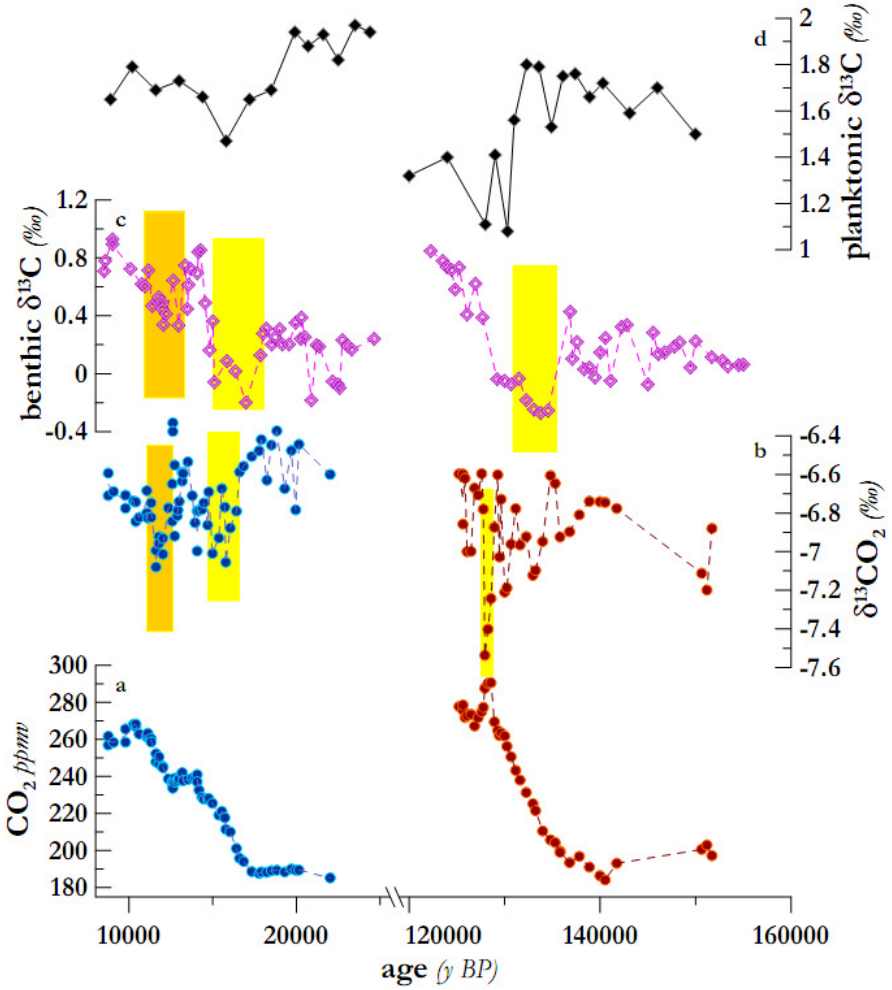

***Figure 5-10**: TI - TII intercomparison of (a) our CO_2 data and (b) our $\delta^{13}CO_2$ data with (c) benthic $\delta^{13}C$ records from the Iberian margin, showing 2 negative $\delta^{13}C$ excursions during TI vs. only one during TII (Skinner and Shackleton, 2006) and (d) planktic $\delta^{13}C$ records from the equat. Pacific region, depicting a much higher ^{13}C-depletion for TII when compared to TI (Spero and Lea, 2002)*

V.5.1. Amplitude of variations

Higher amplitudes during TII are observed for all climatic signals seen in fig. 5-8 (CO_2, deuterium, CH_4, $\delta^{13}CO_2$). Petit et al., 1999 found that the warming silhouette differs between the two deglaciations with warmer Antarctic temperature, while the concentrations of GHGs, such as CO_2 and CH_4 were higher in MIS 5e than during the Holocene. A similar larger amplitude is observed for the ss-Na^+ chemical signal (fig. 5-9d), in accordance with more ^{13}C-depleted planktic signal of intermediate waters in the equatorial Pacific (fig.5-10d), implying a more intense oceanic event during TII than TI. The rest of chemical signals (*i.e.* those depicting continental transport, fig. 5-9b;c) are found less amplified than TI, meaning a reduced dust input to the S. Ocean.

V.5.2. $\delta^{13}C$ depletion

Our $\delta^{13}CO_2$ signal is more ^{13}C-depleted during TII than TI (fig. 5-8d). A recent coupled experimental and modelling study of Duplessy et al., 2007 demonstrated higher NADW related to enhanced temperatures during MIS 5e *vs.* present. On the contrary, during TII probably lower SSTs prevailed than TI, leading towards a weakened NADW. This weakened NADW formation, could have been responsible for the depleted benthic $\delta^{13}C$ values, due to AABW enhancement finally leading to a depleted $\delta^{13}CO_2$ signal.

V.5.3. Phase differences

It has been proposed that CO_2 lags from deuterium evolution for both deglaciations (Broecker and Henderson, 1998; Fischer et al., 1999), with TII potentially experiencing higher time lags than TI. However, Fischer et al., 1999 were focused on the early deglacial changes and not the entire transitions. Despite some relative timing inconsistencies, a consensus over the leading role of Antarctic temperature over atmospheric CO_2 by 1.3±1.0 ka and of CO_2 over the global ice volume development (by 2.7±1.3 ka) prevails for the ensemble of the deglaciations (Mudelsee, 2001). Still, in the new EDC CO_2 record, the phasing comparison with δD is not that evident with the tools at hand; a more delicate statistical analysis and data treatment is needed to reach a definite conclusion. Still, a lead of CO_2 over sea ice retreat can be evident with the help of ss-Na^+ proxy.

In *Ch. I*, the orbital forcing theory on deglaciations generation was exposed, as well as the 'causality problem' for TII. This can be linked with the above amplitude and phasing differences. Broecker and Henderson, 1998 suggested the maximum SH insolation, which precedes the NH one, to play an important role on the glacial terminations triggering. Their suggestion, visualized in fig.5-11a, can explain (i) the different lag magnitudes of climatic sequences for both deglaciations and (ii) the different timing of the initial SH warming between the two deglaciations. A higher 60°S insolation peak magnitude prior the 'main' NH one is encountered during TII, compared to the one corresponding to TI. This may explain the smaller timing lags observed for TI, compared to TII. This can also explain the more rapid initial deglacial melting, according to Ruddiman et al., 1980. In the same fig.5-11b, insolation differences between the two deglaciations are also provided. A greater insolation anomaly is seen for MIS 5e vs. Holocene, which might justify the higher climatic variables amplitudes and duration.

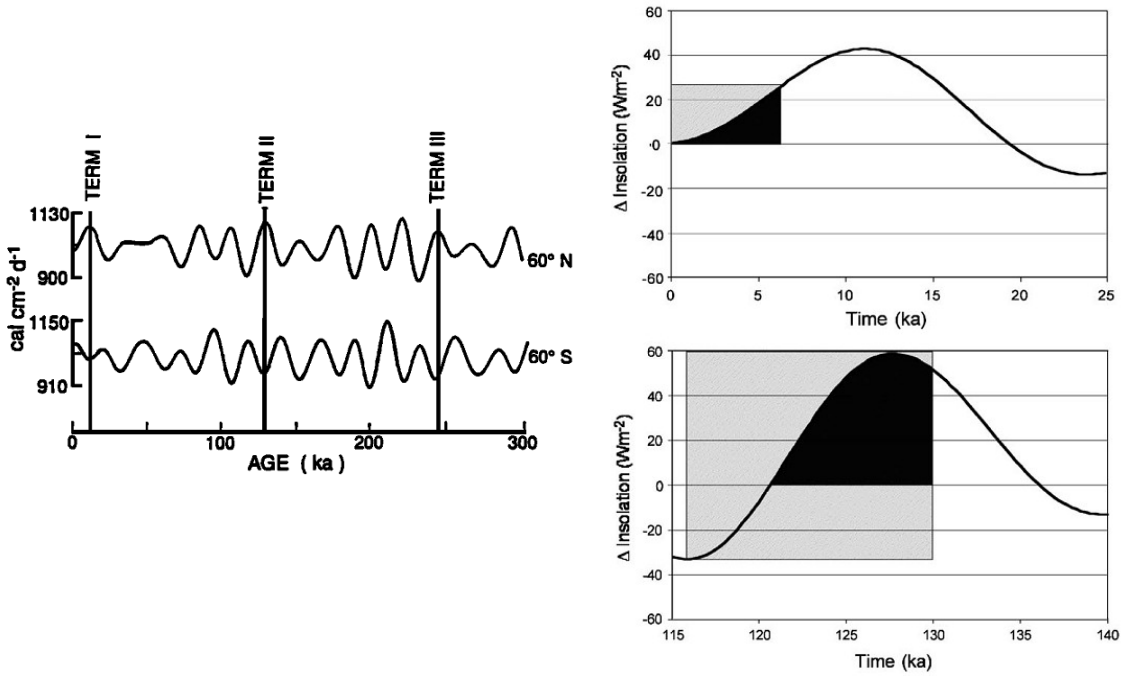

Figure 5-11: (left panel) *on the relative magnitudes of NH and SH insolation TI-TII differences and their causal relationship upon the deglaciation startup (Broecker and Henderson, 1998);* ***(right panel)****: mean summer insolation anomalies ($W m^{-2}$) expressed as the departure from present at 65°N from 25ky to present (upper panel) and from 140-115 ky (lower panel). Solid black areas represent the region where summer insolation and sea level were at or above present, while the interglacial duration (defined as the time when sea level is at or above present) is shown in the shaded box. Taken from CAPE, 2006*

V.5.4. Existence of a seesaw pattern

Millennial-scale climatic oscillations, been anti-phased between the two hemispheres and affecting ocean circulation patterns and SSTs, constitute the bipolar seesaw (Broecker and Henderson, 1998).

As mentioned above, there exist a YD-like event, as well as a H11, registered in NH records. We are not 100% sure of their relative synchronization, as well as their absolute dating occurrence (Lototskaya et al., 1998; Cheng et al., 2006). Both cold TII events, are considered smoother than those of TI (H11 being of lower IRD %, CH_4 not presenting a minimum but a 'standstill' during TII). This was further validated from stalagmite records (Yuan et al., 2004). Skinner and Shackleton, 2006 discuss the "B/A analogue" missing during TII, which is also explained from the CH_4 record and the benthic $\delta^{13}C$ minimum seen for TII vs. TI (fig. 5-10c)

For both terminations CO_2 and CH_4 start rising concomitantly and evolve in a similar way throughout TII. This implies the absence of the bipolar seesaw pattern from the CO_2 and CH_4 variations. Still, the upper is contrasting with what is recorded in marine sediments for TII. This, combined with the relative abrupt climate episodes phasing, inspire us towards a different interpretation of the two deglaciations, on millennial time scales.

Cooling rebounds have been reported also for the SH (Bianchi and Gersonde, 2002; Cortese et al., 2007). These cooling rebounds seen in both hemispheres could have been concomitant. Additionally, both CO_2 and CH_4 experience in-phase slowdown in their increasing trend, just before the climatic optimum. Based on the actual ice core resolution, one can observe similar patterns between the two gases, in contrast with what has been discussed for TI, questioning the inter-hemispheric anti-correlation hypothesis. This is maybe due to the fact that for TII the YD-like pause, as well as H11 event were smoothed out in the atmospheric signal, being originally weaker than the equivalent events of TI.

Since B/A-equivalent period is absent from TII, no matches between the in-phase evolution of $\delta^{13}CO_2$ with CH_4 are observed. On the contrary, the C-cycle seems to be also very dynamic, as for TI, since CO_2 and its stable carbon isotope change gradients mainly in an anti-phased manner (see fig. 5-2 and table 5-2).

Overall, the inter-hemispheric anti-correlation is not that evident when considering solely the ice record for TII.

V.6. Sequence of events during TII

TI and TII could have shared the same main causes of deglaciation, in terms of climatic feedback on the initial orbital forcing, as presented in *Ch. I and Ch. IV*. From the oceanic evidence we dispose, the dominant mechanisms being related to S. Ocean main forcings are also active for TII as for TI. The ensemble of these indicators show a more amplified timing pattern towards MIS 5e.

On a theoretical basis, high austral summer insolation could have generated warm-wet conditions in Patagonia, causing alpine glacial recession and reducing dust; this might have led to lower Fe fertilization in the S. Ocean and thus an enhanced out-gassing of CO_2 towards the atmosphere. Dust fluxes revealed to be weaker for TII than TI but their effect on our CO_2 signal is more propagated than for TI. Dust mechanism is active during 10 ky for TII, compared to 4 ky for TI. This difference includes a CO_2 50 ppmv rise for TII, against 36 ppmv rise for TI. The above can justify the more ^{13}C-depleted pattern encountered for TII, since productivity drawdown induces a CO_2 increase and $\delta^{13}CO_2$ decline.

We consider the sea ice retreat (ss-Na^+ evidence) to have played a major role to the CO_2 and $\delta^{13}CO_2$ evolution, since (i) it finds absolute timing correspondence with the S. Ocean stratification breakdown proxy, i.e. planktic $\delta^{13}C$, (ii) both proxies show a decreasing pattern until 129 ky BP, leading to a major CO_2 outgassing from the deep, old ocean which is depleted in ^{13}C (*cf. Ch. I*).

MIS 5e optimum coincides with maxima in CO_2 and CH_4 mixing ratios, high equatorial, NH and SH SSTs, a NH terrestrial biospheric growth, a marked shift in deuterium excess and a minimum in our atmospheric $\delta^{13}CO_2$. All this occur just after S. Ocean vertical mixing enhancement and sea ice retreat ~2 ky after the dust flux minimum.

Already the synchronized trend of at least the gas parameters has not been encountered previously. From even the phase diagram of $\delta^{13}CO_2$ against CO_2 (fig. 5-12), one easily observes the different interpretation one should proceed for the yellow-rounded frame, belonging to the MIS5e optimum (since it appears to have been governed by different processes):

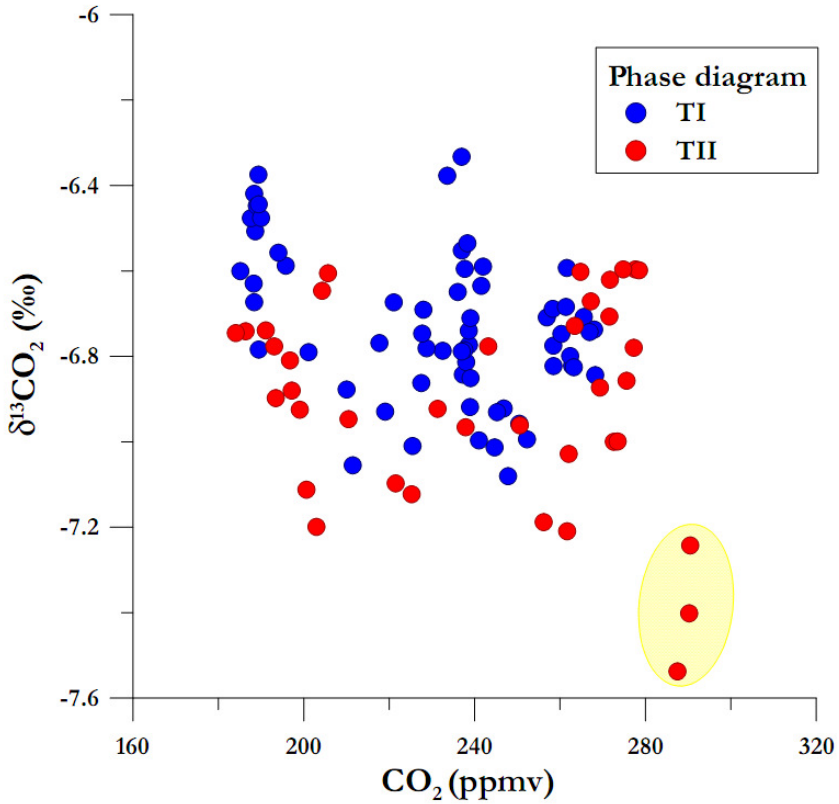

***Figure 5-12**: phase diagram of $\delta^{13}CO_2$ against CO_2 for both deglaciations, plotted to search for common leading processes*

We propose the following "amplifier" mechanism:

The difference in SH summer insolation magnitude results in a delayed reaction of the S. Ocean to the initial forcings. Therefore, dust deposition persists throughout TII (seen also by more intense atmospheric circulation indices) and sea ice remains for a longer time period than TI on the S. Ocean surface. In the meantime, a similar delayed reaction might have also occurred for the NH, as revealed by the weakened NADW throughout TII. The gradual dust flux decrease from the Antarctic record, combined with the even more gradual sea ice retreat over 10 ky, while equally involving the external solar forcing long-term effect, may have provoked a larger climatic

response on the MIS 5e, as seen by the SST maxima, equally depicted on the carbon cycle protagonists (higher CO_2 mixing ratio and such a $\delta^{13}CO_2$ decline). The climatic and C cycle perturbations may have been also accompanied by an intense atmospheric circulation and changes in the hydrological cycle, as expressed from the drift in the *d* record. In the meantime, terrestrial biosphere responds to this perturbation (seen by land change in Europe as well as CH_4 peak in phase with CO_2), which then leads towards the CO_2 decline, combined with the post-optimum $\delta^{13}CO_2$ rise observed in our ice core record.

An earlier proposed suggestion

Based on their highly-resolved N. Atlantic record, Lototskaya and Ganssen, 1999 suggested the following sequence of events, as visualized in fig. 5-13:

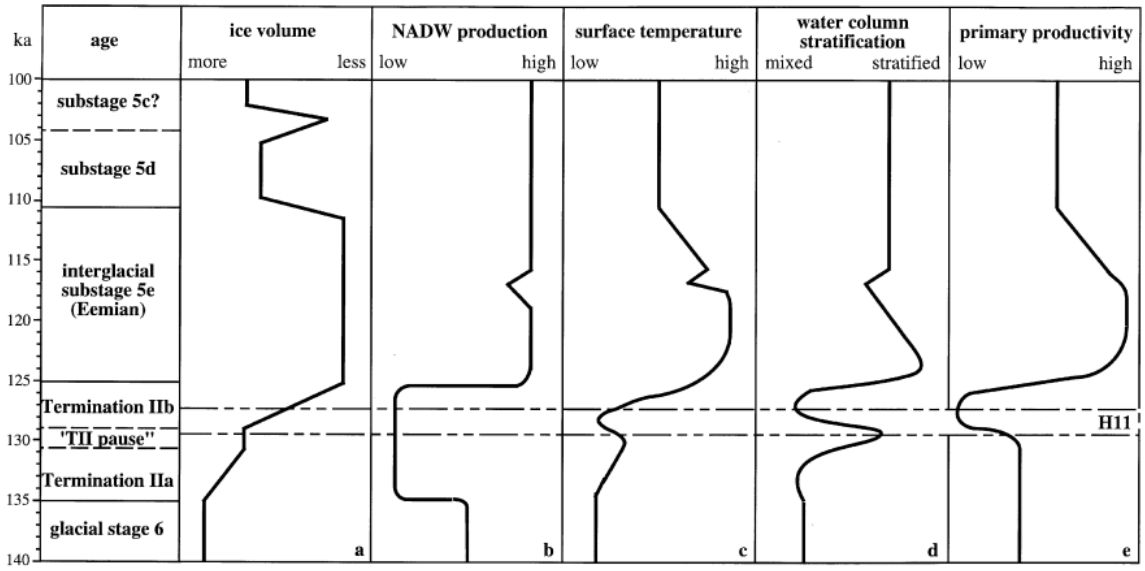

***Figure 5-13**: Sequence of events for TII, as proposed from Lototskaya and Ganssen, 1999 – to be followed in a future study*

The upper figure could be the future basis on a model-based interpretation of this dataset in the near future.

V.7. Clathrated ice and TII results

In *Ch. III*, we exposed the results obtained on the transition between bubbly and clathrated ice, dealing with the AIM 12 period in EDC and comparing it with the same time frame of the purely bubbly ice of Berkner. We found an average 12-ppmv depletion of the CO_2 mixing ratio for the transit zone of EDC vs. the bubbly ice of Berkner, while the $\delta^{13}CO_2$ results of both cores were found interestingly comparable.

All results presented in *Ch. III* and remarks made upon, included only analytical corrections, as presented in Ch. III[7]. When gravitational correction is applied, the EDC $\delta^{13}CO_2$ dataset was found depleted on average by 0.2‰ *vs.* the equally corrected Berkner one, and with a larger scattering. Analogously, returning to data presented in this chapter, one could attribute the more ^{13}C-depleted TII results (compared to TI) to such fractionation artifact on ice including clathrates. Below, some arguments against the upper statement are exposed:

- In *Ch. II*, a higher gas instability at the transit "brittle" zone was demonstrated by the studies of Ikeda et al., 1999; Ikeda-Fukazawa et al., 2001 when compared to the purely clathrated one. Indeed, the upper statement can be valid in our EDC record: although TII data scattering was slightly higher than for TI, it is much better than that observed for the same ice on the AIM 12 time frame. Table 5-3 resumes the results deduced out of the same calculations for the main sampling periods exposed above (TI, AIM 12 and TII):

Variable	EDC TI	Berkner Island	EDC AIM 12	EDC TII
CO_2	1.21	1.16	2.64	1.87
$\delta^{13}CO_2$	0.098	0.142	0.243	0.102
$\delta^{18}O\text{-}CO_2$	0.487	0.497	0.733	0.472

***Table 5-3**: σ-calculations of the three measured variables for the main sampling periods representing EDC ice with different ice properties : first two columns dealing with bubble ice, third column corresponds to the "brittle" zone sample and last column clathrated ice (note: calculation did not include the 5 outliers of TII)*

- The higher scatter found for the transit brittle EDC zone during AIM 12, could be partially attributed to the physical state of the ice, being full of fractures and cracks; this was not the case for TII
- Benthic $\delta^{13}C$ data during TII were found in their great majority ^{13}C-depleted, when compared to TI. This was attributed to differences in oceanic circulation. Since the ocean is thought to have been the protagonist for the CO_2 G-IG evolution, our more ^{13}C-depleted data are coherent with marine observations
- Part of the uncorrected- corrected inconsistency may be attributed to the correction nature itself, for this case being $\delta^{15}N$ experimental data. For the sampling periods of TI and TII, $\delta^{15}N$ EDC data were provided by G. Dreyfus and were found in a very good correlation with the "modeled" $\delta^{15}N$, out of the relation with deuterium (*cf. Ch. II*). I do not have such information for the Berkner core, nor $\delta^{15}N$ measurements exist for the

[7] All kinds of data treatment and exploitation are in charge of H. Schaefer. In this manuscript, only data produced by me are commented. Still, for the discussion part here, some elements deduced from the work of H. Schaefer are exposed, (esp. the gravitational correction subject)

EDC brittle zone. The above statement is further supported when proceeding to a comparison of initial and corrected mean $\Delta\delta^{13}CO_2$ values for the Berkner – EDC (AIM 12 period) and EDC (TI) and EDC (TII) coupled cores and shown in table 5-4:

	AIM 12		**deglaciations**		**$\Delta\delta^{13}CO_2$ between cores**
	Berkner	EDC	EDC_TI	EDC_TII	
Initial	-6.333	-6.239	-6.255	-6.406	0.094 vs. 0.151
Corrected			-6.724	-6.902	0.2 vs. 0.178
$\Delta\delta^{13}CO_2$ corr			-0.469	-0.496	

Table 5-4*: comparing the two experiments: (1) bubble and brittle ice (AIM 12 test) and (2) bubble and clathrated ice (deglaciations experiment), in terms of deviations between them before and after corrections applied*

The above table shows that there is an inconsistency between the pre- and post corrected $\delta^{13}CO_2$ difference between the two cases studied: uncorrected $\Delta\delta^{13}CO_2$ for the AIM 12 cores (of 0.094 ‰) lead to higher corrected $\Delta\delta^{13}CO_2$ of 0.2 ‰) than those of the deglaciations case (0.151 vs. 0.178‰), the proportion of the latter staying constant when excluding the difference added from the correction. Such high corrections difference in such a short period frame, may possibly imply ice core artifacts

- When comparing the CO_2 values from Vostok with those provided by this study, one finds harmonious trends and absolute values (R^2=0.98, *cf. above*). The Vostok ice was also 100% clathrated at the time of drilling. But contrary to EDC, it was then stored for more than 15 years at -20°C before being analyzed at high resolution over TII (Petit et al., 1999; Pépin et al., 2001). This implies that a significant portion of clathrates decomposed during storage. This is evident optically, as the Vostok ice is now far less transparent than EDC ice (decomposed clathrates form cracks, rendering the ice more opaque).
- Certainly, the clathrates-effect was well present during the analytical procedure, in terms of the three expansions characteristics (*cf. Ch. III and annex V*). The grinding efficiency was also lower than for TI. Still, this efficiency even for TI was far less than 100% (been one of the drawbacks of this method, *cf. Ch. III*). Both TI and TII datasets, fit well with previously presented data from either EDC or Vostok cores, which can lead to the conclusion that a lower grinding efficiency has no effect on the absolute atmospheric obtained value (it has nevertheless an effect on its scattering, σ)

Firm quantification of a possible extraction artifact on 100 % clathrated ice could be evaluated later on, by comparing again EDC and Berkner ice over the early CO_2 changes taking place at the MIS 5e – MIS 5d transition. According to the gas dating of the bottom part of Berkner,

stratigraphic continuity is observed back to 110 ka in this core. Although the corresponding depth in the core is around 900 m, the pressure-temperature combination is not suitable for clathrates to form in this deep Berkner ice. On the other hand, EDC ice below 1200 m of depth should be fully clathrated (as observed at Vostok), which corresponds to a gas age of ~80 ka (*i.e.* MIS 5a).

V.8. Conclusion

In this chapter, a new dataset on the CO_2 and its stable carbon isotope ratio evolution throughout the penultimate deglaciation is presented. Since such data are the first ones for the EDC core, we defined in the first place the distinct sub-periods driven by altered CO_2 trends. As for TI, increasing CO_2 tendencies are generally accompanied by an opposite pattern in its stable C isotopic ratio, validating the dynamic character of deglaciations. Being constrained from higher dating uncertainties than for the case of TI, we still proceeded in an intercomparison of the two glacial terminations studied, by superposing our data with other ice core records. We assume a strong impact of orbital forcing differences between the two deglaciations on the climatic amplifiers (seen in deuterium record) and to the C cycle parameters (atm. CO_2 and $\delta^{13}CO_2$), which further implies a robust link between the three of them. S. Ocean is the key region for the start-up of both deglaciations, since (internal) forcing parameters such as sea ice retreat or dust input, reconstructed by Antarctic chemistry data, are active for both sampling periods. Still, for the case of TII, S. Ocean proxies appear more attenuated. This, combined with orbital differences may be responsible for the delayed response of the NH in terms of oceanic circulation and SSTs, both been weakened throughout the first ~10 ky of TII, when compared to TI. This reduced circulation pattern has been depicted in the oceanic signal, which probably explains our more ^{13}C-depleted atmospheric one (*vs.* TI) we measured for the EDC core.

The marine data testify the occurrence of two cold episodes during TII: a YD-like "standstill" and the H11 event. In parallel, they state the absence of a "B/A analogue". One main difference between the two deglaciations in our ice core record, lies in the signals phasing of CO_2 and CH_4 (until SP-6, *i.e.* the post-optimum decline). This, combined to the difficulty we encountered in localizing the cold events in our ice core record, as seen in marine sediments, may mean an absence of the see-saw pattern during TII in EDC record.

As far as the terrestrial biosphere is concerned, similar to SH and NH reaction to orbital forcings, it responds with a delay, after the climatic optimum, associated with a CO_2 depletion accompanied by a $\delta^{13}CO_2$ rise.

Applying the same crushing technique in ice generated from the brittle zone as in bubbly ice, showed no fractionation bias on the uncorrected results (*cf. Ch. III*). Therefore the atmospheric ^{13}C-depletion seen for TII can be attributed to atmospheric signal. This is reinforced by the more negative benthic $\delta^{13}C$ values from the marine archive that have been measured for TII compared to TI.

Some propositions, inspired from this study would engage further measurements on clathrate ice and comparison with bubble ice that represent the same time span. The need of highly resolved marine data is evident in order to better localize the abrupt climatic changes that characterized TII. The upper will furthermore allow to establish a well-constrained sequence of events, which will be further tested with simple box models or GCMs.

Chapter VI. Conclusions

VI.1. Technical conclusions

This study dealt with the delicate treatment of ice samples and the quantitative extraction of the CO_2 gas, as well as its stable isotopic ratios from ancient air occluded in ice cores. The analytical acquisition of CO_2 and its stable carbon isotope ratio, $\delta^{13}CO_2$, on the same sample and extraction steps allowed us to safely compare the two signals, without suffering from bias different datasets would impose. Corrections were applied on a daily basis concerning mass spectrometry measurements, by analysing several sub-samples of a standard gas of known composition. In addition, data were corrected for gravitational fractionation, the main physical process altering the isotopic ratios of CO_2 in interstitial air of the firn down to the ice. The overall precision of the measurements range on average by 1.50 ppmv and 0.099 ‰ for our measurements performed on 100% bubbly to 100% clathrated ice. Replicate measurements on contiguous samples confirmed the validity of this analytical precision. The final signals obtained on Termination I and II fit well to previous data series.

The same experimental protocol was used on ice samples of different nature; this allowed us to conduct an intercomparison test between (i) 100% bubbly ice, (ii) ice belonging to the transition zone from bubble to clathrate ice ("brittle zone"), and (iii) 100% clathrated ice, for evaluating possible bias associated with the non-quantitative extraction of trapped gases using our dry extraction procedure. We find greater efficiency on 100% bubbly ice than on 100% clathrated ice. There are indications that some trapped gas is still released by the crushed sample between consecutive gas expansions into the pre-concentration line, when working on 100% clathrated ice. This phenomenon seems not to affect the carbon isotopic ratio of the extracted CO_2, but brings some additional scattering to the measured CO_2 mixing ratio. When comparing 100% bubbly ice with ice of similar age but from the brittle zone of another ice core, we observe a relatively large depletion of the CO_2 mixing ratio (of max. 12 ppmv), combined with larger scattering (max. 4.5 ppmv), in the brittle zone ice. Previous studies have reported four-fold larger fractionations for CO_2, though. There is also an effect on the CO_2 carbon isotopic ratio, being about 0.2‰ more depleted in the brittle zone ice. Still, this depletion appears after gravitational correction.

Although future attempts should be made to still improve the reproducibility of the experimental procedure, our analytical system proved to be suitable for revealing significant changes in the

carbon isotopic composition of atmospheric CO_2 through time, on a glacial- interglacial time scale. The main limit is the large amount of time required for each analysis. During most of this PhD, we could measure typically one sample per day, when the mass spectrometer behaved well. By slightly modifying the pre-analysis steps, we achieved in measuring in 2008 two samples per day. Automation of part of the protocole should be envisaged in the future, to reduce the stress put on the experimentalist.

VI.2. Summary of the new key dataset

In fig. 6-1, we expose the whole CO_2 record, accompanied by the evolution of its stable isotopic ratios, produced throughout this PhD study. This permits a direct intercomparison on the boundary limits of each atmospheric variable on the four different studied periods.

Fig. 6-2 provides the superposition of our new CO_2 data with the published ones from Vostok core.

Fig. 6-3 compares our data synthesis with existing records from the EDC core, concerning δD, $\delta^{18}O$ and CH_4 records (all 3 being higher resolved that Vostok CO_2 data).

The main features of our $\delta^{13}CO_2$ record can be summarized as follows :

- $\delta^{13}CO_2$ mostly varies when the rate of CO_2 increase changes through the last two deglaciations,
- the maximum amplitude of the overall $\delta^{13}CO_2$ changes is of the magnitude of 1‰,
- there is a general decreasing trend of $\delta^{13}CO_2$ through the major part of the two last deglaciations, with a larger amplitude for TII compared to TI,
- rapid CO_2 changes are associated with large $\delta^{13}CO_2$ decreases, in a proportional way
- the $\delta^{13}CO_2$ profile throughout TI can best be simplified as a W-shape signal, with two minima corresponding to the H1 and Younger Dryas cold events in the N. Hemisphere,
- over TII, $\delta^{13}CO_2$ appears significantly more negative than during TI, possibly related to the overall reduced thermohaline circulation throughout TII relative to TI, as deduced from $\delta^{13}C$ benthic records in the ocean.

We confirm the higher CO_2 mixing ratios taking place at the start of MIS 5e, compared with the Early Holocene, with a mean value close to 290 ppmv; we further show for the first time that the final transition to this maximum happened within less than 300 y, through a rapid increase of more than 20 ppmv.

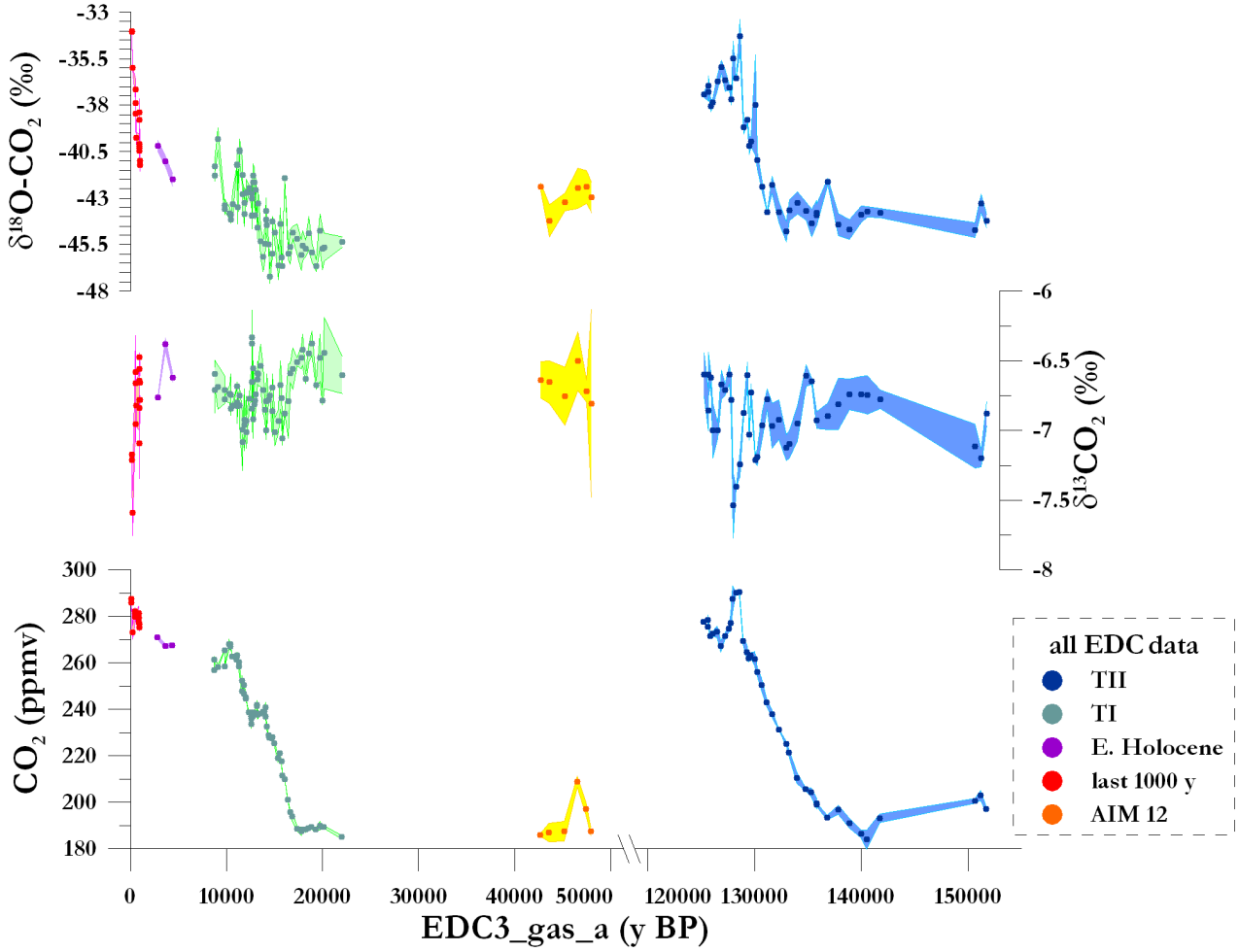

Fig. 6-1: *(from bottom to top): evolution of CO_2, $\delta^{13}CO_2$ and $\delta^{18}O\text{-}CO_2$ throughout studied periods covering the last 160 ky in the EDC core. 1σ for all 3 atm. variables is included*

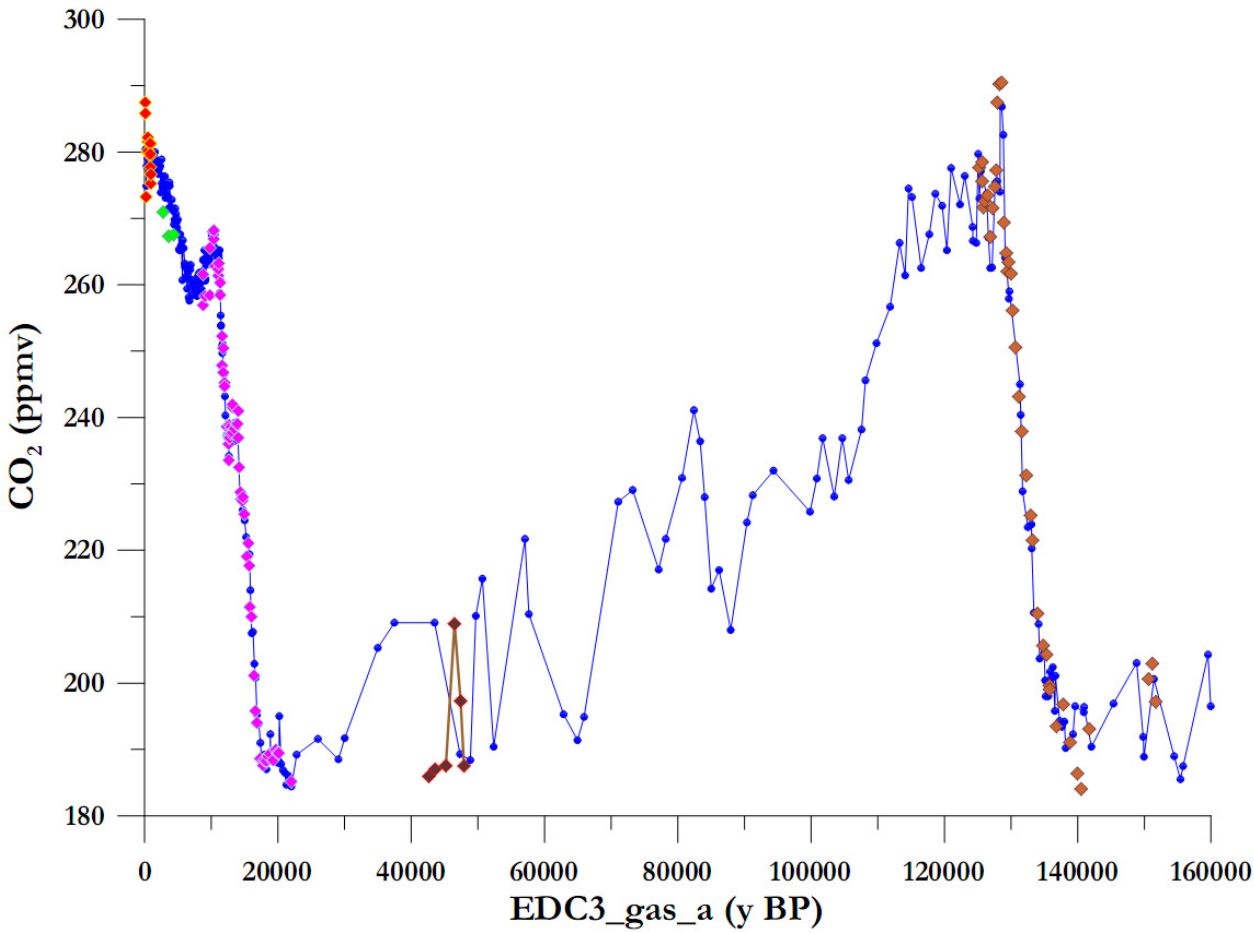

Fig. 6-2: *Vostok CO_2 record –blue circles- plotted against EDC3_gas_a, superimposed by the ensemble of the CO_2 data measured during this PhD. The difference over AIM 12 reflects the lack of resolution in the existing Vostok profile*

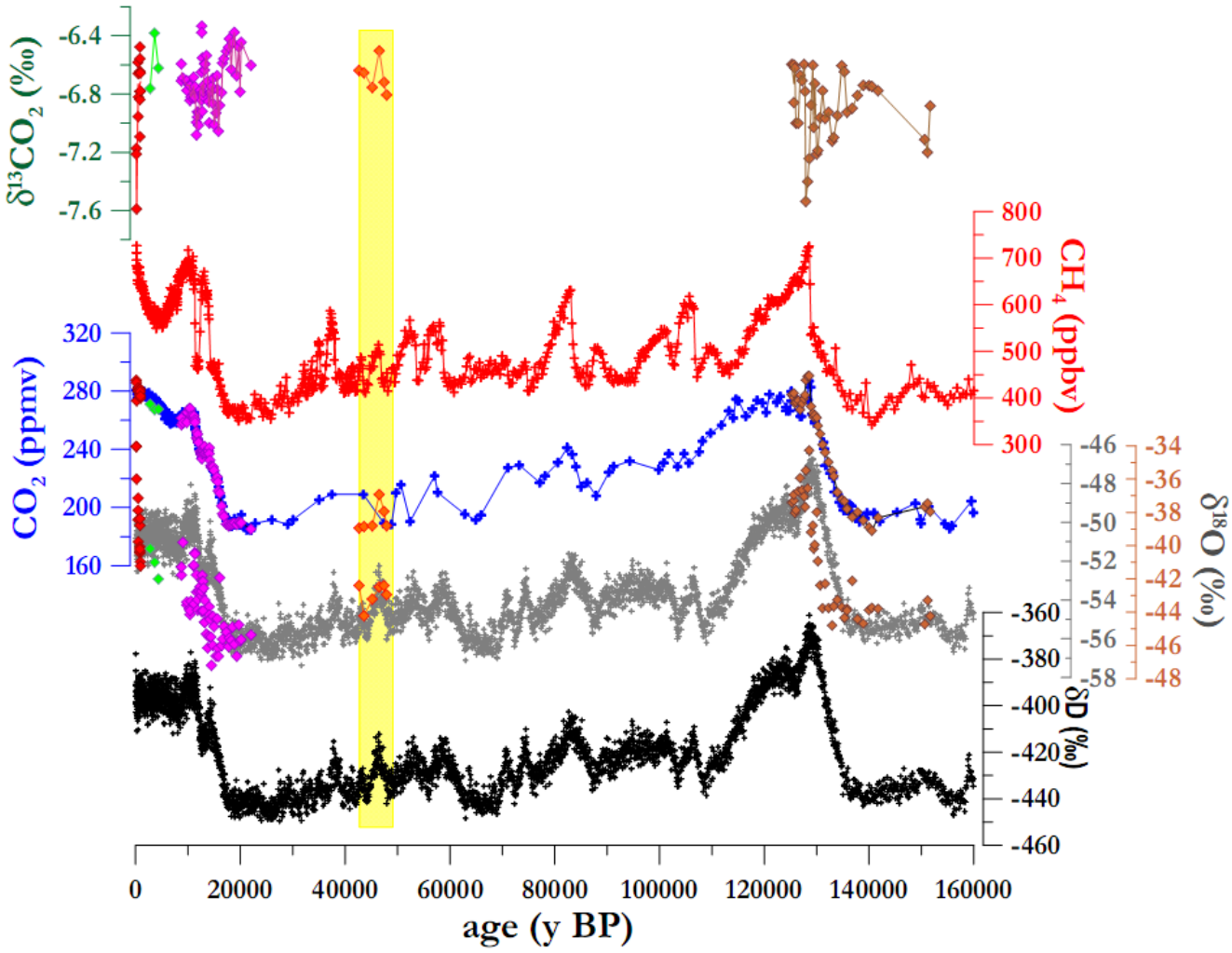

Fig. 6-3 *different ice core-deduced variables superposition. From bottom to top: EDC deuterium record (black line); EDC $\delta^{18}O$ record (grey line), plotted together with our atmospheric $\delta^{18}O$-CO_2 values (colored diamonds, same as for fig. 6-2), showing the equilibration happening among ice (H_2O) and CO_2; Vostok CO_2 record –blue crosses- plotted against EDC3_gas_a, superimposed by the ensemble of our EDC CO_2 data; EDC CH_4 record (red crosses); our EDC $\delta^{13}CO_2$ signal. Yellow frame covers the AIM 12 event, for which we found a CO_2 peak in EDC core, not previously shown in Vostok one; the rest climatic variables confirm the dynamic character of this event, by showing also max. peak signals*

VI.3. Conclusions on the carbon cycle / climate interactions

This study focuses on deglaciations, characterized by a ~80-100 ppmv CO_2 rise within only ~10 ky. The parallel study of the mixing and stable carbon isotopic ratios of CO_2 contribute in better constraining the carbon budget, by evaluating possible causes and interactions related to this deglacial CO_2 rise and ultimately quantifying the CO_2 sources. On such time frame, the reason of the CO_2 rise lies on the interplay of oceanic and terrestrial biospheric carbon reservoirs with the atmospheric one.

Alone our data, when compared with other proxies in *e.g.* the oceans, can provide qualitative statements on the potential major players between different carbon cycle mechanisms coupling climate change with the CO_2 increase. Still, carbon cycle modelling is required to project those mechanisms in a quantitative frame. Two C cycle box models were applied in interpreting the atmospheric signal we obtained from the ice record during the last deglaciation. Both model results were coherent in concluding that S. Ocean reconfigurations, linked to vertical mixing enhancement and marine productivity slowdown, were the leading forcing factors of the initial deglacial CO_2 rise, accompanied by a large and progressive $\delta^{13}CO_2$ decrease. This implies that the initial external insolation perturbation initiating the deglaciation affected first the S. Hemisphere and the austral ocean dynamics and productivity, then leading to a CO_2 change further amplifying the insolation forcing. A terrestrial biosphere imprint probably started during the Bölling/Alleröd warm period and continued through the YD. This could explain (i) the positive $\delta^{13}CO_2$ peak observed during the B/A (and the relative stabilization of CO_2, thus acting synergistically with the Antarctic temperature) and (ii) the subsequent $\delta^{13}CO_2$ decrease during the YD, according to the BICYCLE box model. Overall, while the whole CO_2 signal can mostly be explained by oceanic mechanisms (notably residing in the S. Ocean), the $\delta^{13}CO_2$ signal seems also prone to rapid fluctuations related to biospheric changes, in addition to the large oceanic imprint.

Termination II shows a different pattern than TI, although the general downward trend of $\delta^{13}CO_2$ show up, with a larger amplitude. We speculate that the main solar insolation differences between the two deglaciations affect the response time of SH. A qualitative comparison with existing proxy records of sea-ice cover, biological pump strength through iron fertilization, or strength of ventilation between deep and surface waters suggest that the major S. Ocean processes were also active in affecting CO_2 and $\delta^{13}CO_2$ during TII, but of different duration and magnitude. Sea ice and S. Ocean stratification breakdown would also be responsible for the CO_2 rise and $\delta^{13}CO_2$ decline occurring during ~10 ky after the initial temperature and CO_2 rise for TII. This, combined to the delay in shut-down of dust deposition during TII compared to TI,

could explain the different rates in the CO_2 rise and the $\delta^{13}CO_2$ decrease at the MIS 5e optimum. Thereafter, the effect of terrestrial biosphere growth could be responsible for both the depletion of CO_2 after the early MIS 5e maximum and the concomitant rise in $\delta^{13}CO_2$. Finally, the very good phasing between CO_2 and CH_4, notably expressed by the absence of a B/A analogue (which is also the case in the marine and pollen records), points to a possible absence of a bipolar seesaw pattern during TII.

VI.4. Perspectives

This work represents a first important contribution of LGGE to a desired signal from ice cores, on which several teams and researchers have devoted a lot of energy and efforts over the last ~20 years. This is not the final word. Although the current analytical system and procedure that we applied during this PhD provides conditions suitable for depicting significant $\delta^{13}CO_2$ changes through time, it will require some improvements in order to obtain better reproductibility, hopefully using a partially automated procedure. Approaches could be developed for instance to extract the gas mechanically but with a better efficiency of the current grinding system.
Future applications of the analytical system should focus at least on two important items :

- Comparing 100% bubbly and 100% clathrated ice having the same gas age. This will be feasible by studying the time period between ~80 and 110 ka, where Berkner and EDC ice are available, the former still including 100% bubbly ice
- Measuring $\delta^{13}CO_2$ over MIS 5e and the following glacial inception, when CO_2 remains relatively stable whereas Antarctica cools down. $\delta^{13}CO_2$ should represent a nice tracer of the possible contribution from continental biosphere carbon release during this period
- Ice core data alone are not enough to fully constrain the carbon cycle/climate relationship. Our interpretation has often been limited by the quality and resolution of carbon cycle proxies from the marine realm. Their dating with respect to the ice core chronology clearly represents another limiting factor. Improvements are necessary on both aspects.
- Lastly, we expect that progresses with modelling tools will help to get the maximum out of our experimental data. One promising way is the application of models of intermediate complexity, such as CLIMBER, in which the proxies are directly simulated. $\delta^{13}C$ is one of them in the CLIMBER-carbon version. As they can be run in transient conditions, they will prove much useful to compare with the $\delta^{13}CO_2$ profiles already produced during our PhD, and with the upcoming ones from LGGE and other ice core groups in the world.

References

Aballain O. (2002) Reconstruction de l'évolution passée du rapport isotopique $^{13}C/^{12}C$ du méthane atmosphérique à partir de l'analyse de l'air extrait du névé polaire. In *Laboratoire de Glaciologie et Géophysique de l'Environnement*, p. 134. Université Joseph Fourrier Grenoble I, St Martin d'Hères.

Adams J. M., Faure H., Faure-Denard L., McGlade J. M. and Woodward F. I. (1990) Increases in terrestrial carbon storage from the Last Glacial Maximum to the present. *Nature* **348**, 711-714.

Adkins J. F., Boyle E. A., Keigwin L. and Cortijo E. (1997) Variability of the North Atlantic THC during the last interglacial period. *Nature* **390**, 154-156.

Adkins J. F., McIntyre K. and Schrag D. P. (2002) The Salinity, Temperature, and $\delta^{18}O$ of the Glacial Deep Ocean. *Science* **298**, 1769 - 1773.

Ahn J., Wahlen M., Deck B. L., Brook E. J., Mayewski P. A., Taylor K. C. and White J. W. C. (2004) A record of atmospheric CO_2 during the last 40,000 years from the Siple Dome, Antarctica ice core. *Journal of Geophysical Research* **109**.

Ahn J. and Brook E. J. (2007) Atmospheric CO_2 and climate from 65 to 30 ka B.P. *Geophysical Research Letters* **34**.

Ahn J. and Brook E. J. (2008) Atmospheric CO_2 and Climate on Millennial Time Scales During the Last Glacial Period. *Science* **322**, 83-85.

Alley R. B. (1987) Firn densification by grain boundary sliding: a first model. *J. Phys. Colloques* **48**, 249-256.

Andersen K. K., Svensson A., Johnsen S. J., Rasmussen S. O., Bigler M., Röthlisberger R., Ruth U., Siggaard-Andersen M.-L., Steffensen J. P., Dahl-Jensen D., Vinther B. M. and Clausen H. B. (2007) The Greenland Ice Core Chronology 2005, 15–42 ka. Part 1: constructing the time scale. *Quaternary Science Reviews* **25**, 3246-3257

Anklin M., Barnola J.-M., Schwander J., Stauffer B. and Raynaud D. (1995) Processes affecting the CO_2 concentrations measured in Greenland ice. *Tellus* **47B**, 461-470.

Anklin M., Schwander J., Stauffer B., Tschumi J., Fuchs A., Barnola J. M. and Raynaud D. (1997) CO_2 record between 40 and 8 kyr B.P. from the Greenland Ice Core Project ice core. *Journal of Geophysical Research* **102**, 26539-26545.

Archer D. and Maier-Reimer E. (1994) Effect of deep-sea sedimentary calcite preservation on atmospheric CO_2 concentration. *Nature* **367**, 260 - 263.

Archer D., Kheshgi H. and Maier-Reimer E. (1998) Dynamics of fossil fuel CO_2 neutralization by marine $CaCO_3$. *Global Biogeochemical Cycles* **12**, 259-276.

Archer D., Winguth A., Lea D. and Mahowald N. (2000) What caused the glacial/interglacial atmospheric pCO_2 cycles? *Reviews of Geophysics* **38**, 159-190.

Archer D. E., Martin P. A., Milovich J., Brovkin V., Plattner G.-K. and Ashendel C. (2003) Model sensitivity in the effect of Antarctic sea ice and stratification on atmospheric pCO_2. *Paleoceanography* **18**.

Arnaud L. (1997) Modélisation de la transformation de la neige en glace à la surface des calottes polaires; Etude du transport des gaz dans ces milieux poreux. . In *Laboratoire de Glaciologie et Géophysique de l'Environnement*, p. 300. Université Joseph Fourrier Grenoble I, St Martin d'Hères.

Arrhenius S. (1896) On the Influence of Carbonic Acid in the Air upon the Temperature of the Ground. *Philosophical Magazine* **41**, 237-276.

Arzt E., Ashby M. F. and Easterling K. E. (1983) Practical applications of hot-isostatic Pressing diagrams: Four case studies. *Metallurgical and Materials Transactions A* **14**, 211-221.

Bains S., Norris R., Corfield R. and Faul K. (2000) Termination of global warmth at the Palaeocene/Eocene boundary through productivity feedback *Nature* **407**, 171-174.

Bard E., Rostek F. and Sonzogni C. (1997) Interhemispheric synchrony of the last deglaciation inferred from alkenone palaeothermometry. *Nature* **385**, 707-710.

Bard E., Rostek F., Turon J.-L. and Gendreau S. (2000) Hydrological Impact of Heinrich Events in the Subtropical Northeast Atlantic. *Science* **289**, 1321 - 1324.

Bard E. (2002) Climate Shock: Abrupt Changes over Millennial Time Scales. *Physics Today* **55**, 32-38.

Barnola J. M., Raynaud D., Neftel A. and Oeschger H. (1983) Comparison of CO_2 measurements by two laboratories on air from bubbles in polar ice. *Nature* **303**, 410-413.

Barnola J.-M. (1984) Etude des variations passées du CO_2 atmosphérique à partir de l'analyse de l'air piégé dans la glace; détermination de la Teneur "Pré-Industrielle"; Etude de la Transition Dernier Age Glaciaire – Holocène. In *Laboratoire de Glaciologie et Géophysique de l'Environnement*, Université Joseph Fourrier Grenoble I, St Martin d'Hères.

Barnola J. M., Raynaud D., Korotkevich Y. S. and Lorius C. (1987) Vostok ice core provides 160,000-year record of atmospheric CO_2. *Nature* **329**, 408-414.

Barnola J.-M. (1999) Status of the atmospheric CO_2 reconstruction from ice cores analyses. *Tellus* **51B**, 151–155.

Baskaran M. and Krishnamurthy R. V. (1993) Speleothems as Proxy for the Carbon Isotope Composition of Atmospheric CO_2. *Geophysical Research Letters* **20**, 2905-2908.

Bauch H. A., Erlenkeuser H., Jung S. J. A. and Thiede J. (2000) Surface and Deep Water Changes in the Subpolar North Atlantic During Termination II and the Last Interglaciation. *Paleoceanography* **15**, 76-84.

Bauch H. A. and Kandiano E. S. (2007) Evidence for early warming and cooling in North Atlantic surface waters during the last interglacial. *Paleoceanography* **22**.

Bellier B. (2004) Etude des variations du cycle du carbone au cours de l'Holocène à partir de l'analyse couplée CO_2-CH_4 piégés dans les glaces polaires. In *Laboratoire de Glaciologie et Géophysique de l'Environnement*, p. 160. Université Joseph Fourrier Grenoble I, St Martin d'Hères.

Bender M., Sowers T. and Brook E. (1997) Gases in ice cores. *Proceedings of the National Academy of Sciences of the United States of America* **94**, 8343-8349.

Bender M. L. (2002) Orbital tuning chronology for the Vostok climate record supported by trapped gas composition. *Earth and Planetary Science Letters* **204**, 275-289.

Berger W. H. (1982) Increase of carbon dioxide in the atmosphere during deglaciation: the coral reef hypothesis. *Naturwissenschaften* **69**, 87-88.

Bernard S. (2004) Evolution temporelle du méthane et du protoxyde d'azote dans l'atmosphère : contrainte par l'analyse de leurs isotopes stables dans le névé et la glace polaires. In *Laboratoire de Glaciologie et Géophysique de l'Environnement*, p. 280. Université Joseph Fourier Grenoble I, St Martin d'Hères.

Berner R. A. (1994) GEOCARB II; a revised model of atmospheric CO_2 over Phanerozoic time. *American Journal of Science* **294**, 56-91.

Berner R. A. and Kothavala Z. (2001) Geocarb III: A Revised Model of Atmospheric CO_2 over Phanerozoic Time. *American Journal of Science* **301**, 182-204.

Bianchi C. and Gersonde R. (2002) The Southern Ocean surface between Marine Isotope Stages 6 and 5d: Shape and timing of climate changes. *Palaeogeography, Palaeoclimatology, Palaeoecology* **187**, 151-177.

Bianchi C. and Gersonde R. (2004) Climate evolution at the last deglaciation: the role of the Southern Ocean. *Earth and Planetary Science Letters* **228**, 407-424.

Bird M. I., Lloyd J. and Farquhar G. D. (1994) Terrestrial carbon storage at the LGM. *Nature* **371**.

Blunier T., Chappellaz J., Schwander J., Dällenbach A., Stauffer B., Stocker T. F., Raynaud D., Jouzel J., Clausen H. B., Hammer C. U. and Johnsen S. J. (1998) Asynchrony of Antarctic and Greenland climate change during the last glacial period. *Nature* **394**, 739-743.

Blunier T. and Brook E. J. (2001) Timing of Millennial-Scale Climate Change in Antarctica and Greenland During the Last Glacial Period. *Science* **291**, 109 - 112.

Blunier T., Spahni R., Barnola J.-M., Chappellaz J., Loulergue L. and Schwander J. (2007) Synchronization of ice core records via atmospheric gases. *Clim. Past* **3**, 325-330.

Bopp L., Kohfeld K. E., Quéré C. L. and Aumont O. (2003) Dust impact on marine biota and atmospheric CO_2 during glacial periods. *Paleoceanography* **18**.

Bowen G. J., Beerling D. J., Koch P. L., Zachos J. C. and Quattlebaum T. (2004) A humid climate state during the Palaeocene/Eocene thermal maximum. *Nature* **432**, 495-499.

Brand W. A. (1996) High Precision Isotope Ratio Monitoring Techniques in Mass Spectrometry. *Journal of Mass Spectrometry* **31**, 225-235.

Broecker W. S. and van_Donk J. (1970) Insolation Changes, Ice Volumes, and the $\delta^{18}O$ Record in Deep-Sea Cores. *Reviews of Geophysics and Space Physics* **8**.

Broecker W. S. and Peng T. H. (1982) *Tracers in the sea*. Eldigio Press.

Broecker W. S., Rooth C. and Peng T.-H. (1985) Ventilation of the deep Northeastern Atlantic. *Journal of Geophysical Research* **90**, 6940-6944.

Broecker W. S. and Peng T. H. (1986) Carbon cycle: 1985 glacial to interglacial changes in the operation of the global carbon cycle. *Radiocarbon* **28**, 309-327.

Broecker W. S. (1994) Massive iceberg discharges as triggers for global climate change. *Nature* **372**, 421-424.

Broecker W. S. (1998) Paleocean Circulation during the Last Deglaciation: A Bipolar Seesaw? *Paleoceanography* **13**, 119-121.

Broecker W. S. and Henderson G. M. (1998) The sequence of events surrounding Termination II and their implications for the cause of glacial-interglacial CO_2 changes. *Paleoceanography* **13**, 352-364.

Broecker W. S. (2003) Does the Trigger for Abrupt Climate Change Reside in the Ocean or in the Atmosphere? *Science* **300**, 1519 - 1522.

Broecker W. S. (2005) *The Role of the Ocean in Climate Yesterday, Today and Tomorrow*.

Brook E. J., Harder S., Severinghaus J., Steig E. J. and Sucher C. M. (2000) On the Origin and Timing of Rapid Changes in Atmospheric Methane During the Last Glacial Period. *Global Biogeochemical Cycles* **14**, 559–572.

Brovkin V., Hofmann M., Bendtsen J. and Ganopolski A. (2002) Ocean biology could control atmospheric $\delta^{13}C$ during glacial-interglacial cycle. *Geochem., Geophys., Geosyst.* **3**.

Brovkin V., Ganopolski A., Archer D. and Rahmstorf S. (2007) Lowering of glacial atmospheric CO_2 in response to changes in oceanic circulation and marine biogeochemistry. *Paleoceanography* **22**.

Caillon N., Severinghaus J. P., Barnola J.-M., Chappellaz J., Jouzel J. and Parrenin F. (2001) Estimation of temperature change and of gas age - ice age difference, 108 kyr B.P., at Vostok, Antarctica. *Journal of Geophysical Research* **106**, 31893–31901.

Caillon N., Severinghaus J. P., Jouzel J., Barnola J.-M., Kang J. and Lipenkov V. Y. (2003) Timing of Atmospheric CO_2 and Antarctic Temperature Changes Across Termination III. *Science* **299**, 1728 - 1731.

Campen R. K., Sowers T. and Alley R. B. (2003) Evidence of microbial consortia metabolizing within a low-latitude mountain glacier. *Geology* **31**, 231-234.

Cannariato K. G. and Kennett J. P. (2005) Structure of the penultimate deglaciation along the California margin and implications for Milankovitch theory. *Geology* **33**, 157-160.

CAPE L. I. P. M.-. (2006) Last Interglacial Arctic warmth confirms polar amplification of climate change. *Quaternary Science Reviews* **25**, 1383-1400.

Carlson A. E., Stoner J. S., Donnelly J. P. and Hillaire-Marcel C. (2008) Response of the southern Greenland Ice Sheet during the last two deglaciations. *Geology* **36**, 359 - 362.

Cerling T. E., Quade J., Wang Y. and Bowman J. R. (1989) Carbon isotopes in soils and palaeosols as ecology and palaeoecology indicators. *Nature* **341**, 138-139.

Cerling T. E. (1991) Carbon dioxide in the atmosphere; evidence from Cenozoic and Mesozoic Paleosols. *American Journal of Science* **291**, 377-400

Chapman M. R. and Shackleton N. J. (1999) Global ice-volume fluctuations, North Atlantic ice-rafting events, and deep-ocean circulation changes between 130 and 70 ka. *Geology* **27**, 795-798.

Chappellaz J., Barnola J. M., Raynaud D., Korotkevich Y. S. and Lorius C. (1990) Ice-core record of atmospheric methane over the past 160,000 years. *Nature* **345**, 127-131.

Chappellaz J. A., Fung I. Y. and Thompson A. M. (1993) The atmospheric CH_4 increase since the Last Glacial Maximum. I - Source estimates. *Tellus B* **45B**, 228-241.

Chappellaz J., Brook E., Blunier T. and Malaizé B. (1997) CH_4 and $\delta^{18}O$ of O_2 records from Antarctic and Greenland ice: A clue for stratigraphic disturbance in the bottom part of the Greenland Ice Core Project and the Greenland Ice Sheet Project 2 ice cores. *Journal of Geophysical Research* **102**, 26547–26557.

Chen J. H., Edwards R. L. and Wasserburg G. J. (1986) ^{238}U-^{234}U-^{232}Th in seawater. *Earth and Planetary Science Letters* **80**, 214-251.

Cheng H., Edwards R. L., Wang Y., Kong X., Ming Y., Kelly M. J., Wang X., Gallup C. D. and Liu W. (2006) A penultimate glacial monsoon record from Hulu Cave and two-phase glacial terminations. *Geology* **34**, 217-220.

Ciais P., Tans P., White J., Trolier M., Francey R., Berry J., Randall D., Sellers P., Collatz J. and Schimel D. (1995a) Partitioning of ocean and land uptake of CO_2 as inferred by $\delta^{13}C$ measurements from the NOAA Climate Monitoring and Diagnostics Laboratory Global Air Sampling Network. *Journal of Geophysical Research* **100**, 5051-5070.

Ciais P., White J. W. C., Jouzel J. and Petit J. R. (1995b) The origin of present-day Antarctic precipitation from surface snow deuterium excess data. *Journal of Geophysical Research* **100**, 18917-18927.

Ciais P., Denning A. S., Tans P. P., Berry J. A., Randall D. A., Collatz G. J., Sellers P. J., White J. W. C., Trolier M., Meijer H. A. J., Francey R. J., Monfray P. and Heimann M. (1997) A three-dimensional synthesis study of $\delta^{18}O$ in atmospheric CO_2 1. Surface fluxes. *Journal of Geophysical Research* **102**, 5857–5872.

Colbeck S. C. (1989) Air movement in snow due to wind pumping. *Journal of Glaciology* **35**, 209-213.

Coplen T. B., Brand W. A., Gehre M., Gröning M., Meijer H. A. J., Toman B. and Verkouteren R. M. (2006) After two decades a second anchor for the VPDB $\delta^{13}C$ scale. *Rapid Communications in Mass Spectrometry* **20**, 3165-3166.

Cortese G., Abelmann A. and Gersonde R. (2007) The last five glacial-interglacial transitions: A high-resolution 450,000-year record from the subantarctic Atlantic. *Paleoceanography* **22**.

Cortijo E., Duplessy J. C., Labeyrie L., Leclaire H., Duprat J. and Wearing T. C. E. v. (1994) Eemian cooling in the Norwegian Sea and North Atlantic ocean preceding continental ice-sheet growth. *Nature* **372**, 446-449.

Cortijo E., Lehman S., Keigwin L., Chapman M., Paillard D. and Labeyrie L. (1999) Changes in meridional temperature and salinity gradients in the North Atlantic Ocean (30°-72°N) during the last interglacial period. *Paleoceanography* **14**, 23-33.

Craig H. (1957) Isotopic standards for carbon and oxygen and correction factors for mass-spectrometric analysis of carbon dioxide. *Geochimica et Cosmochimica Acta* **12**, 133-149.

Craig H., Horibe Y. and Sowers T. (1988) Gravitational Separation of Gases and Isotopes in Polar Ice Caps. *Science* **242**, 1675 - 1678.

Curry W. B., Duplessy J. C., Labeyrie L. D. and Shackleton N. J. (1988) Changes in the Distribution of $\delta^{13}C$ of Deep Water ΣCO_2 Between the Last Glaciation and the Holocene. *Paleoceanography* **3**, 317-341.

Dansgaard W., Johnsen S. J., Clausen H. B., Dahl-Jensen D., Gundestrup N. S., Hammer C. U., Hvidberg C. S., Steffensen J. P., Sveinbjörnsdottir A. E., Jouzel J. and Bond G. (1993) Evidence for general instability of past climate from a 250-kyr ice-core record. *Nature* **364**, 218 - 220.

Dargaville R. J., Doney S. C. and Fung I. Y. (2003) Inter-annual variability in the interhemispheric atmospheric CO_2 gradient: contributions from transport and the seasonal rectifier. *TellusB* **55**, 711-722.

de Angelis M., Steffensen J. P., Legrand M. R., Clausen H. B. and Hammer C. U. (1997) Primary aerosol (sea salt and soil dust) deposited in Greenland ice during the last climatic cycle: Comparison with east Antarctic records. *Journal of Geophysical Research* **102**, 26681-26698.

Delmas R. J., Ascencio J.-M. and Legrand M. (1980) Polar ice evidence that atmospheric CO_2 20,000 yr BP was 50% of present. *Nature* **284**, 155-157.

Delmas R. J. (1993) A natural artefact in Greenland ice-core CO_2 measurements. *TellusB* **45**.

Denning A. S., Fung I. Y. and Randall D. (1995) Latitudinal gradient of atmospheric CO_2 due to seasonal exchange with land biota. *Nature* **376**, 240-243.

Denning A. S., Takahashi T. and Friedlingstein P. (1999) Can a strong atmospheric CO_2 rectifier effect be reconciled with a "reasonable" carbon budget? *TellusB* **51**, 249-253.

Duplessy J.-C. and Shackleton N. J. (1985) Response of global deep-water circulation to Earth's climatic change 135,000-107,000 years ago. *Nature* **316**, 500-507.

Duplessy J. C., Shackleton N. J., Fairbanks R. G., Labeyrie L., Oppo D. and Kallel N. (1988) Deepwater Source Variations During the Last Climatic Cycle and Their Impact on the Global Deepwater Circulation. *Paleoceanography* **3**, 343-360.

Duplessy J. C., Roche D. M. and Kageyama M. (2007) The Deep Ocean During the Last Interglacial Period. *Science* **316**, 89-91.

Durand G., Weiss J., Lipenkov V., Barnola J. M., Krinner G., Parrenin F., Delmonte B., Ritz C., Duval P., Röthlisberger R. and Bigler M. (2006) Effect of impurities on grain growth in cold ice sheets. *Journal of Geophysical Research* **111**.

Edgar K. M., Wilson P. A., Sexton P. F. and Suganuma Y. (2007) No extreme bipolar glaciation during the main Eocene calcite compensation shift. *Nature* **448**, 908-911.

Elliot M., Labeyrie L. and Duplessy J.-C. (2002) Changes in North Atlantic deep-water formation associated with the Dansgaard–Oeschger temperature oscillations (60–10 ka). *Quaternary Science Reviews* **21**, 1153-1165.

EPICA Community Members (2004) Eight glacial cycles from an Antarctic ice core. *Nature* **429**, 623-628.

EPICA Community Members (2006) One-to-one coupling of glacial climate variability in Greenland and Antarctica. *Nature* **444**, 195-198.

Etheridge D. M., Pearman G. I. and Fraser P. J. (1992) Changes in tropospheric methane between 1841 and 1978 from a high accumulation-rate Antarctic ice core. *Tellus* **44B**, 282-294.

Etheridge D. M., Steele L. P., Langenfelds R. L., Francey R. J., Barnola J.-M. and Morgan V. I. (1996) Natural and anthropogenic changes in atmospheric CO_2 over the last 1000 years from air in Antarctic ice and firn. *Journal of Geophysical Research* **101**, 4115–4128.

Etheridge D. M., Steele L. P., Francey R. J. and Langenfelds R. L. (1998) Atmospheric methane between 1000 A.D. and present: Evidence of anthropogenic emissions and climatic variability. *Journal of Geophysical Research* **103**, 15979-15994.

Eyer M. (2004) Highly resolved $\delta^{13}C$ measurements on CO_2 in air from Antarctic ice cores. In *Physikalisches Institut der Universität Bern*, p. 94. University of Bern, Bern, Switzerland.

Fairbanks R. G. (1989) A 17,000-year glacio-eustatic sea level record: influence of glacial melting rates on the Younger Dryas event and deep-ocean circulation. *Nature* **342**, 637 - 642

Fairbanks R. G. (1990) The age and origin of the Younger Dryas climate event in Greenland ice cores. *Paleoceanography* **5**, 937-948.

Farquhar G. D., Lloyd J., Taylor J. A., Flanagan L. B., Syvertsen J. P., Hubick K. T., Wong S. C. and Ehleringer J. R. (1993) Vegetation effects on the isotope composition of oxygen in atmospheric CO_2. *Nature* **363**, 439 - 443.

Ferretti D. F., Lowe D. C., Martin R. J. and Brailsford G. W. (2000) A new gas chromatograph-isotope ratio mass spectrometry technique for high-precision, N_2O-free analysis of $\delta^{13}C$ and $\delta^{18}O$ in atmospheric CO_2 from small air samples. *Journal of Geophysical Research* **105**, 6709-6718.

Fichefet T., Hovine S. and Duplessy J.-C. (1994) A model study of the Atlantic thermohaline circulation during the last glacial maximum. *Nature* **372**, 252-255.

Field M. H., Huntley B. and Müller H. (1994) Eemian climate fluctuations observed in a European pollen record. *Nature* **371**, 779-783.

Firestone R. B., West A., Kennett J. P., Becker L., Bunch T. E., Revay Z. S., Schultz P. H., Belgya T., Kennett D. J., Erlandson J. M., Dickenson O. J., Goodyear A. C., Harris R. S., Howard G. A., Kloosterman J. B., Lechler P., Mayewski P. A., Montgomery J., Poreda R., Darrah T., Hee S. S. Q., Smith A. R., Stich A., Topping W., Wittke J. H. and Wolbach W. S. (2007) Evidence for an extraterrestrial impact 12,900 years ago that contributed to the megafaunal extinctions and the Younger Dryas cooling. *Proc Natl Acad Sci U S A.* **104**, 16016-16021.

Fischer H., Wahlen M., Smith J., Mastroianni D. and Deck B. (1999) Ice Core Records of Atmospheric CO_2 Around the Last Three Glacial Terminations. *Science* **283**, 1712-1714.

Fischer H., Wahlen M. and Smith J. (2003) Reconstruction of glacial/interglacial changes in the global carbon cycle from CO_2 and $\delta^{13}CO_2$ in Antarctic ice cores. *Memoirs of National Institute of Polar Research. Special issue* **57**, 121-138.

Fisher R., Lowry D., Wilkin O., Sriskantharajah S. and Nisbet E. G. (2005) High-precision, automated stable isotope analysis of atmospheric methane and carbon dioxide using continuous-flow isotope-ratio mass spectrometry. *Rapid Communications in Mass Spectrometry* **20**, 200-208.

Francey R. J. and Farquhar G. D. (1982) An explanation of $^{13}C/^{12}C$ variations in tree rings. *Nature* **297**, 28-31.

Francey R. J., Allison C. E., Etheridge D. M., Trudinger C. M., Enting I. G., Leuenberger M., Langenfelds R. L., Michel E. and Steele L. P. (1999) A 1000-year high precision record of $\delta^{13}C$ in atmospheric CO_2. *Tellus B* **51**, 170–193.

François R., Altabet M. A., Yu E.-F., Sigman D. M., Bacon M. P., Frank M., Bohrmann G., Bareille G. and Labeyrie L. D. (1997) Contribution of Southern Ocean surface-water stratification to low atmospheric CO_2 concentrations during the last glacial period. *Nature* **389**, 929-935.

Friedli H., Moor E., Oeschger H., Siegenthaler U. and Stauffer B. (1984) $^{13}C/^{12}C$ Ratios in CO_2 Extracted from Antarctic Ice. *Geophysical Research Letters* **11**, 1145-1148.

Friedli H., Lötscher H., Oeschger H., Siegenthaler U. and Stauffer B. (1986) Ice core record of the $^{13}C/^{12}C$ ratio of atmospheric CO_2 in the past two centuries. *Nature* **324**, 237-238.

Friedlingstein P. (2008) A steep road to climate stabilization. *Nature* **451**, 297-298.

Frumkin A., Ford D. C. and Schwarcz H. P. (2000) Paleoclimate and vegetation of the last glacial cycles in Jerusalem from a speleothem record. *Global Biogeochemical Cycles* **14**, 863-870.

Fuchs A., Schwander J. and Stauffer B. (1993) A new ice mill allows precise concentration determination of methane and most probably also other trace gases in the bubble air of very small ice samples. *Journal of Glaciology* **39**, 199-203.

Fuchs A. and Leuenberger M. C. (1996) $\delta^{18}O$ of atmospheric oxygen measured on the GRIP ice core document stratigraphic disturbances in the lowest 10% of the core. *Geophysical Research Letters* **23**, 1049-1052.

Fuhrer K., Neftel A., Anklin M. and Maggi V. (1993) Continuous measurements of hydrogen peroxide, formaldehyde, calcium and ammonium concentrations along the new GRIP ice core from Summit, Central Greenland. *Atmospheric Environment* **12**, 1873-1880.

Gallet J.-C. (2006) Relations CO_2-Climat lors des Entrées en Glaciation. In *Laboratoire de Glaciologie et géophysique de l'Environnement*, p. 57. Université Joseph Fourrier Grenoble I, St Martin d'Hères.

Gallup C. D., Cheng H., Taylor F. W. and Edwards R. L. (2002) Direct Determination of the Timing of Sea Level Change During Termination II. *Science* **295**, 310-313.

Gaspari V., Barbante C., Cozzi G., Cescon P., Boutron C. F., Gabrielli P., Capodaglio G., Ferrari C., Petit J. R. and Delmonte B. (2006) Atmospheric iron fluxes over the last deglaciation: Climatic implications. *Geophysical Research Letters* **33**.

Gersonde R., Crosta X., Abelmann A. and Armand L. (2005) Sea-surface temperature and sea ice distribution of the Southern Ocean at the EPILOG Last Glacial Maximum—a circum-Antarctic view based on siliceous microfossil records. *Quaternary Science Reviews* **24**, 869-896.

Gherardi J.-M. (2006) Changements de la Circulation Océanique au cours de la Déglaciation : Apport des traceurs $^{231}Pa/^{230}Th$ du sédiment et Mg/Ca des foraminifères benthiques In *Laboratoire des Sciences du Climat de l'Environnement*, p. 266. Université Paris VI, Gif-Sur-Yvette, Paris.

Ghosh P. and Brand W. A. (2003) Stable isotope ratio mass spectrometry in global climate change research. *International Journal of Mass Spectrometry* **228**, 1-33.

Gildor H., Tziperman E. and Toggweiler J. R. (2002) Sea ice switch mechanism and glacial-interglacial CO_2 variations. *Global Biogeochemical Cycles* **16**.

Goldstein A. and Shaw S. (2003) Isotopes of volatile organic compounds: an emerging approach for studying atmospheric budgets and chemistry. *Chem Rev.* **103**, 5025-5048.

Gouzy A., Malaizé B., Pujol C. and Charlier K. (2004) Climatic "pause" during Termination II identified in shallow and intermediate waters off the Iberian margin. *Quaternary Science Reviews* **23**, 1523-1528.

Grachev A. M. and Severinghaus J. P. (2003) Laboratory determination of thermal diffusion constants for 29N2/28N2 in air at temperatures from −60 to 0°C for reconstruction of magnitudes of abrupt climate changes using the ice core fossil–air paleothermometer. *Geochimica et Cosmochimica Acta* **67**, 345-360.

Grootes P. M., Stuiver M., White J. W. C., Johnsen S. and Jouzel J. (1993) Comparison of oxygen isotope records from the GISP2 and GRIP Greenland ice cores. *Nature* **366**, 552-554.

Grousset F. E., Cortijo E., Huon S., Hervé L., Richter T., Burdloff D., Duprat J. and Weber O. (2001) Zooming in on Heinrich Layers. *Paleoceanography* **16**, 240-259.

Guimbaud C., Grannas A. M., Shepson P. B., Fuentes J. D., Boudries H., Bottenheim J. W., Dominé F., Houdier S., Perrier S., Biesenthal T. B. and Splawn B. G. (2002) Snowpack processing of acetaldehyde and acetone in the Arctic atmospheric boundary layer. *Atmospheric Environment* **36**, 2743-2752.

Güllük T., Slemr F. and Stauffer B. (1998) Simultaneous measurements of CO_2, CH_4, and N_2O in air extracted by sublimation from Antarctica ice cores: Confirmation of the data obtained using other extraction techniques. *Journal of Geophysical Research* **103**, 15971-15978.

Haan D. (1996) Teneurs en monoxyde de carbone de l'air contenu dans la glace de l'Antarctique et du Groenland. In *Laboratoire de Glaciologie et Géophysique de l'Environnement*, p. 182. Université Joseph Fourier Grenoble I, St Martin d'Hères.

Hachikubo A., Kosaka T., Kida M., Krylov A., Sakagami H., Minami H., Takahashi N. and Shoji H. (2007) Isotopic fractionation of methane and ethane hydrates between gas and hydrate phases. *Geophysical Research Letters* **34**.

Hall J. A., Barth J. A. C. and Kalin R. M. (1999) Routine Analysis by High Precision Gas Chromatography/Mass Selective Detector/ Isotope Ratio Mass Spectrometry to 0.1 Parts Per Mil. *Rapid Communications in Mass Spectrometry* **13**, 1231-1236.

Heinrich H. (1988) Origin and consequences of cyclic ice rafting in the Northeast Atlantic Ocean during the past 130,000 years. *Quaternary Research* **29**, 142-152.

Heinze C., Maier-Reimer E. and Winn K. (1991) Glacial pCO_2 reduction by the world ocean: Experiments with the Hamburg carbon cycle. *Paleoceanography* **6**, 395-430.

Hemming S. R. (2004) Heinrich events: Massive late Pleistocene detritus layers of the North Atlantic and their global climate imprint. *Reviews of Geophysics* **42**.

Henderson G. M. and Slowey N. C. (2000) Evidence from U–Th dating against Northern Hemisphere forcing of the penultimate deglaciation. *Nature* **404**, 61-66.

Hirayama Y., Kase Y., Tanihara N., Sumiyama Y., Kusuki Y. and Haraya K. (1999) Permeation properties to CO_2 and N_2 of poly(ethylene oxide)-containing and crosslinked polymer films. *Journal of Membrane Science* **160**, 87-99.

Hodell D. A., Venz K. A., Charles C. D. and Ninnemann U. S. (2003) Pleistocene vertical carbon isotope and carbonate gradients in the South Atlantic sector of the Southern Ocean. *Geochemistry, Geophysics, Geosystems* **4**.

Holbourn A., Kuhnt W., Schulz M. and Erlenkeuser H. (2005) Impacts of orbital forcing and atmospheric carbon dioxide on Miocene ice-sheet expansion. *Nature* **438**, 483-487.

Houdier S., Perrier S., Dominé F., Cabanes A., Legagneux L., Grannas A. M., Guimbaud C., Shepson P. B., Boudries H. and Bottenheim J. W. (2002) Acetaldehyde and acetone in the Arctic snowpack during the ALERT2000 campaign. Snowpack composition, incorporation processes and atmospheric impact. *Atmospheric Environment* **36**.

Howard W. R. and Prell W. L. (1994) Late Quaternary $CaCO_3$ production and preservation in the Southern Ocean: Implications for oceanic and atmospheric carbon cycling. *Paleoceanography* **9**, 453-482.

Huber C., Leuenberger M. and Zumbrunnen O. (2003) Continuous Extraction of Trapped Air from Bubble Ice or Water for On-Line Determination of Isotope Ratios. *Analytical Chemistry* **75**, 2324-2332.

Huber C., Beyerle U., Leuenberger M., Schwander J., Kipfer R., Spahni R., Severinghaus J. P. and Weiler K. (2006) Evidence for molecular size dependent gas fractionation in firn air derived from noble gases, oxygen, and nitrogen measurements. *Earth and Planetary Science Letters* **243**, 61-73.

Hughen K. A., Eglinton T. I., Xu L. and Makou M. (2004) Abrupt Tropical Vegetation Response to Rapid Climate Changes. *Science* **304**, 1955-1959.

Hulbe C. L., MacAyeal D. R., Denton G. H., Kleman J. and Lowell T. V. (2004) Catastrophic ice shelf breakup as the source of Heinrich event icebergs. *Paleoceanography* **19**.

Hut G. (1987) Consultants' group meeting on stable isotope reference samples for geochemical and hydrological investigations. In *Report to the Director General*. International Atomic Energy Agency, Vienna.

Ikeda T., Fukazawa H., Mae S., Pepin L., Duval P., Champagnon B., Lipenkov V. Y. and Hondoh T. (1999) Extreme fractionation of gases caused by formation of clathrate hydrates in Vostok Antarctic ice. *Geophysical Research Letters* **26**, 91-94.

Ikeda-Fukazawa T., Hondoh T., Fukumura T., Fukazawa H. and Mae S. (2001) Variation in N_2/O_2 ratio of occluded air in Dome Fuji antarctic ice. *Journal of Geophysical Research* **106**, 17799–17810.

Ikeda-Fukazawa T., Fukumizu K., Kawamura K., Aoki S., Nakazawa T. and Hondoh T. (2005) Effects of molecular diffusion on trapped gas composition in polar ice cores. *Earth and Planetary Science Letters* **229**, 183-192.

Indermühle A., Stocker T. F., Joos F., Fischer H., Smith H. J., Wahlen M., Deck B., Mastroianni D., Tschumi J., Blunier T., R.Meyer and Stauffer B. (1999) Holocene carbon-cycle dynamics based on CO_2 trapped in ice at Taylor Dome, Antarctica *Nature* **398**, 121-126.

Indermühle A., Monnin E., Stauffer B. and Stocker T. F. (2000) Atmospheric CO_2 concentration from 60 to 20 kyr BP from the Taylor Dome ice core, Antarctica. *Geophysical Research Letters* **27**, 735-738.

IPCC. (1995) Climate change 1995: The Science of Climate Change: Contribution of Working Group I to the Second Assessment of the Intergovernmental Panel on Climate Change.

IPCC. (2001) Intergovernmental Panel on Climate Change: Climate Change 2001, the Scientifc Basis (Edited by press C. U.).

IPCC. (2007) Climate Change 2007: The Physical Science Basis. Contribution of Working Group I to the Fourth Assessment Report of the Intergovernmental Panel on Climate Change [Solomon, S., D. Qin, M. Manning, Z. Chen, M. Marquis, K.B. Averyt, M. Tignor and H.L. Miller (eds.)]. *Cambridge University Press, Cambridge, United Kingdom and New York, NY, USA*, 996 pp.

Joos F. and Spahni R. (2008) Rates of change in natural and anthropogenic radiative forcing over the past 20,000 years. *PNAS* **105**, 1425-1430.

Jouzel J., Masson-Delmotte V., Cattani O., Dreyfus G., Falourd S., Hoffmann G., Minster B., Nouet J., Barnola J. M., Chappellaz J., Fischer H., Gallet J. C., Johnsen S., Leuenberger M., Loulergue L., Luethi D., Oerter H., Parrenin F., Raisbeck G., Raynaud D., Schilt A., Schwander J., Selmo E., Souchez R., Spahni R., Stauffer B., Steffensen J. P., Stenni B., Stocker T. F., Tison J. L., Werner M. and Wolff E. W. (2007) Orbital and Millennial Antarctic Climate Variability over the Past 800,000 Years. *Science* **317**, 793 - 796.

Karner D. B. and Muller R. A. (2001) A Causality Problem for Milankovitch. *Science* **288**, 2143 - 2144.

Kaspers K. A., Wal R. S. W. v. d., Broeke M. R. v. d., Schwander J., Lipzig N. P. M. v. and Brenninkmeijer C. A. M. (2004) Model calculations of the age of firn air across the Antarctic continent. *Atmospheric Chemistry and Physics* **4**, 1365–1380.

Kawamura K., Yokoyama K., Fujii Y. and Watanabe O. (2001) A Greenland ice core record of low molecular weight dicarboxylic acids, ketocarboxylic acids, and α-dicarbonyls: A trend from Little Ice Age to the present (1540 to 1989 A.D.). *Journal of Geophysical Research* **106**, 1331–1345.

Kawamura K., Nakazawa T., Aoki S., Sugawara S., Fujii Y. and Watanabe O. (2003) Atmospheric CO_2 variations over the last three glacial interglacial climatic cycles deduced from the Dome Fuji deep ice core, Antarctica using a wet extraction technique. *Tellus B* **55**, 126-137.

Kawamura K., Severinghaus J. P., Ishidoya S., Sugawara S., Hashida G., Motoyama H., Fujii Y., Aoki S. and Nakazawa T. (2006) Convective mixing of air in firn at four polar sites. *Earth and Planetary Science Letters* **244**, 672-682.

Keeling C. D., Whorf T. P., Wahlen M. and Plichtt J. v. d. (1995) Interannual extremes in the rate of rise of atmospheric carbon dioxide since 1980. *Nature* **375**, 666-670.

Keigwin L. D. and Lehman S. J. (1994) Deep Circulation Change Linked to HEINRICH Event 1 and Younger Dryas in a Mid-depth North Atlantic Core. *Paleoceanography* **9**, 185-194.

Keigwin L. D., Curry W. B., Lehman S. J. and Johnsen S. (1994) The role of the deep ocean in North Atlantic climate change between 70 and 130 kyr ago. *Nature* **371**, 323-326.

Keir R. (1993) Are atmospheric CO_2 content and Pleistocene climate connected by wind speed over a polar Mediterranean sea? *Global and Planetary Change* **8**, 59-68.

Kienast M., Steinke S., Stattegger K. and Calvert S. E. (2001) Synchronous Tropical South China Sea SST Change and Greenland Warming During Deglaciation. *Science* **291**, 2132-2134.

Kienast M., Kienast S. S., Calvert S. E., Eglinton T. I., Mollenhauer G., François R. and Mix A. C. (2006) Eastern Pacific cooling and Atlantic overturning circulation during the last deglaciation. *Nature* **443**, 846-849.

Kipfstuhl S., Pauer F., Kuhs W. F. and Shoji H. (2001) Air Bubbles and Clathrate Hydrates in the Transition Zone of the NGRIP Deep Ice Core. *Geophysical Research Letters* **28**, 591–594.

Knox F. and McElroy M. B. (1984) Changes in atmospheric CO_2 - Influence of the marine biota at high latitude. *Journal of Geophysical Research* **89**, 4629-4637.

Kohfeld K. E., Quéré C. L., Harrison S. P. and Anderson R. F. (2005) Role of Marine Biology in Glacial-Interglacial CO_2 Cycles. *Science* **308**.

Kohfeld S. b.-K. E. (in preparation) Figure on the smörgåsbord" of biogeochemical forcings. In *SOLAS book* (Edited by Quéré C. L.).

Köhler P. and Fischer H. (2004) Simulating changes in the terrestrial biosphere during the last glacial/interglacial transition. *Global and Planetary Change* **43**, 33-55.

Köhler P., Fischer H., Munhoven G. and Zeebe R. E. (2005) Quantitative interpretation of atmospheric carbon records over the last glacial termination. *Global Biogeochemical Cycles* **19**, GB4020.

Köhler P. and Fischer H. (2006) Simulating low frequency changes in atmospheric CO_2 during the last 740 000 years. *Climate of the Past* **2**, 57-78.

Köhler P., Fischer H., Schmitt J. and Munhoven G. (2006) On the application and interpretation of Keeling plots in paleo climate research – deciphering $\delta^{13}C$ of atmospheric CO_2 measured in ice cores. *Biogeosciences* **3**, 539-556.

Koutavas A., Lynch-Stieglitz J., Jr. T. M. M. and Sachs J. P. (2002) El Niño-Like Pattern in Ice Age Tropical Pacific Sea Surface Temperature. *Science* **297**, 226 - 230.

Kuhlbrodt T., Griesel A., Montoya M., Levermann A., Hofmann M. and Rahmstorf S. (2007) On the driving processes of the Atlantic meridional overturning circulation. *Reviews of Geophysics* **45**.

Kumar N., Anderson R. F., Mortlock R. A., Froelich P. N., Kubik P., Dittrich-Hannen B. and Suter M. (1995) Increased biological productivity and export production in the glacial Southern Ocean. *Nature* **378**.

Kuypers M. M. M., Pancost R. D. and Damsté J. S. S. (1999) A large and abrupt fall in atmospheric CO_2 concentration during Cretaceous times. *Nature* **399**, 342-345.

Labeyrie L., Jouzel J., Lévi C. and Cortijo E. (2004) Changements abrupts dans un monde glaciaire. *Comptes Rendus Geosciences* **336**, 721-732.

Labeyrie L., Waelbroeck C., Cortijo E., Michel E. and Duplessy J.-C. (2005) Changes in deep water hydrology during the Last Deglaciation. *Comptes Rendus Geosciences* **337**, 919-927.

Lagerklint I. M. and Wright J. D. (1999) Late glacial warming prior to Heinrich event 1: The influence of ice rafting and large ice sheets on the timing of initial warming. *Geology* **27**, 1099-1102.

Landais A., Chappellaz J., Delmotte M., Jouzel J., Blunier T., Bourg C., Caillon N., Cherrier S., Malaizé B., Masson-Delmotte V., Raynaud D., Schwander J. and Steffensen J. P. (2003) A tentative reconstruction of the last interglacial and glacial inception in Greenland based on new gas measurements in the Greenland Ice Core Project (GRIP) ice core. *Journal of Geophysical Research* **108**.

Landais A. (2004) Variabilité climatique rapide en Atlantique Nord: l'apport des isotopes de l'air piégé dans la glace du Groenland. In *Laboratoire des Sciences du Climat et de l'Environnement*, Vol. PhD dissertation, p. 281. Université Paris VI, Gif-Sur-Yvette.

Landais A., Barnola J. M., Kawamura K., Caillon N., Delmotte M., Ommen T. V., Dreyfus G., Jouzel J., Masson-Delmotte V., Minster B., Freitag J., Leuenberger M., Schwander J., Huber C., Etheridge D. and Morgan V. (2006) Firn-air $\delta^{15}N$ in modern polar sites and glacial-interglacial ice: a model-data mismatch during glacial periods in Antarctica? *Quaternary Science Reviews* **25**, 49-62.

Lavric J. V., Chappellaz J., Barnola J.-M., Lourantou A., Raynaud D. and Michel E. (in prep.) Measurement of carbon isotope composition and mixing ratio of CO_2 in ancient air from ice core samples.

Lea D. W., Pak D. K. and Spero H. J. (2000) Climate Impact of Late Quaternary Equatorial Pacific Sea Surface Temperature Variations. *Science* **289**, 1719-1724.

Lea D. W., Martin P. A., Pak D. K. and Spero H. J. (2002) Reconstructing a 350 ky history of sea level using planktonic Mg/Ca and oxygen isotope records from a Cocos Ridge core. *Quaternary Science Reviews* **21**, 283-293.

Lea D. W., Pak D. K., Peterson L. C. and Hughen K. A. (2003) Synchroneity of Tropical and High-Latitude Atlantic Temperatures over the Last Glacial Termination. *Science* **301**, 1361 - 1364.

Leckrone K. J. and Hayes J. M. (1998) Water-Induced Errors in Continuous-Flow Carbon Isotope Ratio Mass Spectrometry. *Analytical Chemistry* **70**, 2737 -2744.

Legrand M., Hammer C., Angelis M. D., Savarino J., Delmas R., Clausen H. and Johnsen S. J. (1997) Sulfur-containing species (methanesulfonate and SO4) over the last climatic cycle in the Greenland Ice Core Project (central Greenland) ice core. *Journal of Geophysical Research* **102**, 26663-26680.

Leuenberger M., Siegenthaler U. and Langway C. C. (1992) Carbon isotope composition of atmospheric CO_2 during the last ice age from an Antarctic ice core. *Nature* **357**, 488-490.

Leuenberger M., Nyfeler P., Moret H. P., Sturm P. and Huber C. (2000) A new gas inlet system for an isotope ratio mass spectrometer improves reproducibility. *Rapid Communications in Mass Spectrometry* **14**, 1543-1551.

Leuenberger M. and Lang P. M. (2002) *Thermal diffusion: an important aspect in studies of static air columns such as firn air, sand dunes and soil air*. International Atomic Energy Agency, Vienna.

Leuenberger M. C., Eyer M., Nyfeler P., Stauffer B. and Stocker T. F. (2003) High-resolution $\delta^{13}C$ measurements on ancient air extracted from less than 10 cm^3 of ice. *Tellus B* **55**, 138-144.

Levi C., Labeyrie L., Bassinot F., Guichard F., Cortijo E., Waelbroeck C., Caillon N., Duprat J., Garidel-Thoron T. d. and Elderfield H. (2007) Low-latitude hydrological cycle and rapid climate changes during the last deglaciation. *Geochemistry Geophysics Geosystems* **8**.

Lichtfouse E. (2000) Compound-specific isotope analysis. Application to archaelogy, biomedical sciences, biosynthesis, environment, extraterrestrial chemistry, food science, forensic science, humic substances, microbiology, organic geochemistry, soil science and sport. *Rapid Communications in Mass Spectrometry* **14**, 1337-1344.

Lisiecki L. E. and Raymo. M. E. (2005) A Pliocene-Pleistocene stack of 57 globally distributed benthic $\delta^{18}O$ records. *Paleoceanography* **20**.

Lloyd J. and Farquhar G. D. (1996) The CO_2 dependence of photosynthesis, plant growth responses to elevated atmospheric CO_2 concentrations and their interaction with soil nutrient status. I. General principles and forest ecosystems. *Functional Ecology* **10**, 4-32.

Lototskaya A., Ziveri P., Ganssen G. M. and Hinte J. E. v. (1998) Calcareous nannofloral response to Termination II at 45°N, 25°W (northeast Atlantic). *Marine Micropaleontology* **34**, 47-70.

Lototskaya A. and Ganssen G. M. (1999) The structure of Termination II (penultimate deglaciation and Eemian) in the North Atlantic. *Quaternary Science Reviews* **18**, 1641-1654.

Loulergue L. (2007) Contraintes chronologiques et biogéochimiques grâce au méthane dans la glace naturelle: une application aux forages du projet EPICA. In *Laboratoire de Glaciologie et Géophysique de l'Environnement*, p. 211. Université Joseph Fourrier Grenoble I, St Martin d'Hères.

Loulergue L., Parrenin F., Blunier T., Barnola J.-M., Spahni R., Schilt A., Raisbeck G. and Chappellaz J. (2007) New constraints on the gas age-ice age difference along the EPICA ice cores, 0–50 kyr. *Clim. Past* **3**, 527-540.

Loulergue L., Schilt A., Spahni R., Masson-Delmotte V., Blunier T., Lemieux B., Barnola J.-M., Raynaud D., Stocker T. F. and Chappellaz J. (2008) Orbital and millennial-scale features of atmospheric CH_4 over the past 800,000 years. *Nature* **453**, 383-386.

Lowenstein T. K. and Demicco R. V. (2006) Elevated Eocene Atmospheric CO_2 and Its Subsequent Decline. *Science* **313**, 1928.

Lüthi D., Floch M. L., Bereiter B., Blunier T., Barnola J.-M., Siegenthaler U., Raynaud D., Jouzel J., Fischer H., Kawamura K. and Stocker T. F. (2008) High-resolution carbon dioxide concentration record 650,000–800,000 years before present. *Nature* **453**, 379-382.

Lynch-Stieglitz J., Adkins J. F., Curry W. B., Dokken T., Hall I. R., Herguera J. C., Hirschi J. J.-M., Ivanova E. V., Kissel C., Marchal O., Marchitto T. M., McCave I. N., McManus J. F., Mulitza S., Ninnemann U., Peeters F., Yu E.-F. and Zahn R. (2007) Atlantic Meridional Overturning Circulation During the Last Glacial Maximum. *Science* **316**, 66-69.

MacAyeal D. R. (1993) Binge/purge oscillations of the Laurentide ice sheet as a cause of the North Atlantic's Heinrich events. *Paleoceanography* **8**, 775-784.

Marchitto J. T. M., Curry W. B. and Oppo D. W. (1998) Millennial-scale changes in North Atlantic circulation since the last glaciation. *Nature* **393**, 557-561.

Marchitto T. M., Lynch-Stieglitz J. and Hemming S. R. (2005) Deep Pacific $CaCO_3$ compensation and glacial–interglacial atmospheric CO_2. *Earth and Planetary Science Letters* **231**, 317-336.

Marchitto T. M., Lehman S. J., Ortiz J. D., Flückiger J. and Geen A. v. (2007) Marine Radiocarbon Evidence for the Mechanism of Deglacial Atmospheric CO_2 Rise. *Science* **316**, 1456 - 1459.

Martin J. H., Gordon R. M. and Fitzwater S. E. (1990) Iron in Antarctic waters. *Nature* **345**, 156 - 158.

Masson-Delmotte V., Jouzel J., Landais A., Stievenard M., Johnsen S. J., White J. W. C., Werner M., Sveinbjornsdottir A. and Fuhrer K. (2005) GRIP Deuterium Excess Reveals Rapid and Orbital-Scale Changes in Greenland Moisture Origin. *Science* **309**, 118 - 121.

Matsumoto K., Hashioka T. and Yamanaka Y. (2007) Effect of temperature-dependent organic carbon decay on atmospheric pCO_2. *Journal of Geophysical Research* **112**.

McCabe A. M. and Clark P. U. (1998) Ice-sheet variability around the North Atlantic Ocean during the last deglaciation. *Nature* **392**, 373-377.

McKinney C. R., McCrea J. M., Epstein S., Allen H. A. and Urey H. C. (1950) Improvements in Mass Spectrometers for the Measurement of Small Differences in Isotope Abundance Ratios. *Rev. Sci. Instrum.* **21**.

McManus J. F., Bond G. C., Broecker W. S., Johnsen S., Labeyrie L. and Higgins S. (1994) High-resolution climate records from the North Atlantic during the last interglacial. *Nature* **371**

McManus J. F., Francois R., Gherardi J.-M., Keigwin L. D. and Brown-Leger S. (2004) Collapse and rapid resumption of Atlantic meridional circulation linked to deglacial climate changes. *Nature* **428**, 834-837

Mendeleev D. (1889) The Periodic Law of the Chemical Elements. *Journal of the Chemical Society (London)* **55**, 634-656.

Merlivat L. and Jouzel J. (1979) Global Climatic Interpretation of the Deuterium-Oxygen 18 Relationship for Precipitation. *Journal of Geophysical Research* **84**, 5029-5033.

Miller S. L. (1969) Clathrate Hydrates of Air in Antarctic Ice. *Science* **165**, 489 - 490.

Molyneux E. G., Hall I. R., Zahn R. and Diz P. (2007) Deep water variability on the southern Agulhas Plateau: Interhemispheric links over the past 170 ka. *Paleoceanography* **22**.

Monnin E., Indermühle A., Dällenbach A., Flückiger J., Stauffer B., Stocker T. F., Raynaud D. and Barnola J.-M. (2001) Atmospheric CO_2 Concentrations over the Last Glacial Termination. *Science* **291**, 112 - 114.

Monnin E., Steig E., Siegenthaler U., Kawamura K., Schwander J., Stauffer B., Stocker T., Morse D., Barnola J.-M., Bellier B., Raynaud D. and Fischer H. (2004) Evidence for substantial accumulation rate variability in Antarctica during the Holocene, through synchronization of CO_2 in the Taylor Dome, Dome C and DML ice cores *Earth and Planetary Science Letters* **224**, 45-54.

Mook W. G. (1986) ^{13}C in atmospheric CO_2. *Netherlands Journal of Sea Research* **20**, 211-223.

Mook W. G. (2000) *Environmental isotopes in the hydrological cycle: principles and applications*, Paris.

Moor E. and Stauffer B. (1984) A new dry extraction system for gases in ice. *Journal of Glaciology* **30**, 358-361.

Morales-Maqueda M. A. and Rahmstorf S. (2002) Did Antarctic sea-ice expansion cause glacial CO_2 decline? *Geophysical Research Letters* **29**.

Mudelsee M. (2001) The phase relations among atmospheric CO_2 content, temperature and global ice volume over the past 420 ka. *Quaternary Science Reviews* **20**, 583-589.

Müller U. C. and Kukla G. J. (2004) North Atlantic Current and European environments during the declining stage of the last interglacial. *Geology* **32**, 1009-1012.

Mulvaney R., Oerter H., Peel D. A., Graf W., Arrowsmith C., Pasteur E. C., Knight B., Littot G. C. and Miners W. D. (2002) 1000 year ice-core records from Berkner Island, Antarctica. *Annals of Glaciology* **35**, 45-51.

Munhoven G. and François L. M. (1996) Glacial-interglacial variability of atmospheric CO_2 due to changing continental silicate rock weathering: A model study. *Journal of Geophysical Research* **101**, 21,423–21,437.

Neftel A., Oeschger H., Schwander J., Stauffer B. and Zumbrunn R. (1982) Ice core sample measurements give atmospheric CO_2 content during the past 40,000 yr. *Nature* **295**, 220-223.

Neflel A., Oeschger H., Schwander J. and Stauffer B. (1983) Carbon dioxide concentration in bubbles of natural cold ice. *J. Phys. Chem.* **87**, 4116-4120.

Neftel A., Oeschger H., Staffelbach T. and Stauffer B. (1988) CO_2 record in the Byrd ice core 50,000–5,000 years BP. *Nature* **331**, 609-611.

Ninnemann U. S. and Charles C. D. (1997) Regional Differences in Quaternary Subantarctic Nutrient Cycling: Link to Intermediate and Deep Water Ventilation. *Paleoceanography* **12**, 560–567.

Norris R. D. and Röhl U. (1999) Carbon cycling and chronology of climate warming during the Palaeocene/Eocene transition. *Nature* **401**, 775-778.

Oeschger H., Stauffer B., Neftel A., Schwander J. and Zumbrunn R. (1983) Atmospheric CO_2 content in the past deduced from ice core analyses. *Annals of Glaciology* **3**, 227-232.

O'Leary M. (1981) Carbon isotope fractionation in plants. *Phytochemistry* **20**, 553-567.

Oppo D. W., Horowitz M. and Lehman S. J. (1997) Marine core evidence for reduced deep water production during Termination II followed by a relatively stable substage 5e (Eemian). *Paleoceanography* **12**, 51-64.

Oppo D. W., Keigwin L. D., McManus J. F. and Cullen J. L. (2001) Persistent suborbital climate variability in marine isotope stage 5 and Termination II. *Paleoceanography* **16**, 280-292.

Pagani M., Arthur M. A. and Freeman K. H. (1999) Miocene Evolution of Atmospheric Carbon Dioxide. *Paleoceanography* **14**, 273-292.

Pahnke K. and Zahn R. (2005) Southern Hemisphere Water Mass Conversion Linked with North Atlantic Climate Variability. *Science* **307**, 1741-1746.

Paillard D., Labeyrie L. and Yiou P. (1996) Macintosh program performs time-series analysis. *EOS, transactions American Geophysical Union* **77**.

Parrenin F. and Paillard D. (2003) Amplitude and phase of glacial cycles from a conceptual model. *Earth and Planetary Science Letters* **214**, 243-250.

Parrenin F., Rémy F., Ritz C., Siegert M. J. and Jouzel J. (2004) New modeling of the Vostok ice flow line and implication for the glaciological chronology of the Vostok ice core. *Journal of Geophysical Research* **109**.

Parrenin F., Barnola J.-M., Beer J., Blunier T., Castellano E., Chappellaz J., Dreyfus G., Fischer H., Fujita S., Jouzel J., Kawamura K., Lemieux-Dudon B., Loulergue L., Masson-Delmotte V., Narcisi B., Petit J.-R., Raisbeck G., Raynaud D., Ruth U., Schwander J., Severi M., Spahni R., Steffensen J. P., Svensson A., Udisti R., Waelbroeck C. and Wolff E. (2007) The EDC3 chronology for the EPICA Dome C ice core. *Clim. Past* **3**, 485-497.

Pauer F., Kipfstuhl J. and Kuhs W. F. (1995) Raman Spectroscopic Study on the Nitrogen/Oxygen Ratio in Natural Ice Clathrates in the GRIP Ice Core. *Geophysical Research Letters* **22**, 969–971.

Pauer F., Kipfstuhl J. and Kuhs W. F. (1997) Raman spectroscopic and statistical studies on natural clathrates from the Greenland Ice Core Project ice core, and neutron diffraction studies on synthetic nitrogen clathrates. *Journal of Geophysical Research* **102**, 26519-26526.

Pépin L. (2000) Variation de la teneur en CO_2 de l'atmosphère au cours des 4 derniers cycles glaciaire-interglaciaires, à partir de l'analyse de la carotte de Vostok (Antarctique). Implication sur l'évolution du climat et du cycle du carbone. In *Laboratoire de Glaciologie et Géophysique de l'Environnement*, p. 203. Université Joseph Fourrier Grenoble I, St Martin d'Hères.

Pépin L., Raynaud D., Barnola J.-M. and Loutre M. F. (2001) Hemispheric roles of climate forcings during glacial-interglacial transitions as deduced from the Vostok record and LLN-2D model experiments. *Journal of Geophysical Research* **106**, 31885–31892.

Peterson B. J. and Fry B. (1987) Stable Isotopes in Ecosystem Studies. *Annual Review of Ecology and Systematics* **18**, 293-320.

Petit J. R., Jouzel J., Raynaud D., Barkov N. I., Barnola J.-M., Basile I., Bender M., Chappellaz J., Davis M., Delaygue G., Delmotte M., Kotlyakov V. M., Legrand M., Lipenkov V. Y., Lorius C., Pépin L., Ritz C., Saltzman E. and Stievenard M. (1999) Climate and atmospheric history of the past 420,000 years from the Vostok ice core, Antarctica. *Nature* **399**, 429-436.

Pimienta P. (1987) Etude du comportement mécanique des glaces polycristallines aux faibles contraintes; applications aux glaces des calottes polaires. In *Laboratoire de Glaciologie et Géophysique de l'Environnement*. Université Joseph Fourrier Grenoble I, St Martin d'Hères.

Prentice K. C. and Fung I. Y. (1990) The sensitivity of terrestrial carbon storage to climate change. *Nature* **346**, 48-51.

Price P. B. (1995) Kinetics of Conversion of Air Bubbles to Air Hydrate Crystals in Antarctic Ice. *Science* **267**, 1802-1804.

Rahmstorf S. (2002) Ocean circulation and climate during the past 120,000 years. *Nature* **419**, 207-214.

Raymo M. E., Grant B., Horowitz M. and Rau G. H. (1996) Mid-Pliocene warmth: stronger greenhouse and stronger conveyor. *Marine Micropaleontology* **27**, 313-326.

Raynaud D. and Whillans I. M. (1982) Air content of the Byrd core and past changes in the West Antarctic ice sheet. *Annals of Glaciology* **3**, 269-273.

Raynaud D., Lipenkov V., Lemieux-Dudon B., Duval P., Loutre M.-F. and Lhomme N. (2007) The local insolation signature of air content in Antarctic ice. A new step toward an absolute dating of ice records. *Earth and Planetary Science Letters* **261**, 337–349.

Ribas-Carbo M., Still C. and Berry J. (2002) Automated system for simultaneous analysis of ^{13}C, ^{18}O and CO_2 concentrations in small air samples. *Rapid Communications in Mass Spectrometry* **16**, 339-345.

Rickaby R. E. M. and Elderfield H. (2005) Evidence from the high-latitude North Atlantic for variations in Antarctic Intermediate water flow during the last deglaciation. *Geochemistry Geophysics Geosystems* **6**, Q05001.

Ridgwell A. J. (2001) Glacial-interglacial perturbations in the global carbon cycle. In *School of Environmental Sciences*, p. 146. University of East Anglia, Norwich.

Ridgwell A. J., Watson A. J. and Archer D. A. (2002) Modelling the response of the oceanic Si inventory to perturbation, and consequences for atmospheric CO_2. *Global Biogeochemical Cycles* **16**.

Ridgwell A. J. (2003) An end to the "rain ratio" reign? *Geochemistry Geophysics Geosystems* **4**.

Ridgwell A. and Zeebe R. E. (2005) The role of the global carbonate cycle in the regulation and evolution of the Earth system. *Earth and Planetary Science Letters* **234**, 299-315.

Ridgwell A. and Kohfeld K. E. (2006) Glacial-interglacial changes in atmospheric CO_2 - A smörgåsbord of marine biogeochemical forcings. *Geochimica et Cosmochimica Acta* **70**, A534-A534.

Robinson S. G., Maslin M. A. and McCave I. N. (1995) Magnetic Susceptibility Variations in Upper Pleistocene Deep-Sea Sediments of the NE Atlantic: Implications for Ice Rafting and Paleocirculation at the Last Glacial Maximum. *Paleoceanography* **10**, 221-250.

Robinson L. F., Adkins J. F., Keigwin L. D., Southon J., Fernandez D. P., Wang S.-L. and Scheirer D. S. (2005) Radiocarbon variability in the western North Atlantic during the last deglaciation. *Science* **310**.

Roche D. (2006) Isotopes de l'oxygène en paléoclimatologie : l'apport d'un modèle de complexité intermédiaire. In *Laboratoire des Sciences du Climat de l'Environnement*, p. 221. Université Paris VI, Saclay, Paris.

Rommelaere V., Arnaud L. and Barnola J.-M. (1997) Reconstructing recent atmospheric trace gas concentrations from polar firn and bubbly ice data by inverse methods. *Journal of Geophysical Research-Atmospheres* **102**.

Röthlisberger R., Bigler M., Wolff E. W., Joos F., Monnin E. and Hutterli M. A. (2004) Ice core evidence for the extent of past atmospheric CO_2 change due to iron fertilization. *Geophysical Research Letters* **31**.

Ruddiman W. F., Molfino B., Esmay A. and Pokras E. (1980) Evidence bearing on the mechanism of rapid deglaciation. *Climatic Change* **3**, 65-87.

Ruddiman W. F. (2003) The Anthropogenic Greenhouse Era Began Thousands of Years Ago. *Climatic Change* **61**, 261-293.

Rühlemann C., Mulitza S., Müller P. J., Wefer G. and Zahn R. (1999) Warming of the tropical Atlantic Ocean and slowdown of thermohaline circulation during the last deglaciation. *Nature* **402**, 511-514.

Salamatin A. N., Lipenkov V. Y. and Hondoh T. (2003) Air-hydrate crystal growth in polar ice. *Journal of Crystal Growth* **247**, 412-426.

Sánchez-Goñi M. F., Loutre M. F., Crucifix M., Peyron O., Santos L., Duprat J., Malaizé B., Turon J.-L. and Peypouquet J.-P. (2005) Increasing vegetation and climate gradient in Western Europe over the Last Glacial Inception (122–110 ka): data-model comparison. *Earth and Planetary Science Letters* **231**, 111-130.

Santrock J., Studley S. and Hayes J. (1985) Isotopic analyses based on the mass spectrum of carbon dioxide. *Analytical Chemistry* **57**, 1444-1448.

Sanyal A., Hemming N. G., Hanson G. N. and Broecker W. S. (1995) Evidence for a higher pH in the glacial ocean from boron isotopes in foraminifera. *Nature* **373**, 234 - 236

Sarmiento J. L. and Toggweiler J. R. (1984) A new model for the role of the oceans in determining atmospheric pCO_2. *Nature* **308**, 621-624.

Sarnthein M. and Tiedemann R. (1990) Younger Dryas-style cooling events at glacial terminations I-VI at ODP Site 658: Associated benthic $\delta^{13}C$ anomalies constrain meltwater hypothesis. *Paleoceanography* **5**, 1041-1055.

Schmitt J. (2006) A sublimation technique for high-precision $\delta^{13}C$ on CO_2 and CO_2 mixing ratio from air trapped in deep ice cores. In *Alfred-Wegener-Institut für Polar und Meeresforschung*, p. 118. Universität Bremen, Bremerhaven.

Schmitt J., Fischer H. and Behrens M. (2007) What caused the CO_2 fluctuations of the pre-industrial Holocene? Clues from the carbon isotopic composition of CO_2 from the EDML ice core. In *European Geosciences Union, General Assembly*, Austria, Vienna.

Schmitt J. and Fischer H. (to be submitted) A sublimation technique for high-precision $\delta^{13}C$ on CO_2 and CO_2 mixing ratio from air trapped in deep ice cores. *submitted to Rapid Communications in Mass Spectrometry*

Schmittner A., Brook E. and Ahn J. (2007) Impact of the Ocean's Overturning Circulation on Atmospheric CO_2. *AGU Geophysical Monograph Series* **173**, 209-246.

Schnyder H., Schäufele R. and Wenzel R. (2004) Mobile, outdoor continuous-flow isotope-ratio mass spectrometer system for automated high-frequency ^{13}C- and ^{18}O-CO_2 analysis for Keeling plot applications. *Rapid Communications in Mass Spectrometry* **18**, 3068-3074.

Schulz M., Seidov D., Sarnthein M. and Stattegger K. (2001) Modeling ocean-atmosphere carbon budgets during the Last Glacial Maximum - Heinrich 1 Meltwater Event - Bølling transition. *Int. Journ. Earth Sciences* **90**, 412-425.

Schulz K. G. and Zeebe R. E. (2006) Pleistocene glacial terminations triggered by synchronous changes in Southern and Northern Hemisphere insolation: The insolation canon hypothesis. *Earth and Planetary Science Letters* **249**, 326-336.

Schwander J., Stauffer B. and Sigg A. (1988) Air mixing in firn and the age of the air at pore close-off. *Annals of Glaciology* **10**, 141-145.

Schwander J., Barnola J.-M., Andrié C., Leuenberger M., Ludin A., Raynaud D. and Stauffer B. (1993) The Age of the Air in the Firn and the Ice at Summit, Greenland. *Journal of Geophysical Research* **98**, 2831–2838.

Schwander J. (1996) *Gas diffusion in firn*. E.W. Wolff, and R.C. Bales, Berlin Heidelberg.

Seidenkrantz M.-S., Bornmalm L., Johnsen S. J., Knudsen K. L., Kuijpers A., Lauritzen S.-E., Leroy S. A. G., Mergeal I., Schweger C. and Vliet-Lanoë B. V. (1996) Two-step deglaciation at the oxygen isotope stage 6/5E transition: The Zeifen-Kattegat climate oscillation. *Quaternary Science Reviews* **15**, 63-75.

Severinghaus J. P., Sowers T., Brook E. J., Alley R. B. and Bender M. L. (1998) Timing of abrupt climate change at the end of the Younger Dryas interval from thermally fractionated gases in polar ice *Nature* **391**, 141-146.

Severinghaus J. P. and Brook E. J. (1999) Abrupt Climate Change at the End of the Last Glacial Period Inferred from Trapped Air in Polar Ice. *Science* **286**, 930 - 934.

Severinghaus J. P., Grachev A. and Battle M. (2001) Thermal fractionation of air in polar firn by seasonal temperature gradients. *Geochemistry, Geophysics, Geosystems* **2**, 1048.

Severinghaus J. P., Grachev A., Luz B. and Caillon N. (2003) A method for precise measurement of argon 40/36 and krypton/argon ratios in trapped air in polar ice with applications to past firn

thickness and abrupt climate change in Greenland and at Siple Dome, Antarctica. *Geochimica et Cosmochimica Acta* **67**, 325-343.

Severinghaus J. P. and Battle M. O. (2006) Fractionation of gases in polar ice during bubble close-off: New constraints from firn air Ne, Kr and Xe observations. *Earth and Planetary Science Letters* **244**, 474-500.

Shackleton N. J. (1967) Oxygen isotope analyses and Pleistocene temperatures re-assessed. *Nature* **215**, 15-17.

Shackleton N. J. and Opdyke N. D. (1973) Oxygen isotope and paleomagnetic stratigraphy of equatorial Pacific core V28-238: oxygen isotope temperatures and ice volumes on 10^6 yr scale. *Quaternary Research* **3**, 39-55.

Shoji H. and Langway C. C. (1982) Air hydrate inclusions in fresh ice core. *Nature* **298**, 548-550.

Siani G., Paterne M., Michel E., Sulpizio R., Sbrana A., Arnold M. and Haddad G. (2001) Mediterranean Sea Surface Radiocarbon Reservoir Age Changes Since the Last Glacial Maximum. *Science* **294**, 1917 - 1920.

Siegenthaler U. and Wenk T. (1984) Rapid atmospheric CO_2 variations and ocean circulation. *Nature* **308**, 624-626.

Siegenthaler U., Friedli H., Loetschewr H., Moor E., Neftel A., Oeschger H. and Stauffer B. (1988) Stable-isotope ratios and concentration of CO_2 in air from polar ice cores. *Annals of Glaciology* **10**, 151-156.

Siegenthaler U., Monnin E., Kawamura K., Spahni R., Schwander J., Stauffer B., Stocker T. F., Barnola J.-M. and Fischer H. (2005) Supporting evidence from the EPICA Dronning Maud Land ice core for atmospheric CO_2 changes during the past millennium. *TellusB* **57**.

Sigman D. M., McCorkle D. C. and Martin W. R. (1998) The Calcite Lysocline as a Constraint on Glacial/Interglacial Low-Latitude Production Changes. *Global Biogeochemical Cycles* **12**, 409–427.

Sigman D. and Boyle E. (2000) Glacial/interglacial variations in atmospheric carbon dioxide. *Nature* **407**, 859-869.

Sima A., Paul A. and Schulz M. (2004) The Younger Dryas-an intrinsic feature of late Pleistocene climate change at millennial timescales. *Earth and Planetary Science Letters* **222**, 741-750.

Skinner L. C. and Shackleton N. J. (2006) Deconstructing Terminations I and II: revisiting the glacioeustatic paradigm based on deep-water temperature estimates. *Quaternary Science Reviews* **25**, 3312-3321.

Smith H. J., Wahlen M., Mastroianni D. and Taylor K. C. (1997a) The CO_2 Concentration of Air Trapped in GISP2 Ice from the Last Glacial Maximum-Holocene Transition. *Geophysical Research Letters* **24**, 1-4.

Smith H. J., Wahlen M., Mastroianni D., Taylor K. and Mayewski P. (1997b) The CO_2 concentration of air trapped in GISP2 ice formed during periods of rapid climate change. *Journal of Geophysical Research-Oceans* **112**.

Smith H. J., Fischer H., Wahlen M., Mastroianni D. and Deck B. (1999) Dual modes of the carbon cycle since the Last Glacial Maximum. *Nature* **400**, 248-250.

Souchez R., Lemmens M. and Chappellaz J. (1995) Flow-Induced mixing in the GRIP basal ice deduced from the CO_2 and CH_4 Records. *Geophysical Research Letters* **22**, 41-44.

Sowers T., Bender M. and Raynaud D. (1989) Elemental and isotopic composition of occluded O_2 and N_2 in polar ice. *Journal of Geophysical Research* **94**, 5137–5150.

Sowers T., Bender M., Raynaud D., Korotkevich Y. S. and Orchardo J. (1991) The $\delta^{18}O$ of atmospheric O_2 from air inclusions in the Vostok ice core : timing of CO_2 and ice volume changes during the penultimate deglaciation. *Paleoceanography* **6**, 679-696.

Sowers T., Bender M., Raynaud D. and Korotkevich Y. S. (1992) $\delta^{15}N$ of N_2 in Air Trapped in Polar Ice: a Tracer of Gas Transport in the Firn and a Possible Constraint on Ice Age-Gas Age Differences. *Journal of Geophysical Research* **97**, 15683–15697.

Sowers T., Brook E., Etheridge D., Blunier T., Fuchs A., Leuenberger M., Chappellaz J., Barnola J.-M., Wahlen M., Deck B. and Weyhenmeyer C. (1997) An interlaboratory comparison of techniques for extracting and analyzing trapped gases in ice cores. *Journal of Geophysical Research* **102**, 26527-26538.

Spero H. J. and Lea D. W. (2002) The Cause of Carbon Isotope Minimum Events on Glacial Terminations. *Science* **296**, 522-525.

Spötl C., Mangini A., Frank N., Eichstädter R. and Burns S. J. (2002) Start of the last interglacial period at 135 ka: Evidence from a high Alpine speleothem. *Geology* **30**, 815-818.

Stauffer B., Fischer G., Neftel A. and Oeschger H. (1985) Increase of Atmospheric Methane Recorded in Antarctic Ice Core. *Science* **229**, 1386-1388.

Stauffer B., Lochbronner E., Oeschger H. and Schwander J. (1988) Methane concentration in the glacial atmosphere was only half that of the pre-industrial Holocene. *Nature* **332**, 812-814.

Stauffer B., Blunier T., A.Dällenbach, Indermühle A., Schwander J., Stocker T. F., Tschumi J., Chappellaz J., Raynaud D., Hammer C. U. and Clausen H. B. (1998) Atmospheric CO_2 concentration and millennial-scale climate change during the last glacial period. *Nature* **392**, 59-62.

Stauffer B., Fluckiger J., Monnin E., Schwander J., Barnola J.-M. and Chappellaz J. (2002) Atmospheric CO_2, CH_4 and N_2O records over the past 60 000 years based on the comparison of different polar ice cores. *Annals of Glaciology* **35**, 202-208.

Stauffer B., Flückiger J., Wolff E. W. and Barnes P. (2004) The EPICA deep ice cores: First results and perspectives. *Annals of Glaciology* **39**, 93-100.

Stephens B. B. and Keeling R. F. (2000) The influence of Antarctic sea ice on glacial-interglacial CO_2 variations. *Nature* **404**, 171-174.

Taylor K. C., Hammer C. U., Alley R. B., Clausen H. B., Dahl-Jensen D., Gow A. J., Gundestrup N. S., Kipfstuhl J., Moore J. C. and Waddington E. D. (1993) Electrical conductivity measurements from the GISP2 and GRIP Greenland ice cores. *Nature* **366**, 549-552.

Teller J. T., Leverington D. W. and Mann J. D. (2002) Freshwater outbursts to the oceans from glacial Lake Agassiz and their role in climate change during the last deglaciation. *Quaternary Science Reviews* **21**, 879-887.

Thiemens M. H. and Heidenreich J. E. (1983) The Mass-Independent Fractionation of Oxygen: A Novel Isotope Effect and Its Possible Cosmochemical Implications. *Science* **219**, 1073 - 1075.

Thorsteinsson T. (1996) Textures and fabrics in the GRIP ice core, in relation to climate history and ice deformation. In *Reports on Polar Research*, Vol. 205, p. 146. Alfred Wegener Institute for Polar and Marine Research, Bremerhaven.

Toggweiler J. R. and Samuels B. (1995) Effect of Sea Ice on the Salinity of Antarctic Bottom Waters. *Journal of Physical Oceanography* **25**, 1980–1997.

Toggweiler J. R. (1999) Variation of atmospheric CO_2 by ventilation of the ocean's deepest water. *Paleoceanography* **14**, 571-588.

Trudinger C. M., Enting L. G., Etheridge D. M., Francey R. J., Levchenko V. A., Steele L. P., Raynaud D. and Arnaud L. (1997) Modelling air movement and bubble trapping in firn. *Journal of Geophysical Research* **102**, 6747–6763.

Tschumi J. and Stauffer B. (2000) Reconstructing past atmospheric CO_2 concentration based on ice-core analyses: open questions due to in situ production of CO_2 in the ice. *Journal of Glaciology* **46**, 45-53.

Uchida T., Hondoh T., Mae S., Duval P. and Lipenkov V. Y. (1994) Effects of temperature and pressure on the transformation rate from air bubbles to air-hydrate crystals in ice sheets. *Annals of Glaciology* **20**, 143-147.

Urey H. C. (1947) The thermodynamic properties of isotopic substances. *J. Chem. Soc.*, 562-581.

Van Breugel Y., Schouten S., Tsikos H., Erba E., Price G. D. and Damsté J. S. S. (2007) Synchronous negative carbon isotope shifts in marine and terrestrial biomarkers at the onset of the early Aptian oceanic anoxic event 1a: Evidence for the release of ^{13}C-depleted carbon into the atmosphere. *Paleoceanography* **22**.

Van Kreveld S. A., Knappertsbusch M., Ottens J., Ganssen G. M. and Hinte J. E. v. (1996) Biogenic carbonate and ice-rafted debris (Heinrich layer) accumulation in deep-sea sediments from a Northeast Atlantic piston core. *Marine Geology* **131**, 21-46.

Vecsei A. and Berger W. H. (2004) Increase of atmospheric CO_2 during deglaciation: Constraints on the coral reef hypothesis from patterns of deposition. *Global Biogeochemical Cycles* **18**.

Veizer J., Ala D., Azmy K., Bruckschen P., Buhl D., Bruhn F., Carden G. A. F., Diener A., Ebneth S., Godderis Y., Jasper T., Korte C., Pawellek F., Podlaha O. G. and Strauss H. (1999) $^{87}Sr/^{86}Sr$, $\delta^{13}C$ and $\delta^{18}O$ evolution of Phanerozoic seawater. *Chemical Geology* **161**, 59-88.

Visser K., Thunell R. and Stott L. (2003) Magnitude and timing of temperature change in the Indo-Pacific warm pool during deglaciation. *Nature* **421**, 152-155.

Waelbroeck C., Levi C., Duplessy J. C., Labeyrie L. and Michel E. (2006) Distant origin of circulation changes in the Indian Ocean during the last deglaciation. *Earth and Planetary Science Letters* **243**, 244-251.

Waelbroeck C., Frank N., Jouzel J., Parrenin F., Masson-Delmotte V. and Genty D. (2008) Transferring radiometric dating of the last interglacial sea level high stand to marine and ice core records. *Earth and Planetary Science Letters* **265**, 183-194.

Wahlen M., Allen D., Deck B. and Herchenroder A. (1991) Initial measurements of CO_2 concentrations (1530 to 1940 AD) in air occluded in the GISP2 ice core from central Greenland. *Geophysical Research Letters* **18**, 1457-1460.

Watson A. J. and Garabato A. C. N. (2006) The role of Southern Ocean mixing and upwelling in glacial-interglacial atmospheric CO_2 change. *Tellus B* **58**, 73-87.

Weaver A. J., Saenko O. A., Clark P. U. and Mitrovica J. X. (2003) Meltwater Pulse 1A from Antarctica as a Trigger of the Bølling-Allerød Warm Interval. *Science* **299**, 1709 - 1713.

Weiss R. F., Mühle J., Salameh P. K. and Harth C. M. (in press) Nitrogen trifluoride in the global atmosphere. *Geophysical Research Letters.*

Werner R. A. and Brand W. A. (2001) Referencing strategies and techniques in stable isotope ratio analysis. *Rapid Communications in Mass Spectrometry* **15**, 501-519.

Werner R. A., Rothe M. and Brand W. A. (2001) Extraction of CO_2 from air samples for isotopic analysis and limits to ultra high precision ^{18}O determination in CO_2 gas. *Rapid Communications in Mass Spectrometry* **15**, 2152-2167.

Wilson A. T. and Long A. (1997) New approaches to CO_2 analysis in polar ice cores. *Journal of Geophysical Research* **102**, 26601-26606.

Wolff E. W., Miners W. D., Moore J. C. and Paren J. G. (1997) Factors controlling the Electrical Conductivity of ice from the polar regions - a summary. *J. Phys. Chem.* **101B**, 6090-6094.

Wolff E. W., Fischer H., Fundel F., Ruth U., Twarloh B., Littot G. C., Mulvaney R., Röthlisberger R., de Angelis M., Boutron C. F., Hansson M., Jonsell U., Hutterli M. A., Lambert F., Kaufmann P., Stauffer B., Stocker T. F., Steffensen J. P., Bigler M., Siggaard-Andersen M. L., Udisti R., Becagli S., Castellano E., Severi M., Wagenbach D., Barbante C., Gabrielli P. and Gaspari V. (2006) Southern Ocean sea-ice extent, productivity and iron flux over the past eight glacial cycles. *Nature* **440**, 491-496.

Yakir D. and Sternberg L. d. S. L. (2000) The use of stable isotopes to study ecosystem gas exchange. *Oecologia* **123**, 297-311.

Yeom C. K., Lee S. H. and Lee J. M. (2000) Study of transport of pure and mixed CO_2/N_2 gases through polymeric membranes. *Journal of Applied Polymer Science* **78**, 179 - 189.

Yiou F., Raisbeck G. M., Baumgartner S., Beer J., Hammer C., Johnsen S., Jouzel J., Kubik P. W., Lestringuez J., Stiévenard M., Suter M. and Yiou P. (1997) Beryllium 10 in the Greenland Ice Core Project ice core at Summit, Greenland. *Journal of Geophysical Research* **102**, 26783-26794.

Yokoyama Y., Lambeck K., Deckker P. D., Johnston P. and Fifield L. K. (2000) Timing of the Last Glacial Maximum from observed sea-level minima. *Nature* **406**, 713-716.

Young E. D., Galy A. and Nagahara H. (2002) Kinetic and equilibrium mass-dependent isotope fractionation laws in nature and their geochemical and cosmochemical significance. *Geochimica et Cosmochimica Acta* **66**, 1095-1104.

Yu E.-F., François R. and Bacon M. (1996) Similar rates of modern and last-glacial ocean thermohaline circulation inferred from radiochemical data. *Nature* **379**, 689-694.

Yuan D., Cheng H., Edwards R. L., Dykoski C. A., Kelly M. J., Zhang M., Qing J., Lin Y., Wang Y., Wu J., Dorale J. A., An Z. and Cai Y. (2004) Timing, Duration, and Transitions of the Last Interglacial Asian Monsoon. *Science* **304**, 575 - 578.

Zachos J., Pagani M., Sloan L., Thomas E. and Billups K. (2001) Trends, Rhythms, and Aberrations in Global Climate 65 Ma to Present. *Science* **292**, 686-693.

Zachos J. C., Dickens G. R. and Zeebe R. E. (2008) An early Cenozoic perspective on greenhouse warming and carbon-cycle dynamics. *Nature* **451**, 279-283.

Zeebe R. E. and Wolf-Gladrow D. (2003) *CO_2 in seawater: equilibrium, kinetics, isotopes*, Elsevier: Amsterdam, The Netherlands.

Zemmelink H. J., Delille B., Tison J. L., Hintsa E. J., Houghton L. and Dacey J. W. H. (2006) CO_2 deposition over the multi-year ice of the western Weddell Sea. *Geophysical Research Letters* **33**.

Zumbrunn R., Neftel A. and Oeschger H. (1982) CO_2 measurements on 1-cm^3 ice samples with an IR Laser Spectrometer (IRLS) combined with a new dry extraction device *Earth and Planetary Science Letters* **60**, 318-324.

Annex I. TI and TII calendar

Below the extended laboratory calendar is exposed for both deglaciations, from which one can conclude on the main sampling differences.

	Monday	Tuesday	Wednesday	Thursday	Friday
2006					
April	3	4	5 748_1 +777_1	6 748_2	7 777_2 + 820_1
	10 820_2	11 1011 + 912	12 686_1 + 981	13 716_1 + 761_1	14 716_2 + 795_1
	17	18 795_2	19 785_1	20 861	21 989
	24	25	26 785_2	27	28 761_2
May	1	2	3 751	4 631_1	5 686_2
	8	9	10 631_2	11 405	12 726
	15	16 325	17 647	18 366	19 969
	29	30	31 843		
June				1 941	2 957
	5 855	6 1052	7	8 966	9 846
	12 895	13 816_1	14 988	15 917	16 976
	19	20 936	21 926	22 886	23 837
	26	27 946	28 1006	29 998	30 826
July	3	4 807	5 1015	6	7
	10 865_1	11 815_1	12	13 875	14
	17	18 835_1	19 825_1	20 888	21 835_2
	24	25 865_2	26 815_2	27 869	28 879
August	7 829	8 907	9	10 825_2	11
October					27 919
	30 816_2				
November					3 710

***Table I-1**: Analytical calendar of TI period, measured in 2006.*

The number of daily measurements was doubled in 2008, compared to TI period, corresponding to the analysis of AIM12 and TII. This allowed us to fully cover the penultimate deglaciation despite the limited time period separating the analysis period and the defense day.

	Monday	Tuesday	Wednesday	Thursday	Friday
2006					
October	9 3401	10 3406	11 3396		
2008					
February	18	19 $3036_{1;2}$+3046_1	20 3046_2+3056	21 3066+3076	22 3086
	25 3096_1	26 3106 + 3116_1	27 3126 + 3166	28 BFI	29 $1327_{2\#BK}$+1566_2
March	3 3201+$1345_{2\#BK}$	4 3226+3246	5 1456_2+$1360_{2\#BK}$	6 3256_1+3276	7 3256_2+$1354_{2\#BK}$
	10 $1338_{1\#BK}$+3286	11 3296+3301	12 3136+3146	13 $DC04W_1$+1486_1	14 $DC04W_{2;3}$
	17 3156+$DC04W_4$	18 1516_1+3266_1	19 3251+3236 +3266_2	20 3151_1+3101 +3051	21 1528_1+$DC04W_5$
	25 1516_2 +1466_1	26 1495_1 +1546_1	27 1551_1 +1528_2	28 1486_2	29
April	21	22 stand. gas	23 $DC04W_6$	24 1566_2 +1536_2	25 1551_2 +1506_2
	28 1476_2 +1495_2	29 $1338_{2\#BK}$	30 $1345_{3\#BK}$		
May	5 3151_2+3172	6 3192+3212	7 3222+3182	8 3096_2+3116_2	9 3312

***Table I-2**: Analytical calendar of TII period, mainly measured in 2008 (3 samples of MIS 6 had been analyzed in 2006). Since the sampling period 2008 was partitioned between two experimentalists, in blue we specify the measurements accomplished by H. Schaefer in-between our own TII measurements*

Annex II. Data

Below two series of tables are exposed: those including the ensemble of analyzed data, outliers included, and tables of gravitationally corrected data. For both cases magenta colours represent rejected values, mainly with the method exposed in annex IV.

II.1. TI all expansions (uncorrected)

no bag	depth (high)	date	CO_2 uncorr.	$\delta^{13}C$ uncorr.	$\delta^{18}O$ uncorr.	EDC3_gas_a
631	346,50	04/05/2006	259,31	-6,094	-40,987	8756
			258,41	-6,327	-40,557	
			261,04	-6,398	-39,630	
631	346,50	10/05/2006	264,91	-6,106	-40,466	8756
			263,43	-5,992	-40,520	
			262,37	-6,186	-39,864	
647	355,30	17/05/2006	259,41	-6,204	-39,328	9072
			260,17	-6,339	-38,942	
			261,25	-6,023	-38,145	
686	376,75	12/04/2006	267,55	-6,147	-42,808	9793
			267,54	-6,289	-42,385	
			270,65	-6,471	-41,175	
686	376,75	05/05/2006	260,51	-6,298	-42,646	9793
			260,17	-6,273	-42,171	
710	389,95	03/11/2006	268,55	-6,267	-43,006	10278
			271,66	-6,179	-42,545	
			271,72	-6,123	-41,719	
716	393,25	13/04/2006	268,19	-6,341	-43,286	10401
			269,77	-6,130	-42,969	
			270,29	-6,026	-41,768	
716	393,25	14/04/2006	270,29	-6,336	-42,877	10401
			273,21	-6,586	-42,544	
			278,08	-6,871	-41,460	
726	398,75	12/05/2006	264,35	-6,303	-42,780	10604
			265,07	-6,298	-42,654	
			265,09	-6,348	-41,512	
748	410,85	05/04/2006	263,39	-6,184	-40,213	11064
			252,21	-6,555	-40,318	
748	410,85	06/04/2006	263,68	-6,129	-40,753	11064
			264,15	-6,410	-40,388	
			265,32	-6,358	-39,397	
751	412,50	03/05/2006	263,87	-6,348	-43,279	11124
			265,31	-6,292	-42,700	
			266,56	-6,339	-41,515	
761	418,00	13/04/2006	262,57	-6,180	-39,451	11324
			262,29	-6,249	-39,267	
			265,12	-6,013	-38,023	

761	418,00	28/04/2006	258,76	-6,283	-39,982	11324
			261,31	-6,160	-39,615	
			261,65	-6,426	-38,670	
777	426,80	05/04/2006	251,27	-6,417	-41,207	11612
			248,33	-6,711	-40,212	
			252,12	-7,021	-39,438	
777	426,80	07/04/2006	251,78	-6,459	-42,204	11612
			255,48	-6,454	-42,170	
			255,49	-6,520	-40,884	
785	431,20	19/04/2006	247,66	-6,295	-43,482	11796
			248,46	-6,309	-42,982	
			249,84	-6,689	-42,191	
785	431,20	26/04/2006	250,42	-6,509	-42,920	11796
			252,99	-6,440	-42,502	
			253,57	-6,452	-41,335	
795	436,70	14/04/2006	246,54	-6,567	-41,763	12029
			247,65	-6,319	-41,669	
			253,32	-6,834	-40,113	
795	436,70	18/04/2006	246,72	-6,480	-42,348	12029
			246,28	-6,653	-41,984	
			246,51	-6,444	-40,940	
807	443,30	04/07/2006	240,15	-6,272	-41,602	12346
			240,67	-6,322	-41,419	
			242,28	-6,120	-40,414	
815	447,70	11/07/2006	236,45	-6,045	-42,686	12585
			237,23	-6,201	-42,253	
			239,34	-6,328	-41,327	
815	447,70	26/07/2006	238,04	-6,371	-42,198	12585
			238,09	-6,558	-41,968	
			240,59	-6,224	-41,311	
816	448,25	13/06/2006	237,94	-5,642	-43,474	12614
			237,85	-5,975	-43,314	
			240,13	-5,991	-42,280	
816	448,25	29/10/2006	235,01	-6,070	-43,474	12614
			233,63	-5,931	-43,344	
			237,06	-5,740	-42,160	
820	450,45	07/04/2006	245,34	-6,706	-40,605	12734
			241,32	-6,355	-41,288	
			239,88	-6,549	-40,399	
820	450,45	10/04/2006	238,55	-6,139	-41,916	12734
			239,06	-6,032	-41,615	
			238,41	-6,084	-40,101	
825	453,20	19/07/2006	242,60	-6,668	-41,203	12889
			243,25	-6,785	-40,219	
			245,65	-6,649	-38,980	
825	453,20	10/08/2006	239,47	-6,214	-41,891	12889
			239,98	-6,352	-41,388	
			239,74	-6,466	-40,345	
826	453,75	30/06/2006	238,49	-6,226	-43,139	12918
			240,14	-6,418	-42,849	
			241,50	-6,537	-41,563	
829	455,40	07/08/2006	238,40	-6,251	-42,098	13000
			241,08	-6,363	-41,861	
			241,54	-6,188	-40,863	
835	458,70	18/07/2006	241,68	-6,136	-43,857	13174

			244,93	-6,176	-43,415	
835	458,70	21/07/2006	243,26	-6,064	-44,101	13174
			244,37	-6,062	-43,826	
			243,60	-6,207	-43,002	
837	459,80	23/06/2006	237,88	-6,176	-43,061	13235
			241,52	-6,030	-42,395	
			238,90	-6,164	-41,598	
843	463,10	31/05/2006	242,18	-5,732	-43,765	13415
			247,16	-6,100	-40,849	
846	464,75	09/06/2006	239,70	-5,903	-44,963	13511
			239,51	-6,067	-44,684	
			240,96	-6,210	-43,418	
855	469,70	05/06/2006	239,52	-6,039	-45,871	13780
			241,17	-6,339	-45,421	
			241,53	-6,324	-44,289	
861	473,00	20/04/2006	240,92	-6,284	-45,132	13945
			240,08	-6,435	-44,891	
			241,44	-6,378	-43,435	
865	475,20	10/07/2006	240,61	-6,450	-43,249	14066
			242,72	-6,583	-42,983	
			244,90	-6,543	-41,941	
865	475,20	25/07/2006	238,42	-6,231	-43,745	14066
			238,59	-6,343	-43,471	
			239,06	-6,378	-42,431	
869	477,40	27/07/2006	233,00	-6,364	-43,968	14176
			233,70	-6,090	-43,670	
			236,03	-6,460	-42,784	
875	480,70	13/07/2006	230,13	-6,303	-44,606	14357
			230,83	-6,277	-44,391	
			230,58	-6,497	-43,372	
879	482,90	28/07/2006	228,84	-6,259	-46,536	14473
			229,87	-6,288	-45,971	
			232,93	-6,420	-45,035	
886	486,75	22/06/2006	228,67	-6,270	-45,175	14697
			229,53	-6,524	-44,940	
			231,39	-6,319	-43,730	
888	487,85	20/07/2006	229,00	-6,281	-43,466	14756
			230,33	-6,145	-43,105	
			233,17	-6,241	-42,147	
895	491,70	12/06/2006	226,63	-6,617	-44,327	14978
			227,46	-6,474	-43,524	
			229,98	-6,679	-42,714	
907	498,30	08/08/2006	218,84	-6,378	-46,372	15369
			220,57	-6,522	-45,901	
			222,34	-6,519	-44,847	
912	501,05	11/04/2006	222,38	-6,182	-44,217	15541
			222,83	-6,071	-43,715	
			222,61	-6,414	-42,525	
917	503,80	15/06/2006	219,21	-6,214	-45,523	15718
			219,23	-6,406	-44,996	
			221,80	-6,845	-43,835	
919	504,9	27/10/2006	212,34	-6,567	-45,800	15781
			213,47	-6,638	-45,673	
			216,99	-6,445	-44,505	
926	508,75	21/06/2006	213,55	-6,114	-41,959	16041

			211,44	-6,431	-41,022	
			206,76	-6,550	-39,296	
936	514,25	20/06/2006	202,15	-6,163	-45,343	16413
			202,79	-6,540	-44,892	
			203,50	-6,069	-43,532	
941	517,00	01/06/2006	196,66	-6,154	-45,409	16611
			197,10	-6,229	-45,189	
			197,48	-6,093	-43,692	
946	519,75	27/06/2006	193,84	-6,242	-44,240	16834
			196,74	-6,032	-43,764	
			197,77	-6,510	-41,849	
957	525,80	02/06/2006	188,68	-6,082	-45,029	17335
			190,29	-6,126	-44,602	
			190,49	-6,073	-43,472	
966	530,75	08/06/2006	187,11	-5,984	-45,924	17766
			188,31	-6,147	-45,490	
			190,94	-6,069	-44,317	
969	532,40	19/05/2006	189,16	-5,901	-45,338	17906
			189,80	-6,123	-44,994	
			189,73	-5,991	-43,825	
976	536,25	16/06/2006	188,65	-6,242	-45,189	18239
			190,25	-6,194	-44,566	
			188,91	-6,380	-43,408	
981	539,00	12/04/2006	191,07	-6,086	-44,836	18502
			189,30	-6,065	-44,313	
			190,18	-5,970	-43,087	
988	542,85	14/06/2006	189,77	-6,032	-45,467	18824
			191,35	-5,907	-44,762	
			193,74	-6,033	-43,626	
989	543,40	21/04/2006	152,93	-6,186	-45,026	18873
			153,89	-6,381	-44,624	
998	548,35	29/06/2006	189,14	-6,286	-46,047	19300
			189,97	-6,240	-45,601	
			192,15	-6,518	-43,959	
1006	552,75	28/06/2006	190,57	-5,921	-44,583	19703
			189,78	-6,247	-44,312	
			193,26	-6,007	-42,867	
1011	555,50	11/04/2006	190,11	-6,412	-45,652	19950
			190,49	-6,367	-45,459	
			191,36	-6,346	-43,589	
1015	557,70	05/07/2006	191,09	-5,887	-45,420	20149
			189,92	-5,883	-45,037	
			190,94	-6,329	-43,983	
1052	578,05	06/06/2006	186,87	-6,093	-44,739	22009
			185,78	-6,287	-44,348	
			189,16	-6,372	-42,970	

Cases with magenta were rejected (*cf. annex IV*)

II.2. TI Corrected data

no bag	depth (high)	date	CO_2 corr	$\delta^{13}C$ corr	$\delta^{18}O$ corr	EDC3_gas_a
631	346,50	04/05/2006	257,35	-6,593	-41,984	8756
			256,46	-6,826	-41,554	
			259,06	-6,897	-40,627	
631	346,50	10/05/2006	262,90	-6,604	-41,463	8756
			261,44	-6,491	-41,517	
			260,38	-6,684	-40,861	
647	355,30	17/05/2006	257,44	-6,705	-40,329	9072
			258,19	-6,839	-39,943	
			259,26	-6,523	-39,146	
686	376,75	12/04/2006	265,56	-6,637	-43,787	9793
			265,54	-6,779	-43,364	
			268,64	-6,960	-42,154	
686	376,75	05/05/2006	258,57	-6,787	-43,625	9793
			258,23	-6,763	-43,150	
710	389,95	03/11/2006	266,45	-6,781	-44,035	10278
			269,54	-6,693	-43,574	
			269,59	-6,637	-42,747	
716	393,25	13/04/2006	266,12	-6,848	-44,301	10401
			267,69	-6,638	-43,985	
			268,20	-6,534	-42,783	
716	393,25	14/04/2006	268,21	-6,844	-43,893	10401
			271,10	-7,093	-43,559	
			275,93	-7,379	-42,475	
726	398,75	12/05/2006	262,31	-6,809	-43,792	10604
			263,03	-6,804	-43,666	
			263,05	-6,854	-42,523	
748	410,85	05/04/2006	261,39	-6,684	-41,214	11064
			250,30	-7,056	-41,319	
748	410,85	06/04/2006	261,67	-6,629	-41,754	11064
			262,14	-6,911	-41,389	
			263,30	-6,858	-40,398	
751	412,50	03/05/2006	261,86	-6,848	-44,278	11124
			263,30	-6,791	-43,698	
			264,53	-6,838	-42,514	
761	418,00	13/04/2006	260,44	-6,713	-40,517	11324
			260,17	-6,782	-40,333	
			262,97	-6,546	-39,089	
761	418,00	28/04/2006	256,66	-6,816	-41,048	11324
			259,20	-6,693	-40,681	
			259,53	-6,959	-39,736	
777	426,80	05/04/2006	249,30	-6,933	-42,240	11612
			246,38	-7,228	-41,245	
			250,14	-7,537	-40,471	
777	426,80	07/04/2006	249,80	-6,975	-43,237	11612
			253,47	-6,970	-43,202	
			253,49	-7,036	-41,917	
785	431,20	19/04/2006	245,81	-6,786	-44,464	11796
			246,60	-6,800	-43,964	
			247,97	-7,180	-43,172	
785	431,20	26/04/2006	248,56	-7,000	-43,902	11796
			251,10	-6,931	-43,484	
			251,67	-6,943	-42,317	
795	436,70	14/04/2006	244,71	-7,055	-42,739	12029

			245,81	-6,806	-42,645	
	436,70		251,44	-7,321	-41,088	
795	436,70		244,90	-6,968	-43,323	12029
		18/04/2006	244,46	-7,141	-42,960	
			244,68	-6,931	-41,915	
807	443,30		238,41	-6,749	-42,555	12346
		04/07/2006	238,93	-6,799	-42,372	
			240,52	-6,597	-41,367	
815	447,70		234,80	-6,504	-43,603	12585
		11/07/2006	235,58	-6,659	-43,170	
			237,67	-6,786	-42,243	
815	447,70		236,38	-6,829	-43,115	12585
		26/07/2006	236,43	-7,017	-42,885	
			238,91	-6,682	-42,228	
816	448,25		236,26	-6,106	-44,402	12614
		13/06/2006	236,17	-6,438	-44,241	
			238,43	-6,454	-43,207	
816	448,25		233,35	-6,533	-44,401	12614
		29/10/2006	231,98	-6,395	-44,271	
			235,39	-6,204	-43,087	
820	450,45		243,60	-7,173	-41,539	12734
		07/04/2006	239,61	-6,822	-42,222	
			238,18	-7,016	-41,333	
820	450,45		236,86	-6,606	-42,850	12734
		10/04/2006	237,36	-6,499	-42,548	
			236,72	-6,551	-41,034	
825	453,20		240,87	-7,137	-42,142	12889
		19/07/2006	241,51	-7,254	-41,158	
			243,90	-7,118	-39,919	
825	453,20		237,76	-6,684	-42,831	12889
		10/08/2006	238,27	-6,822	-42,328	
			238,03	-6,935	-41,284	
826	453,75		236,81	-6,689	-44,066	12918
		30/06/2006	238,45	-6,881	-43,775	
			239,80	-7,000	-42,490	
829	455,40		236,69	-6,724	-43,044	13000
		07/08/2006	239,35	-6,836	-42,807	
			239,81	-6,661	-41,809	
835	458,70	18/07/2006	239,92	-6,615	-44,815	13174
			243,15	-6,655	-44,373	
835	458,70		241,49	-6,543	-45,059	13174
		21/07/2006	242,59	-6,541	-44,783	
			241,82	-6,686	-43,959	
837	459,80		236,18	-6,648	-44,005	13235
		23/06/2006	239,79	-6,502	-43,339	
			237,19	-6,636	-42,542	
843	463,10	31/05/2006	240,46	-6,199	-44,699	13415
			245,40	-6,567	-41,783	
846	464,75		237,96	-6,379	-45,913	13511
		09/06/2006	237,78	-6,542	-45,634	
			239,22	-6,685	-44,368	
855	469,70		237,79	-6,516	-46,824	13780
		05/06/2006	239,42	-6,816	-46,375	
			239,78	-6,801	-45,242	
861	473,00		239,14	-6,770	-46,103	13945
		20/04/2006	238,31	-6,920	-45,862	
			239,66	-6,863	-44,405	
865	475,20	10/07/2006	238,88	-6,922	-44,192	14066

			240,98	-7,054	-43,926	
			243,14	-7,014	-42,883	
865	475,20		236,71	-6,702	-44,688	14066
		25/07/2006	236,88	-6,815	-44,414	
			237,35	-6,849	-43,374	
869	477,40		231,29	-6,847	-44,933	14176
		27/07/2006	231,99	-6,573	-44,635	
			234,30	-6,942	-43,749	
875	480,70		228,41	-6,794	-45,589	14357
		13/07/2006	229,10	-6,768	-45,374	
			228,85	-6,988	-44,354	
879	482,90		227,19	-6,733	-47,482	14473
		28/07/2006	228,22	-6,761	-46,918	
			231,25	-6,893	-45,982	
886	486,75		227,05	-6,735	-46,106	14697
		22/06/2006	227,91	-6,990	-45,871	
			229,75	-6,785	-44,661	
888	487,85		227,33	-6,759	-44,422	14756
		20/07/2006	228,65	-6,623	-44,061	
			231,48	-6,719	-43,103	
895	491,70		225,03	-7,081	-45,255	14978
		12/06/2006	225,86	-6,938	-44,453	
			228,36	-7,143	-43,642	
907	498,30		217,32	-6,835	-47,285	15369
		08/08/2006	219,04	-6,979	-46,814	
			220,79	-6,975	-45,760	
912	501,05		220,86	-6,633	-45,121	15541
		11/04/2006	221,30	-6,523	-44,618	
			221,08	-6,865	-43,428	
917	503,80		217,68	-6,674	-46,441	15718
		15/06/2006	217,70	-6,865	-45,915	
			220,25	-7,304	-44,753	
919	504,9		210,88	-7,019	-46,705	15781
		27/10/2006	212,00	-7,091	-46,579	
			215,50	-6,897	-45,410	
926	508,75		212,10	-6,562	-42,853	16041
		21/06/2006	210,00	-6,878	-41,917	
			205,36	-6,997	-40,190	
936	514,25		200,80	-6,602	-46,221	16413
		20/06/2006	201,44	-6,978	-45,770	
			202,14	-6,508	-44,410	
941	517,00		195,38	-6,583	-46,267	16611
		01/06/2006	195,81	-6,658	-46,047	
			196,20	-6,522	-44,550	
946	519,75		192,61	-6,663	-45,081	16834
		27/06/2006	195,48	-6,452	-44,605	
			196,51	-6,930	-42,689	
957	525,80		187,49	-6,496	-45,857	17335
		02/06/2006	189,09	-6,540	-45,429	
			189,30	-6,486	-44,299	
966	530,75		185,94	-6,394	-46,744	17766
		08/06/2006	187,14	-6,557	-46,311	
			189,75	-6,479	-45,137	
969	532,40		187,97	-6,315	-46,167	17906
		19/05/2006	188,61	-6,537	-45,823	
			188,54	-6,405	-44,653	
976	536,25	16/06/2006	187,47	-6,653	-46,012	18239
			189,06	-6,605	-45,389	

			187,72	-6,791	-44,231	
981	539,00	12/04/2006	189,89	-6,494	-45,651	18502
			188,13	-6,472	-45,128	
			189,00	-6,377	-43,902	
988	542,85	14/06/2006	188,60	-6,437	-46,278	18824
			190,17	-6,313	-45,572	
			192,55	-6,438	-44,436	
989	543,40	21/04/2006	151,96	-6,602	-45,857	18873
			152,92	-6,797	-45,456	
998	548,35	29/06/2006	187,96	-6,696	-46,867	19300
			188,79	-6,650	-46,421	
			190,96	-6,928	-44,779	
1006	552,75	28/06/2006	189,36	-6,339	-45,419	19703
			188,57	-6,664	-45,147	
			192,03	-6,425	-43,702	
1011	555,50	11/04/2006	188,93	-6,821	-46,470	19950
			189,31	-6,776	-46,277	
			190,17	-6,755	-44,407	
1015	557,70	05/07/2006	189,89	-6,298	-46,242	20149
			188,74	-6,295	-45,860	
			189,74	-6,740	-44,806	
1052	578,05	06/06/2006	185,70	-6,504	-45,560	22009
			184,62	-6,697	-45,169	
			187,98	-6,782	-43,791	

II.3. TII all data (uncorrected)

no bag	depth (high)	dates for T2	CO_2 vs. amplitude	$\delta^{13}C$ uncorr.	$\delta^{18}O$ uncorr.	EDC3_gas_a
3036	1669,25	19/02/2008	268,62	-5,861	-37,294	125223
3036	1669,25	19/02/2008	279,96	-6,182	-36,474	125223
			279,79	-5,962	-36,249	
			272,95	-5,619	-35,672	
3046	1674,75	19/02/2008	271,55	-6,446	-37,073	125633
			277,20	-6,236	-36,606	
			278,39	-6,443	-35,918	
3046	1674,75	20/02/2008	278,23	-6,265	-36,346	125633
			281,21	-5,961	-36,082	
			282,68	-6,017	-35,310	
3051	1677,5	20/03/2008	272,51	-6,107	-37,217	125859
			273,82	-6,074	-37,187	
			275,06	-6,154	-36,643	
3056	1680,25	20/02/2008	273,42	-6,339	-36,940	126058
			275,35	-6,376	-36,911	
			275,61	-6,703	-36,577	
3066	1685,75	21/02/2008	272,99	-6,519	-35,915	126484
			276,13	-6,533	-35,997	

			277,68	-6,423	-35,237	
3076	1691,25		266,97	-6,194	-35,177	126856
		21/02/2008	268,98	-6,020	-34,953	
			272,14	-6,210	-34,493	
3086	1696,75		272,34	-6,208	-36,084	127225
		22/02/2008	274,48	-6,194	-35,752	
			274,49	-6,129	-34,957	
3096	1702,25		295,70	-7,440	-32,144	127595
		25/02/2008	297,26	-7,552	-31,919	
			328,88	-9,020	-27,234	
3096	1702,25		275,36	-5,999	-36,051	127595
		08/05/2008	277,43	-6,041	-36,066	
			278,42	-6,136	-35,816	
3101	1705		275,47	-6,082	-36,845	127773
		20/03/2008	280,85	-6,366	-36,696	
			282,41	-6,261	-36,228	
3106	1707,75		284,55	-6,868	-35,082	127934
		26/02/2008	289,21	-6,827	-34,700	
			296,02	-7,253	-33,325	
3116	1713,25		299,47	-7,390	-34,215	128268
		26/02/2008	299,74	-7,322	-33,873	
			303,77	-7,389	-33,324	
3116	1713,25		287,42	-6,190	-37,572	128268
		08/05/2008	292,72	-6,843	-35,450	
			310,43	-7,792	-32,350	
3126	1718,75		292,14	-6,591	-33,896	128585
		27/02/2008	294,60	-6,748	-33,450	
			292,06	-6,745	-32,180	
3136	1724,25		270,38	-6,316	-38,344	128920
		12/03/2008	271,53	-6,282	-38,239	
			273,07	-6,357	-37,654	
3146	1729,75		264,46	-6,010	-37,840	129273
		12/03/2008	265,84	-5,986	-37,746	
			270,74	-6,156	-37,476	
3151	1732,5		270,50	-6,944	-36,454	129446
		20/03/2008	281,04	-7,375	-35,225	
			294,20	-7,700	-33,038	
3151	1732,5		262,24	-6,431	-39,446	129446
		05/05/2008	265,14	-6,502	-39,253	
			265,29	-6,506	-38,570	
3156	1735,25		264,48	-6,129	-39,054	129628
		17/03/2008	266,44	-6,156	-38,993	
			265,99	-6,247	-38,485	
3166	1740,75		255,50	-6,413	-39,307	130008
		27/02/2008	261,52	-6,681	-38,794	
			266,24	-6,646	-34,981	
3172	1744,05		256,67	-6,580	-40,182	130236
		05/05/2008	257,82	-6,692	-40,085	
			260,28	-6,682	-39,336	
3182	1749,55		249,85	-6,347	-41,564	130678
		07/05/2008	252,43	-6,420	-41,446	
			255,55	-6,541	-40,978	
3192	1755,05		243,92	-6,316	-42,713	131153
		06/05/2008	246,25	-6,209	-42,761	
			245,31	-6,661	-41,995	
3201	1760	03/03/2008	240,99	-6,474	-41,570	131621
			240,34	-6,618	-41,517	

			237,88	-6,294	-40,740	
3212	1766,05	06/05/2008	232,80	-6,279	-43,148	132267
			233,15	-6,448	-43,026	
			233,18	-6,560	-42,119	
3222	1771,55	07/05/2008	226,31	-6,648	-44,173	132954
			226,22	-6,745	-44,159	
			228,13	-6,560	-43,206	
3226	1773,75	04/03/2008	221,60	-6,638	-43,000	133238
			223,21	-6,528	-43,086	
			224,53	-6,726	-42,083	
3236	1779,25	19/03/2008	209,60	-6,467	-42,744	133981
			211,83	-6,375	-42,627	
			214,45	-6,625	-41,660	
3246	1784,75	04/03/2008	206,41	-6,080	-43,210	134805
			207,92	-6,234	-42,928	
			206,87	-6,166	-42,267	
3251	1787,5	19/03/2008	203,50	-6,210	-44,126	135295
			206,53	-6,205	-43,685	
			206,79	-6,246	-42,668	
3256	1790,25	06/03/2008	199,89		-43,288	135791
			199,24		-43,349	
			203,64		-42,159	
3256	1790,25	07/03/2008	199,57	-6,443	-43,509	135791
			201,22	-6,562	-43,267	
			200,19	-6,495	-42,397	
3266	1795,75	18/03/2008	193,88	-6,545	-41,137	136803
			195,51	-6,408	-41,401	
			199,15	-6,156	-41,169	
3266	1795,75	19/03/2008	208,72	-7,409	-38,525	136803
			232,37	-8,391	-34,149	
3276	1801,25	06/03/2008	195,85	-6,260	-43,970	137817
			199,78	-6,596	-43,885	
			198,53	-6,305	-42,871	
3286	1806,75	10/03/2008	190,03	-6,237	-44,414	138872
			192,62	-6,455	-43,859	
			194,20	-6,298	-43,325	
3296	1812,25	11/03/2008	185,66	-6,183	-43,325	139966
			188,27	-6,427	-43,275	
			188,78	-6,367	-42,532	
3301	1815	11/03/2008	180,74	-6,211	-43,027	140514
			186,14	-6,476	-43,068	
			188,90	-6,283	-42,573	
			193,42	-6,339	-41,959	
3312	1821,05	09/05/2008	193,03	-6,301	-43,114	141740
			195,64	-6,396	-42,754	
			199,17	-6,702	-41,187	
3396	1867,25	11/10/2006	200,92	-6,747	-44,130	150636
			201,81	-6,789	-44,005	
			203,08	-6,497	-43,395	
3401	1870	09/10/2006	202,32	-6,836	-42,740	151179
			203,95	-6,744	-42,671	
			206,65	-6,715	-41,851	
3406	1872,75	10/10/2006	196,93	-6,384	-43,563	151703
			198,87	-6,418	-43,573	
			199,62	-6,547	-42,951	

II.4. TII corrected data

no bag	depth (high)	dates for T2	CO_2 corr	$\delta^{13}C$ corr	$\delta^{18}O$ corr	EDC3_gas_a
3036	1669,25	19/02/2008	266,48	-6,385	-38,343	125223
3036	1669,25	19/02/2008	277,73	-6,707	-37,523	125223
			277,56	-6,486	-37,298	
			270,77	-6,144	-36,721	
3046	1674,75	19/02/2008	269,42	-6,964	-38,108	125633
			275,02	-6,754	-37,641	
			276,20	-6,961	-36,953	
3046	1674,75	20/02/2008	276,05	-6,783	-37,381	125633
			279,00	-6,479	-37,117	
			280,46	-6,534	-36,345	
3051	1677,5	20/03/2008	270,40	-6,616	-38,235	125859
			271,70	-6,584	-38,206	
			272,93	-6,663	-37,661	
3056	1680,25	20/02/2008	271,23	-6,866	-37,995	126058
			273,15	-6,903	-37,966	
			273,40	-7,230	-37,632	
3066	1685,75	21/02/2008	270,88	-7,026	-36,931	126484
			274,00	-7,041	-37,012	
			275,54	-6,931	-36,252	
3076	1691,25	21/02/2008	264,82	-6,724	-36,237	126856
			266,81	-6,550	-36,012	
			269,95	-6,740	-35,552	
3086	1696,75	22/02/2008	270,14	-6,738	-37,144	127225
			272,27	-6,724	-36,812	
			272,28	-6,659	-36,016	
3096	1702,25	25/02/2008	293,28	-7,977	-33,220	127595
			294,83	-8,090	-32,994	
			326,20	-9,558	-28,309	
3096	1702,25	08/05/2008	273,11	-6,536	-37,126	127595
			275,17	-6,579	-37,142	
			276,15	-6,674	-36,892	
3101	1705	20/03/2008	273,19	-6,625	-37,932	127773
			278,53	-6,910	-37,783	
			280,07	-6,805	-37,315	
3106	1707,75	26/02/2008	282,15	-7,423	-36,192	127934
			286,77	-7,382	-35,811	
			293,52	-7,808	-34,435	
3116	1713,25	26/02/2008	296,93	-7,948	-35,332	128268
			297,20	-7,881	-34,990	
			301,19	-7,947	-34,441	
3116	1713,25	08/05/2008	284,98	-6,748	-38,689	128268
			290,23	-7,401	-36,567	
			307,80	-8,350	-33,466	
3126	1718,75	27/02/2008	289,70	-7,139	-34,992	128585
			292,15	-7,296	-34,547	
			289,62	-7,293	-33,276	
3136	1724,25	12/03/2008	268,09	-6,871	-39,454	128920
			269,24	-6,837	-39,350	
			270,76	-6,912	-38,764	
3146	1729,75	12/03/2008	262,24	-6,562	-38,943	129273

			263,61	-6,537	-38,850	
			268,47	-6,707	-38,579	
3151	1732,5	20/03/2008	268,24	-7,493	-37,551	129446
			278,70	-7,923	-36,323	
			291,74	-8,249	-34,136	
3151	1732,5	05/05/2008	260,05	-6,980	-40,544	129446
			262,92	-7,051	-40,350	
			263,08	-7,054	-39,668	
3156	1735,25	17/03/2008	262,27	-6,680	-40,157	129628
			264,21	-6,708	-40,095	
			263,76	-6,798	-39,588	
3166	1740,75	27/02/2008	253,38	-6,960	-40,400	130008
			259,35	-7,227	-39,887	
			264,03	-7,192	-36,074	
3172	1744,05	05/05/2008	254,58	-7,117	-41,255	130236
			255,71	-7,228	-41,159	
			258,16	-7,219	-40,409	
3182	1749,55	07/05/2008	247,85	-6,873	-42,614	130678
			250,41	-6,945	-42,497	
			253,51	-7,066	-42,028	
3192	1755,05	06/05/2008	242,02	-6,830	-43,742	131153
			244,32	-6,724	-43,789	
			243,39	-7,175	-43,023	
3201	1760	03/03/2008	239,14	-6,978	-42,578	131621
			238,50	-7,122	-42,525	
			236,06	-6,798	-41,748	
3212	1766,05	06/05/2008	231,05	-6,773	-44,136	132267
			231,40	-6,942	-44,014	
			231,43	-7,054	-43,106	
3222	1771,55	07/05/2008	224,68	-7,120	-45,117	132954
			224,60	-7,217	-45,103	
			226,49	-7,032	-44,150	
3226	1773,75	04/03/2008	220,03	-7,104	-43,933	133238
			221,62	-6,995	-44,020	
			222,94	-7,193	-43,016	
3236	1779,25	19/03/2008	208,14	-6,925	-43,660	133981
			210,36	-6,833	-43,544	
			212,96	-7,083	-42,576	
3246	1784,75	04/03/2008	205,01	-6,526	-44,101	134805
			206,52	-6,680	-43,820	
			205,47	-6,611	-43,158	
3251	1787,5	19/03/2008	202,18	-6,637	-44,979	135295
			205,19	-6,631	-44,538	
			205,45	-6,672	-43,521	
3256	1790,25	06/03/2008	198,60		-44,138	135791
			197,95		-44,198	
			202,33		-43,008	
3256	1790,25	07/03/2008	198,29	-6,867	-44,358	135791
			199,92	-6,987	-44,116	
			198,90	-6,920	-43,246	
3266	1795,75	18/03/2008	192,64	-6,967	-41,979	136803
			194,26	-6,829	-42,244	
3266	1795,75	19/03/2008	197,88	-6,577	-42,012	136803
			207,38	-7,831	-39,368	

			230,89	-8,812	-34,992	
3276	1801,25	06/03/2008	194,59	-6,682	-44,815	137817
			198,50	-7,019	-44,730	
			197,25	-6,727	-43,715	
3286	1806,75	10/03/2008	188,84	-6,647	-45,233	138872
			191,42	-6,865	-44,678	
			192,99	-6,708	-44,144	
3296	1812,25	11/03/2008	184,49	-6,598	-44,156	139966
			187,08	-6,843	-44,107	
			187,58	-6,783	-43,363	
3301	1815	11/03/2008	179,58	-6,633	-43,871	140514
			184,94	-6,898	-43,913	
			187,69	-6,705	-43,418	
			192,18	-6,762	-42,803	
3312	1821,05	09/05/2008	191,78	-6,729	-43,970	141740
			194,37	-6,824	-43,610	
			197,87	-7,130	-42,043	
3396	1867,25	11/10/2006	199,60	-7,182	-44,999	150636
			200,47	-7,223	-44,874	
			201,74	-6,932	-44,264	
3401	1870	09/10/2006	200,98	-7,271	-43,608	151179
			202,60	-7,178	-43,539	
			205,28	-7,149	-42,719	
3406	1872,75	10/10/2006	195,64	-6,814	-44,424	151703
			197,57	-6,849	-44,434	
			198,31	-6,978	-43,812	

Annex III. $\delta^{18}O\text{-}CO_2$

Oxygen equilibrates between CO_2 and H_2O. The same phenomenon is expected to occur between the atmospheric CO_2 found in air occluded in the ice, with the ice itself (being the solid form of water).

In the framework of the experimental protocol presented in *Ch. III*, analysis of the stable oxygen isotopic ratio of CO_2, $\delta^{18}O\text{-}CO_2$, was accomplished in parallel with the $\delta^{13}CO_2$ measurements. This signal is superposed with measurements of $\delta^{18}O$ in EDC ice, and presented individually for TI and TII in fig. III-1 and III-2, respectively.

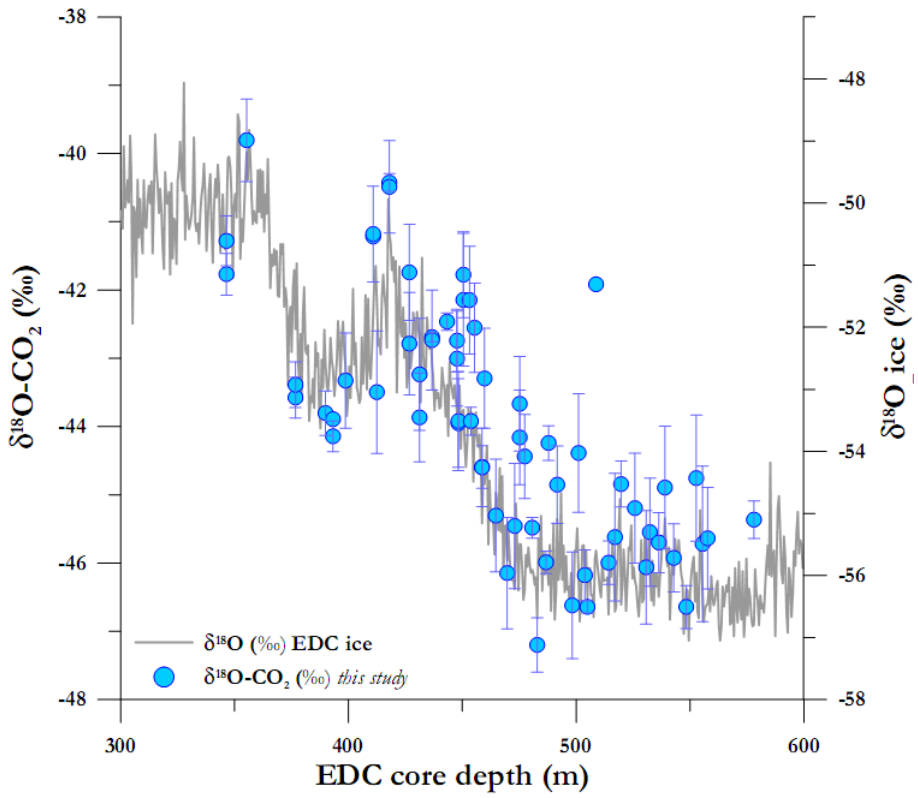

Fig. III-1: *mean $\delta^{18}O\text{-}CO_2$ points with error bars from the ensemble of samples covering TI period, superposed with data of $\delta^{18}O$ from EDC ice (V. Masson-Delmotte, personal communication)*

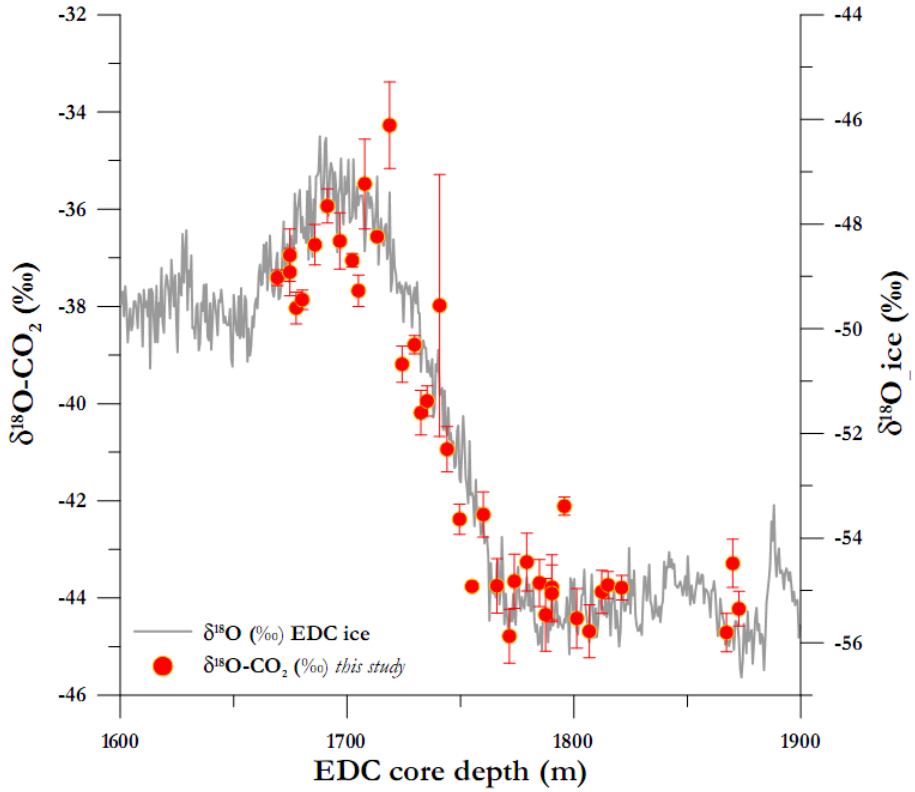

Fig. III-2: *mean $\delta^{18}O$-CO_2 points with error bars from the ensemble of samples covering TII period, superposed with data of $\delta^{18}O$ from EDC ice (V. Masson-Delmotte, personal communication)*

A higher TII $\delta^{18}O$-CO_2 amplitude is observed, accompanying analogous tendencies of the ice $\delta^{18}O$ isotope. During TII, ice $\delta^{18}O$ shifts by ~8‰, whereas during TI the shift is only 6‰; in an equivalent way, $\delta^{18}O$-CO_2 behaves in a similar way, with the same relative shifts than for ice $\delta^{18}O$. This may be due to higher temperature amplitudes observed for TII than TI, phenomenon directly depicted in the ice $\delta^{18}O$ signal (and also, by equilibration, to the atmospheric $\delta^{18}O$-CO_2).

We observe an average 11‰ difference between the CO_2 and ice results, the latter being more ^{18}O-depleted than the gas data. Note that ice $\delta^{18}O$ is calibrated vs. SMOW scale, whereas our results are vs. V-PDB, the two scales been related with the following equation:

$$\delta^{18}O_{VSMOW} = 1.03091 \times \delta^{18}O_{VPDB} + 30.91 \qquad (anIII\text{-}1)$$

Overall, this conversion accounts for a difference of approximately 30‰ (Coplen et al., 2002). For both sampling periods, if we re-scale our VPDB data against SMOW, this ~11‰ enrichment would fall down to a ~41‰ depletion compared to the ice data. This number has been associated with the CO_2 – water equilibration process, equally found in earlier studies on other ice cores – Siple, S. Pole, Byrd - (Siegenthaler et al., 1988). A proposed fractionation between the ice and

CO_2 is 47.9‰ for –25°C (hypothetical storage temperature, information found within Eyer, 2004). The shift we find against this value, may be due to higher fractionation temperatures.

With this study, we validate the exchange of oxygen atoms between CO_2 and the ice matrix. The obtained $\delta^{18}O$-CO_2 values are far depleted when compared to the actual atmospheric air isotopic signature (of ~0‰, Coplen et al., 2002). This implies a fractionation setup from the air trapped in firn air until the analysis in the laboratory. Assonov et al., 2005 by measuring firn $\delta^{18}O$-CO_2 values in EDC core found isotopic shifts from atmospheric value increasing with depth and thus, with age of CO_2 gas. They suggested fractionation processes, directly linked with the firn column.

The time of ice storage, as well as the temperature conditions under which the ice sample is kept, constitute primordial factors for oxygen fractionation. Assonov et al., 2005 found values of $\delta^{18}O$-CO_2 in the EDC firn of ~-2‰, expected to reach ~-35.1‰ after equilibration with ice. Our atmospheric values were found more ^{18}O-depleted (especially the corrected ones, shown here) than this suggested value. This is primarily attributed to the storage conditions.

In fig. III-3, a final intercomparison between UBern and LGGE on TI $\delta^{18}O$-CO_2 data in EDC core is provided.

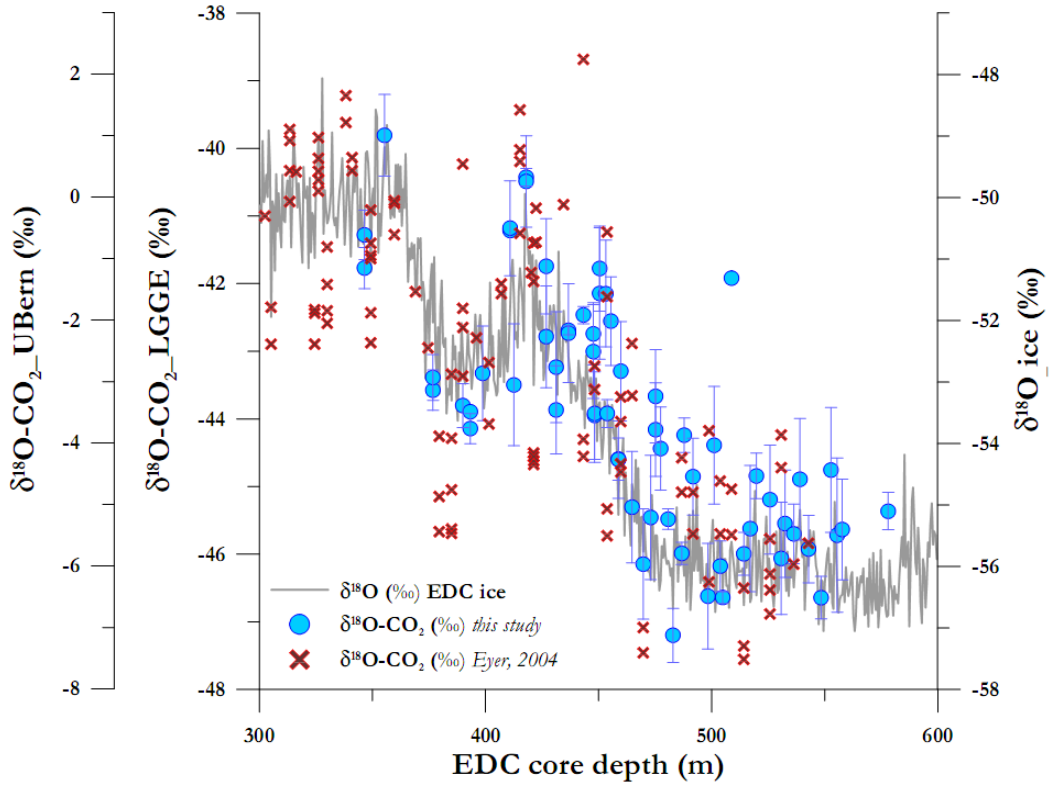

Fig. III-3: *intercomparison of $\delta^{18}O$-CO_2 data from EDC ice between this study and results provided by Eyer, 2004; the former being calibrated vs. VPDB and the latter against SMOW*

Assonov S. S., Brenninkmeijer C. A. M. and Jöckel P. (2005) The 18O isotope exchange rate between firn air CO2 and the firn matrix at three Antarctic sites. *Journal of Geophysical Research* **110**.

Coplen T. B., Bohlke J. K., Bievre P. D., Ding T., Holden N. E., Hopple J. A., Krouse H. R., Lamberty A., Peiser H. S., Revesz K., Rieder S. E., Rosman K. J. R., Roth E., Taylor P. D. P., Jr. R. D. V. and Xiao Y. K. (2002) Isotope-abundance variations of selected elements (IUPAC Technical Report). *Pure Appl. Chem.* **74**, 1987-2017.

Eyer M. (2004) Highly resolved d13C measurements on CO2 in air from Antarctic ice cores. In *Physikalisches Institut der Universität Bern*, p. 94. University of Bern, Bern, Switzerland.

Siegenthaler U., Friedli H., Loetschewr H., Moor E., Neftel A., Oeschger H. and Stauffer B. (1988) Stable-isotope ratios and concentration of CO2 in air from polar ice cores. *Annals of Glaciology* **10**, 151-156.

Annex IV. Statistical & experimental means of rejecting outliers

In Chapter III, we demonstrated the tendencies of each expansion for the 3 atmospheric variables: CO_2, $\delta^{13}CO_2$ and $\delta^{18}O\text{-}CO_2$, on a statistical basis. To achieve this, the following calculation took place:

$$deviation_x = value_x - \sum_{n=1}^{3} value_n \qquad \text{(IV-1)}$$

With $\boldsymbol{x}$ the expansion number

In our ice case, the above equation gives for instance $deviation_1 < deviation_2$ for CO_2 and $\delta^{18}O\text{-}CO_2$ since the variable rises with time, while the opposite is seen for $\delta^{13}CO_2$. In the following, the next step of this exercise is exposed, which deals with the σ- calculation of each variable. This consists in extracting the total of the above result for all the samples of the studied period in question from the individual upper calculation:

$$\sigma = st.deviation \quad (deviation_x - \sum_{k=1}^{q} deviation_x) \qquad \text{(IV-2)}$$

With $\boldsymbol{q}$ the number of samples measured for each sampling period.

The step in-between, i.e. the extracted calculation of $(deviation_x - \sum_{k=1}^{q} deviation_x)$ is plotted in the following for all 3 variables. This helps in validating the "normal distribution" of our datasets, as well as in rejecting the abnormal values (defined as >3σ calculated in eq. IV-2).

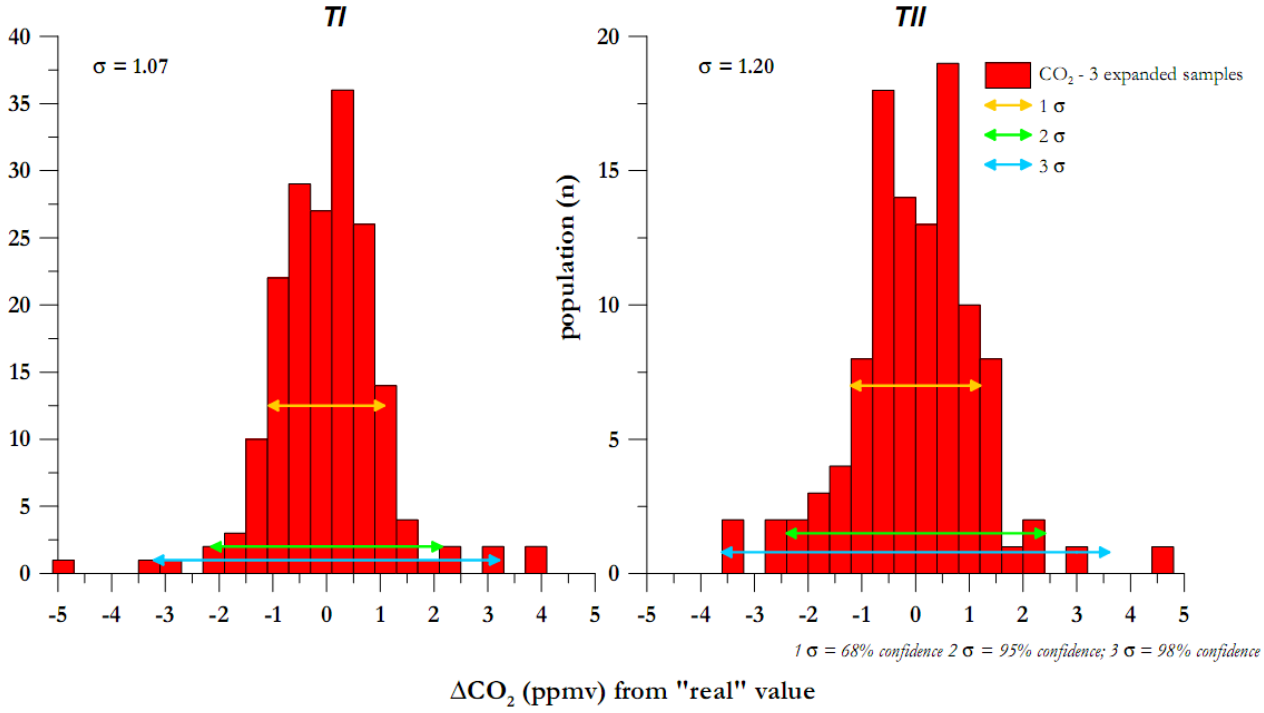

***Fig. IV-1**: Statistical approach in excluding "extreme" values for CO_2; coloured arrows indicate the covered area of 1σ, 2σ and 3σ. Histograms represent the population (number of samples) against deviation from the (mean) calculated value, used as reference*

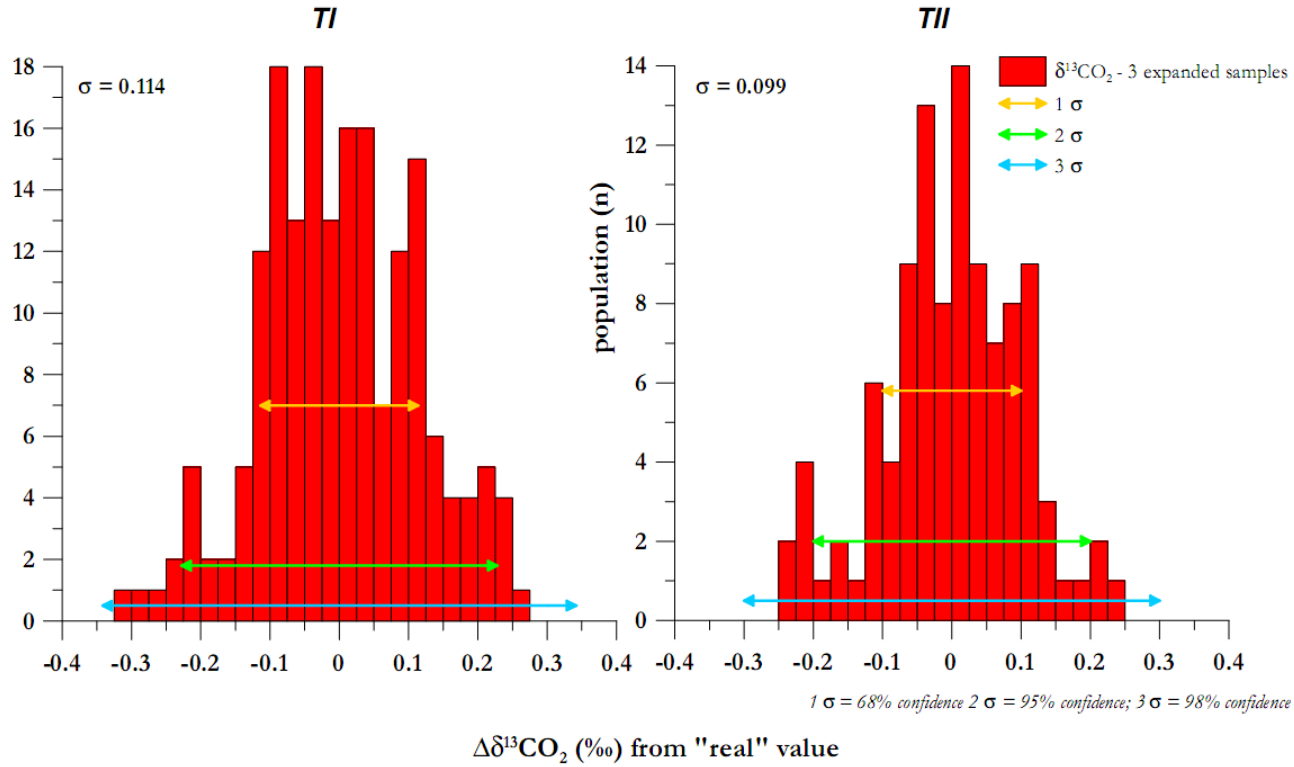

***Fig. IV-2**: Statistical approach in excluding "extreme" values for $\delta^{13}CO_2$; coloured arrows indicate the covered area of 1σ, 2σ and 3σ. Histograms represent the population (number of samples) against deviation from the (mean) calculated value, used as reference*

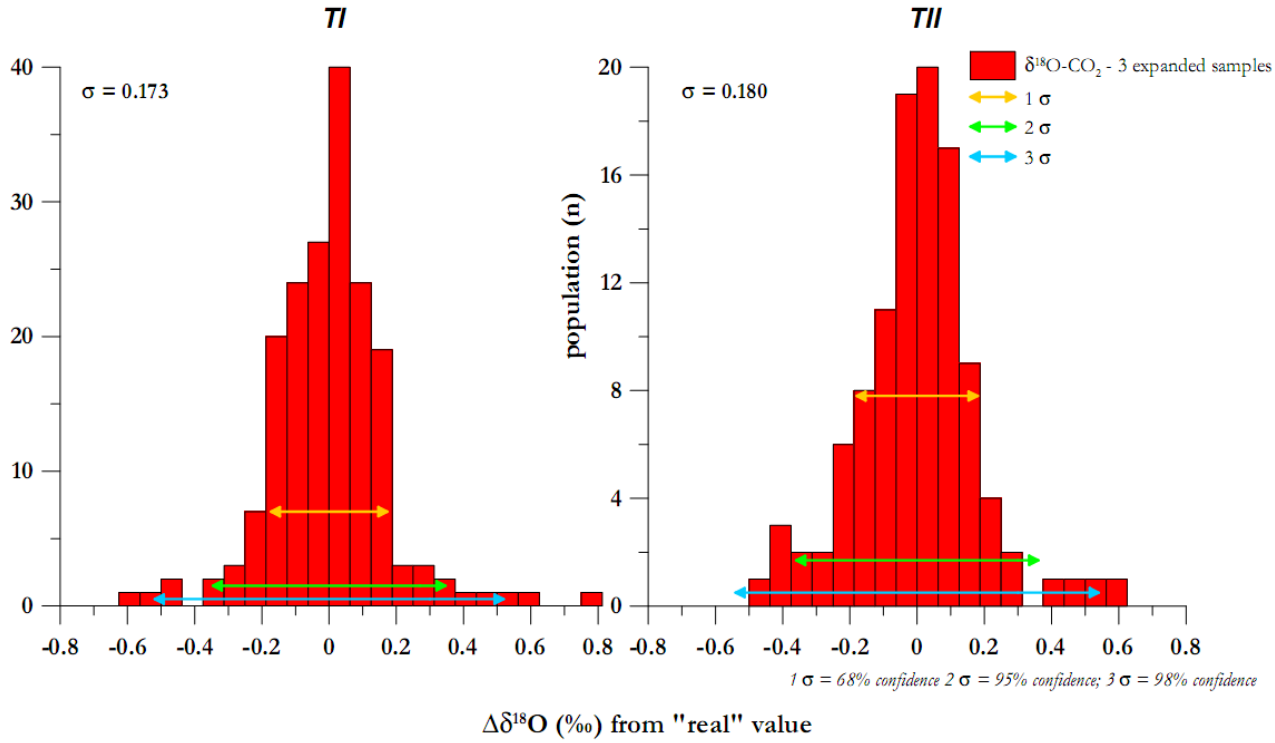

***Fig. IV-3**: Statistical approach in excluding "extreme" values for $\delta^{18}O\text{-}CO_2$; coloured arrows indicate the covered area of 1σ, 2σ and 3σ. Histograms represent the population (number of samples) against deviation from the (mean) calculated value, used as reference*

In the following, the gradient evolution of variables measured throughout time will be plotted against the obtained variables for the same time frame.

The gradient calculation lies on the simple equation :

$$gradient = \frac{\Delta_{variable}}{\Delta_{time}} \qquad \text{(IV-3)}$$

The calculation been conducted between two neighbour values. The obtained result, plotted against the older sample of each couple, is presented in the following:

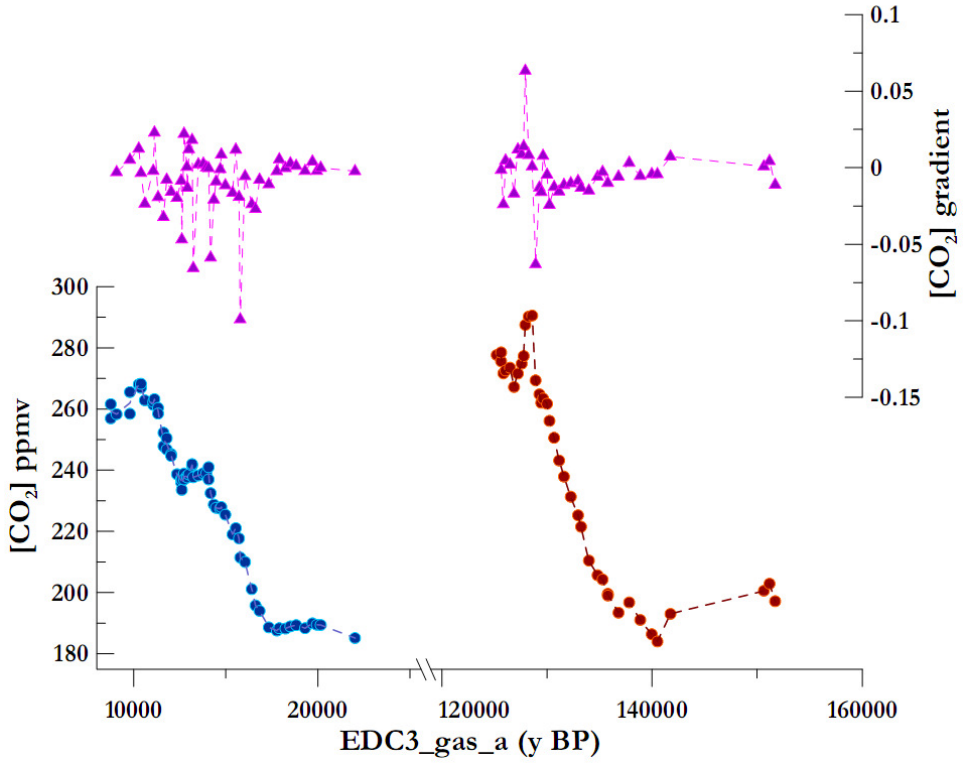

Fig. IV-4: *CO_2 gradient evolution throughout time, superposed with the real CO_2 values for the same time period*

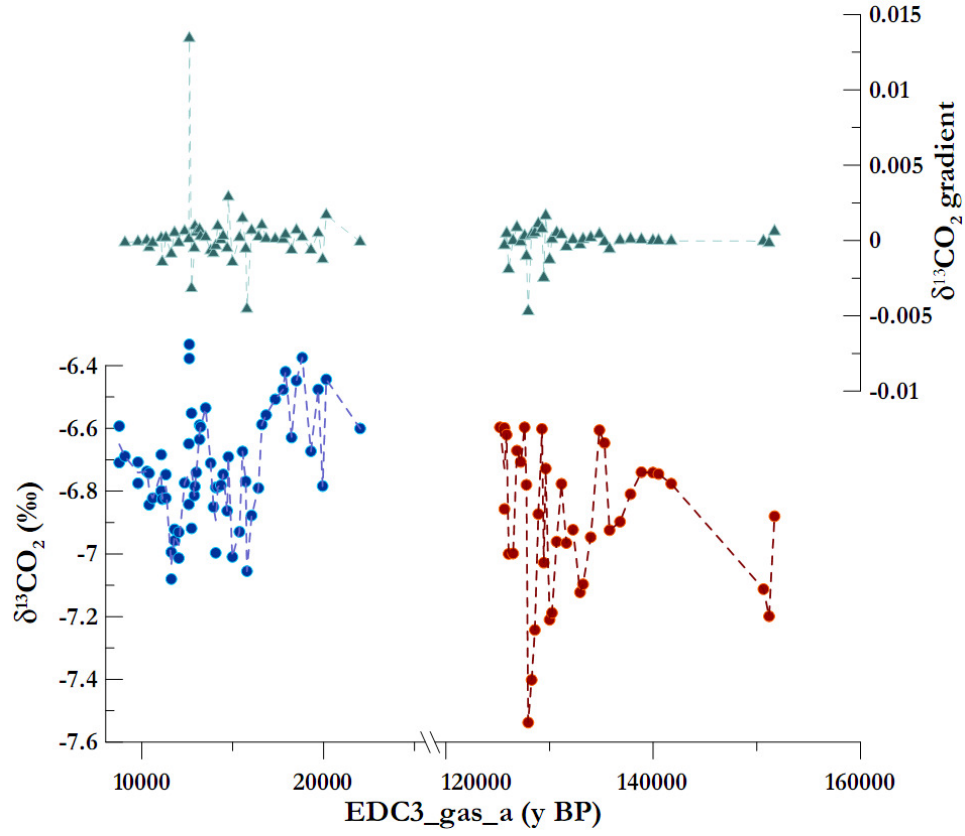

Fig. IV-5: *$\delta^{13}CO_2$ gradient evolution throughout time, superposed with the real $\delta^{13}CO_2$ values for the same time period*

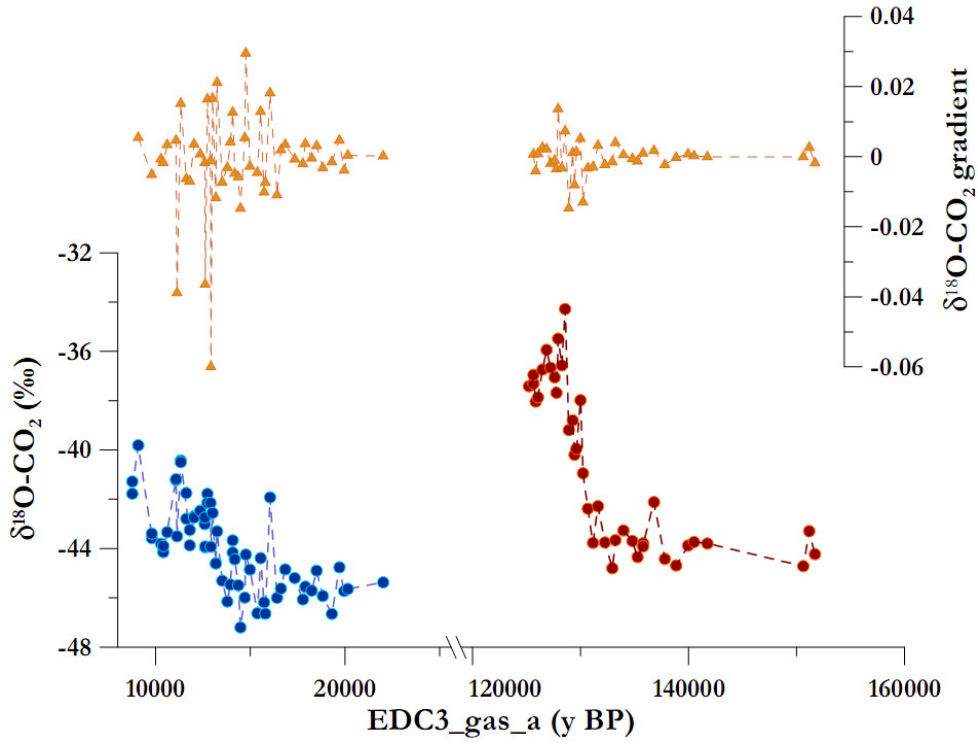

Fig. IV-6: *$\delta^{18}O\text{-}CO_2$ gradient evolution throughout time, superposed with the real $\delta^{18}O\text{-}CO_2$ values for the same time period*

From the above, one observes higher gradient scatter of samples of TI period, despite the more complex physical ice properties and the bigger amplitudes seen for TII samples

Annex V. Technical calculations[1]

In order to check any relation of the ice core state against grinding efficiency of our milling device, we proceeded in a series of calculations, by taking into account the ice sample mass, the different expansions pressure, the line and sample baths temperature throughout the experimental procedure.

These calculations permitted us:

1. to predict the line volume, calculated for all analyzed samples, based on equation *V-1* and compare this value to the theoretical one;

$$V_l = (V_m - V_{ice}) \times \left(\frac{P_1}{T_{m,1}} - \frac{P_2}{T_{m,2}} \right) \times \frac{T_{l,2}}{P_2} \qquad (V\text{-}1)$$

Where ***V*** represents the volume, ***P*** the expanded pressure and ***T*** the temperature, while ***l*** corresponds to line parameters, ***m*** to (ice) mill and numbers either the 1st or 2nd sample expansion.

2. to verify the accuracy of our system, by "predicting" the expansion Pressure and thus, validating with the measurement efficiency when comparing it with the real measured one

$$P_n = \left[\frac{P_{n+1}}{T_{m,n+1}} \times (V_m - V_{ice}) + P_{n+1} \times \frac{V_l}{T_{l,n+1}} \right] \times \frac{T_{m,n+1}}{(V_m - V_{ice})} \qquad (V\text{-}2)$$

The symbols in equation *V*-2 are the same as for eq. *V*-1; in order to predict the 1st expansion Pressure, temperature conditions of the 2nd expansion are necessary.

3. to compare the air content, deduced from each sample and discuss any deviations related to the physical processes of the ice

$$V/m = \left[\frac{V_m - V_{ice}}{T_{m,1}} + \frac{V_l}{T_{l,1}} \right] \times \frac{T_0}{P_0 \times m} \qquad (V\text{-}3)$$

[1] an inspiration of Jean-Marc Barnola and his initial intention to prove that the experimental procedure is problematic!

Where additionally to same symbols as previous equations, ***m*** represents the sample mass, T_0 273K and P_0 1013hPa (standard conditions).

Fig. V-1 presents the obtained results for the two major periods of this study, TI (bubble ice) and TII (clathrate ice). The air content calculated result, superposed with known values are already exposed in Ch. III (fig. 3-24c)

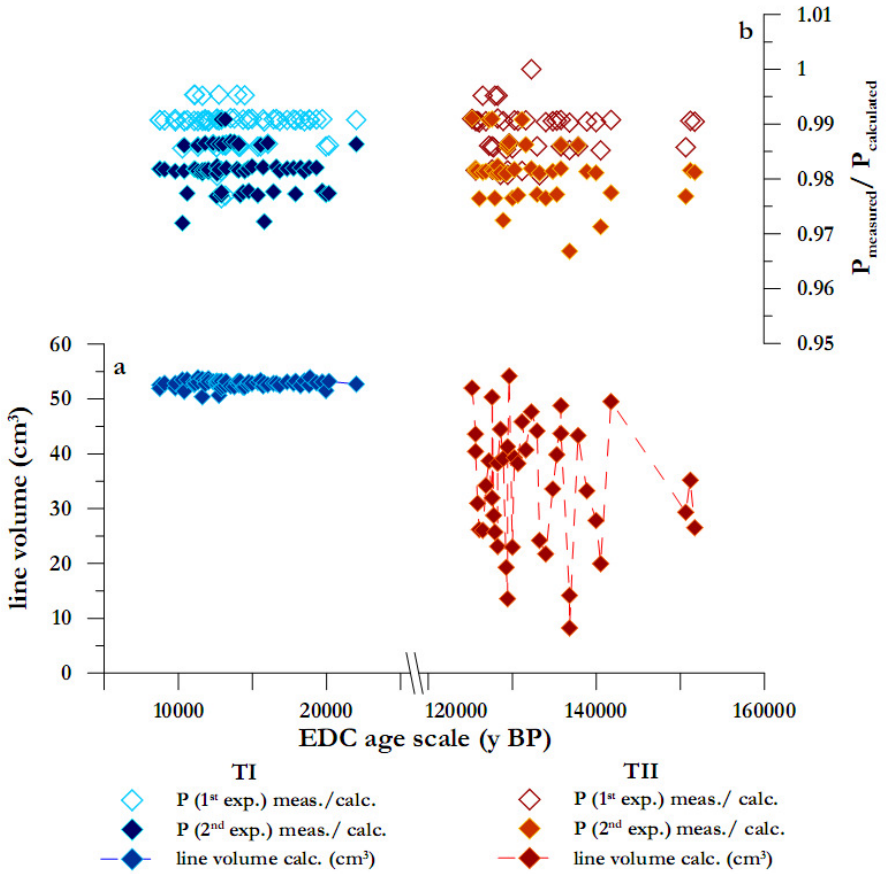

Fig. V-1 *notably Vline, calculated* $P_{expansion}$ *vs real P*

From the above figure we deduce the following major points: in fig. V-1a the inadequacy of TII samples to obtain a reproducible number for the line volume, compared to what is observed for period TI is obvious. For TI, mean line volume was found at 52.76±0.66 cm^3. For TII samples, the results were disastrous: 34.43±11.21 cm^3! Certainly, the V_{line} cannot oscillate; besides, the real line volume is estimated ~48 cm^3 (*J.-V. Lavric, personal communication*), i.e. very close to our calculated TI-one.

The ratios of measured/ theoretical expansion pressure has the same magnitude and dispersion for both TI and TII. This validates the accuracy of the calculations themselves and the conviction

that the higher scatter seen in fig. 3-24b of TII vs. TI, combined with the outcome of fig. V-1a, are deduced from the ice nature itself. This is further enhanced from the calculations of the air content (the result visualized in fig. 3-24c), where it is found lower for the TII, while the existing published values are of the same magnitude (Raynaud et al., 2007). We conclude that all this can be explained by the reduced grinding efficiency by 14% from TI to TII and the change from bubble ice to clathrate ice to be the main responsible factor for this.

Grinding efficiency = air content as calculated (1st expansions)/air content published (V-4)

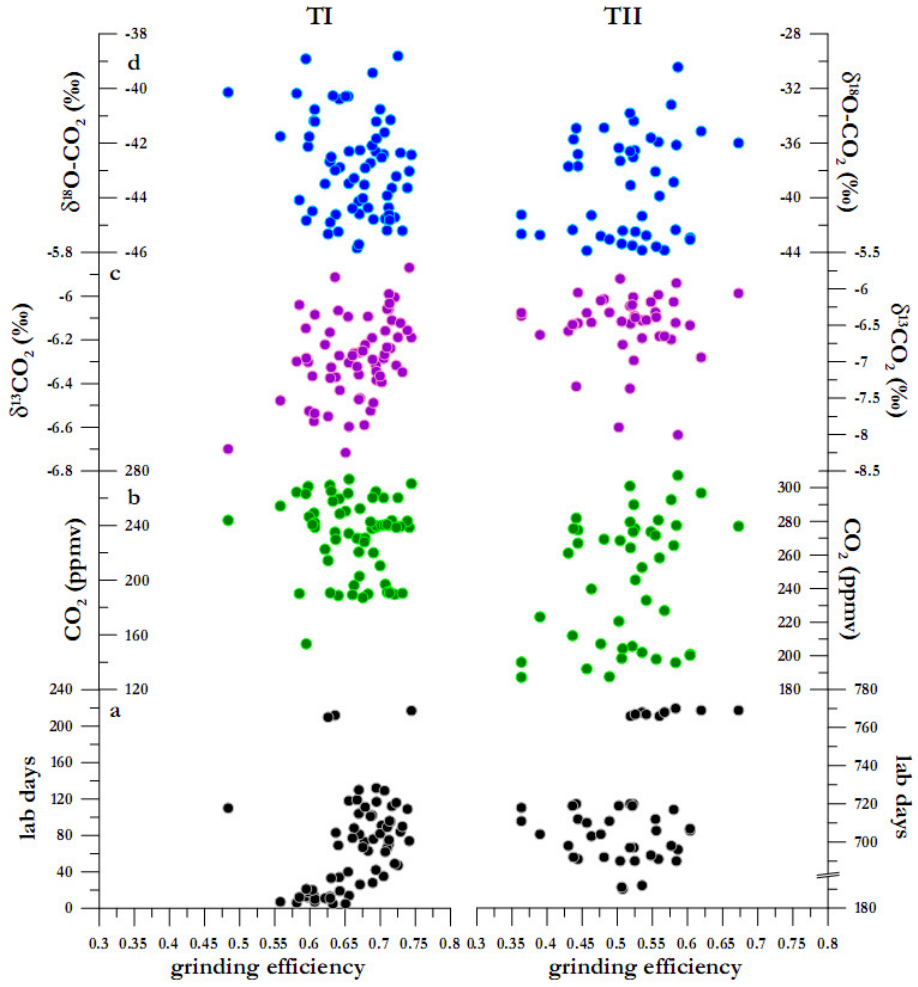

Fig. V-2 *(a) lab days; (b) CO_2; (c) $\delta^{13}CO_2$; (d) $\delta^{18}O$-CO_2 against grinding efficiency for TI(left) and TII(right)*

Being aware of this grinding efficiency shift, the question now arises on whether the obtained values are biased upon the used air extraction technique. Fig. V-2 plots all CO_2 and isotope data obtained, as well as the number of days (from 01-04-2006) against the calculated grinding efficiency for both TI and TII data, in order to prove that no such bias is observed. We still keep some uncertainty on the trend seen for the case of lab days and grinding efficiency for the TI case only.

Annex VI. Data from the last 1000 years

VI.1. Non-corrected data[1]

EDC depths representing the last 1000 y were analyzed in order to compare our $\delta^{13}CO_2$ data with the study-milestone from Law Dome (Francey et al., 1999) and re-consider the corrections to be further accomplished to our raw data. The depth range studied was particular, since it coincides with the transition zone from firn to ice formation. The bubbles not being well formed at this stage, permit the easy air circulation within this depth range. Higher scatter of duplicated samples is expected out of this.

no bag	depth	dates	CO_2	$\delta^{13}C$	$\delta^{18}O$	EDC3_gas_a
187	102,30	08/11/2007	289,74	-6,657	-33,001	120
			280,98	-6,558	-33,154	
			284,59	-6,712	-32,458	
187	102,30	05/12/2007	288,09	-6,698	-33,011	120
			290,34	-6,993	-33,145	
191	104,50	05/10/2007	273,30	-6,966	-35,027	192
			277,49	-7,196	-34,929	
			267,73	-7,205	-34,121	
191	104,50	07/11/2007	308,73	-7,646	-31,161	192
			311,92	-7,655	-31,049	
			314,85	-7,794	-30,452	
206	112,75	04/10/2007	283,07	-6,373	-36,434	472
			279,29	-5,878	-36,504	
			283,81	-5,976	-35,481	
206	112,75	29/11/2007	285,34	-6,358	-37,038	472
			282,00	-6,541	-36,710	
	112,75		288,65	-6,596	-35,992	
206	112,75	06/12/2007	284,00	-6,075	-37,749	472
			283,67	-6,196	-37,521	
			285,47	-6,191	-37,033	
210	114,95	04/12/2007	262,59	-10,331	-45,085	546
			264,62	-10,257	-44,599	
			269,86	-9,728	-43,058	

[1] The majority of this dataset has been analyzed by H. Schaefer; the corrections and superposition with previously published data, by me

210	114,95	12/12/2007	279,84	-6,143	-39,032	546
			284,37	-6,355	-38,825	
			282,92	-6,438	-38,388	
227	124,30	03/10/2007	280,22	-6,314	-39,553	859
			284,37	-6,036	-39,100	
			286,13	-6,465	-38,493	
227	124,30	13/11/2007	282,22	-5,932	-39,789	859
			283,78	-5,995	-39,626	
			278,69	-5,967	-38,872	
227	124,30	27/11/2007	278,51	-6,114	-39,636	859
			281,33	-6,094	-39,505	
			279,82	-5,929	-38,713	
227	124,30	11/12/2007	283,33	-6,328	-39,198	859
			275,12	-6,364	-39,255	
			284,29	-5,897	-37,681	
227	124,30	25/01/2008	280,42	-6,389	-38,193	859
			283,87	-6,490	-37,918	
			286,13	-6,869	-37,189	
227	124,30	04/02/2008	283,42	-6,164	-38,008	859
			281,86	-6,099	-37,483	
			280,39	-6,138	-36,585	
231	126,50	30/11/2007	276,29	-6,050	-39,899	941
			278,35	-6,268	-40,051	
			284,89	-6,025	-38,986	
231	126,50	07/12/2007	277,08	-6,162	-40,456	941
			280,36	-6,403	-40,006	
			271,48	-6,070	-39,395	

VI.2. Corrected data

Two types of corrections were effectuated for this period: one based on the same relation $\delta^{15}N$-δD, as previously applied for the two terminations case (provided by G. Dreyfus):

$$\delta^{15}N = 0.0020032 \times \delta D + 1.2969 \qquad \text{(VI-1)}$$

The second lies on a stable value of $\delta^{15}N=0.520$ provided by (Landais et al., 2006) for the end of firn air. The correlation of proposed and modelled $\delta^{15}N$ was satisfactory: the $\Delta\delta^{15}N$ difference varied from 0.00 to 0.02‰, with an increasing tendency towards higher depths. Equally for the corrected mixing ratio and stable isotopic values, the difference was higher with increasing depth,

reaching maximum differences of 0.10 ppmv and 0.024‰ and 0.048‰ for CO_2, $\delta^{13}CO_2$ and $\delta^{18}O$-CO_2, respectively at the older sample.

Beneath the equation-based correction is provided, in order all measured EDC samples to be uniformly corrected, avoiding more experimental biases:

no bag	depth	dates	CO_2 corr	$\delta^{13}C$ corr	$\delta^{18}O$ corr	EDC3_gas_a
187	102,30	08/11/2007	287,47	-7,172	-34,032	120
	102,30		278,78	-7,074	-34,185	120
	102,30		282,36	-7,227	-33,488	120
187	102,30	05/12/2007	285,84	-7,213	-34,042	120
	102,30		288,07	-7,508	-34,175	120
191	104,50	05/10/2007	271,18	-7,475	-36,044	192
	104,50		275,34	-7,704	-35,946	192
	104,50		265,66	-7,713	-35,138	192
191	104,50	07/11/2007	306,34	-8,155	-32,179	192
	104,50		309,51	-8,164	-32,066	192
	104,50		312,41	-8,303	-31,469	192
206	112,75	04/10/2007	280,90	-6,878	-37,444	472
	112,75		277,15	-6,383	-37,513	472
	112,75		281,63	-6,481	-36,491	472
206	112,75	29/11/2007	283,15	-6,863	-38,048	472
	112,75		279,84	-7,046	-37,720	472
	112,75		286,44	-7,101	-37,002	472
206	112,75	06/12/2007	281,83	-6,580	-38,759	472
	112,75		281,50	-6,701	-38,531	472
	112,75		283,28	-6,695	-38,042	472
210	114,95	04/12/2007	260,56	-10,839	-46,101	546
	114,95		262,58	-10,765	-45,615	546
	114,95		267,78	-10,236	-44,074	546
210	114,95	12/12/2007	277,68	-6,651	-40,048	546
	114,95		282,18	-6,863	-39,840	546
	114,95		280,73	-6,945	-39,404	546
227	124,30	03/10/2007	278,05	-6,824	-40,574	859
	124,30		282,16	-6,546	-40,120	859
	124,30		283,92	-6,975	-39,513	859
227	124,30	13/11/2007	280,03	-6,443	-40,809	859
	124,30		281,58	-6,505	-40,647	859
	124,30		276,53	-6,477	-39,892	859
227	124,30	27/11/2007	276,35	-6,624	-40,656	859

	124,30		279,15	-6,604	-40,525	859
	124,30		277,65	-6,439	-39,733	859
227	124,30	11/12/2007	281,13	-6,839	-40,219	859
	124,30		272,98	-6,874	-40,275	859
	124,30		282,08	-6,407	-38,701	859
227	124,30	25/01/2008	278,24	-6,899	-39,213	859
	124,30		281,67	-7,000	-38,939	859
	124,30		283,91	-7,379	-38,209	859
227	124,30	04/02/2008	281,22	-6,675	-39,028	859
	124,30		279,67	-6,609	-38,503	859
	124,30		278,22	-6,648	-37,605	859
231	126,50	30/11/2007	274,21	-6,546	-40,891	941
	126,50		276,25	-6,764	-41,043	941
	126,50		282,74	-6,521	-39,978	941
231	126,50	07/12/2007	274,99	-6,658	-41,448	941
	126,50		278,24	-6,899	-40,998	941
	126,50		269,43	-6,566	-40,387	941

VI.3. Comparison with other data

Below, our accepted gravitationally corrected data are superposed with previously published from (a) direct air samples from Cape Grim (Francey et al., 1999), (b) firn air samples from Law Dome (Francey et al., 1999) and (c) ice samples from Law Dome (Francey et al., 1999) and Siple core (Friedli et al., 1986) :

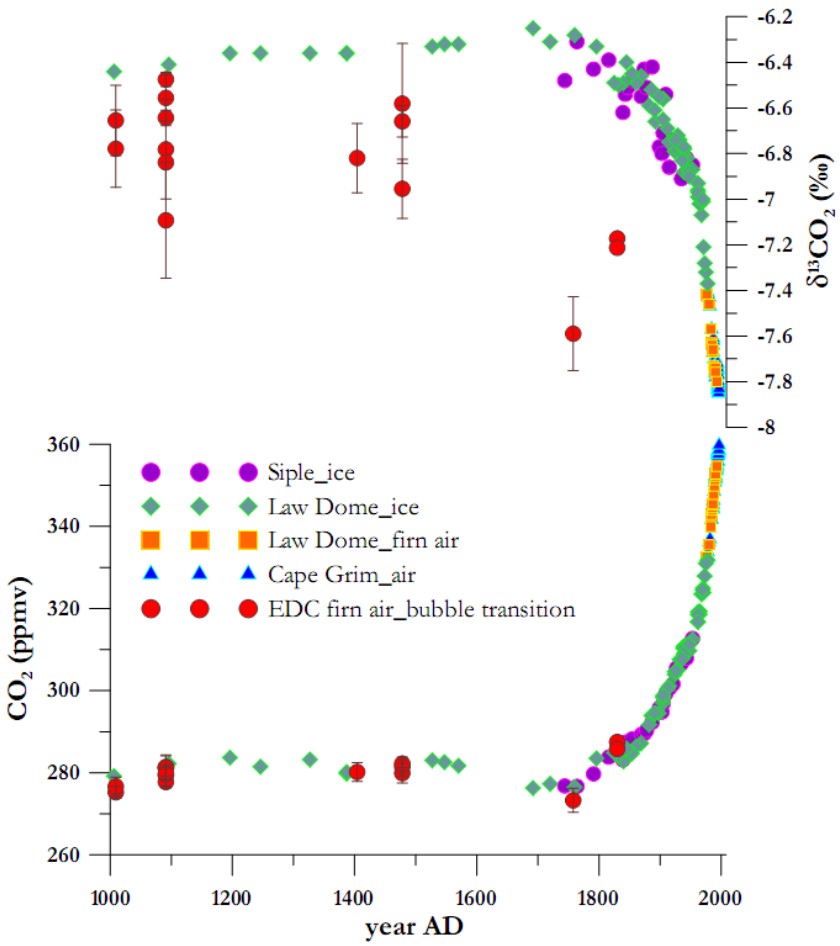

Fig. VI-1 : *Superposition of our data taken from the firn-bubble closure transition with air, firn and ice samples (Friedli et al., 1986; Francey et al., 1999)*

While our CO_2 data fall within the Law Dome values, this is not the case for the $\delta^{13}CO_2$ data, ours being more ^{13}C-depleted than the published data by an average 0.3‰. Still, the decreasing trend is reproduced by the EDC core, implying application of further corrections in the future in resolving the discrepancy. The first candidate to be applied as correction factor may be deduced from the bubble free ice tests and the obtained max fractionation of ~0.25‰.

Francey R. J., Allison C. E., Etheridge D. M., Trudinger C. M., Enting I. G., Leuenberger M., Langenfelds R. L., Michel E. and Steele L. P. (1999) A 1000-year high precision record of $\delta^{13}C$ in atmospheric CO_2. *Tellus B* **51**, 170–193.

Friedli H., Lötscher H., Oeschger H., Siegenthaler U. and Stauffer B. (1986) Ice core record of the $^{13}C/^{12}C$ ratio of atmospheric CO_2 in the past two centuries. *Nature* **324**, 237-238.

Landais A., Barnola J. M., Kawamura K., Caillon N., Delmotte M., Ommen T. V., Dreyfus G., Jouzel J., Masson-Delmotte V., Minster B., Freitag J., Leuenberger M., Schwander J., Huber C., Etheridge D. and Morgan V. (2006) Firn-air $\delta^{15}N$ in modern polar sites and glacial-interglacial ice: a model-data mismatch during glacial periods in Antarctica? *Quaternary Science Reviews* **25**, 49-62.

Annex VII. EPICA $\delta^{13}C$ consortium and gas intercomparison process and results

A common strategy was established between the laboratories who belong to EPICA Consortium and deal with $\delta^{13}C$ measurements, in late 2006, in order to comprehend the analytical differences of each protocol, on a short-term scale, the long-term goal being the attainment of an analytical consensus. Thus LGGE, UBern and AWI, engaged in first measuring gas cylinders of known composition on a round-robin application and second, apply their differing protocols to the same real ice sample. Here the first approach is exposed, in which I participated, with the support of H. Schaefer.

3 cylinders were analyzed, with the following composition:

Cylinder n°	CO_2	$\delta^{13}C$	$\delta^{18}O$
1 INSTAAR n° CA06195	182.09	-7.919	-4.756
2 INSTAAR n° CA06818	296.80	-8.420	-4.800
3 measured by I. Levin, Heidelberg	277.67	-2.757	-14.720

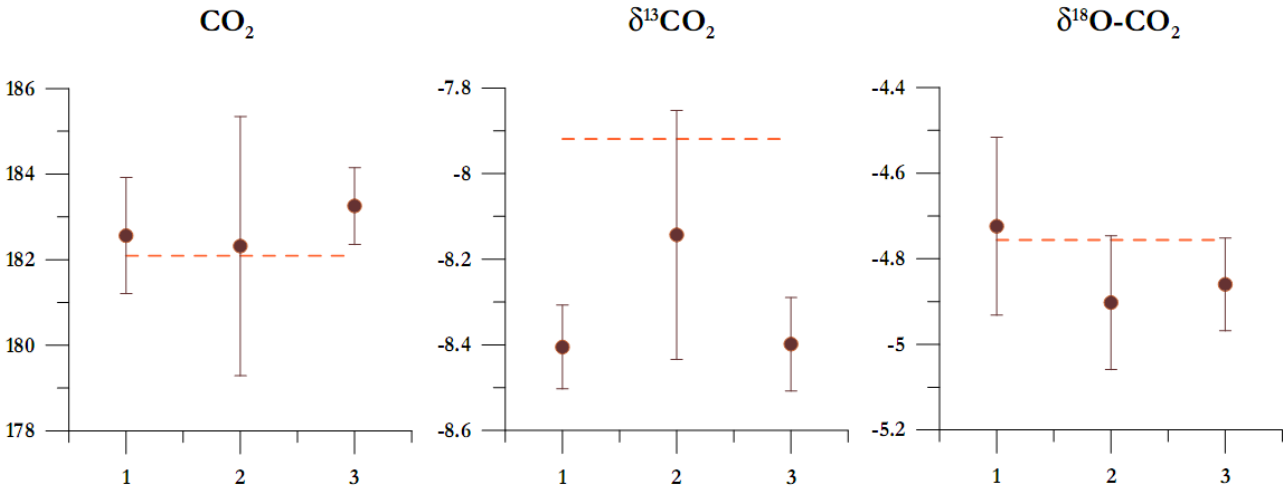

Fig. VII-1: *Cylinder 1 real value (dotted line) and mean measured one + error bars; x axis: n° sampling day*

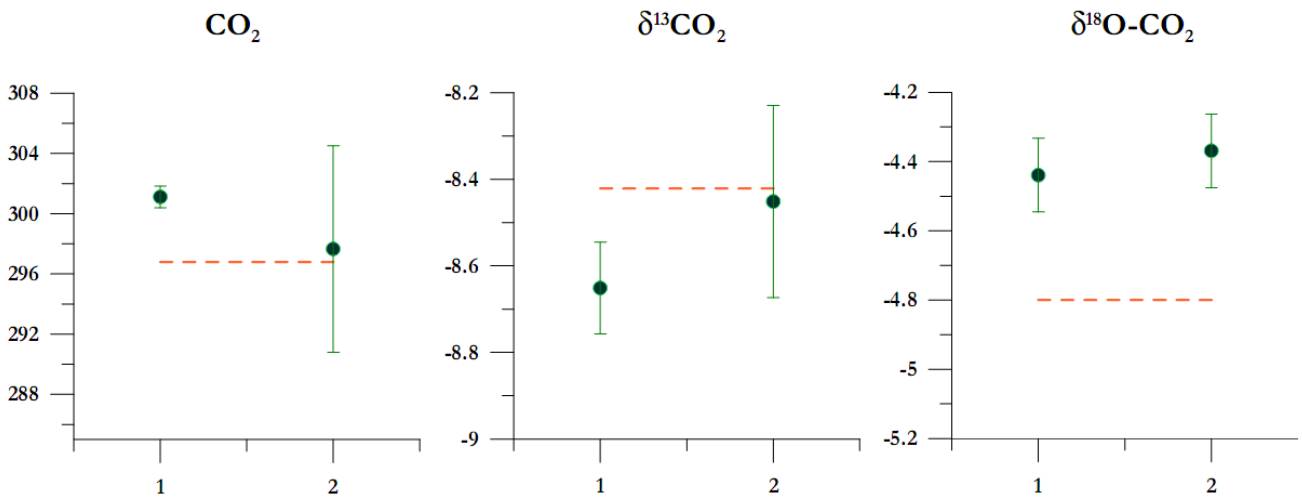

Fig. VII-2: *Cylinder 2 real value (dotted line) and mean measured one + error bars; x axis: n° sampling day*

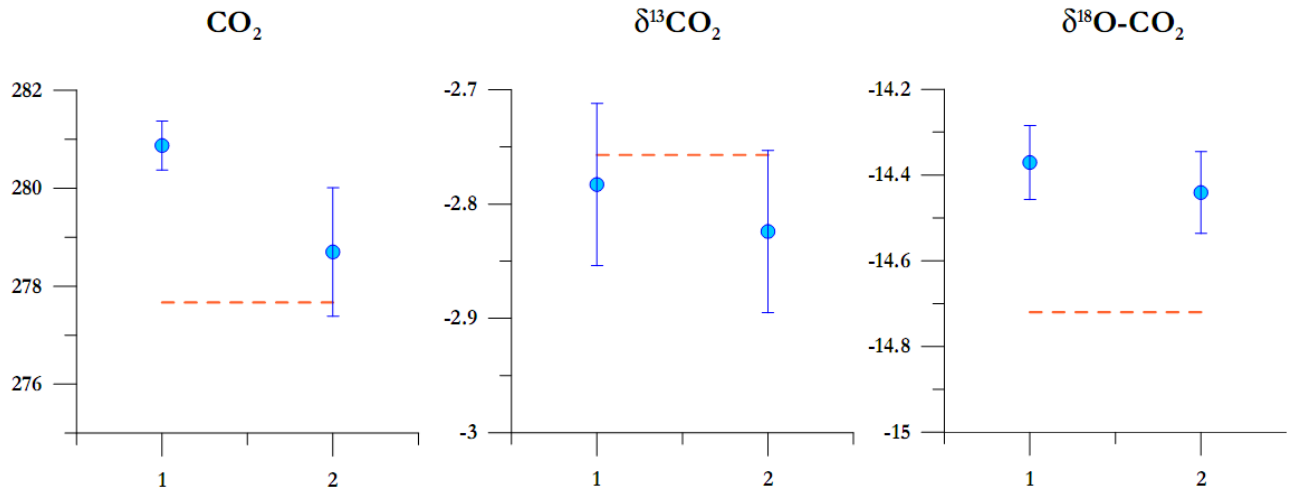

Fig. VII-3: *Cylinder 3 real value (dotted line) and mean measured one + error bars; x axis: n° sampling day*

Annex VIII. BOXKIT

VIII.1. BOXKIT description

BOXKIT model (Paillard et al., 1993) is a conceptual mathematical approach that helps in discerning the principal f-actors of the C-cycle, by effectuating sensitivity tests.

Input variables

According to the code, one is free in constructing the number of oceanic boxes one desires, by being then obliged in setting the background needed, in terms of :

- geometry and ocean flux setup (box volume and area, ocean circulation loops definition and quantification)
- C-cycle parameters (nutrients –PO_4 considered as the limiting factor-, Total Alkalinity, *TAlk*, Dissolved Inorganic Carbon, *DIC*, Redfield and Rain Ratios, oxidation / dissolution percentages..)
- Marine productivity (defined either from Michaelis-Menton equation, or from a pre-defined fixed production on which each surface box has a certain percentage)
- Sea Surface Temperature and Salinity setup; the former for only surface boxes, the latter for all boxes involved

The exercise accomplished involved a PANDORA-like box configuration (Broecker and Peng, 1986), in an effort to represent the most accurately possible the one seen in the BICYCLE version (Köhler et al., 2005a).

Output variables

The model provides us with the following outputs/ results:

- Distribution of C-cycle parameters initially introduced (e.g. PO_4, TAlk, DIC..) to all involved oceanic boxes
- Oceanic $\delta^{13}C$ and $\Delta^{14}C$

- Productivity in every surface box
- Temperature, salinity, oxygen distribution in deep boxes
- pCO_2 calculated for every surface box
- atmospheric CO_2, $\delta^{13}C$ and $\Delta^{14}C$ calculations

Model steps/ Way of thinking

Everything depends in the first place on the phosphate concentration: according to the kind of productivity selected (among the pre-mentioned options), the phosphate repartition under equilibrium conditions is calculated for every single surface box. The model then calculates what inserts and exits every box, based on the circulation scheme, by additionally defining the flux of organic matter that corresponds to these movements. DIC, Dissolved Oxygen, *DO*, and TAlk are calculated via the Redfield Ratios. Air-sea exchanges are further considered for the case of DO, DIC, $\delta^{13}C$ and $\Delta^{14}C$. In the following a specimen of BOXKIT work area is exposed, with all pre-mentioned input parameters mentioned:

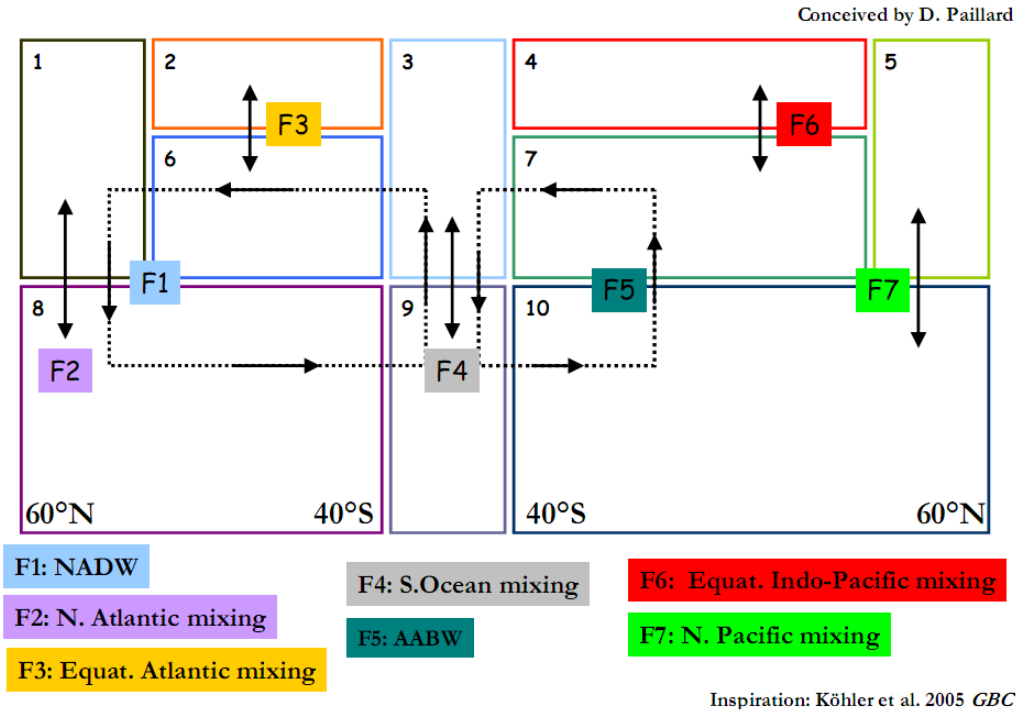

Fig. VIII-1: *BOXKIT configuration used for sensitivity tests, discussed in Ch. IV*

Annex IX. Nouveau Chapitre de la thèse

Association Bernard Gregory
www.abg.asso.fr

Valorisation des compétences des docteurs
«un nouveau chapitre de la thèse ®»

Anna Lourantou

Ecole doctorale : ***Terre, Univers et Environnement (TUE)***

Université ou organisme de rattachement : ***Université Joseph Fourrier***

Nom du "mentor" : ***Jean-Christophe Klein***

Nouvelle contrainte sur la cause de l'augmentation du gaz carbonique lors les déglaciations

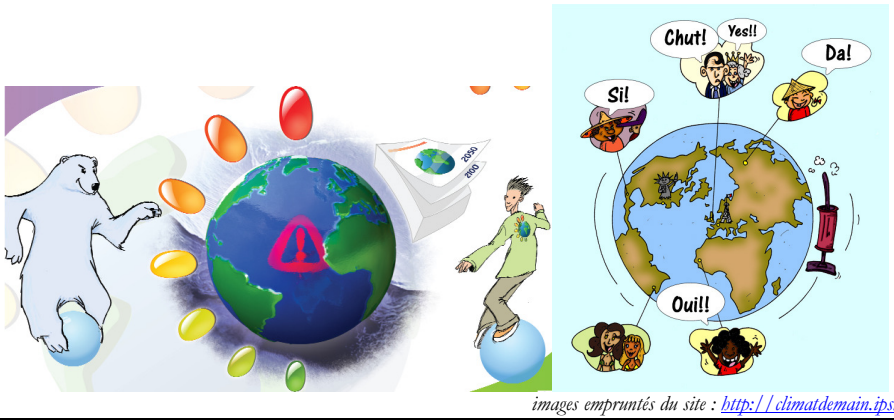

images empruntés du site : http://climatdemain.ipsl.jussieu.fr/index.html

Date probable de présentation orale du « NCT » : 19 Novembre 2008

Sujet académique de la thèse : "On the causes of the rise of CO_2 during deglaciations : new constraints using its stable carbon isotope ratio, $\delta^{13}C$"

Nom du directeur de thèse : Jérôme Chappellaz

Date probable de soutenance de la thèse : 22 Décembre 2008

IX.2. Cadre général, enjeux et présentation de votre projet de recherche

IX.2.1. Présentation succincte

L'enjeu scientifique consiste à expliquer l'origine du gaz carbonique (CO_2) dans l'atmosphère, lors les transitions (naturelles) glaciaires-interglaciaires du passé. Cette étude est basée sur les caractéristiques physico-chimiques de ce gaz. Elle a pour but de contraindre les scénarios du changement climatique dans le futur, en examinant des hypothèses sur l'avenir tout en s'appuyant sur le climat du passé.

L'enjeu technique comprend des mesures originales, délicates, pionnières, auxquelles il faut consacrer du temps et de l'énergie considérables pour la production, l'interprétation et la communication (des résultats) aux différentes communautés.

L'enjeu sociétal est le devenir des futures générations dépendantes des conditions climatiques, les « mélanges inter-sociétaux » qui se produiront lors les grandes vagues d'« immigration climatique », ainsi que l'adaptation de l'homme aux créations ou réductions des emplois de travail.

L'enjeu économique représente l'accoutumance de l'homme aux besoins des nouvelles formes d'énergie, liées à la décroissance des ressources en carbone, combinées à l'essor démographique et au prolongement de l'espérance de vie.

De nos jours, on associe la notion d'« effet de serre » avec le réchauffement anormal actuel de la planète. Pourtant, c'est un processus d'origine naturelle : il s'agit du piégeage des rayonnements solaires par certains éléments dans l'atmosphère, les gaz à effet de serre (GES). Le gaz carbonique (CO_2) constitue un des GES les plus importants. L'étude des carottes de glace permet de reconstituer l'évolution passée du CO_2, d'où on déduit un lien fort entre le climat (représenté par la température) et ce GES. On distingue régulièrement dans le passé des périodes froides (glaciaires) accompagnées par des teneurs en CO_2 basses, suivies par des périodes chaudes (interglaciaires) avec des teneurs en CO_2 élevé. Actuellement, on vit dans la dernière « interglaciaire », période associée à la prospérité culturelle, vu les conditions climatiques optimales que l'on parcourt. Pourtant, on est en train d'intervenir sur cette périodicité naturelle, en utilisant de plus en plus des moyens de transports et en multipliant l'activité industrielle, émettant ainsi de plus en plus du CO_2 dans l'atmosphère. Ceci a comme conséquence un réchauffement anormal de la planète. Afin de mieux saisir la réversibilité de la situation, il fallait en premier lieu comprendre la raison de l'évolution « naturelle » du CO_2 dans le passé, qui reste jusque maintenant incertaine. L'outil que l'on emploie pour identifier la provenance du CO_2, c'est

le rapport entre la forme 'lourde' (^{13}C) et la forme 'légère' (^{12}C) naturelle du carbone dans le CO_2 ; ces formes se comportent différemment lors des processus qui se produisent aux différents réservoirs (océan, biosphère). Imaginons le suivant : que ces deux formes de CO_2 ont une couleur différente ; cette couleur est liée au bleu de l'océan et au vert des plantes. En trouvant l'analogie du bleu au vert dans le CO_2, on trouve indirectement la contribution de l'océan ou la biosphère terrestre comme source d'origine de ce gaz dans le passé.

Depuis les années '60, on fait des forages dans les pôles afin de récupérer des carottes de glace ; plus on va vers le fond, plus la glace devient vieille et plus loin on va dans l'histoire.

L'objectif principal de cette thèse est l'étude du cycle du carbone et les interactions entre les différents réservoirs pendant les deux dernières déglaciations.

IX.2.2. Ma thèse dans son contexte

a) UJF [1] → TUE [2] → **LGGE** [3] → thème paléoclimat → équipe 'gaz' → Anna

b) UE [4] → CNRS [5] → **LGGE** [3]

Deux axes principaux ont été superposés dans le schéma ci-dessus :

(a) la suite '**administrative**', commençant par l'UJF[1] (où je me suis inscrite dans le cadre de ma thèse), qui amène vers l'école doctorale 'TUE[2] (domaine Sciences de la Terre) et

(b) la suite '**financière**' partant de l'UE[4] et le 'siège administratif' à Bruxelles, passant à travers le CNRS[5] (organisme par lequel je suis payée); ces 2 axes mènent au LGGE[3] (laboratoire d'accueil).

Le personnel du LGGE[3] se monte à 100 personnes, étant chercheurs, ingénieurs, enseignants, techniciens, personnel administratif, stagiaires ou doctorants. Ce personnel est divisé en quatre groupes scientifiques : les 'thèmes'. Ma thèse fait partie du thème : « paléoclimatologie », qui contient plusieurs équipes : 'chimie', 'mécanique de la glace', 'poussières', 'datation de la glace', 'métaux lourds' et 'gaz' : la dernière c'est l'équipe à laquelle j'appartiens. Elle contient actuellement 7 personnes qui étudient l'air piégé dans la glace. Mes analyses consistent à extraire le CO_2 de la glace, à le séparer des autres gaz et à le quantifier pour finalement récupérer de façon quantitative ses différentes formes du carbone.

Lors de cette thèse, l'acquisition des données de qualité pour un site en Antarctique a été la priorité. Le choix du site continental « Dome C », foré par une collaboration de 10 pays européens, impose que cette thèse s'implique directement au projet international « EPICA[6] ». En

[1] Université Joseph Fourier
[2] Terre, Univers, Environnement
[3] Laboratoire de Glaciologie et Géophysique de l'Environnement
[4] Union Européenne
[5] Centre National de Recherche Scientifique
[6] European Project for Ice Coring in Antarctica

Europe, il existe 3 laboratoires qui sont en collaboration (plutôt concurrence) en ce qui concerne l'acquisition, exploitation et validation des données : (1) Climate and Environmental Physics, Physics Institute, UBern[7] en Suisse, (2) AWI[8] à Bremerhaven en Allemagne et (3) LGGE[3] sur Grenoble en France.

Compétences scientifiques mises à disposition de mon sujet de recherche : le réseau informatique du LGGE[3] contient des bases de données qui permettent d'effectuer des recherches bibliographiques, élément indispensable pour mon travail. Lors de mon détachement sur Paris (fin 1ère année), en collaboration avec des scientifiques spécialisés en 'mise en place numérique', un travail sur l'initiation en interprétation des données a été réalisé.

Compétences techniques mises à disposition de mon sujet de recherche : lors du démarrage de ma thèse, un entraînement sur le traitement des échantillons de glace, le travail en chambre froide, l'usage en sécurité de l'azote liquide (-196°C), les techniques d'extraction de l'air, le piégeage du CO_2 et l'utilisation des machines de chimie a été réalisé afin que je sois autonome au laboratoire. Le LGGE[3] dispose d'un nombre de facilités afin qu'une thèse se déroule sous conditions optimales : un bureau, des 'utilités' comme papeterie, ligne téléphonique, connexion internet, imprimantes ont été mis à mon service. Un ordinateur portable sous forme de station de travail a été également acheté pour me faciliter les déplacements.

Compétences humaines mises à disposition de mon sujet de recherche : les secrétaires du LGGE[3] m'ont aidée sur l'organisation des missions et pour la mise au point de la littérature accessible. Le personnel administratif a été à ma disposition pour des questions bureaucratiques. Dans l'atelier, les techniciens garantissent toutes les réparations possibles et informent sur la sécurité. Un post-doctorant m'a encadrée et surveillée lors du travail analytique. Le personnel du labo, tant permanents que doctorants a été indispensable lors des périodes difficiles et a toujours été proche de moi quand je l'ai sollicité, tant scientifiquement que humainement.

Cette thèse est enregistrée dans le réseau européen des actions 'Marie Curie' (étant un 'Réseau de Recherche et d'Entraînement') sur le changement global de l'environnement, soutenu par le 6ème programme-cadre de l'UE[4] (2004-2008), nommé **GREENCYCLES**. Ce réseau relie des centres européens majeurs dans le domaine du changement global de l'environnement situés dans 7 pays européens, et a pour but de contribuer à la formation de la prochaine génération 'scientifique' du système 'Terre'. Ce travail est également lié au projet **EPICA**[6], un programme scientifique joint de la Fondation de la Recherche Européenne/ UE[4], avec des engagements nationaux de 10 différents pays européens. Ces partenaires travaillent autour des résultats de la carotte de glace

[7] University of Bern
[8] Alfred Wegener Institute for Polar and Marine Research

forée sur le site Antarctique 'Dome C'. Cette thèse est davantage liée au projet **'DESIRE**[9]'(2007-2009), financé par NERC[10] QUEST[11] (UK) et par l'INSU[12] (France), dans le cadre d'une de ses thématiques qui vise à la compréhension de la nature et diversité des cycles glaciaires-interglaciares s du CO_2 envers le climat.

Lors de cette thèse, à ces partenariats internationaux s'ajoutent les océanographes et les chercheurs du système terre du **LSCE**[13] à Paris ainsi qu'un chercheur du paléoclimatologie de l'**AWI**[8] à Bremerhaven en Allemagne.

IX.2.3. Moi dans ce contexte

Le monde de la recherche m'a toujours tenu à cœur, vu la curiosité perpétuelle et l'esprit d'alerte qu'il engage. Pourtant, je n'ai pas directement enchaîné vers une thèse dès la fin de mes études en master : un engagement de 3 ans (réglementation française pour la durée d'une thèse) vers un sujet particulier demande un raisonnement plus élaboré qu'auparavant. Les enjeux au niveau personnel étaient également considérables : ville inconnue, laboratoire inconnu, thématique de recherche inconnu. J'ai toujours aimé travailler pour l'environnement, découvrir ses multiples richesses à travers les divers sujets que j'ai étudiés : pollution des lacs naturels et artificiels; suivi de la qualité de l'eau des écosystèmes diversifiés avec une implication sur le management, qui s'appuie sur la législation locale et européenne. Il me manquait des références de base, une recherche historique, des acquis du passé : j'ai donc décidé d'étudier l'histoire du climat à travers les carottes de glace, passer dans des échelles de temps mystérieuses pour moi, traiter la glace dans le froid, ce que je n'avais pas expérimenté avant. Utiliser des outils techniques auxquels j' étais pas habituée, faire de la science 'du passé' entièrement nouvelle pour moi !

Le sujet de cette thèse a été proposé dans le cadre du projet européen GREENCYCLES dans le site web CORDIS[14] de la UE[4]. Le choix du recrutement a été basé entièrement sur le dossier envoyé, comprenant mon curriculum vitae, ma lettre de motivation et mes références. A cette époque-là je travaillais en Belgique comme 'attachée scientifique' pour l'ULg[15], quand j'ai passé l'entretien téléphonique avec mon futur 'employeur' et l'ensemble de l'équipe. Il me semble que c'est plutôt ma curiosité et ma motivation qui ont été retenues afin d'être acceptée parmi les candidats. A la question concrète me demandant la raison de mon choix envers ce sujet, j'ai eu un seul mot à dire : « challenge » (=enjeu).

[9] Dynamics of the Earth System and the Ice core REcord
[10] Natural Environment Research Council
[11] Quantifying and Understanding the Earth SysTem
[12] Institut National des Sciences et de l'Univers
[13] Laboratoire des Sciences du Climat de l'Environnement
[14] Community Research and Development Information Service for Science, Research and Development
[15] Université de Liège

Vu les conditions du recrutement, le sujet était bien défini même avant la sélection des candidats potentiels. Aucune contribution de mon côté n'a été apportée sur la construction du sujet. Lors de la fin du 3ème mois de ma thèse, après une période de recherche bibliographique et des communications internationales, le sujet a dérivé vers l'étude d'autres gaz dans la glace (du monoxyde du carbone, CO, et du méthane, CH_4 on passe au CO_2). Ce changement a eu lieu grâce au travail avancé du post-doctorant au laboratoire, permettant ainsi le démarrage d'une thèse *a priori* opérationnelle.

IX.3. Déroulement, gestion et coût de votre projet

IX.3.1. Préparation et cadrage du projet

L'évaluation des facteurs de succès ou de risques a été effectuée lors les premiers 3 mois de ma thèse en parallèle à l'avancement du travail du post-doctorant au laboratoire. Le principal facteur de risque consistait à mettre en place un nouveau protocole expérimental, qui (i) risquait de rester seulement en termes techniques, sans science impliquée derrière, ce qui n'a pas été mon souhait d'origine et (ii) impliquerait un changement fondamental de la structure mise en place par un post-doctorant pendant 1,5 ans de travail et qui juste venait d'être opérationnel ! La décision a donc été de prolonger le travail du post-doctorant, sans davantage envisager les facteurs de risques, malgré le caractère pionnier et complexe de l'acquisition des données, ainsi que l'ambiance compétitive avec les partenaires européens. Quant aux facteurs de succès, ils contiennent le financement a priori acquis, combiné avec le caractère « prestigieux » du laboratoire d'accueil (connu dans le monde entier pour sa recherche pionnière et sa rigueur scientifique), et le classement de mon nouveau sujet de la thèse comme sujet prioritaire.

Le choix des partenaires au niveau international a été dans un premier temps 'imposé' par le réseau européen, dans le cadre duquel cette thèse s'inscrit, **GREENCYCLES**. D'autres partenariats européens ont été établis bien avant cette thèse, dû à l'intérêt du site d'étude en Antarctique, **EPICA**[6]. D'autres collaborateurs 'individuels' ont été rajoutés tout au long de cette thèse, produit de l'initiative personnel et de celui de mon directeur de thèse : *Elisabeth Michel et Didier Paillard (LSCE[13]), Peter Köhler (AWI[8]).*

Il n'y a pas eu de contribution à la mobilisation de financements externes à l'équipe de ma part (car je n'ai pas participé à la rédaction des appels d'offre).

Dans les réseaux où je suis impliquée, il existe le principe implicite sur la confidentialité des données qui ne sont pas publiées, en les communiquant et les gardant 'intra-muros'.

IX.3.1.1. Conduite du projet

Début thèse 1 an 2 ans 3 ans

Initialisation	Acquisition données	Exploitation	Exploitation	Acquisition données	Exploitation
Intégration	Réunion équipe		Evaluation	Exploitation	Récapitulation
Acquisition données	Exploitation		Acquisition données	Réunion équipe	Réunion thème
			Réunion équipe	Réunion thème	

Ma thèse s'est déroulée de la manière suivante : (i) **initialisation** : identification du sujet général, mise en place des objectifs, réorientation du sujet originel de la thèse ; (ii) **intégration** : formation sur les aspects techniques et l'acquisition des données ; (iii) **acquisition des données**; (iv) **exploitation** : d'après des réunions, combinés avec la recherche bibliographique, j'ai établi des hypothèses sur l'interprétation des résultats acquis ; (v) **évaluation** : fondation des collaborations, communications, validation des résultats acquis et leur interprétation, comme elle a été conçue lors des diverses collaborations, en rédigeant un article scientifique [étapes (iii) à (v) réalisées deux fois] ; (vi) **récapitulation** : rédaction du manuscrit de thèse. Parmi les étapes pré-mentionnées, des **réunions** ont eu lieu, dans un premier temps avec mon directeur de thèse, puis avec les membres de l'équipe 'gaz' et avec le thème 'paléoclimat'. Leur fréquence oscillait selon la disponibilité des gens et l'urgence des circonstances.

La gestion des relations avec certains partenaires scientifiques, plus concrètement avec le « gaz consortium » du projet « EPICA[6] et les 3 laboratoires européens mentionnés auparavant, n'a pas été facile. Le problème concerne les publications jointes (imposées par la 'stratégie' du projet) et le rôle de chaque laboratoire en son sein. Notre cas n'est pas purement scientifique, mais aussi éthique et humain, car la bonne (ou pas) volonté des gens pour l'avancement de la science devrait se mettre au-delà des intérêts personnels ou nationaux. Ceci n'a pas été le cas tout au long de ma thèse, au détriment de celle-ci, pendant laquelle des résultats importants ont été produits dont la publication a pris du retard.

Lors du déroulement de cette thèse, certains problèmes ont été soulevés et le caractère impératif de leur solution a été posé. Commençant par les soucis à petite échelle, allant vers ceux de grande échelle :

(a) lors des 2 premières années de thèse, il n'y a pas eu beaucoup d'interaction avec les membres de mon équipe; ceci a renforcé mon autonomie, certes, mais je me suis retrouvée à travailler toute seule, faire face aux difficultés rencontrées sans en parler aux autres. Je m'en suis sortie par l'intermédiaire des cours de support du collège doctoral qui m'ont aidé à relativiser la gravité de la situation, à contrôler mes sentiments et à approcher sereinement les gens impliqués en leur expliquant la situation et en leur demandant leur sollicitation. En parallèle, lors des conférences et

des réunions de toutes sortes, j'ai rencontré des scientifiques dont le domaine de recherche est similaire au mien, ce qui m'a permis d'établir un réseau hors-LGGE[3] tout au long de ma thèse ; pour cela je suis reconnaissante à mon directeur de thèse et en général à la politique générale du LGGE[3], qui encourage les jeunes chercheurs (dont les doctorants) assister aux conférences nationales et internationales.

(b) Un problème déjà mentionné auparavant concerne les aspects diplomatiques dans le grand réseau européen, EPICA[6]. Tout au long de ma thèse, dès que j'ai présenté à la communauté mes résultats, les partenaires Suisses ont été hostiles. La raison se trouve dans les conflits d'intérêt entre les 2 partenaires sur le « premier nom » des publications. Auparavant ils avaient produit la même série des données mais plus dispersée (en termes analytiques) qui n'a pas pu être publiée, malgré leurs efforts considérables. Par conséquent, leur opposition à publier mes données paraît 'normale'. La solution proposée par la communauté était l'établissement d'une série d'inter-comparaisons entre les trois laboratoires, afin d'atteindre un consensus et de trouver la source du désaccord. Nous avons tout accompli à temps ; par contre, nos partenaires n'ont pas été si rapides..

IX.3.2. Evaluation et prise en charge du coût du projet

Ressources humaines : le personnel engagé (directement ou indirectement) à ce travail de thèse, en termes de catégorie, leur temps disposé pour ce travail, leur salaire mensuel (charges patronales inclus) et leur salaire correspondant à ce travail par rapport à leur temps de disposition sont affichés dans le tableau suivant :

Type de personnel	Salaire mensuel (charges patronales incl)	Temps consacré à mon projet	Montant correspondant à ce travail	Total « personnel »
Directeur de Recherche CNRS 1	6371.41	3 ans : 1j/6mois → *total 6j*	1274.28	
Directeur de Recherche CNRS 2	6371.41	1er an : 1j/3 mois ; 2ème an : 1j/2 mois ; 3ème an : 1j/3 semaines → *total 28j*	5946.64	
Chargé de Recherche CNRS	6371.41	1er an : 1j/3 mois ; 2ème an : 1j/6 mois ; 3ème an : 1j/an → *total 7j*	1486.66	
Technicien/ permanent CNRS	2938.13	1j/an → *total 3j*	293.82	
Post-doctorant CNRS 1*	3079.06	*20 mois*	61581.20	
Post-doctorant CNRS 2	3515.15	*5 mois*	17575.75	
Thésarde CNRS/ Marie Curie	3376.85	*36 mois*	121566.60	
				209724.96

* financé par le prix Balzan de Claude Lorius

Dépenses associées au projet : les différents types des dépenses (amortissements, déplacements, infrastructure…) sont projetés au tableau suivant :

Type de dépense	Temps / nombre	Montant correspondant	Total dépense
Amortissement-Manips labo :			
*Tout matériel acheté dans le passé [IRMS[17] *+ GC[18] + Interface GC-IRMS + consommables ligne préconcentration**, pompes, onduleur + chambre froide, de 317000 euros au total] a été amorti* Bouteilles He		4550	
Echantillons de glace EPICA (nº 130)	A 50 euros/ échantillon	6500	
PC + logiciels		3500	
			14550
Installation bureau :			
Ordinateur portable/ station de travail, photocopies, papeterie, logiciels	3 ans		
			3000
Infrastructure :			
2006 + 2007 + 2008 (prévision)	100 personnes	208907 + 225019 + 221400	
			6553.26
Déplacements :			
2006 + 2007 + 2008 (prévision)	5 (dont 3 payées par EPICA et GREENCYCLES) + 9 (dont 1 payée par CNRS centrale) + 2 missions	1562.67 + 3339.22 + 543.77 (+prévu 600 euros)	
			6045.66

* acheté aux crédits Fondation de France et EPICA[6]
** achetés aux crédits EPICA-MIS et INSU-QUEST projet « DESIRE[9] »

Evaluation du coût total du projet : En faisant l'addition des tableaux ci-dessus, le coût total de cette thèse se monte aux 239873.88 euros.

IX.3.3. Camembert de ventilation :(a) théorique ; (b) réel

Il s'agit des informations communiquées par la « Project Manager » de GREENCYCLES, Marion Chabrillat. Je la remercie énormément pour sa disponibilité, sa confiance et son aide précieux en ce qui concerne les budgets annuels. Je dois également remercier mon directeur de thèse d'avoir donné le feu vert pour que j'aie accès à ce type d'information qui a priori est confidentiel entre CNRS[5] et l'UE[4].

[17] Isotope Ratio Mass Spectrometer
[18] Gas Chromatograph

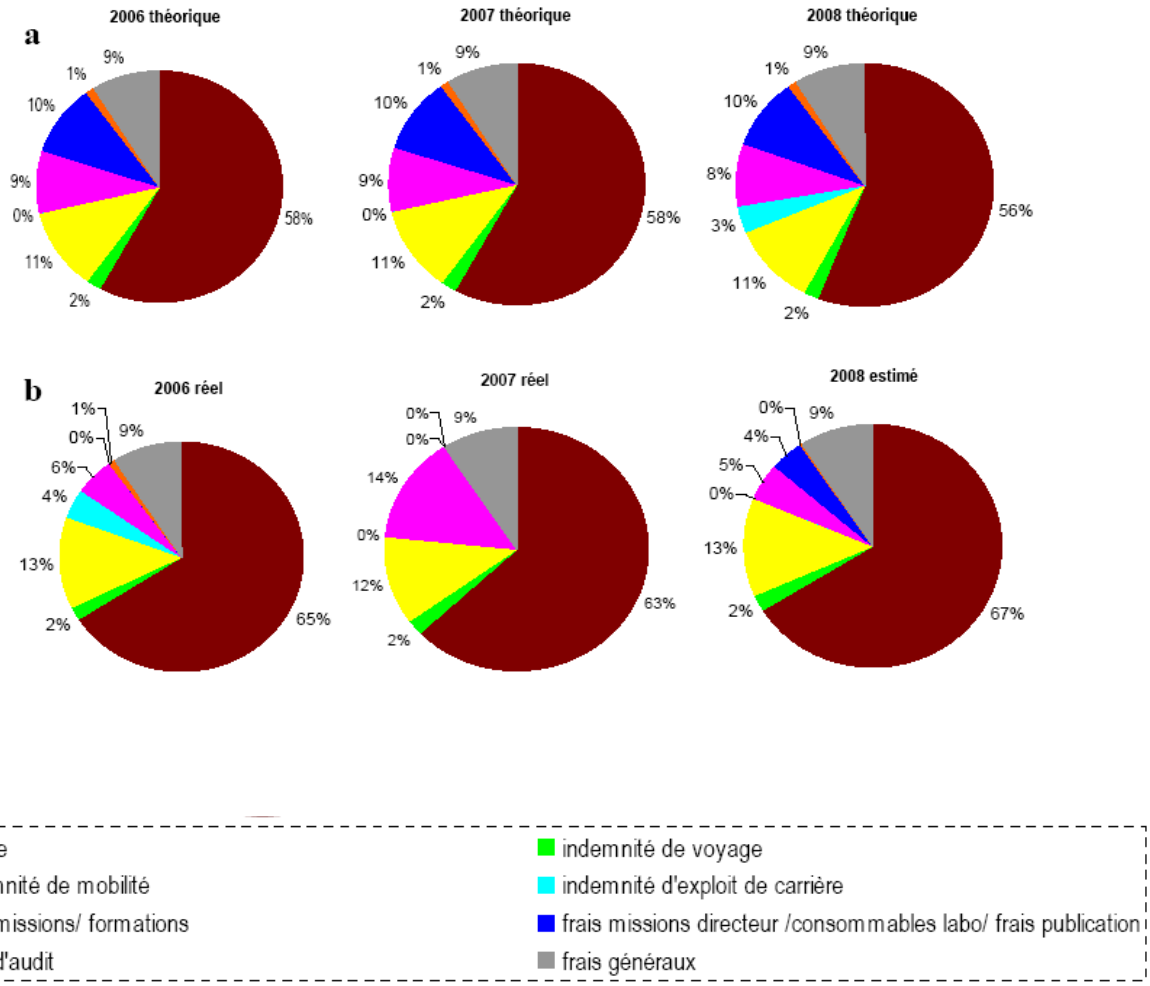

Ma bourse contient plusieurs catégories de financement, 'strictement' cadrées (*ex.* charges pour assister uniquement aux conférences), qui exigent la justification des dépenses, sous contrôles réguliers de l'UE[4]. La partie 'théorique' de la ventilation de ces différentes catégories, consiste aux sommes individuelles, bien anticipées et calculées afin d'être de suite disposées aux bénéficiaires. Elle diffère de la partie réelle, non pas dû aux contradictions de la somme initialement prévue et ultérieurement versée, ni au fait que par exemple mon salaire était bien plus élevé que prévu (comme quelqu'un pourrait bien se dire en regardant la différence des 'camembers' ci-dessus), mais plutôt dû au fait que le bénéficiaire n'utilise qu'une partie de cette somme prévu pour faciliter sa vie scientifique (ici dans le cadre de ma thèse je n'ai pas utilisé le 100% des sommes versées par l'UE[4]), rendant ainsi une partie à la 'source' (UE[4]).

IX.4. Identification, hiérarchisation et illustration des diverses compétences mises en œuvre

Domaines d'expertise et de savoir-faire acquis lors de cette thèse:

- **niveau scientifique** : Cette thèse, m'a permis d'approfondir mes connaissances sur les évènements climatiques majeurs qui ont eu lieu lors les deux dernières déglaciations. Je me suis initiée à la complexité du lien entre le cycle du carbone et le climat à travers l'histoire. J'ai appris comment appliquer un nouvel outil, afin de tracer l'évolution du CO_2 dans le passé et le présent. J'ai essayé de contribuer aux problématiques de la synchronisation entre les différents enregistrements polaires et marins partout dans le globe. Ceci impliquait l'étude du rôle des différents indicateurs chimiques et biologiques utilisés pour reconstituer les évènements importants du passé, qui m'a permis d'interagir avec des scientifiques de multiples disciplines.
- **niveau technique** : Lors de cette thèse, je me suis éduquée sur la manipulation de la glace et sur les techniques diverses d'extractions de l'air piégé. J'ai appris comment travailler dans des chambres froides à -20°C, ainsi que respecter un protocole élaboré sur le principe de séparation des gaz. Je me suis initiée sur des nouvelles techniques, aux principes des machines analytiques, comme le GC[18] et le IRMS[17]. Je me suis également formée sur l'utilisation des logiciels afin de traiter mes résultats.

Connaissances acquises de manière plus large : Lors de cette thèse, j'ai senti l'importance d'étudier le passé pour mieux anticiper pour l'avenir et je me suis sensibilisée sur le changement climatique et ses effets à long terme sur toute espèce vivante . Je me suis rendue compte que le système « Terre » est complexe, à travers les séminaires assistés lors les écoles d'été et par mon travail. Je me suis renseignée sur les applications diverses des isotopes stables des divers éléments chimiques dans l'industrie, la chimie, la nutrition, l'histoire, l'espace et les origines de la vie sur terre. J'ai assisté aux séminaires du LGGE[3] qui traitaient le système « Terre » sous plusieurs angles. A travers les partenaires GREENCYCLES j'ai appris la reconstitution de la végétation en utilisant différents systèmes numériques. Avant tout, j'ai acquis que la science n'a pas de nationalité et qu'un scientifique humain est une qualité rare, car, finalement ni la nationalité ni le niveau d'éducation fait la qualité de l'homme..

Compétences méthodologiques: Elles ont été à l'origine envisagées par l'UE[4], qui proposait des rapports informels semestriels (le « Carrer Development Plan ») : j'étais sensée mettre régulièrement à jour mes activités récentes et celles de l'avenir proche, ce qui engageait un esprit critique et d'anticipation continu. L'UJF[1] et le LGGE[3] envisageaient également la rédaction annuelle de la *charte de la thèse* et d'un *échéancier*, pour les mêmes raisons.

Le travail au laboratoire consistait à suivre à la lettre un protocole qui ne permet pas d'erreur. Son principe de rétention des gaz au temps précis, imposait l'utilisation des 2 chronomètres. Par conséquent, l'acquisition des données, fortement biaisée par le paramètre 'temps', a également renforcé le savoir-faire organisationnel (développé ci-dessous)

Savoir-faire organisationnel : La création d'une base des données bibliographique, la rédaction et le suivi d'un protocole élaboré pour le travail au laboratoire, ainsi que la projection dans l'avenir immédiat en rédigeant des rapports informels pour l'UE[4] et pour TUE[2]/UJF[1] sont en première ligne. S'ajoute mon effort d'être à temps aux obligations diverses (respect de délai pour les soumissions/présentations orales et écrites aux conférences, la rédaction des rapports officiels pour l'UE[4], pour le calendrier de la thèse et sa rédaction).

Compétences communicatives/ négociatrices/ management : En raison de la nature de ma bourse européenne qui encourage la mobilité des jeunes chercheurs, j'ai assisté un nombre considérable de workshops et conférences; lors de ces réunions, la communication de l'avancement de mon travail a eu lieu, ce qui a contribué à l'amélioration de mon bien-être et 'me bien-vendre' vis à vis du public. De nouvelles idées de manipulation, d'acquisition des données ou d'interprétation se présentent périodiquement aux différents membres de l'équipe, afin d'engager des conversations.

Mon sens de la négociation a été également développé, vu les intérêts multiples dans le cadre du projet EPICA[6], sous condition que la partie 'opposée' soit de bonne volonté pour atteindre un compromis.

La gestion du temps est difficile à envisager ; comme j'ai mentionné auparavant j'ai eu des objectifs ambitieux, qui imposait le travail aux heures supplémentaires pour les atteindre. Les axes principaux sont : acquisition- réflexion –collaboration - interprétation, effectués en deux différentes périodes. Au début de ma thèse j'ai été encadrée par un post-doctorant, état indispensable afin que je puisse être autonome pour la partie expérimentale. J'ai ensuite travaillé seule pendant les 2 premières années. Vers la fin de ma 2ème année un nouveau post-doctorant est arrivé et que j'ai encadré ; depuis on partage le labo en respectant nos besoins respectifs.

Savoir-être/compétences humaines : Effectuer une thèse est une compétition perpétuelle avec soi-même. On se sent bien dans sa thèse chaque fois que l'on se dépasse. Mon sens d'autonomie se cultive et s'évolue au fur et à mesure, ce qui permet la construction d'un organigramme (des travaux au laboratoire vers la rédaction de la thèse), souvent revisité et actualisé.

Savoir-faire linguistique : étant Grecque d'origine, je travaille dans un laboratoire français et je communique en français avec mes partenaires français, alors que ma bourse européenne me permet de collaborer avec des laboratoires partout dans l'Europe et d'assister un grand nombre de conférences, tout en s'exprimant en anglais. Mon manuscrit de thèse sera en anglais alors que le nouveau chapitre de la thèse en français !

Qualités personnelles : Je mettrais en première ma motivation et curiosité permanente à l'apprentissage, comme s'est déduit à travers la recherche dans différents domaines de l'environnement que j'ai parcouru tout au long de mes études. Ma capacité d'analyse et de synthèse serait aussi une des qualités acquise lors de cette thèse vu des nombreuses rédactions des rapports annuels officiels à l'UE[4], ainsi que d'un article scientifique. Mes aptitudes à l'animation et la communication sont également présentes, suite à la participation aux évènements de vulgarisation scientifique et mon intervention avec le grand public et les enfants. La rigueur, comme elle est acquise par l'application d'un protocole élaboré et performant, en permettant toutefois de vérifier cette performance en effectuant des tests, devrait aussi être mentionnée. Pour finir, j'ajouterais mon adaptabilité aux nouvelles conditions, le travail dans la chambre froide et l'initiation aux techniques inconnues faisant preuve.

Construction d'un réseau professionnel personnel : Ma participation aux conférences nationales et internationales, m'a permis de rencontrer des scientifiques dont le domaine de recherche m'intéresse, d'interagir et se réunir ultérieurement pour une collaboration ou pour plus de discussions. Le réseau web a également contribué aux 'connaissances' même 'inter-atlantiques' ou 'inter-pacifiques' via e-mail, à travers duquel des discussions fructueuses ont eu lieu. Le fait que j'appartiens à 3 réseaux européens et avoir assisté 2 écoles d'été m'a également permis de connaître de jeunes chercheurs. Toutes ces connaissances, pourraient éventuellement servir comme 'soutien '/'appui' vis-à-vis aux nouveaux/ futurs réseaux.

Transférabilité de ces compétences en dehors de mon domaine de recherche

	ACTUEL	**NOUVEAU**
ACTUEL	• curiosité scientifique ; questionnement constants ; recherche de l'information ; rédaction des articles → **chercheur** • travail expérimental ; traitement des données → **ingénieur de recherche**	• intérêt sur l'histoire du passé et l'océan → passage de la paléoclimatologie au **paléoceanographie** • flexibilité aux déplacements → **représentant d'entreprise / missionnaire**
NOUVEAU	• communication ; vulgarisation → **journaliste scientifique** • interaction avec les étudiants → **maître des conférences** • sensibilisation sur l'environnement → **chargée d'études dans un bureau d'études**	• intéractions avec jeune public → **professeur ; institutrice ; responsable de formation/ communication** • compétences linguistiques → **traductrice ; guide** • travail en équipe → **coordinateur ; chef d'entreprise** • sens de négociation → **diplomate / négociateur**

IX.5. Résultats, impact de la thèse

-pour le laboratoire : j'ai été une doctorante avec une bourse Marie Curie, impliquée dans 3 différents projets européens ; ce fait combiné avec la production des données importantes pour la communauté scientifique, permettra au LGGE[3] d'être de nouveau mentionné. Tous les investissements ont été rentabilisés au niveau scientifique et personnel. Ce genre de contrats européens devrait être propagé partout pour dynamiser la mobilisation des chercheurs en encourageant les partenariats internationaux. Seul point faible : le bilan final en carbone de tous ces déplacements…Faudrait-il envisager des téléconférences ?

-pour l'équipe : le rôle d'un doctorant dans cette équipe est multidisciplinaire : il assure la production des données pendant une période prévu, la communication auprès des scientifiques et du public (lors des nombreuses visites au labo des écoles, journalistes, hommes politiques, chercheurs..) et le passage de savoir-faire envers les nouveaux arrivants. L'acquisition des résultats pendant cette thèse a de nouveau confirmé le rôle pionnier de cette équipe vers la production des données de qualité. Des nouvelles collaborations sont établies qui pourraient servir dans l'avenir.

-pour les partenaires du projet : pour GREENCYCLES, malgré le fait que mon domaine de recherche diffère des autres partenaires, la conception générale de mon étude (couplage travail technique et interprétation en utilisant des outils numériques) les a intéressés sur l'évolution de ce travail. La preuve en est que le 'GREENCYCLES_part 2' vient d'être 'candidatée' à la UE[4], ayant comme axe principal ce couplage pré-mentionné. En ce qui concerne les autres projets, les résultats de cette thèse pourront être exploités par des physiciens/mathématiciens afin de mieux comprendre les mécanismes du climat du passé.

-pour la Recherche : un pas vers la lumière, la connaissance ; un pas vers le doute, les questionnements ; un pas vers la vérité, vers l'anticipation pour l'avenir !

-pour l'Economie : cette thèse apporte un rôle indirect mais significatif sur l'identification des potentielles futures sources d'énergie vu que ses sources actuelles diminuent. Il rappelle le caractère urgent de mise en place des protocoles/directives-cadres sur l'environnement.

-pour la Société : l'histoire nous apprend que la période interglaciaire (chaude et stable) correspond à l'euphorie et au bien-vivre de l'être humain. Actuellement on modifie cette stabilité, ce qui risque d'avoir un impact sérieux sur la société, couplé avec le mondialisation et le développement démographique. Cette thèse souligne que l'anticipation immédiate est nécessaire pour le bien-être des prochaines générations.

Cette thèse m'a cultivée sur l'histoire en me permettant d'approfondir un nouveau domaine sur l'environnement, de travailler avec des nouvelles techniques expérimentales, de me diriger vers le monde inconnu de l'interprétation numérique, d'assister un grand nombre de réunions, de renforcer mon sens de communication, de travailler avec des chercheurs brillants, de voyager partout dans l'Europe et d'interagir tant scientifiquement que humainement. Je suis profondément reconnaissante à mon directeur de thèse de m'avoir donné cette opportunité de faire face à tout cela. Le monde de la recherche me plaît ; j'aimerais continuer sur ce chemin là, soit en tant que chercheuse ou ingénieur de recherche. Pour l'instant une chose est sure : je n'abandonnerai pas l'environnement, ses richesses à investiguer, ainsi que la communication, le transfert de la connaissance et l'interaction avec les jeunes qui sont l'espoir du futur.